Les nanocapsules lipidiques chargées en Rhénium-188 : nouvel outil pour la radiothérapie interne du carcinome hépatocellulaire et du gliome

Claire Vanpouille-Box

UNIVERSITE D'ANGERS Année 2011

N° 1097

Les nanocapsules lipidiques chargées en Rhénium-188 : nouvel outil pour la radiothérapie interne du carcinome hépatocellulaire et du gliome

Thèse DE DOCTORAT

Spécialité : Pharmacologie Expérimentale et Clinique

ECOLE DOCTORALE : BIOLOGIE SANTE

Présentée et soutenue publiquement

Par **Claire Vanpouille-Box**

Le 3 février 2011

Devant le jury ci-dessous :

Dr. Claire BILLOTEY Docteur à l'Université de Lyon	Rapporteur
Pr. Frédéric COURBON Professeur à l'Université de Toulouse, INSERM U563	Rapporteur
Pr. Etienne GARIN Professeur à l'Université de Rennes, INSERM U991	Examinateur
Pr. Patrice MARCHE Directeur de recherche INSERM, INSERM U823, Grenoble	Examinateur
Pr. Philippe MENEI Professeur à l'Université d'Angers, INSERM U646	Examinateur
Dr. Emmanuel GARCION Chargé de recherche CR1 INSERM, INSERM U646, Angers	Examinateur
Dr. François HINDRE Docteur à l'Université d'Angers, INSERM U646	Co-Directeur de Thèse
Pr. Olivier COUTURIER Professeur à l'Université d'Angers, INSERM U646	Directeur de Thèse

REMERCIEMENTS

Je remercie Jean-Pierre Benoit, Professeur de l'Université d'Angers, pour m'avoir accueillie au sein de son unité pendant ces trois années enrichissantes.

Je tiens à exprimer mes plus sincères remerciements aux membres du jury pour avoir accepté et pris de leur temps pour évaluer ce travail.

Un grand merci à Etienne Garin, Professeur de l'Université de Rennes ; à Patrice Marche, Directeur de recherche INSERM de l'Université de Grenoble et à Philippe Menei, Professeur de l'Université d'Angers pour avoir accepté d'évaluer ce travail en tant qu'examinateurs.

Un merci particulier à Claire Billotey, Maître de conférences à l'Université de Lyon et à Frédéric Courbon, Professeur à l'Université de Toulouse de me faire l'honneur d'être rapporteur de cette thèse.

Je tiens à remercier Olivier Couturier, Professeur à l'Université d'Angers, pour avoir pris le temps de suivre ce travail.

J'exprime ma plus profonde gratitude au Docteur François Hindré, Maître de conférences à l'Université d'Angers et co-directeur de ce travail. Merci pour ta sympathie, ton enthousiasme et ta confiance. Les mots me manquent pour exprimer toute ma reconnaissance. Merci encore.

Un grand merci à Emmanuel Garcion, Chargé de recherche INSERM à l'Université d'Angers. Merci pour tes conseils et ton intérêt pour ce travail, sans toi, je n'aurai pas eu assez de recul pour la partie biologie de ce projet. Je garde de nombreux souvenirs en tant

que collègue de bureau ! Entre discussions sérieuses et blagues, le temps à l'IBT a semblé passer super vite !

J'adresse mes remerciements à La Ligue contre le Cancer du Maine-et-Loire, le Cancéropôle Grand Ouest et les Collectivité territoriales pour les aides financières octroyées.

Je tiens à remercier :

Le Professeur Nicolas Noiret, le Docteur Virginie Cadeillan et Sabine Orain, de l'Ecole Nationale Supérieure de Chimie de Rennes, pour m'avoir gentiment accueilli pendant une semaine pour une formation accélérée de la synthèse du ligand. Merci également pour m'avoir donné les kits de rhénium-188.

Le Docteur Nicolas Lepareur, Centre Eugène Marquis de Rennes, pour les nombreuses élutions de rhénium-188.

Le Professeur Christophe Aubé et le Docteur Frédérique Oberti, laboratoire HIFI EA3589, pour leur intérêt et les précieux conseils pour ce projet de thèse.

Merci à Camille Belloche, technicienne de laboratoire au sein de l'unité. Merci pour toute ton aide, je pense que les marquages immuno n'ont plus aucuns secrets pour toi! Merci également pour m'avoir fait découvrir ce qu'était le véritable échange stagiaire-encadrant ! J'ai vraiment apprécié de travailler avec toi et j'espère sincèrement que tu réussiras dans ta vie professionnelle et personnelle.

Je tiens à remercier Jérôme Roux et Pierre Legras pour leurs précieux conseils en expérimentation animale. Je garde de précieux souvenirs avec vous à l'animalerie aussi bien pour le travail que pour les moments de détente. Je n'oublie pas Dom et Laurent qui sont su s'occuper de mes petits rats en mon absence …

Je voudrais remercier les personnes qui ont travaillé avec moi de près ou de loin, notamment Franck pour ses précieux conseils, Francis pour les scintigraphies, Laurent et Florence pour l'IRM.

Merci à Emeline Brocard, pour ta sympathie, ton enthousiasme et surtout pour ton travail de qualité. Je suis vraiment contente que tu aies pu trouver un poste intéressant à Nantes. Je te souhaite de réussir, tu le mérites.

Mention particulière pour:

mes nouveaux coloc' de bureau : Anne, Jérôme et Marie qui ont su me faire une place et écouter mes complaintes pendant la rédaction de ce travail.

Emilien pour les biodis qu'on a traversé ensemble et les fous rires ! J'espère que tu as trouvé ce qu'il te plaisait…

Séverine pour nos discussions de fille. Je ne dirai qu'une chose : vive cocoon!!

Gaétan merci pour ton humour et tout le reste ! Bonne chance à Miami ! Je n'oublie pas Clem (celle qui a des migraines avec les orages ☺!) merci pour les soirées passées ensemble et celles à venir.

Kahena pour ton amitié, ton humour, nos discussions constructives et drôles ! On se verra sur Toulouse promis !

Je voudrais également remercier tous mes autres collègues pour la bonne ambiance au labo ! Edith pour sa disponibilité et sa bonne humeur, Laurence, Olivier, Claudia, Marie-Claire, Nathalie, Patrick, Jean-Luc, Franck B, Frédéric, Catherine, Stéphanie (le mois prochain, promis, je viens avec toi au sport !), Elodie (il faut qu'on retourne au VnB), Erika (bon courage, tu es sur la dernière ligne droite…), Sandy (félicitations encore pour ton poste !), JP (alias Dr. Amore), Nolwenn (je me demande encore comment tu fais pour avoir 10 de tension et courir partout !), Brice (occupe toi bien de ton p'tit bout), Florian, Nicolas, Audrey, Leila, Anne-Laure, Sido (surtout ne change pas !) Marie W, Thanh, Kien, Trâm, Samuli, Guillaume, Thomas, Maud, Mathilde…J'espère n'oublier personne…

Je tiens à remercier mes amis qui ont toujours été avec moi, même de très loin : Sandra (c'est bientôt ton tour !), Thomas, Matthieu (mon ex-binôme ! quand j'y repense, ça me fait encore sourir), Steffie, Emilie, Florian, Jench, Olivier, Loraine, Mika, Laurette, Raphaël… Merci pour tous les fous rires qui m'ont permis de m'aérer l'esprit !

J'adresse des remerciements les plus sincères à ma famille : mes parents et mon frère pour leur soutien inconditionnel ! Merci d'avoir simplement écouté lorsque j'en avais besoin !

Merci à ma belle-famille : mes beaux parents, mes belles soeurs, mes beaux frères, pour vos nombreux encouragements.

Enfin, merci à Nico ton soutien, ton écoute (surtout les jeudis) et ton humour m'ont permi de faire ce travail alors que je m'en croyais incapable.

ABBREVIATIONS

^{131}I: Iode-131

^{131}I-lipiodol : Lipiodol radiomarqué à l'Iode-131

^{188}Re : Rhénium-188

^{188}Re-lipiodol : Lipiodol radiomarqué au Rhénium-188

$^{188}ReO_4^-$: ^{188}Re-perrhénate

^{188}Re-SSS : Complexe lipophile de Rhénium-188

^{90}Y: Yttrium-90

^{90}Y-DOTATOC: [^{90}Y]-DOTA^{0}-D-Phe^{1}-Tyr^{3}-octreotide

^{90}Y-lipiodol: Lipiodol radiomarqué à l'Yttrium-90

^{90}Y-microsphere: Microsphères chargées en Yttrium-90

^{99m}Tc : Technétium-99m

^{99m}Tc-MAA: Macroagrégats d'Albumine marqués au Technétium-99m

ADN : Acide Désoxyribonucléique

ALT : Alanine Aminotransférase

ARN : Acide Ribonucléique

AST : Aspartate Aminotransférase

BBB: Blood Brain Barrier

BCNU: Bis-Chloronitrosourea

BHE : Barrière Hémato-Encéphalique

CED : Convection Enhanced-Delivery

CHC : Carcinome Hépatocellulaire

CMHI : Complexe Majeur d'Histocompatibilité de classe I

CMHII : Complexe Majeur d'Histocompatibilité de classe II

CT: Computed Tomography

DAPI: 4', 6-Diamidino-2-phenylindole dihydrochloride

DEB: Drug Eluting Bead

DENA: Diéthylnitrosamine

DHFR: Dihydrofolate Réductase

DOTA: 1, 4, 7, 10-tetraazacyclododecane-1, 4, 7, 10-tetraacetic acid

E/H : Eau dans Huile

EBR : External Beam Radiation

EDTB : N,N,N',N''-tetrakis-(2-benzymidazolylméthyl)-1,2-éthanediamine

EGF: Epidermal Growth Factor

EGFR: Epidermal Growth Factor Receptor

EGFRvIII: Epidermal Growth Factor Receptor variant type III

EMEM: Eagle's minimal essential medium

EPR: Enhancement Permeability Retention

FCS: Fœtal Calf Serum

FDA: Food and Drug Administration

Flt3L: fems-like tyrosine 3 Ligand

FSE: Fast Spin Echo

fSR: Fractionated Stereotactic Radiotherapy

GBM: Glioblastoma

H/E : Huile dans Eau

HAMA: Human Anti-Mouse Antibodies

HCC: Hepatocellular Carcinoma

HMGB-1: High-Mobility-Group protein B1

h-R3: Nimotuzumab

ICAM-1: Inter-Cellular Adhesion Molecule 1

IFNɣ: Interféron-ɣ

IL-2: Interleukine-2

IMST %: Increase in Median Survival Time (%)

IRM: Imagerie par Résonance Magnétique

LNC: Lipid Nanocapsule

LNC^{188}Re-SSS: Lipid Nanocapsules loaded with Rhenium-188

MAb: Monoclonal Antibody

MGMT: O^6-methylguanine-DNA-methyltransferase

MRI: Magnetic Resonance Imaging

MTD: Maximum Tolerated Dose

NCL : Nanocapsule Lipidique

$NCL^{188}Re$-SSS : Nanocapsule Lipidique chargée en complexe de Rhénium-188

P1 : Protocole 1 (SI+SI)

P2 : Protocole 2 (CED+CED)

P3 : Protocole 3 (CED+SI)

P4 : Protocole 4 (SI+CED)

PEG : poly(ethylene glycol)

PES: Post-Embolization Syndrome

$PhCS_2H$: Dithiobenzoate de sodium

RCP: Radiochemical Purity

RILD: Radiation-Induced Liver Disease

RIT: Radioimmunotherapy

SCRC: Surgically Created Resection Cavity

SI: Simple Injection

SIRT: Selective Internal Radiotherapy

SPECT: Single Photon Emission Computed Tomography

SR: Stereotactic Radiosurgery

SSS: Super Six Sulfur

SST: Somatostatin

SSTR: Somatostatin Receptor

TEL: Transfert Linéaire d'Energie

TIP: Température d'Inversion de Phase

TLR4: Toll Like Receptor 4

TMZ: Temozolomide

TN: Tenascin

VEGF: Vascular Endothelium growth Factor

VHB : Virus de l’Hépatite B

VHC : Virus de l’Hépatite C

ZIP : Zone d’Inversion de Phase

SOMMAIRE

Introduction Générale

PREAMBULE

Les progrès incessants réalisés, tant en matière de traitement que de détection de nombreuses pathologies, ont permis un bénéfice global pour les patients. Ils ont également conduit à ce que les cancers deviennent la 1ère cause de mortalité avant les maladies cardiovasculaires d'où la nécessité du développement de nouvelles stratégies thérapeutiques anti-cancéreuses.

La radiothérapie conventionnelle pour la thérapie des cancers, présente l'inconvénient majeur d'une toxicité locale. Dans ce contexte, la radiothérapie interne, visant à focaliser les radiations ionisantes dans une zone d'intérêt précise, a fait l'objet d'intenses recherches. Une des stratégies proposées est d'améliorer l'efficacité thérapeutique, la spécificité et la sécurité biologique par l'utilisation de vecteurs capables de véhiculer des radioéléments. Leur encapsulation, au sein de systèmes particulaires, permet de modifier leur profil de distribution après injection, puisque les propriétés physico-chimiques du vecteur prévalent sur celles du radioélément (Caruthers, Wickline et al. 2007). Leur ciblage passif ou actif conduit à une cytotoxicité sélective au niveau des cellules cancéreuses tout en préservant les cellules saines adjacentes (Ting, Chang et al. 2009).

La radiothérapie interne vectorisée peut donc présenter un réel avantage pour des pathologies cancéreuses où la sensibilité des tissus sains adjacents à la tumeur est accrue. Le carcinome hépatocellulaire (CHC) et les gliomes sont deux pathologies pour lesquelles les traitements curatifs sont très limités voire inexistants. La difficulté d'une radiothérapie conventionnelle pour ces pathologies, réside dans la toxicité locale mais aussi dans la sensibilité des tissus hépatiques (Dawson and Guha 2008) et cérébraux (Stupp, Mason et al. 2005).

Seules les microsphères d'Yttrium-90 ont été développées en tant que radiothérapie vectorisée après injection intra-hépatique pour le traitement du carcinome hépatocellulaire. Ainsi, la radiothérapie interne nanovectorisée peut constituer un axe de recherche

intéressant, en tant que nouvelle modalité de traitement pour le CHC et les gliomes pour lesquelles des thérapies antitumorales locales sont déjà maîtrisées.

Notre travail s'inscrit donc dans l'évaluation de nanovecteurs, les nanocapsules lipidiques chargées en Rhénium-188 (NCL^{188}Re-SSS), pour le traitement du CHC et des gliomes. Après un rappel des données existantes sur les diverses thérapies conventionnelles, nous nous concentrerons sur l'évaluation des NCL^{188}Re-SSS en tant que nouvel outil pour la radiothérapie interne nanovectorisée du CHC, puis sur l'optimisation des NCL^{188}Re-SSS pour la radiothérapie interne des gliomes. Enfin, une discussion générale permettra d'ouvrir de nouvelles perspectives.

I-LE CANCER

Afin de maintenir l'intégrité de l'organisme, les cellules incapables de réparer une ou plusieurs altérations de leur fonction principale entrent en apoptose, la mort programmée de la cellule. Cependant, dans de rares cas, les cellules peuvent subir de profonds changements métaboliques et comportementaux avec l'inactivation de l'apoptose et une division cellulaire permanente (Figure 1) (Colotta, Allavena et al. 2009) conduisant à une prolifération anarchique et à l'échappement du système immunitaire (Merlo, Pepper et al. 2006). Les cellules devenues « immortelles », dites tumorales, vont se diviser pour former un amas de cellules déréglées. Cette masse, asymptomatique pendant une longue période, va peu à peu altérer les fonctions physiologiques à l'origine de plusieurs symptômes variant selon la localisation, la taille et la propagation des cellules tumorales au sein de l'organisme (métastases tumorales).

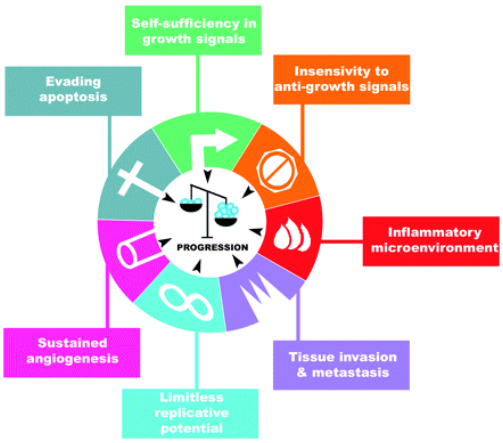

Figure 1 : Modifications nécessaires pour la cancérisation d'une cellule.
(d'après Colotta et al.)

Cette pathologie, désignée sous le terme de cancer, est la première cause de mortalité devant les maladies cardiovasculaires avec 12,4 millions de nouveaux cas et un taux de mortalité de 6,7 millions en 2008. Le taux de mortalité par cancer a doublé entre 1975 et 2000 et va certainement tripler en 2030 avec un taux prévisionnel de 38% (Boyle and Levin 2008). L'augmentation alarmante de l'incidence mondiale trouve son origine dans

l'accroissement de la population mondiale corrélée à la hausse de l'espérance de vie (ex : espérance de vie en Inde : 32-33 ans en 1947 ; 62 ans en 1997) (Are, Colburn et al.), l'élaboration d'un meilleur diagnostic clinique ainsi qu'une exposition plus importante aux agents étiologiques (l'occidentalisation des pays en développement, le tabagisme, l'obésité, l'alcoolémie, la pollution…).

II- THERAPIES CONTRE LE CANCER

Aujourd'hui, la prise en charge des patients implique une approche pluridisciplinaire regroupant la chirurgie, l'oncologie médicale, l'imagerie, la chimiothérapie et la radiothérapie, basée sur la connaissance de la biologie du cancer qui peut être très variable selon le type tumoral. L'optimisation du traitement contre le cancer dépend alors de l'orchestration de différentes modalités ayant pour objectif un bénéfice maximal pour le patient (Kerr, Bevan et al. 2002).

II-1- Chirurgie

La chirurgie, traitement standard visant à réséquer la masse tumorale, permet de diminuer l'effet de masse et donc des symptômes. Elle joue également un rôle important dans l'approche pluridisciplinaire en affirmant le diagnostique histologique. Ainsi, l'évolution tumorale pourra être appréhendée et le traitement anti-cancéreux adapté au patient. De plus, la réduction de la masse tumorale améliore l'efficacité des traitements adjuvants (Al-Shammaa, Li et al. 2008), fournit un accès vasculaire très utile dans le cadre d'une stratégie chimiothérapeutique (Tilney, Kirkman et al. 1986) et diminue les symptômes liées à la compression de la tumeur (Mitchell, Ellison et al. 2005). Cependant, la chirurgie peut être limitée devant la nature infiltrante de certaines tumeurs (gliomes) et la présence de

métastases, c'est pourquoi, elle est accompagnée par les modalités de chimio- et radiothérapie.

II-2- Chimiothérapie

La chimiothérapie est l'utilisation de molécules chimiques pour le traitement des cancers. Cytotoxiques et/ou radiosensibilisants, le choix de ces molécules dépend de l'analyse histologique et cytologique de la tumeur, puisque le traitement est variable selon le type tumoral. Plusieurs classes d'agents chimiothérapeutiques ont été développées selon l'effet biologique qu'ils engendrent au niveau cellulaire (intercalant d'ADN, inhibiteurs de mitose…) et/ou au niveau du microenvironnement tumoral (stratégies pro-apoptotiques, anti-angiogéniques…). Quatre exemples sont ici présentés (Figure 2):

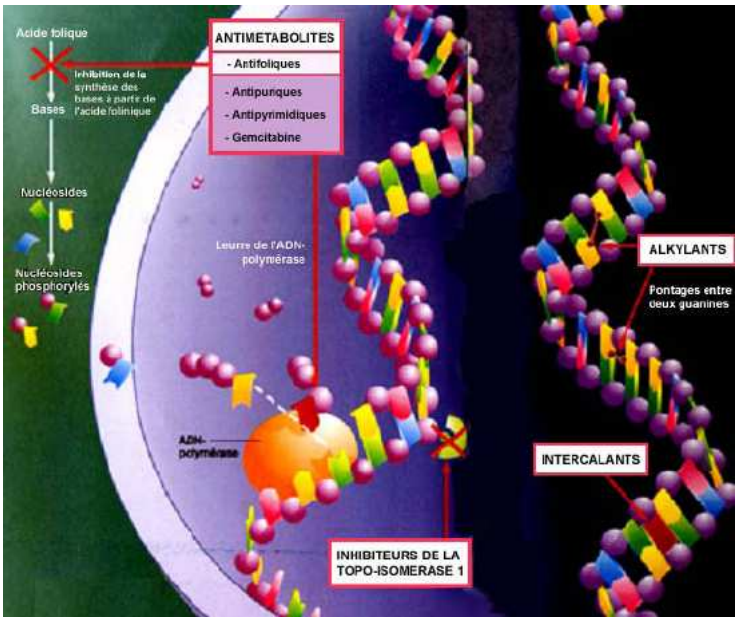

Figure 2 : Mécanismes et sites d'action des molécules chimiothérapeutiques

II-2-1- Les Anti-Métabolites

Ce sont des molécules qui, de part leur similarité structurelle, peuvent interférer avec un métabolite essentiel au bon fonctionnement de la cellule tumorale. Les réserves

intracellulaires sont alors épuisées conduisant à la mort de la cellule cible. L'un des plus anciens exemples est le méthotrexate, un inhibiteur de la dihydrofolate réductase (DHFR), une enzyme catalysant la conversion du dihydrofolate en tétrahydrofolate (Rajagopalan, Zhang et al. 2002). Il s'agit donc d'une inhibition de la voie des folates dès sa 1ère étape (Figure 3). L'affinité du méthotrexate pour la DHFR est 1000 fois supérieure à celle d'un acide folique. Ce dernier est nécessaire à la synthèse de la thymidine, lui-même essentiel à la synthèse de l'acide désoxyribonucléide (ADN). L'acide folique est également nécessaire à la synthèse des bases puriques. Par conséquent, le méthotrexate inhibe la synthèse de l'ADN, de l'acide ribonucléique (ARN) des thymidylates et des protéines. Il agit spécifiquement au cours de la synthèse de l'ADN et de l'ARN. Il est donc cytotoxique au cours de la phase S du cycle cellulaire et a un plus grand effet toxique sur les cellules à division rapide telles que les cellules tumorales.

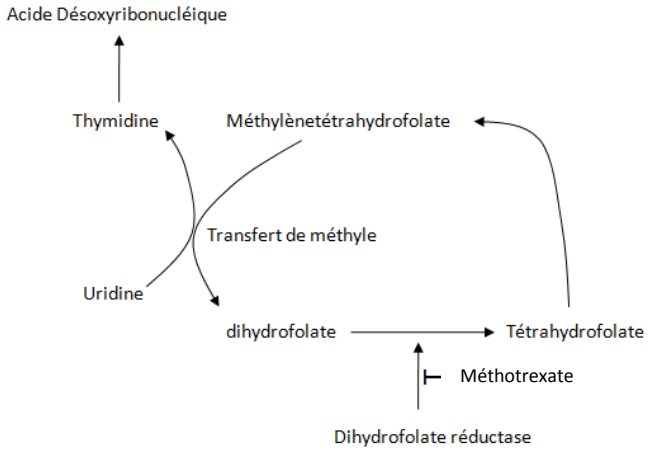

Figure 3 : Mécanisme d'action du méthotrexate (Boyle and Levin 2008).

II-2-2- Adduits d'ADN

Ces molécules peuvent se lier à l'ADN, le déformer en créant soit des adduits monofonctionnels qui interfèrent avec la synthèse de l'ADN, ou soit des réticulations bifonctionnelles qui réunissent les deux brins d'ADN, empêchant ainsi l'accès des différentes polymérases nécessaires à sa réplication. Cette classe comprend les agents alkylants

(cyclophosphamide, nitrosurés, carmustine…), les analogues de platine (cisplatine, carboplatine, oxaliplatine) et la mitomycine C.

- Exemple du cisplatine :

Le cisplatine sur fixe sur l'ADN en formant essentiellement des pontages intracaténaires (Figure 4). Les pontages type 1,2 entre deux guanines adjacentes, ou entre une adénine et une guanine sont prépondérants et représentent près de 90% du platine lié. Cette régiosélectivité est gouvernée par la forte affinité des espèces cationiques du platine pour les sites les plus riches en électrons de l'ADN. Les adduits monobrins, 1,3-intracaténaires, et interbrins constituent moins de 10 % des liaisons cisplatine-ADN (Ahmad 2010).

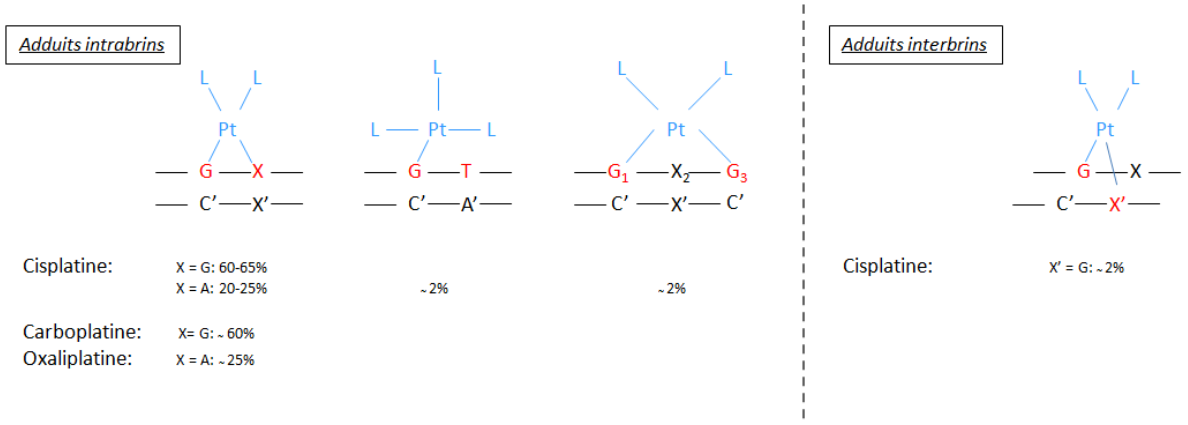

Figure 4 : Adduits d'ADN formés par les analogues de platine.

La fixation des analogues de platine sur l'ADN engendre des distorsions de la double hélice et constituent des obstacles au fonctionnement des ADN polymérases dont la progression est arrêtée au niveau de l'altération, ce qui bloque la réplication de l'ADN. Toutes les ADN polymérases à localisation nucléaire sont inhibées, de même que celle à localisation mitochondriale.

II-2-3- Inhibiteurs de la mitose

Après que la cellule ait doublé sa quantité d'ADN pendant la phase S du cycle cellulaire, elle entre en phase de mitose. Un fuseau mitotique se forme, résultat de l'interaction entre plusieurs protéines avec notamment la tubuline, importante dans l'alignement des chromosomes nouvellement synthétisés. Beaucoup d'agents anti-cancéreux interfèrent avec ce phénomène soit en empêchant la formation du fuseau mitotique, soit en inhibant sa dissolution. Cette classe est composée de taxanes (taxol), de vinca-alkaloïdes et des épothilones.

II-2-4- Prévention de l'ouverture de l'ADN double brin

Les inhibiteurs de la topoisomérase II (doxorubicine, étoposide), de la topoisomérase I (irinitecan, topotecan) interfèrent avec les enzymes responsables de l'ouverture de l'ADN double brin, phénomène essentiel à sa synthèse. Les cellules tumorales entrent alors en apoptose.

II-2-5- Association radio-chimiothérapie

L'irradiation d'une population de cellules produit une cascade d'événements physiques, chimiques, biochimiques puis biologiques maintenant mieux appréhendés (cf. paragraphe II-3-3-). L'ionisation produite par l'irradiation va être responsable de la formation d'un grand nombre de lésions de l'ADN : dommages de bases, cassures simple et double brin. L'ADN est donc la cible principale des radiations ionisantes, les cassures double brin de l'ADN étant plus difficilement réparables et donc principalement responsables de la radiosensibilité. Ces constations ont conduit à tenter de diminuer la réparation des lésions de l'ADN radio-induites pour accroître la radiosensibilité. C'est ainsi que se sont développées des stratégies concomitantes de radio- et de chimiothérapies avec des agents cytotoxiques comme le cisplatine, majorant les lésions de l'ADN, ou comme le 5-fluoro-uracile, inhibant la réparation, ces médicaments jouent alors un rôle radiosensibilisateur.

Du fait de leurs modes d'actions la chimio- et la radiothérapie trouvent un intérêt particulier en situation néoadjuvante et adjuvante à la chirurgie, seul traitement curatif des tumeurs solides à ce jour.

Bien que ces agents chimiothérapeutiques aient des mécanismes d'action différents, ils ont tendance à toucher de façon sélective les compartiments cellulaires où la prolifération cellulaire est rapide lorsqu'ils sont injectés en systémique. Toutefois, cette thérapie conventionnelle s'avère inefficace pour les traitements tels que le carcinome hépatocellulaire (CHC) et le gliome malin en raison de la résistance intrinsèque du CHC et de la présence de la barrière hémato-encéphalique (BHE). Ces problèmes majeurs de toxicité et d'accessibilité de l'agent anti-cancéreux au site tumoral ont conduit à leur administration locale, (exemple : implant de carmustine - gliadel®, agent alkylant pour le traitement locorégional des gliomes), qui se trouve confrontée à une efficacité anti-tumorale insuffisante.

II-3- Radiothérapie

La radiothérapie est l'utilisation de radiations ionisantes pour entraîner la mort des cellules tumorales en bloquant leur capacité à se multiplier. Pour cela, le patient est soumis à un rayonnement dirigé sur un volume précis contenant la masse tumorale. Un rayonnement ionisant induit des ionisations dans la matière qu'il traverse. La pénétration des radiations va dépendre du type de radiation (α, β^-, β^+, X et γ), du transfert d'énergie linéaire (TEL) et de leur énergie.

II-3-1- Type de radiation

La production des rayonnements α, β, et γ résulte d'un réagencement des nucléons à l'intérieur du noyau (transition nucléaire), tandis que les rayonnements X proviennent du

passage d'un électron de niveau d'énergie E_0 à un niveau d'énergie supérieur E_1 (transition électronique).

II-3-1-1- Radioactivité alpha (α)

La radioactivité alpha (ou rayonnement α) est une forme de désintégration radioactive où un noyau atomique X éjecte une particule α et se transforme en un noyau Y de nombre de masse diminué de 4 et de numéro atomique diminué de 2. La désintégration alpha peut être vue comme une forme de fission nucléaire où le noyau père se scinde en deux noyaux fils dont l'un est un noyau d'hélium :

$$ {}^{A}_{Z}X \rightarrow {}^{A-4}_{Z-2}Y + {}^{4}_{2}He \quad \text{ou} \quad {}^{A}_{Z}X \rightarrow {}^{A-4}_{Z-2}Y + \alpha $$

(*A* représente le nombre de masse, *Z* le numéro atomique)

L'émission α ne concerne que les noyaux lourds présentant un excès de protons (nombre de masse >200). Le rayonnement alpha étant constitué d'une particule lourde, il est très peu pénétrant, une simple feuille de papier peut l'arrêter.

Exemple : la désintégration du radium en radon

$^{226}Ra \rightarrow {}^{222}Rn + \alpha.$

II-3-1-2- Radioactivité bêta (β)

La radioactivité β (ou émission β) est un type de désintégration radioactive dans laquelle une particule β (un électron ou un positon) est émise. On parle de désintégration β^- ou β^+ si un électron ou un positon est émis. L'électron ou le positon étant des particules légères, le rayonnement β est beaucoup plus pénétrant que le rayonnement α. Comme les particules sont chargées, elles interagissent facilement avec la matière (seuls les rayonnements β^- sont utilisés en radiothérapie). Il faut une feuille métallique de quelques centimètres d'épaisseur pour arrêter ce rayonnement.

- Emission β^-

La radioactivité β^- affecte les nucléides X présentant un excès de neutrons. Elle se manifeste par la transformation dans le noyau d'un neutron en proton, le phénomène s'accompagnant de l'émission d'un électron (ou *particule* β^-) et d'un antineutrino électronique $\overline{\nu_e}$:

$$^{A}_{Z}\mathrm{X} \rightarrow {}^{A}_{Z+1}\mathrm{Y} + e^- + \bar{\nu}_e$$

Exemple : la désintégration du tritium en hélium

$^3H^+ \rightarrow {}^3He^{2+} + e^- + \overline{\nu_e}$

- Emission β^+

La radioactivité β^+ ne concerne que les nucléides présentant un excès de protons. Elle se manifeste par la transformation dans le noyau d'un proton en neutron, qui abouti à l'émission d'un positon et d'un neutrino électronique ν_e :

$$^{A}_{Z}\mathrm{X} \rightarrow {}^{A}_{Z-1}\mathrm{Y} + e^+ + \nu_e$$

Exemple : la désintégration du fluor en oxygène

$^{18}F \rightarrow {}^{18}O + e^+ + \nu_e$

II-3-1-3- Radioactivité gamma (ɣ)

La radioactivité ɣ est le nom donné au rayonnement électromagnétique produit par la désintégration des noyaux atomiques ou par des phénomènes subatomiques comme l'annihilation d'une paire électron-positron. Ils ont une énergie qui varie dans une plage allant de la centaine à plusieurs centaines de keV. Les rayons ɣ sont plus pénétrants que les rayonnements α et β, mais sont moins ionisants. Ils sont de même nature que les rayons X mais sont d'origine différente. Les rayons ɣ sont produits par des transitions nucléaires tandis que les rayons X sont produits par des transitions électroniques provoquées en général par la collision d'un électron avec un atome, à haute vitesse.

II-3-1-4- Rayonnements X

Les rayons X sont une forme de rayonnement électromagnétique à haute fréquence constitué de photons dont la longueur d'onde est comprise approximativement entre 5 picomètres et 10 nanomètres. L'énergie de ces photons va de quelques eV (électron-volt), à plusieurs dizaines de MeV. Ils peuvent être produits par trois manières :

- Transition électronique : Un électron du niveau d'énergie E_0 va passer au niveau d'énergie supérieur E_1.L'excitation des électrons peut être provoqué par des rayons X ou par un bombardement d'électrons. Il s'agit du principe de la spectrométrie de fluorescence X.
- Accélération des électrons : Tout électron soumis à une accélération émet des ondes électromagnétiques. L'émission de ce rayonnement ainsi émis s'appelle rayonnement de freinage magnétique.

II-3-2- Effets des rayonnements sur la matière

Le transfert d'énergie linéaire (TEL) refléte directement les dommages biologiques d'un rayonnement. En effet, le TEL est la quantité d'énergie libérée par une particule radioactive (ou une onde) le long de son parcours de désintégration. Ainsi, des particules à TEL élevés (particules α et β) vont ioniser les molécules d'eau sur un parcours très court tandis que celles à TEL faible (rayons X et particules ɣ) résultent en une ionisation sur un parcours plus important (Figure 5). Ainsi, pour un TEL élevé, nous pouvons considérer que les ionisations auront lieu dans la même cellule. Dans ce cas, l'ionisation de l'eau va conduire à la formation d'une paire de radicaux OH adjacents qui vont alors se recombiner en péroxide (H_2O_2). Ce péroxide va être à l'origine de lésions oxydatives au sein de la cellule. Dans le cas d'un TEL faible, les ionisations auront lieu dans deux cellules séparées. Ainsi, les radicaux H et OH les plus proches vont intéragir pour former une nouvelle molécule d'eau.

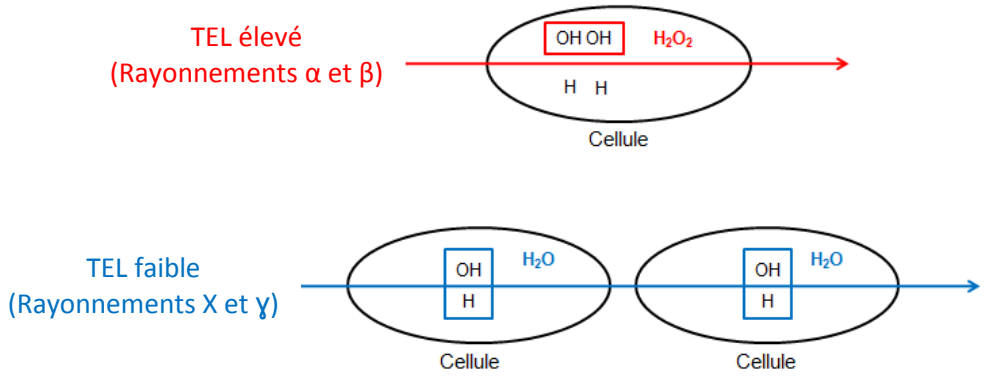

Figure 5 : Ionisation et transfert linéaire d'énergie (TEL)

II-3-2-1- Rayonnements α

En traversant la matière, cette particule interagit principalement avec le cortège électronique des atomes du matériau traversé, ce qui les excite ou les ionise. Ce mécanisme se produit sur une très courte distance (TEL très élevé) car la section efficace d'interaction est élevée: le pouvoir de pénétration des rayonnements alpha est faible (une simple feuille de papier ou 4 à 5 cm d'air les arrêtent totalement) et par conséquent le dépôt d'énergie par unité de longueur traversée sera élevé. Cette énergie dissipée dans la matière traversée se traduira par des excitations et des ionisations et donne lieu à des rayonnements secondaires.

II-3-2-2- Rayonnements β^-

Ce rayonnement interagit avec la matière en provoquant des excitations et des ionisations par diffusion. Le parcours des électrons dans la matière est plus important que celui des particules α (de l'ordre de quelques mètres maximum dans l'air). La perte d'énergie du rayonnement β par unité de longueur traversée sera moindre que celle du rayonnement α. Il en sera de même du nombre d'excitation et d'ionisation produite par unité de longueur (TEL élevé mais inférieur à ceux des particules α).

II-3-2-3- Rayonnements X et ɣ

Au cours de l'interaction entre les rayons X ou γ et la matière, des électrons peuvent être libérés par un effet photoélectrique, un effet Compton ou par production de paires, pour acquérir une énergie cinétique (Figure 6). L'atome cible perd un électron et devient un ion positif. Les électrons libérés rencontrent d'autres électrons le long de leur trajet et sont responsables de la formation de nombreux autres ions. La majeure partie des ions formés provient, en réalité, des électrons et non pas des rayons X eux-mêmes. Les rayons X et γ sont pour cette raison, appelés radiations indirectement ionisantes.

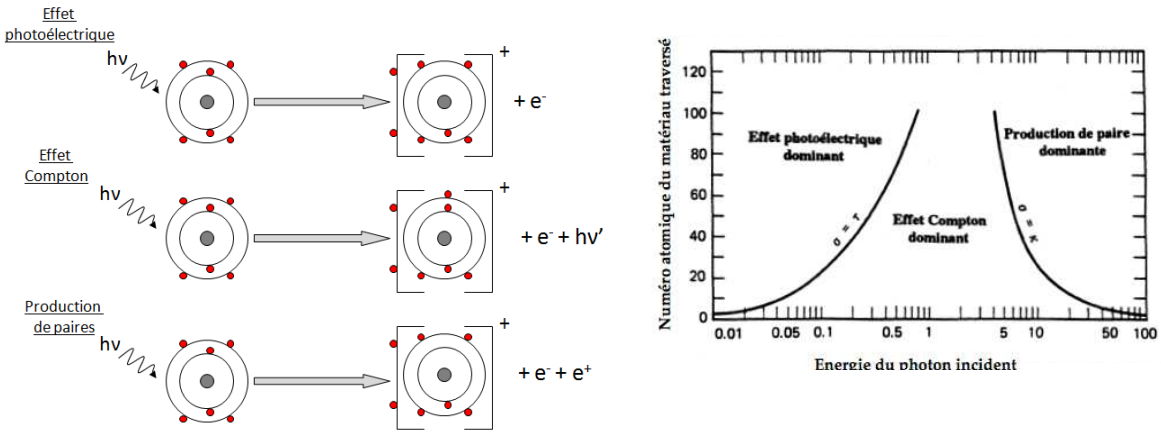

Figure 6 : Schéma de l'absorption des rayons X ou γ par la matière

II-3-3- Radiations ionisantes et effets biologiques

Les dommages cellulaires provoqués par les rayonnements ionisants sont principalement dus à leurs effets sur l'ADN. Les modifications structurelles des molécules d'ADN entraînent des effets génotoxiques, à l'origine de possibles mutations ou de mort cellulaire. Deux types de mécanismes ont été mis en évidence pour expliquer les anomalies de l'ADN. Les rayonnements ionisants ont d'abord un effet direct sur l'ADN. L'ionisation d'un atome constituant la molécule d'ADN est à l'origine d'une recombinaison avec un autre atome, modifiant la structure de l'ADN. L'effet direct est important pour les rayonnements de type α et β, mais a une importance mineure pour les rayons X ou γ.

Le deuxième mécanisme consiste en une ionisation des molécules d'eau (radiolyse de l'eau) et d'oxygène à l'origine des radicaux libres. Ceux-ci entraînent, lors de leur recombinaison, des modifications structurelles des molécules d'ADN (Figure 7).

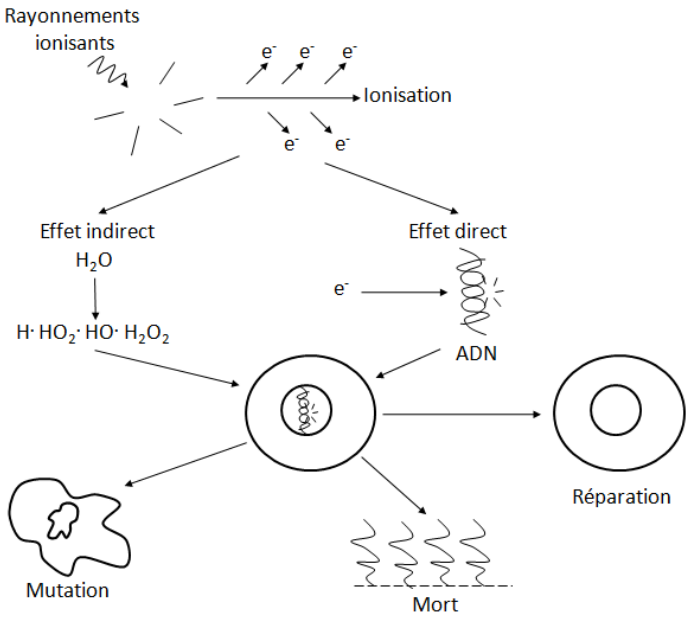

Figure 7 : Effets des radiations ionisantes.

Les dommages de l'ADN peuvent être sans importance pour le codage génétique ou être réparés par la cellule ; dans ce cas, l'effet biologique des radiations se limite à l'échelle moléculaire laissant la cellule intacte.

Lorsque les modifications sur l'ADN provoquées par l'irradiation touchent le codage génétique et lorsque la cellule ne procède pas à sa réparation, les radiations peuvent être à l'origine de mutations ou de mort cellulaire. La mort cellulaire n'intervient généralement que lors de la mitose suivante, on parle alors de mort retardée. La sensibilité de la cellule dépend de facteurs liés à l'irradiation (énergie, débit, fractionnement de la dose), au milieu (oxygène) et à la cellule elle-même. Les cellules sont plus radiosensibles lorsqu'elles sont en phase G2M et plus résistantes en interphase. De plus, les cellules sont d'autant plus sensibles qu'elles sont peu différenciées et qu'elles se divisent beaucoup.

Il est important de souligner les travaux du Pr. Bergonié-Tribondeau (Loi de Radiologie) et du Pr. Claudius Regaud (notion de radiosensibilisation) qui ont permi de poser les bases de fractionnement, d'étalement et de radiosensibilisation, à l'origine de l'augmentation la plus significative de l'index thérapeutique en radiothérapie. C'est donc sur ces notions que la radiothérapie a trouvé son utilité dans le traitement des cancers. L'objectif thérapeutique étant de maximiser l'effet anti-tumoral tout en préservant les tissus sains adjacents (Steel, McMillan et al. 1989). La radiosensibilité intrinsèque des différents types de cellules tumorales a été très largement étudiée, cependant, les mécanismes sous-jacents n'ont été que très peu élucidés.

II-3- 4- Radiations ionisantes et microenvironnement

Plusieurs études se sont focalisées sur les dommages de l'ADN et la capacité de sa réparation au sein de la cellule tumorale (Prise, Schettino et al. 2005) mais ont ignoré le fait que la radiosensibilité des tumeurs *in vivo* est fortement affectée par son caractère immunosuppresseur. En 2007, Galluzzi *et al.* ont démontré une nouvelle voie de mort cellulaire qui est mise en place lors d'un stress cellulaire et contribue à l'activation du système immunitaire (Galluzzi, Maiuri et al. 2007). Les interactions possibles entre la cellule irradiée, son microenvironnement et le système immunitaire sont de mieux en mieux appréhendées (Zeh and Lotze 2005; Apetoh, Ghiringhelli et al. 2007; Formenti and Demaria 2009). Ce processus peut résulter en l'acquisition d'une immunité spécifique anti-tumorale aussi bien au site primaire qu'aux sites métastatiques. Ces effets indirects de l'irradiation à l'intérieur et en dehors du champ de traitement suggèrent de nouvelles opportunités incluant les combinaisons à visée immunothérapeutiques.

<u>Action du système immunitaire face aux radiations ionisantes</u>

Dans certains cas, la cellule tumorale irradiée peut subir plusieurs modifications qui vont participer à la mise en place d'une réponse immunitaire anti-tumorale. En effet, la cellule

tumorale en apoptose va exposer la calréticuline à sa surface pour favoriser sa phagocytose par les cellules dendritiques et ainsi relarguer le facteur nucléaire HMGB1 (high-mobility-group protein B1), cytokine inflammatoire responsable de l'apprêtement antigénique par les cellules dendritiques exprimant le récepteur TLR4 (Figure 8A) (Apetoh, Ghiringhelli et al. 2007; Obeid, Panaretakis et al. 2007; Obeid, Tesniere et al. 2007).

Dans un deuxième temps, lorsque les dommages des radiations ne sont pas suffisants pour induire une mort cellulaire, les cellules tumorales vont surexprimer des molécules d'adhésion telles qu'ICAM-1, le récepteur Fas et le complexe majeur d'histocompatibilité de classe I (CMHI). Ceux-ci vont permettre la reconnaissance des cellules tumorales par les lymphocytes T (Chakraborty, Abrams et al. 2004) qui vont, à leur tour, produire un gradient de cytokines utilisé pour l'attraction des lymphocytes T effecteurs (Figure 8B).

Parallèlement, les cellules dendritiques activées vont présenter les antigènes tumoraux et migrer vers les organes lymphoïdes secondaires (Figure 8C) où elles vont rencontrer des lymphocytes T naïfs. Ces derniers vont alors proliférer, en acquérant des fonctions effectrices et migrer vers le site d'irradiation par un gradient de cytokines (Figure 8B) (Lugade, Sorensen et al. 2008).

Tous les effets pro-immunogéniques décrits dans la littérature ont eu lieu au niveau du site tumoral. Néanmoins, si les lymphocytes T effecteurs sont en nombre suffisant, il est possible qu'ils puissent reconnaître les cellules métastatiques (Figure 8D).

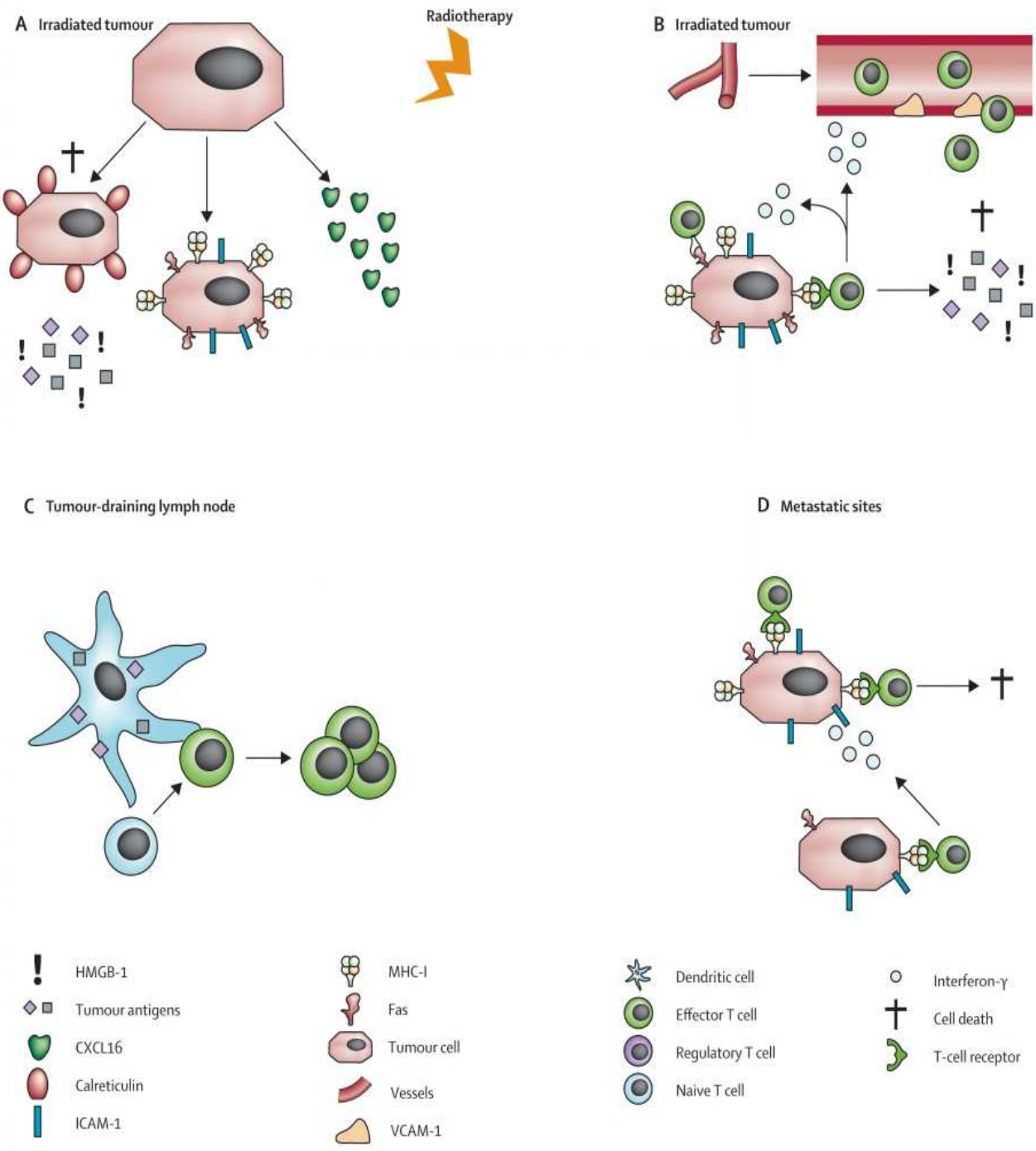

Figure 8 : Etablissement d'une réponse immunitaire spécifique après modifications de la tumeur et de son microenvironnement (Formenti and Demaria 2009).

Aujourd'hui, la radiothérapie, qui peut être associée à la chimiothérapie, est souvent utilisée en situation adjuvante et néoadjuvante pour le traitement des cancers. La source de rayonnements peut être située à l'extérieur de l'organisme, on parle de radiothérapie externe, ou à l'intérieur de l'organisme, il s'agit de la radiothérapie interne.

II-3-5- Radiothérapie externe

II-3-5-1- Accélérateur de particules

Il s'agit de la technique la plus utilisée. Elle consiste en l'utilisation d'un faisceau de rayons X créé par un accélérateur de particules (Figure 9), qui couvre de manière adéquate la tumeur tout en minimisant la dose aux tissus sains adjacents. Néanmoins, même si toutes les précautions sont effectuées pour cibler le tissu tumoral (système de cache…), le faisceau d'irradiation est trop large pour éviter l'irradiation des tissus sains. Dans ce contexte, la radiothérapie stéréotaxique a été développée avec les systèmes Gamma Knife® et CyberKnife®.

Figure 9: Accélérateur linéaire de particules

II-3-5-2- Radiochirurgie stéréotaxique

Le Gamma Knife® et le CyberKnife® sont des dispositifs permettant une irradiation plus focalisée, cependant, le caractère aléatoire des interactions photons/matière entraîne une irradiation significative de l'ensemble des tissus situés entre l'entrée et la sortie du faisceau.

- *Le système Gamma Knife®*

Le système Gamma knife® est destiné aux cancers cérébraux (primaire et métastatique). Les radiations ionisantes sont délivrées par des faisceaux émis par 201 sources de cobalt-60. Les 201 faisceaux se concentrent en un point précis sur lequel les doses de chaque faisceau vont s'additionner (Figure 10). Ainsi, avec ce système, une masse tumorale située dans une zone normalement inaccessible peut être traitée.

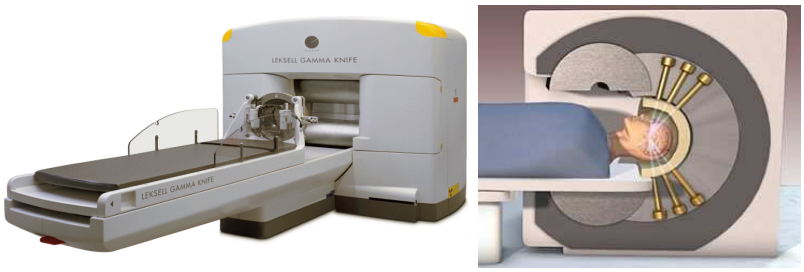

Figure 10: Système Gamma knife®

- *Le système CyberKnife®*

Le système CyberKnife® fait appel à un accélérateur linéaire de particules, monté sur un bras robotisé, pour produire des faisceaux de rayonnement à très haute énergie (Figure 11). Comparativement aux techniques stéréotaxiques standards où un cadre métallique rigide est fixé sur la tête du patient pour l'empêcher de bouger, le système CyberKnife® emploie deux caméras à rayons X installées au plafond pour guider l'imagerie en «temps réel» et corriger instantanément l'ajustement en réponse aux légers mouvements du patient.

Figure 11: Système CyberKnife®

II-3-6- Radiothérapie interne

De nouvelles stratégies permettant de mieux focaliser les radiations ionisantes sur une zone d'intérêt ont été développées avec le concept de radiothérapie interne. L'objectif étant de minimiser la toxicité locale des tissus sains adjacents à la tumeur.

Plusieurs type de radiothérapie interne sont rencontrés: la curiethérapie (ou brachythérapie) et la radiothérapie vectorisée avec des vecteurs tels que les anticorps radiomarqués (Boiardi, Bartolomei et al. 2005), les peptides radiomarqués (Merlo, Hausmann et al. 1999) et les systèmes particulaires (Allard, Hindre et al. 2008).

II-3-6-1- Curithérapie (ou Brachythérapie)

La curiethérapie consiste en l'insertion de dispositifs radioactifs (Iridium-192) (Figure 12A-B) directement au sein de la masse tumorale (Figure 12C). L'irradiation affecte une zone très localisée réduisant ainsi l'exposition des tissus adjacents. Cette technique est utilisée pour le traitement du cancer du col de l'utérus, de la prostate, du sein et de la peau.

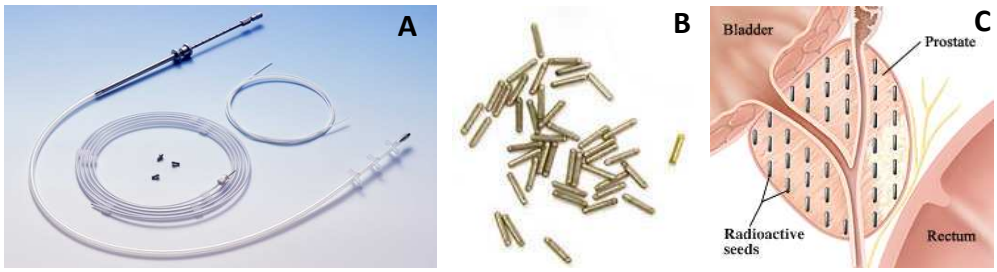

Figure 12: **A**-**B**: Dispositifs radioactifs ; **C**: emplacement des implants radioactifs

Ces objets macroscopiques ne sont pas biodégradables et nécessitent une intervention chirurgicale pour leur mise en place et leur retrait lorsque le traitement est achevé.

II-3-6-2- Radiothérapie vectorisée (ou métabolique)

Avec la connaissance de la biologie des cancers, l'identification de cibles cellulaires a conduit au développement de la radiothérapie vectorisée. Elle utilise des vecteurs radiomarqués, tels que les anticorps monoclonaux et les peptides, possédant un tropisme tumoral pour créer une irradiation localisée (cf. chapitre II). Récemment, l'utilisation de systèmes particulaires a été développée avec l'utilisation de vecteurs micrométriques (microsphères d'Yttrium-90) et nanométriques. L'objectif principal étant d'augmenter l'efficacité, la spécificité et la sécurité biologique du radioélément en améliorant son administration par des vecteurs colloïdaux. Dans ce domaine de compétence, l'unité U646 a développé des nanocapsules lipidiques capables d'encapsuler des radioéléments comme le Rhénium-188.

- Les nanocapsules lipidiques (NCL)

Les nanocapsules lipidiques sont des nanovecteurs constitués d'un cœur lipidique stabilisé par une coque tensioactive (Figure 13). Leur taille varie de 20 à 100 nm selon les proportions d'excipients.

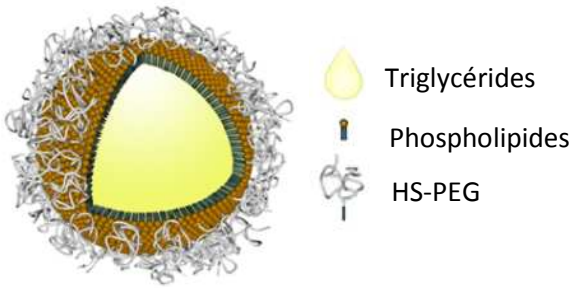

Figure 13 : Représentation schématique des nanocapsules lipidiques.

Elles sont formulées par un processus d'inversion de phase entre une émulsion huile dans eau (H/E) et une émulsion eau dans huile (E/H) suite à une augmentation et une diminution de la température du milieu réactionnel (Heurtault, Saulnier et al. 2002) (Figure 14A). En

fonction des proportions de chaque constituant, une zone d'inversion de phase (ZIP) est déterminée par suivi conductimétrique. Une conductivité très faible (< 10^{-2} µS.cm^{-1}) caractérise une émulsion E/H, tandis qu'une conductivité forte traduit une émulsion H/E (Figure 14B). La stabilisation des NCLs consiste en l'ajout d'eau froide à la température d'inversion de phase, préalablement déterminée lors du suivi conductimétrique. Ainsi, ce refroidissement rapide du système permet l'obtention de NCLs sans recours à un solvant organique et sans consommation importante d'énergie.

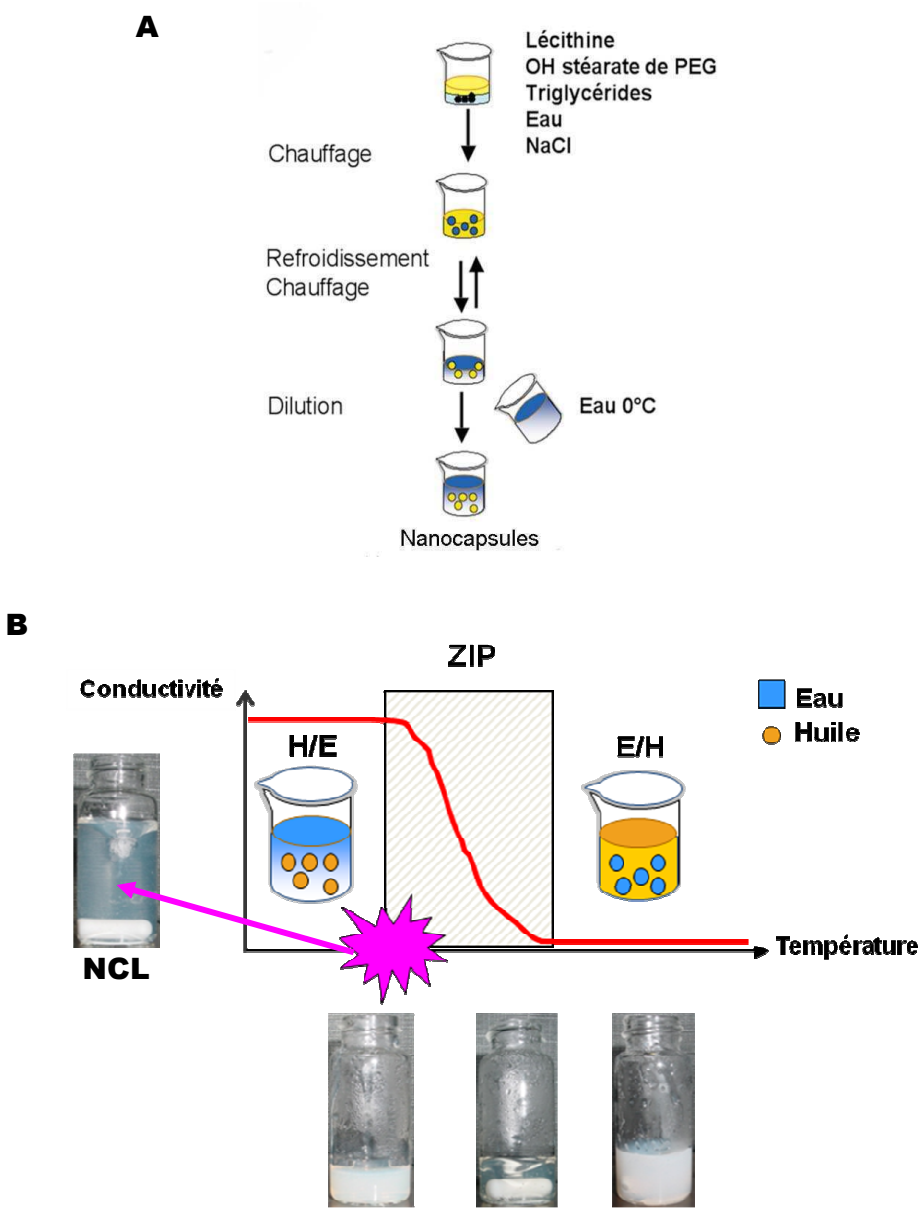

Figure 14: A- Représentation schématique des étapes de la formulation des nanocapsules lipidiques (NCLs). B- Mesure de la conductivité en fonction de la température.

Le cœur lipidique des NCLs impose l'encapsulation de radionucléides lipophiles. En collaboration avec l'unité UMR-CNRS 6226 (Pr. N. Noiret), des progrès dans la chimie du Rhénium-188 ont conduit au développement d'un complexe lipophile de Rhénium-188 pouvant être incorporé dans les NCLs. Le complexe [^{188}Re ($PhCS_3$) $_2$ ($PhCS_2$)] (^{188}Re-SSS)] (Figure 15) est synthétisé en deux étapes, avec un passage par un intermédiaire de degré V chelaté par un ligand labile, le dithiobenzoate de sodium ($PhCS_2H$):

ETAPE 1: ^{188}Re-perrhenate ($^{188}ReO_4^-$) + Sodium Gluconate $\xrightarrow{\text{15 minutes, TA}}$ [^{188}ReO (gluc) $_2^-$]

ETAPE 2: [^{188}ReO (gluc) $_2^-$] + $PhCS_2H$ $\xrightarrow{\text{30 minutes, 100°C}}$ [$^{188}Re(PhCS_3)_2(PhCS_2)$]

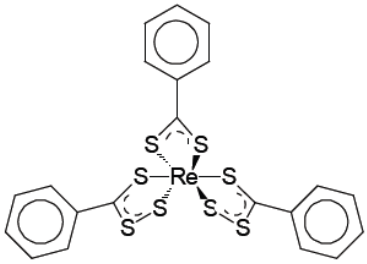

Figure 15 : complexe lipophile de rhénium-188

L'encapsulation de ce complexe lipophile de Rhénium-188 conduit à des objets à haute activité utile pour une stratégie de radiothérapie interne. Son incorporation au sein des NCLs est réalisée selon la méthode d'inversion de phase, décrite précédemment, après avoir ajouté le complexe de Rhénium-188 aux autres composés des NCLs. De plus, leur formulation a également fait l'objet d'une automatisation visant à s'affranchir des problèmes de radioprotection.

Contrairement aux dispositifs médicaux utilisés en curiethérapie, les NCLs chargées en Rhénium-188 sont biodégradables, il n'est donc pas nécessaire de les retirer par une autre intervention chirurgicale comme réalisée en curiethérapie. De plus, leur taille nanométrique

permet une injection stéréotaxique simple (SI) ou par « Convection Enhanced Delivery » (CED), technique d'administration facilitant l'infusion de principes actifs par le phénomène de convection. Ainsi, ce dispositif nanométrique, vecteur de radioélément, pourrait pallier les inconvénients majeurs de la radiothérapie externe et de la radiothérapie interne (implants non-biodégradables...).

III- PATHOLOGIES CANCER : LE CARCINOME HEPATOCELLULAIRE ET LE GLIOME

Le carcinome hépatocellulaire (CHC) et le gliome sont deux pathologies pour lesquelles, les traitements curatifs sont très limités (CHC) voire inexistants (gliome). La toxicité locale et la sensibilité des tissus hépatiques (Dawson and Guha 2008) et cérébraux (Stupp, Mason et al. 2005) limite l'utilisation de la radiothérapie conventionnelle. Dans ce contexte, l'injection locale d'agent anti-cancéreux a toujours représenté une méthode de choix pour le traitement du CHC (injection intra-hépatique) et du gliome (injection stéréotaxique). Plusieurs stratégies de radiothérapie interne locorégionales ont été développées mais celles-ci peuvent être confrontées à certains inconvénients et/ou ne pas présenter de bénéfices significatifs pour les patients (les détails sont abordés au sein des chapitres I et II). Ainsi, une administration locorégionale des nanocapsules lipidiques chargées en Rhénium-188 ($NCL^{188}Re$-SSS) pourrait constituer une potentielle application dans le cas du CHC et du gliome.

L'objectif de ce travail de thèse a été, dans un premier temps, d'évaluer les $NCL^{188}Re$-SSS en tant que vecteur pour la radiothérapie interne du CHC ; et, dans un deuxième temps, d'optimiser et de potentialiser l'efficacité thérapeutique des $NCL^{188}Re$-SSS après injections répétées pour le traitement du gliome.

RÉFÉRENCES

Ahmad, S. (2010). "Platinum-DNA interactions and subsequent cellular processes controlling sensitivity to anticancer platinum complexes." Chem Biodivers **7**(3): 543-66.

Al-Shammaa, H. A., Y. Li, et al. (2008). "Current status and future strategies of cytoreductive surgery plus intraperitoneal hyperthermic chemotherapy for peritoneal carcinomatosis." World J Gastroenterol **14**(8): 1159-66.

Allard, E., F. Hindre, et al. (2008). "188Re-loaded lipid nanocapsules as a promising radiopharmaceutical carrier for internal radiotherapy of malignant gliomas." Eur J Nucl Med Mol Imaging **35**(10): 1838-46.

Apetoh, L., F. Ghiringhelli, et al. (2007). "Toll-like receptor 4-dependent contribution of the immune system to anticancer chemotherapy and radiotherapy." Nat Med **13**(9): 1050-9.

Are, C., L. Colburn, et al. "Disparities in cancer care between the United States of America and India and opportunities for surgeons to lead." J Surg Oncol **102**(1): 100-5.

Boiardi, A., M. Bartolomei, et al. (2005). "Intratumoral delivery of mitoxantrone in association with 90-Y radioimmunotherapy (RIT) in recurrent glioblastoma." J Neurooncol **72**(2): 125-31.

Boyle, P. and B. Levin (2008). "The World Cancer Report " International Agency for Research in Cancer

Caruthers, S. D., S. A. Wickline, et al. (2007). "Nanotechnological applications in medicine." Curr Opin Biotechnol **18**(1): 26-30.

Chakraborty, M., S. I. Abrams, et al. (2004). "External beam radiation of tumors alters phenotype of tumor cells to render them susceptible to vaccine-mediated T-cell killing." Cancer Res **64**(12): 4328-37.

Colotta, F., P. Allavena, et al. (2009). "Cancer-related inflammation, the seventh hallmark of cancer: links to genetic instability." Carcinogenesis **30**(7): 1073-81.

Dawson, L. A. and C. Guha (2008). "Hepatocellular carcinoma: radiation therapy." Cancer J **14**(2): 111-6.

Formenti, S. C. and S. Demaria (2009). "Systemic effects of local radiotherapy." Lancet Oncol **10**(7): 718-26.

Galluzzi, L., M. C. Maiuri, et al. (2007). "Cell death modalities: classification and pathophysiological implications." Cell Death Differ **14**(7): 1237-43.

Heurtault, B., P. Saulnier, et al. (2002). "A novel phase inversion-based process for the preparation of lipid nanocarriers." Pharm Res **19**(6): 875-80.

Kerr, D., H. Bevan, et al. (2002). "Redesigning cancer care." Bmj **324**(7330): 164-6.

Lugade, A. A., E. W. Sorensen, et al. (2008). "Radiation-induced IFN-gamma production within the tumor microenvironment influences antitumor immunity." J Immunol **180**(5): 3132-9.

Merlo, A., O. Hausmann, et al. (1999). "Locoregional regulatory peptide receptor targeting with the diffusible somatostatin analogue 90Y-labeled DOTA0-D-Phe1-Tyr3-octreotide (DOTATOC): a pilot study in human gliomas." Clin Cancer Res **5**(5): 1025-33.

Merlo, L. M., J. W. Pepper, et al. (2006). "Cancer as an evolutionary and ecological process." Nat Rev Cancer **6**(12): 924-35.

Mitchell, P., D. W. Ellison, et al. (2005). "Surgery for malignant gliomas: mechanistic reasoning and slippery statistics." Lancet Neurol **4**(7): 413-22.

Obeid, M., T. Panaretakis, et al. (2007). "Calreticulin exposure is required for the immunogenicity of gamma-irradiation and UVC light-induced apoptosis." Cell Death Differ **14**(10): 1848-50.

Obeid, M., A. Tesniere, et al. (2007). "Calreticulin exposure dictates the immunogenicity of cancer cell death." Nat Med **13**(1): 54-61.

Prise, K. M., G. Schettino, et al. (2005). "New insights on cell death from radiation exposure." Lancet Oncol **6**(7): 520-8.

Rajagopalan, P. T., Z. Zhang, et al. (2002). "Interaction of dihydrofolate reductase with methotrexate: ensemble and single-molecule kinetics." Proc Natl Acad Sci U S A **99**(21): 13481-6.

Steel, G. G., T. J. McMillan, et al. (1989). "The 5Rs of radiobiology." Int J Radiat Biol **56**(6): 1045-8.

Stupp, R., W. P. Mason, et al. (2005). "Radiotherapy plus concomitant and adjuvant temozolomide for glioblastoma." N Engl J Med **352**(10): 987-96.

Tilney, N. L., R. L. Kirkman, et al. (1986). "Vascular access for dialysis and cancer chemotherapy." Adv Surg **19**: 221-70.

Ting, G., C. H. Chang, et al. (2009). "Cancer nanotargeted radiopharmaceuticals for tumor imaging and therapy." Anticancer Res **29**(10): 4107-18.

Zeh, H. J., 3rd and M. T. Lotze (2005). "Addicted to death: invasive cancer and the immune response to unscheduled cell death." J Immunother **28**(1): 1-9.

Chapitre I

Efficacité des nanocapsules Lipidiques chargées en Rhénium-188 dans un modèle de Carcinome Hépatocellulaire

INTRODUCTION

Les cancers primaires du foie sont des pathologies graves qui représentent 5% des cancers avec environ 560 000 nouveaux cas par an. 85-90% sont des carcinomes hépatocellulaires (CHC), ce qui fait de lui le type de cancer primaire du foie le plus fréquent (El-Serag and Rudolph 2007). L'incidence du CHC est très hétérogène (Figure 1). Elle est importante en Asie du Sud et du Sud-Est, en Mongolie, en Afrique et en Amérique du Sud avec 40 cas pour 100 000 personnes. Dans les pays développés, son incidence est beaucoup plus faible avec 5 cas pour 100 000 personnes (Nordenstedt, White et al. 2010). Cependant, le CHC est en constante augmentation avec 15 000 nouveaux cas par an aux Etats-Unis et 4 000 nouveaux cas par an en France. On estime que le taux de mortalité lié au CHC va augmenter chez l'homme et la femme avec des taux prédictifs en 2020 de 150% et de 200% respectivement.

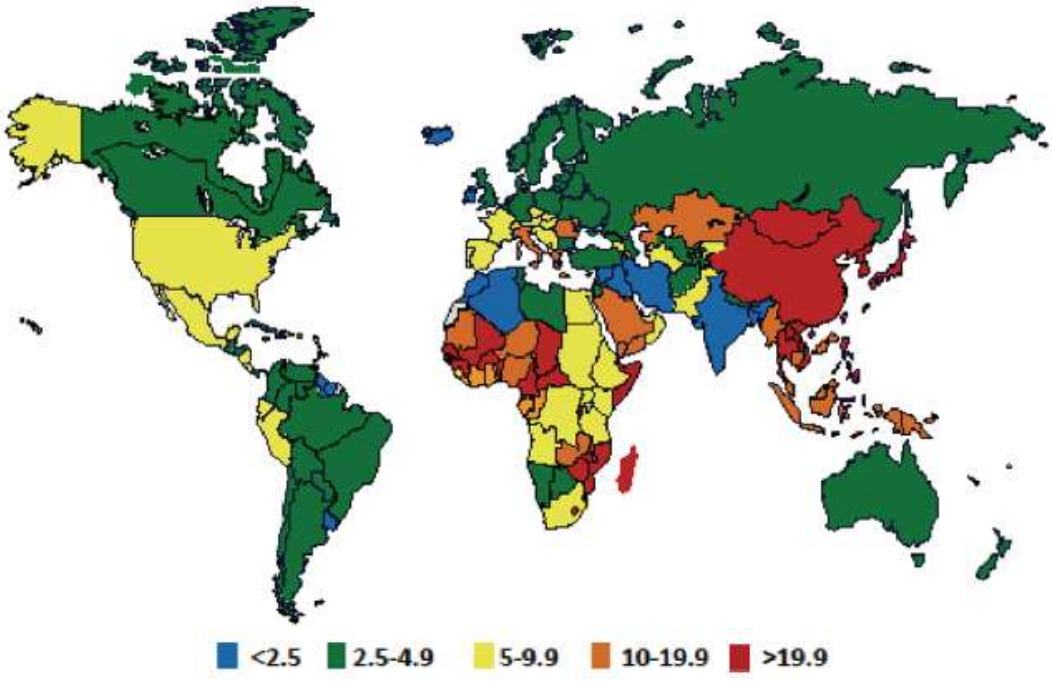

Figure 1 : Taux d'incidence normalisés selon l'âge des cancers primaires du foie dans le monde (d'après Nordenstedt et *al.)*

Les causes du CHC, son mécanisme de carcinogenèse et ses caractéristiques tumorales sont multiples et varient selon la carte géographique de l'incidence du CHC. Ainsi, en Afrique et dans l'Asie du Sud, l'aflatoxine B1 et le virus de l'hépatite B (VHB) jouent un rôle prépondérant dans la carcinogenèse du CHC (Nordenstedt, White et al. 2010). Au Japon, en Egypte et dans le sud de l'Europe, le virus de l'hépatite C (VHC) est la principale cause du CHC tandis que dans le nord et le centre de l'Europe, le VHC et l'alcool sont les causes majeures de cirrhose du foie, facteur aggravant dans le pronostic du CHC (Yang and Roberts 2010). En effet, le CHC se développe dans plus de 95% des cas sur une hépatopathie préexistante, avec 80% des cas affectés par une cirrhose (Nordenstedt, White et al. 2010).

I- TRAITEMENTS DU CARCINOME HEPATOCELLULAIRE

Le pronostic pour cette pathologie est très faible (6 à 20 mois) puisque les possibilités thérapeutiques dépendent de l'extension intra-hépatique et du degré de sévérité de l'hépatopathie sous-jacente. La transplantation hépatique est le seul traitement curatif (Mazzaferro, Regalia et al. 1996). Néanmoins, des récidives, fortement influencées par la taille et le nombre de nodules tumoraux, l'invasion vasculaire et la faible différenciation cancéreuse, sont observées dans 10 à 40% des cas (Jonas, Bechstein et al. 2001; Cillo, Vitale et al. 2007; Ravaioli, Grazi et al. 2008; Mazzaferro, Llovet et al. 2009). De plus, 50% des patients ne deviennent plus éligibles pour une transplantation en raison d'un manque de donneur (Yao, Ferrell et al. 2001; Kassahun, Fangmann et al. 2006). La résection chirurgicale, pour des tumeurs inférieures à 5 cm et monofocales, est également un traitement efficace pour des tumeurs peu évoluées. Cependant, elle n'est applicable qu'à des foies non cirrhotiques, ce qui représente moins de 5% des cas dans les pays occidentaux (Worns and Galle 2010). L'injection intra-tumorale percutanée d'éthanol (éthanolisation) est également un traitement curatif. Elle permet des réponses complètes

dans 70% des cas pour des tumeurs inférieures à 3 cm. L'utilisation de radiofréquences par voie percutanée ou par laparoscopie est une alternative à l'injection éthanol puisque cette méthode permet l'obtention de résultats supérieurs à l'éthanolisation (Kwon 2010; McWilliams, Yamamoto et al. 2010).

Néanmoins, un traitement curatif ne peut être réalisé que dans moins de 25% des cas en raison des contre-indications telles que les cirrhoses avancées, la présence de lésions multifocales, l'invasion de la veine porte ou plus rarement, une dissémination métastatique (Cha, Saif et al. 2010). Dans ce contexte, le patient peut bénéficier d'un traitement palliatif s'il ne présente pas une forme trop avancée du CHC (Bruix and Llovet 2002). Des chimioembolisations ont pu permettre d'obtenir 20 à 40% de réponse objective, mais sans réel gain de survie (Lencioni 2010). Actuellement, seule la chimiothérapie systémique avec le sorafenib (Nexavar®) permet une augmentation de survie de 3 mois, ce qui est encourageant mais reste insuffisant (Llovet, Ricci et al. 2008). Le manque de traitement pour les CHC non opérables a conduit à de nombreuses recherches portant sur la cryothérapie (Xu, Niu et al. 2009) ou l'embolisation (Lencioni 2010). La chimioembolisation artérielle par le lipiodol a donc été développée. Elle consiste en l'injection intra-artérielle d'une émulsion de lipiodol, huile iodée, et de chimiothérapie (Shin 2009). Plusieurs agents chimiothérapeutiques ont été évalués avec l'anthracycline, la doxorubicine, l'épirubicine, la mitomycine, le cisplatine…(Nagamatsu, Hiraki et al. 2010; Sahara, Kawai et al. 2010).

Cette technique est actuellement la plus utilisée en tant que traitement palliatif, cependant, son efficacité est discutée (Hepatocellulaire 1995).

C'est dans ce contexte que la radiothérapie interne a été développée avec le radiomarquage du lipiodol, en raison de son tropisme pour les tumeurs CHC, et l'utilisation de systèmes particulaires vecteurs de radioéléments.

II- RADIOTHERAPIE INTERNE ET CARCINOME HEPATOCELLULAIRE

La radiothérapie interne des tumeurs hépatiques s'effectue principalement par l'artère hépatique. En effet, le foie présente la particularité d'une double vascularisation via l'artère hépatique et la veine porte (Gunven 2008). De plus, l'hépatocarcinome est une tumeur hypervascularisée, principalement irriguée par l'artère hépatique (90%), tandis que le foie sain possède une irrigation par la veine porte à hauteur de 75% (Wallace, Carrasco et al. 1990). Ainsi, l'injection intra-artérielle de radioéléments permet d'obtenir un ratio élevé tumeur/tissu sain et donc de minimiser l'irradiation non sélective du foie sain tout en focalisant les radiations au niveau du tissu tumoral.

- Vecteurs utilisés en radiothérapie interne du carcinome hépatocellulaire

II-1- Le lipiodol

Le vecteur le plus utilisé pour l'administration intra-hépatique est le lipiodol. Il s'agit d'un ester éthylique d'acides gras iodés issus des graines de pavot (Shin 2009). Cette huile iodée est le 1er agent de contraste organique utilisé pour les rayons X en lymphographie. Son tropisme pour les carcinomes hépatocellulaires a permis son utilisation pour la détection du CHC et de ses tumeurs satellites non décelables par les techniques d'imagerie classiques (Ohishi, Uchida et al. 1985; Kan, McCuskey et al. 1994).

Il a été démontré que le lipiodol possédait un tropisme tumoral puisque son temps de rétention intra-tumoral est nettement supérieur à son temps de rétention au niveau du foie sain avec une rétention au sein des tumeurs CHC pouvant atteindre plusieurs mois (Raoul, Bourguet et al. 1988). Plusieurs hypothèses pouvant expliquer ce phénomène ont été émises avec, par exemple, l'accumulation du lipiodol dans les sinusoïdes péritumoraux, sa

fixation sur la membrane des cellules tumorale ou à l'intérieur de celles-ci (Chou, Fang et al. 1995). Cependant, le mécanisme de rétention du lipiodol reste à élucider.

II-1-1- Lipiodol radiomarqué à l'iode-131

L'Iode-131 émet des rayonnements β^- (0,81 MeV) et des rayonnements ɣ (364 keV) et possède une demi-vie de 8,02 jours. Le remplacement de l'iode froid par de l'Iode-131 via une réaction d'échange (Madsen, Park et al. 1988) sur le Lipiodol Ultra-Fluide® (Laboratoires Guerbet, France), permet d'obtenir du lipiodol radiomarqué : ^{131}I-lipiodol (Lipiocis®, CIS-bio international/Schering, France).

La radiothérapie interne par injection intra-artérielle de ^{131}I-lipiodol a été développée pour le traitement du CHC non opérable avec thrombose porte et en tant que traitement adjuvant (après résection tumorale). Il s'agit donc d'un traitement palliatif.

L'utilisation du ^{131}I-lipiodol dans le cas de thrombose portale est possible car ce traitement ne crée pas d'embolisation contrairement à la chimioembolisation. Ainsi, Raoul *et al.* ont démontré un bénéfice significatif de survie comparativement aux traitements classiques avec une survie à 6 mois de 48% pour le groupe traité par l'^{131}I-lipiodol contre 0% pour le groupe contrôle (Raoul, Guyader et al. 1994). Cependant, il s'avère que l'injection de ^{131}I-lipiodol est inadapté pour un traitement répété puisque De Baere et *al*. ont obtenu des toxicités importantes chez des patients atteints d'un CHC avec thrombose portale (de Baere, Taourel et al. 1999).

L'utilisation du lipiodol a également été développée pour le traitement du CHC non opérable sans thombose portale, lorsque la tumeur est trop importante pour son exérèse ou lorsqu'elle est multifocale (Rindani, Hugh et al. 2002). Dans le cas de lésions multifocales, le lipiodol présente l'avantage de se distribuer dans la tumeur principale ainsi que dans les tumeurs satellites. Toutefois, l'^{131}I-lipiodol n'a pas montré d'efficacité supérieure à la chimioembolisation lipiodolée (cisplatine, épirubicine), traitement de référence actuel (Raoul, Guyader et al. 1997). Cependant, le traitement par l'^{131}I-lipiodol est mieux toléré que la chimioembolisation avec une toxicité nettement inférieure.

Bien que l'^{131}I-lipiodol présente des efficacités thérapeutiques intéressantes, certaines limitations peuvent être rencontrées. En effet, l'Iode-131 est un émetteur β^- de faible énergie (0,81 MeV) avec une faible pénétration tissulaire. Les tumeurs volumineuses ne peuvent donc pas être traitées de manière optimale. De plus, sa demi-vie de 8,02 jours et son rayonnement ɣ (364 keV, 81%) conduit à une irradiation indésirable des tissus adjacents. Ainsi, les patients traités par le ^{131}I-lipiodol doivent être placés en chambre d'isolement pendant 6-7 jours.

Devant ces limitations, un certain nombre d'alternatives ont été proposées avec notamment l'utilisation d'autres émetteurs β^- : l'Yttrium-90 et le Rhénium-188.

II-1-2- Lipiodol radiomarqué à l'Yttrium-90 : ^{90}Y-lipiodol

L'Yttrium-90 est un émetteur β^- pur de forte énergie (2,28 MeV) avec une demi-vie de 64 heures. Sa pénétration tissulaire moyenne est de 2,5 mm. Contraitrement à l'Iode-131, il est nécessaire d'utiliser un chélate pour procéder au radiomarquage du lipiodol par l'Yttrium-90. Le radiomarquage du ^{90}Y-lipiodol consiste en un couplage covalent du lipiodol par l'EDTB (N,N,N',N''-tetrakis-(2-benzymidazolylméthyl)-1,2-éthanediamine) (Wang, Lin et al. 1996). Même si l'Yttrium-90 a été suggéré comme étant un isotope de choix pour le marquage du lipiodol, peu d'études ont été réalisées avec l'^{90}Y-lipiodol. La biodistribution de l'^{90}Y-lipiodol chez des rats sains et des rats porteurs d'un CHC est comparable à l'^{131}I-lipiodol avec une distribution préférentielle au niveau du foie. Néanmoins, une fixation osseuse croissante a été reportée (Wang, Lin et al. 1996). L'Yttrium-90 possède une forte affinité pour les os, ce qui explique ces résultats, mais ceci souligne également l'instabilité du complexe, inconvénient majeur dans l'utilisation de l'^{90}Y-lipiodol puisque la moelle osseuse peut potentiellement être touchée par les irradiations.

II-1-3- Lipiodol radiomarqué au Rhénium-188: ^{188}Re-lipiodol

Le Rhénium-188 est un émetteur β^- (2,12 MeV) et ɣ (155 keV), utile pour l'imagerie et la dosimétrie, avec une demi-vie courte de 16,9 heures. Le Rhénium-188 est excrété par les voies rénales et ne se fixe pas dans les os ce qui présente un avantage par rapport à l'Yttrium-90 (Garin, Denizot et al. 2004). Sa demi-vie courte et son émission ɣ, plus faible que l'Iode-131, permet de restreindre les contraintes de radioprotection.

Comme pour l'Yttrium-90, il est nécessaire d'utiliser un chélate pour marquer le lipiodol avec le Rhénium-188. Ainsi le lipiodol peut être marqué avec le Rhénium-188 par l'intermédiaire de l'EDTB (Wang, Lin et al. 1996) ou par la synthèse d'un complexe lipophile de Rhénium-188 de degré V (Mevellec, Lepareur et al. 2002), mis ensuite en solution dans le lipiodol après extraction. Les essais chez l'homme sont encourageants avec des taux de survie à 24 mois jusqu'à 58% (Bernal, Raoul et al. 2007; Kumar, Srivastava et al. 2007). De plus, un essai clinique de phase I concernant l'évaluation du ^{188}Re-SSS-lipiodol est en cours.

II-2- Les microsphères.

L'administration intra-hépatique de microsphères (20-60 µm) est également un traitement palliatif du CHC inopérable. Les microsphères injectées dans l'artère hépatique après cathétérisme de celle-ci, peuvent se répandre dans tout le foie ou se limiter dans certaines zones où elles se logent dans les artérioles. L'apport sanguin à la tumeur peut alors être bloqué. Ces vecteurs micrométriques ont été utilisés pour l'encapsulation de l'Yttrium-90 (Dancey, Shepherd et al. 2000) et du Rhénium-188 (Wunderlich, Pinkert et al. 2005; Hafeli, Pauer et al. 2007). Deux produits commerciaux de microsphères d'Yttrium-90 sont actuellement commercialisés : TheraSphere® et SIR-Sphere® et conduisent à des réductions tumorales jusqu'à 50% (Lau, Ho et al. 1998; Salem, Lewandowski et al. 2005; Kulik, Atassi et al. 2006). La dose moyenne utilisée est de 120 Gy puisqu'il a été démontré par Lau et *al*. une meilleure efficacité des ^{90}Y-microsphères à des doses supérieures à 120

Gy (Lau, Leung et al. 1994). Ainsi, Hilgard *et al.* ont observé des réponses complètes dans 3% des patients, des réponses partielles dans 37%, stabilisation de la maladie de 53%, et la progression primaires dans 6% des patients atteints d'un carcinome hépatocellulaire non-opérable (Hilgard, Hamami et al. 2010).

Les microsphères de Rhénium-188 possèdent une biodistribution comparables à celle des microsphères d'Yttrium-90 avec peu de modification des fonctions hépatiques répertoriée dans les essais cliniques.

La difficulté dans l'injection intra-artérielle de microsphères réside dans la cathétérisation de l'artère hépatique ainsi que de l'existence de shunts artério-veineux pouvant conduire à une irradiation pulmonaire. Ceux-ci sont donc évalués par une scintigraphie abdominale après injection de macroagrégats d'albumine marqués au technétium-99m (^{99m}Tc-MAA) (Lau, Leung et al. 1994; Ahmadzadehfar, Sabet et al. 2010; Knesaurek, Machac et al. 2010).

II-3- Les nanocapsules lipidiques chargées en rhénium-188 : NCL^{188}Re-SSS

Composées d'un cœur lipidique entouré d'une coque tensio-active, les nanocapsules lipidiques (NCL) permettent l'encapsulation de radionucléides tels que le rhénium-188 (Ballot, Noiret et al. 2006).

Tout comme le radiomarquage du ^{188}Re-lipiodol, il est nécessaire de synthétiser un complexe lipophile de rhénium-188 de degré V qui sera ensuite solubilisé dans le labrafac, huile entrant dans la composition des NCLs. La taille nanométrique des NCL^{188}Re-SSS (50 nm) peut se révéler très avantageuse pour le traitement du CHC car les NCL^{188}Re-SSS pourraient pénétrer plus profondément dans le système vasculaire tumoral comparativement aux microsphères d'Yttrium-90, seuls systèmes particulaires vecteurs de radioéléments mis sur le marché.

L’objectif de ce chapitre est donc de mettre en évidence l’intérêt d’une radiothérapie interne nanovectorisée dans un modèle de carcinome hépatocellulaire chez le rat.

RÉFÉRENCES

Ahmadzadehfar, H., A. Sabet, et al. (2010). "The significance of 99mTc-MAA SPECT/CT liver perfusion imaging in treatment planning for 90Y-microsphere selective internal radiation treatment." J Nucl Med **51**(8): 1206-12.

Ballot, S., N. Noiret, et al. (2006). "99mTc/188Re-labelled lipid nanocapsules as promising radiotracers for imaging and therapy: formulation and biodistribution." Eur J Nucl Med Mol Imaging **33**(5): 602-7.

Bernal, P., J. L. Raoul, et al. (2007). "Intra-arterial rhenium-188 lipiodol in the treatment of inoperable hepatocellular carcinoma: results of an IAEA-sponsored multination study." Int J Radiat Oncol Biol Phys **69**(5): 1448-55.

Bruix, J. and J. M. Llovet (2002). "Prognostic prediction and treatment strategy in hepatocellular carcinoma." Hepatology **35**(3): 519-24.

Cha, C. H., M. W. Saif, et al. (2010). "Hepatocellular carcinoma: current management." Curr Probl Surg **47**(1): 10-67.

Chou, F. I., K. C. Fang, et al. (1995). "Lipiodol uptake and retention by human hepatoma cells." Nucl Med Biol **22**(3): 379-86.

Cillo, U., A. Vitale, et al. (2007). "Intention-to-treat analysis of liver transplantation in selected, aggressively treated HCC patients exceeding the Milan criteria." Am J Transplant **7**(4): 972-81.

Dancey, J. E., F. A. Shepherd, et al. (2000). "Treatment of nonresectable hepatocellular carcinoma with intrahepatic 90Y-microspheres." J Nucl Med **41**(10): 1673-81.

de Baere, T., P. Taourel, et al. (1999). "Hepatic intraarterial 131I iodized oil for treatment of hepatocellular carcinoma in patients with impeded portal venous flow." Radiology **212**(3): 665-8.

El-Serag, H. B. and K. L. Rudolph (2007). "Hepatocellular carcinoma: epidemiology and molecular carcinogenesis." Gastroenterology **132**(7): 2557-76.

Garin, E., B. Denizot, et al. (2004). "188Re-SSS lipiodol: radiolabelling and biodistribution following injection into the hepatic artery of rats bearing hepatoma." Nucl Med Commun **25**(10): 1007-13.

Gunven, P. (2008). "Liver embolizations in oncology: a review. Part I. Arterial (chemo)embolizations." Med Oncol **25**(1): 1-11.

Hafeli, U. O., G. J. Pauer, et al. (2007). "Fibrin glue system for adjuvant brachytherapy of brain tumors with 188Re and 186Re-labeled microspheres." Eur J Pharm Biopharm **65**(3): 282-8.

Hepatocellulaire, G. E. T. C. (1995). "A comparison of lipiodol chemoembolization and conservative treatment for unresectable hepatocellular carcinoma. Groupe d'Etude et de Traitement du Carcinome Hepatocellulaire." N Engl J Med **332**(19): 1256-61.

Hilgard, P., M. Hamami, et al. (2010). "Radioembolization with yttrium-90 glass microspheres in hepatocellular carcinoma: European experience on safety and long-term survival." Hepatology **52**(5): 1741-9.

Jonas, S., W. O. Bechstein, et al. (2001). "Vascular invasion and histopathologic grading determine outcome after liver transplantation for hepatocellular carcinoma in cirrhosis." Hepatology **33**(5): 1080-6.

Kan, Z., P. A. McCuskey, et al. (1994). "Role of Kupffer cells in iodized oil embolization." Invest Radiol **29**(11): 990-3.

Kassahun, W. T., J. Fangmann, et al. (2006). "Liver resection and transplantation in the management of hepatocellular carcinoma: a review." Exp Clin Transplant **4**(2): 549-58.

Knesaurek, K., J. Machac, et al. (2010). "Quantitative comparison of yttrium-90 (90Y)-microspheres and technetium-99m (99mTc)-macroaggregated albumin SPECT images for planning 90Y therapy of liver cancer." Technol Cancer Res Treat **9**(3): 253-62.

Kulik, L. M., B. Atassi, et al. (2006). "Yttrium-90 microspheres (TheraSphere) treatment of unresectable hepatocellular carcinoma: downstaging to resection, RFA and bridge to transplantation." J Surg Oncol **94**(7): 572-86.

Kumar, A., D. N. Srivastava, et al. (2007). "Inoperable hepatocellular carcinoma: transarterial 188Re HDD-labeled iodized oil for treatment--prospective multicenter clinical trial." Radiology **243**(2): 509-19.

Kwon, J. H. (2010). "Is Percutaneous Ethanol Injection Therapy Still Effective for Hepatocellular Carcinoma in the Era of Radiofrequency Ablation?" Gut Liver **4**(Suppl. 1): S105-S112.

Lau, W. Y., S. Ho, et al. (1998). "Selective internal radiation therapy for nonresectable hepatocellular carcinoma with intraarterial infusion of 90yttrium microspheres." Int J Radiat Oncol Biol Phys **40**(3): 583-92.

Lau, W. Y., T. W. Leung, et al. (1994). "Diagnostic pharmaco-scintigraphy with hepatic intra-arterial technetium-99m macroaggregated albumin in the determination of tumour to non-tumour uptake ratio in hepatocellular carcinoma." Br J Radiol **67**(794): 136-9.

Lau, W. Y., W. T. Leung, et al. (1994). "Treatment of inoperable hepatocellular carcinoma with intrahepatic arterial yttrium-90 microspheres: a phase I and II study." Br J Cancer **70**(5): 994-9.

Lencioni, R. (2010). "Loco-regional treatment of hepatocellular carcinoma." Hepatology **52**(2): 762-73.

Llovet, J. M., S. Ricci, et al. (2008). "Sorafenib in advanced hepatocellular carcinoma." N Engl J Med **359**(4): 378-90.

Madsen, M. T., C. H. Park, et al. (1988). "Dosimetry of iodine-131 ethiodol in the treatment of hepatoma." J Nucl Med **29**(6): 1038-44.

Mazzaferro, V., J. M. Llovet, et al. (2009). "Predicting survival after liver transplantation in patients with hepatocellular carcinoma beyond the Milan criteria: a retrospective, exploratory analysis." Lancet Oncol **10**(1): 35-43.

Mazzaferro, V., E. Regalia, et al. (1996). "Liver transplantation for the treatment of small hepatocellular carcinomas in patients with cirrhosis." N Engl J Med **334**(11): 693-9.

McWilliams, J. P., S. Yamamoto, et al. (2010). "Percutaneous ablation of hepatocellular carcinoma: current status." J Vasc Interv Radiol **21**(8 Suppl): S204-13.

Mevellec, F., N. Lepareur, et al. (2002). "Chelated hydrazido(3-)rhenium(V) complexes: on the way to the nitrido-M(V) core (M = Tc, Re)." Inorg Chem **41**(6): 1591-7.

Nagamatsu, H., M. Hiraki, et al. (2010). "Intra-arterial therapy with cisplatin suspension in lipiodol and 5-fluorouracil for hepatocellular carcinoma with portal vein tumour thrombosis." Aliment Pharmacol Ther **32**(4): 543-50.

Nordenstedt, H., D. L. White, et al. (2010). "The changing pattern of epidemiology in hepatocellular carcinoma." Dig Liver Dis **42 Suppl 3**: S206-14.

Ohishi, H., H. Uchida, et al. (1985). "Hepatocellular carcinoma detected by iodized oil. Use of anticancer agents." Radiology **154**(1): 25-9.

Raoul, J. L., P. Bourguet, et al. (1988). "Hepatic artery injection of I-131-labeled lipiodol. Part I. Biodistribution study results in patients with hepatocellular carcinoma and liver metastases." Radiology **168**(2): 541-5.

Raoul, J. L., D. Guyader, et al. (1994). "Randomized controlled trial for hepatocellular carcinoma with portal vein thrombosis: intra-arterial iodine-131-iodized oil versus medical support." J Nucl Med **35**(11): 1782-7.

Raoul, J. L., D. Guyader, et al. (1997). "Prospective randomized trial of chemoembolization versus intra-arterial injection of 131I-labeled-iodized oil in the treatment of hepatocellular carcinoma." Hepatology **26**(5): 1156-61.

Ravaioli, M., G. L. Grazi, et al. (2008). "Liver transplantation for hepatocellular carcinoma: results of down-staging in patients initially outside the Milan selection criteria." Am J Transplant **8**(12): 2547-57.

Rindani, R. B., T. J. Hugh, et al. (2002). "131I lipiodol therapy for unresectable hepatocellular carcinoma." ANZ J Surg **72**(3): 210-4.

Sahara, S., N. Kawai, et al. (2010). "Prospective comparison of transcatheter arterial chemoembolization with Lipiodol-epirubicin and Lipiodol-cisplatin for treatment of recurrent hepatocellular carcinoma." Jpn J Radiol **28**(5): 362-8.

Salem, R., R. J. Lewandowski, et al. (2005). "Treatment of unresectable hepatocellular carcinoma with use of 90Y microspheres (TheraSphere): safety, tumor response, and survival." J Vasc Interv Radiol **16**(12): 1627-39.

Shin, S. W. (2009). "The current practice of transarterial chemoembolization for the treatment of hepatocellular carcinoma." Korean J Radiol **10**(5): 425-34.

Wallace, S., C. H. Carrasco, et al. (1990). "Hepatic artery infusion and chemoembolization in the management of liver metastases." Cardiovasc Intervent Radiol **13**(3): 153-60.

Wang, S. J., W. Y. Lin, et al. (1996). "Radiolabelling of Lipiodol with generator-produced 188Re for hepatic tumor therapy." Appl Radiat Isot **47**(3): 267-71.

Wang, S. J., W. Y. Lin, et al. (1996). "Hepatic artery injection of Yttrium-90-lipiodol: biodistribution in rats with hepatoma." J Nucl Med **37**(2): 332-5.

Worns, M. A. and P. R. Galle (2010). "Future perspectives in hepatocellular carcinoma." Dig Liver Dis **42 Suppl 3**: S302-9.

Wunderlich, G., J. Pinkert, et al. (2005). "Labeling and biodistribution of different particle materials for radioembolization therapy with 188Re." Appl Radiat Isot **62**(5): 745-50.

Xu, K. C., L. Z. Niu, et al. (2009). "Sequential use of transarterial chemoembolization and percutaneous cryosurgery for hepatocellular carcinoma." World J Gastroenterol **15**(29): 3664-9.

Yang, J. D. and L. R. Roberts (2010). "Hepatocellular carcinoma: A global view." Nat Rev Gastroenterol Hepatol **7**(8): 448-58.

Yao, F. Y., L. Ferrell, et al. (2001). "Liver transplantation for hepatocellular carcinoma: expansion of the tumor size limits does not adversely impact survival." Hepatology **33**(6): 1394-403.

Publication n°1

Nanocapsules lipidiques chargées en rhénium-188 et hépatocarcinome.

“Lipid nanocapsules loaded with rhenium-188 reduce tumor progression in a rat hepatocellular model.”

Publication acceptée dans « PloS One »

TITLE PAGE

LIPID NANOCAPSULES LOADED WITH RHENIUM-188 REDUCE TUMOR PROGRESSION IN A RAT HEPATOCELLULAR CARCINOMA MODEL

Authors & institutions: Claire Vanpouille-Box[1], Franck Lacoeuille[1,2], Jérôme Roux[3], Christophe Aubé[6,7], Emmanuel Garcion[1], Nicolas Lepareur[4,5], , Frédéric Oberti[7], Francis Bouchet[2], Nicolas Noiret[8,5], Etienne Garin[4,5], Jean-Pierre Benoît[1], Olivier Couturier[1,2], and François Hindré[1*]

[1]LUNAM Université ; Université d'Angers ; INSERM U646 ; 4 rue larrey, F-49000 Angers, France

[2] Nuclear Medicine Department, Angers CHU, F-49100 Angers, France

[3] LUNAM Université ; Université d'Angers ; SCAHU ; UFR Medicine ; F-49100 Angers, France

[4]Medical Imaging Department, CRLCC Eugene Marquis, F-35042 Rennes, France

[5]European University of Brittany, F-35000 Rennes, France

[6] Radiology Department, Angers CHU, F-49033 Angers, France

[7] LUNAM Université ; Université d'Angers ; Laboratory HIFI, UPRES EA3589, F-49100 Angers, France

[8]UMR CNRS 6226, ENSCR, F-35700 Rennes, France

***Corresponding author:** François Hindré, LUNAM Université ; Université d'Angers ; INSERM U646 ; 4 rue larrey, F-49000 Angers, France ; Tel: +33 244 68 85 29; Fax: +33 244 68 85 46; Email: francois.hindre@univ-angers.fr

Number of figures and tables: 8

List of abbreviation: lipid nanocapsules loaded with Rhenium-188 (LNC^{188}Re-SSS), hepatocellular carcinoma (HCC), radiation-induced liver disease (RILD), selective internal

radiotherapy (SIRT), ^{188}Re-perrhenate ($^{188}ReO_4^-$), lipid nanocapsules (LNC), radiochemical purity (RCP), diethylnitrosamine (DENA), alanine aminotransferase (ALT), aspartate aminotransferase, vascular endothelium growth factor (VEGF), magnetic resonance imaging (MRI), fast spin echo (FSE), increase in median survival time (IMST %), enhancement permeability retention (EPR), injected activity per gramm (%IA/g).

Keywords: hepatocellular carcinoma; lipid nanocapsules; Rhenium-188; internal radiotherapy

ABSTRACT (185 WORDS)

Background: Due to their nanometric scale (50nm) along with their biomimetic properties, lipid nanocapsules loaded with Rhenium-188 (LNC^{188}Re-SSS) constitute a promising radiopharmaceutical carrier for hepatocellular carcinoma treatment as its size may improve tumor penetration in comparison with microspheres devices. This study was conducted to confirm the feasibility and to assess the efficacy of internal radiation with LNC^{188}Re-SSS in a chemically-induced hepatocellular carcinoma rat model.

Methodology/Principal Findings: Animals were treated with an injection of LNC^{188}Re-SSS (80MBq or 120 MBq). The treated animals (80 MBq, n=12; 120 MBq, n=11) were compared with sham (n=12), blank LNC (n=7) and ^{188}Re-perrhenate (n=4) animals. The evaluation criteria included rat survival, tumor volume assessment, and vascular endothelial growth factor quantification.

Following treatment with LNC^{188}Re-SSS (80 MBq) therapeutic efficiency was demonstrated by an increase in the median survival from 54 to 107% compared with control groups with up to 7 long-term survivors in the LNC^{188}Re-SSS group. Decreased vascular endothelial growth factor expression in the treated rats could indicate alterations in the angiogenesis process.

Conclusions/Significance: Overall, these results demonstrate that internal radiation with LNC^{188}Re-SSS is a promising new strategy for hepatocellular carcinoma treatment.

INTRODUCTION

Hepatocellular carcinoma (HCC) is the fifth most common malignant tumor worldwide. The prognosis of HCC remains extremely poor, and a curative treatment (liver transplantation, surgical resection, and radiofrequency ablation) can only be carried out in approximately 25% to 30% of cases [1]. The use of conventional external beam radiation therapy in HCC treatment has been limited by the low radiation tolerance of the cirrhotic liver that often resulted in radiation-induced liver disease (RILD) [2]. Selective internal radiotherapy (SIRT) aims to deliver high tumoricidal doses while limiting the development of RILD. This locoregional strategy is defined as the infusion of radioactive carrier including microsphere of Yttrium-90, Iodine-131 iodized oil or similar agent into the hepatic artery [3]. Currently, ^{90}Y-microspheres are the most SIRT technique used. Given the hypervascularity of HCC, ^{90}Y-microspheres injected into the hepatic artery will spread throughout the liver or confined to certain areas, where they can stop blood supply of the tumor by the embolisation process.

Progress in pharmaceutical research field has been exploited in the design of tumor-targeting nanoscale vectors able to deliver radionuclides. Among them, lipid nanocapsules (LNC), a nanovector with biomimetic properties [4], appear to be a useful therapeutic option for HCC treatment. Composed of a liquid lipidic core surrounded by a tensioactive shell, LNC lead to the encapsulation of a lipophilic complex of Rhenium-188 (γ = 155 keV; β^- =2 MeV; $T_{1/2}$ = 16.9h). The formulation, based on a fully automated phase-inversion process, is simple and results in nanoparticles solution presenting a mean diameter between 20 and 100 nm, depending on the quantity of excipients. The nanometric scale of LNC^{188}Re-SSS (50nm) could be highly advantageous, as LNCs may penetrate more deeply inside the tumor blood vessels, the mean diameter of microsphere devices are varying between 20 to 500 µm. Moreover,

enhanced permeability retention effect (EPR), the main strategy for the delivery of nanoparticulate systems, may improve therapeutic efficiency. Indeed, it has been shown that small particles can passively cross the sinusoidal endothelium of the liver through fenestrations with a size of approximately a few hundred nanometers [5, 6].

We report a study of LNC^{188}Re-SSS as a new radiopharmaceutical carrier for internal radiotherapy of rats presenting hepatocellular carcinoma induced by diethylnitrosamine. No early mortality and no intolerance following LNC^{188}Re-SSS intra-arterial injection were observed. Our results provide evidences of therapeutic efficiency of LNC^{188}Re-SSS with a reduction in tumor progression which could be combinated with an altered angiogenesis process as indicated by VEGF quantifications in plasmatic samples in a rat HCC model.

METHODS AND PROCEDURES

Ethics Statement

This study was carried out in strict accordance with the French Minister of Agriculture and the European Communities Council Directive of 24 November 1986 (86/609/EEC). The protocol was approved by the Committee on the Ethics of Animal Experiments of the "Pays de la Loire" (Permit Number: CEEA.2009.6). All surgery was performed under ketamine/xylazine anesthesia, and all efforts were made to minimize suffering.

Materials

Lipoïd® S75-3 (soybean lecithin with 69% of phosphatidylcholine) and Solutol® HS15 (a mixture of polyethylene glycol 660 and polyethylene glycol 660 hydroxystearate) were kindly donated by Lipoïd Gmbh. (Ludwigshafen, Germany) and BASF (Ludwigshafen, Germany), respectively. NaCl and dichloromethane were provided by Sigma (St-Quentin, Fallavier, France). Deionized water was obtained from a Milli-Q plus system (Millipore, Paris, France). Lipophilic Labrafac® CC (caprylic-capric acid triglycerides) was provided by Gattefosse S.A. (Saint-Priest, France).

Preparation of the ^{188}Re-SSS complex

^{188}Re as carrier-free Na [$^{188}ReO_4^-$] in a physiological solution was obtained by saline elution of a ^{188}W/^{188}Re generator (*Institut des Radioéléments* [Institute for Radioelements], Fleurus, Belgium) and then concentrated. The ^{188}Re-SSS complex was prepared according to the method developed by Lepareur *et al*.[7]. In brief, the ^{188}Re-SSS complex was obtained by the reaction of the ligand sodium dithiobenzoate (organic synthesis platform, Rennes, France) with a freeze-dried formulation kit containing 30mg sodium gluconate, 30mg ascorbic acid,

40mg potassium oxalate, and 4mg $SnCl_2.2H_2O$ reconstituted in 0.5mL of physiological serum. 1 110MBq of ^{188}Re-perrhenate ($^{188}ReO_4^-$, in 0.5mL) was added, and the solution was mixed for 15 minutes at room temperature. Then, 20mg of sodium dithiobenzoate (in 0.5mL; pH=7) was added before being heated at 100°C for 30 minutes, which allowed for the formation of the ^{188}Re-SSS complex. Due to its precipitation in aqueous media, the ^{188}Re-SSS complex was extracted with dichloromethane (1mL) and washed three times with 1mL of deionized water. The radiochemical purity (RCP) of the complex was checked by thin-layer chromatography as the ratio of migrated radioactivity to total radioactivity. Thin-layer chromatography was carried out using silica gel 60-F_{254} alumina plates (Merck) and a solution of petroleum ether/dichloromethane (6/4; v/v) as an eluant. Radioactivity was assessed with a phosphor-imaging machine (Packard, Cyclone storage phosphor system).

Nanocapsule formulation and characterization

The overall study was performed on 50nm-diameter LNCs which were prepared according to a phase-inversion process described by Heurtault *et al.* [4]. In brief, 25mg Lipoïd ® S75-3, 282mg Solutol® HS15, 342.7mg Labrafac®, 29.7mg NaCl, and 987.5mg deionized water were mixed by magnetic stirring. The ^{188}Re-SSS complex extracted with dichloromethane (1mL) was then added to the other components of the emulsion. The organic solvent was removed by being heated at 60°C for 15 minutes. Three cycles of progressive heating and cooling between 85°C and 60°C were then carried out and followed by an irreversible shock, induced by dilution with 4.16mL of 0°C deionized water, which was added to the mixture at 70°C leading to 50nm-lipid nanocapsules solution. Afterwards, slow magnetic stirring was applied to the suspension for 5 minutes. LNC^{188}Re-SSS were dialyzed during 2 hours with deionized water at room temperature by magnetic stirring. The mean diameter and polydispersity

index were then determined using a Malvern Zetasizer® Nano Serie DTS 1060 (Malvern Instruments S.A., Worcestershire, UK). The encapsulation yield was assessed with a gamma counter (Packard Auto-Gamma 5,000 series) according to the equation below.

Encapsulation yield (%):

$$= \frac{\text{LNC}^{188}\text{Re-SSS solution activity after dialysis}}{\text{LNC}^{188}\text{Re-SSS solution activity before dialysis}} \text{ X } 100$$

HCC model and treatment

49 Male Wistar rats weighting 150-180g were obtained from the animal house of the Angers University Hospital. The animals were kept in polycarbonate cages in a room with controlled temperature (20-22°C), humidity (50-70%), and light (12-hour light/dark cycles). Room air was renewed at the rate of 10vol/hour. Tap water and food were provided *ad libitum*.

All experiments were performed on 6-week-old male Wistar rats. Hepatic carcinogenesis was induced chemically by adding diethylnitrosamine (DENA) to drinking water (100mg/L) for 8 weeks. Each animal underwent hepatic artery catheterization on Day 10 (D10) after the end of tumor induction. Two LNC^{188}Re-SSS groups were performed with one intra-hepatic artery injection of 80MBq and 120 MBq of LNC^{188}Re-SSS (LNC^{188}Re-SSS – 80MBq, n=12; LNC^{188}Re-SSS – 120 MBq, n=11) as described in the "Hepatic artery catheterization" section below. Three control groups, the $^{188}ReO_4^-$ group (80 MBq, n=4), the sham group (n=12) and the blank LNC group (n=10) were assessed with the same procedure. We set the therapeutic activity at 80MBq and 120MBq, corresponding to an absorbed dose to the liver of 40Gy, which proved to be effective in the treatment of human HCC [8], and of 65Gy in order to appreciate the effect of a higher dose after LNC^{188}Re-SSS internal radiation.

Hepatic artery catheterization

Hepatic artery catheterization was carried out according to the Garin *et al.* method [9]. The experiment was continued under a binocular magnifying glass. The first duodenal loop was pulled down to expose the gastroduodenal artery which was, after identification of the celiac and hepatic arteries, carefully dissected. A final distal ligature of the gastroduodenal artery was performed, and the celiac artery was clamped to temporarily stop arterial flow. After perforation using a 30G needle, a 32G catheter (CS-32, Bioseb, Vitrolles, France) was placed inside the gastroduodenal artery, and a volume of 400µL of LNC^{188}Re-SSS, $^{188}ReO_4^-$, or blank LNC solution was then injected. After washing the syringe with saline solution, the upstream end of the gastroduodenal artery was tied off and arterial flow was restored. Concerning the sham group, the same procedure was performed except the injection which was not realized and a final ligature of the hepatic artery. This control group led to an appreciation of the collateral revascularization which could occur after injection.

Transaminase assessment

Blood samples were collected from the tail vein using heparinized tubes in each group at D12, D18, D24, D25, D30, D45, D55, D65, D80, D90, D105, D130, and D152 after the end of tumor induction in order to assess hepatotoxicity after treatment injection. After centrifugation at 1 000g for 20 minutes, plasma alanine aminotransferase (ALT) and aspartate aminotransferase [10] were assessed using BioMérieux kits (Marcy l'étoile, France) according to the manufacturer's instructions.

Dosage of plasmatic vascular endothelium growth factor (VEGF)

Blood samples were collected from the tail vein using heparinized tubes in each group at D12, D20, D40, D55, D65, D80, and D105 after the end of tumor induction. After centrifugation at 1 000g for 20 minutes, the rat VEGF ELISA test (R&D Systems Europe, Lille, France) was immediately performed according to the manufacturer's instructions.

Magnetic resonance imaging

Six animals from the LNC^{188}Re-SSS – 80 MBq and four animals from the ^{188}Re-perrhenate groups were explored by MRI in order to acquire images of the treatment-induced morphological changes at day 100 after the end of tumor induction. MRI was performed with a 1.5T Signa Excite HD device (General Electric Medical System Milwaukee, Ilinois). Rapid T2-weighted images were obtained using a fast spin echo (FSE) sequence with the following parameters: TR=2500 s, TE=102 s, matrix 320x320, twelve slices, thickness 3mm, gap 0.5mm, FOV=15cm, Nex=4, acquisition time 6'30''). The following day, the animals were sacrificed for macroscopic and histopathological analyses.

Whole-body planar γ-scintigraphy

Three animals from the LNC^{188}Re-SSS – 80 MBq and three animals from the ^{188}Re-perrhenate groups were explored by whole-body planar γ-scintigraphy. Static 15-minutes scintigraphy acquisitions were obtained using a gamma camera (SOPHA DSX γ camera, 155 keV±15%, 128² matrix, HRLE collimator). ^{188}Re-perrhenate and LNC^{188}Re-SSS solutions (80MBq) were injected into the hepatic artery, and images were taken at 1.5 h, 3 h, and 24 h. A scan projection radiograph (Scout View) was acquired on a GE lightspeed system (General Electric

Medical System Milwaukee, Ilinois) and fused with planar scintigraphy of the same animal for the localization of $^{188}ReO_4^-$ and LNC^{188}Re-SSS.

Tissue distribution study

A tissue distribution study was carried out on an extra group of 24 male Wistar rats with chemically-induced HCC. They were divided into two groups: one injected with a $^{188}ReO_4^-$ solution following hepatic artery catheterization (n=12), and the other with LNC^{188}Re-SSS – 80 MBq (n=12). In both groups, the animals were sacrificed at 1.5 h (n=4), 3 h (n=4), and 24 h (n=4) post-injection. The organs were removed, washed, and weighed (blood, liver, spleen, kidneys, heart, lung, stomach, small intestine, large intestine, bladder, bone, muscle, brain, tail, and carcass). The content activity of each organ was determined using a gamma counter (Packard Auto-Gamma 5,000 series).

Statistical analysis

The Kaplan-Meier method was carried out to plot animal survival. Statistical significance was assessed using the log-rank test (Mantel-Cox Test). StatView software was used for this purpose, and the tests were considered significant at p values less than 0.05. The different groups were compared in terms of survival time, increase in median survival time (IMST %), maximal survival time, and long-term survivors (rats were considered to be long-term survivors if they survived twice the median survival time of control groups [11]).

RESULTS

Encapsulation of the ^{188}Re-SSS complex in LNCs

The ^{188}Re-SSS complex presents a good purity as satisfactory RCP of more than 98% was obtained. Physico-chemical characteristics of the LNC are provided in Table 1. Blank LNCs were measured at 50.7 ± 5.7 nm. ^{188}Re-SSS entrapping did not change the characteristics of nanoparticles with a size of 49.7 ± 2.7 nm. Blank LNC and LNC^{188}Re-SSS solutions were monodispersed with a polydispersity index of 0.05 (Table 1). The encapsulation yield was approximately 97.9%, 97.7% and 97.5% after 2h, 24h and 48h of dialysis, against phosphate buffer solution (pH=7.4), respectively; therefore, ^{188}Re-SSS release of 2.5% observed at 48h can be neglected.

Table 1: *Physico-chemical characteristics of blank and ^{188}Re-SSS LNCs*

	Mean particle size	Polydispersity index	Encapsulation yield (%)
Blank LNC	50.7 ± 5.7	0.05 ± 0.02	-
LNC^{188}Re-SSS	49.7 ± 2.7	0.05 ± 0.03	97.9 ± 0.2

Biodistribution study

Planar scintigraphy led to the monitoring of the radioactivity distribution of LNC^{188}Re-SSS and $^{188}ReO_4^-$ following hepatic artery injection (Figure 1a). Results highlighted a liver uptake following LNC^{188}Re-SSS injections and a stomach uptake after $^{188}ReO_4^-$ injection up to 24 hours. LNC^{188}Re-SSS were essentially confined to the liver, with an increased uptake up to 24h (1.5h post-injection: 1.67 ± 0.39 %IA/g; 3h post-injection: 2.93 ± 0.75 %IA/g; 24h post-injection: 4.51 ± 0.72 %IA/g) in correlation with an increased of the blood clearance (1.5h

post-injection: 0.79 ± 0.16 %IA/g; 3h post-injection: 0.21 ± 0.12 %IA/g; 24h post-injection: 0.06 ± 0.01 %IA/g). Contrary, the tissue distribution study of ^{188}Re-perrhenate solution revealed a rapid stomach uptake (1.5h post-injection: 3.21 ± 1.47 %IA/g; 3h post-injection: 4.58 ± 0.85 %IA/g; 24h post-injection: 1.28 ± 0.51 %IA/g).

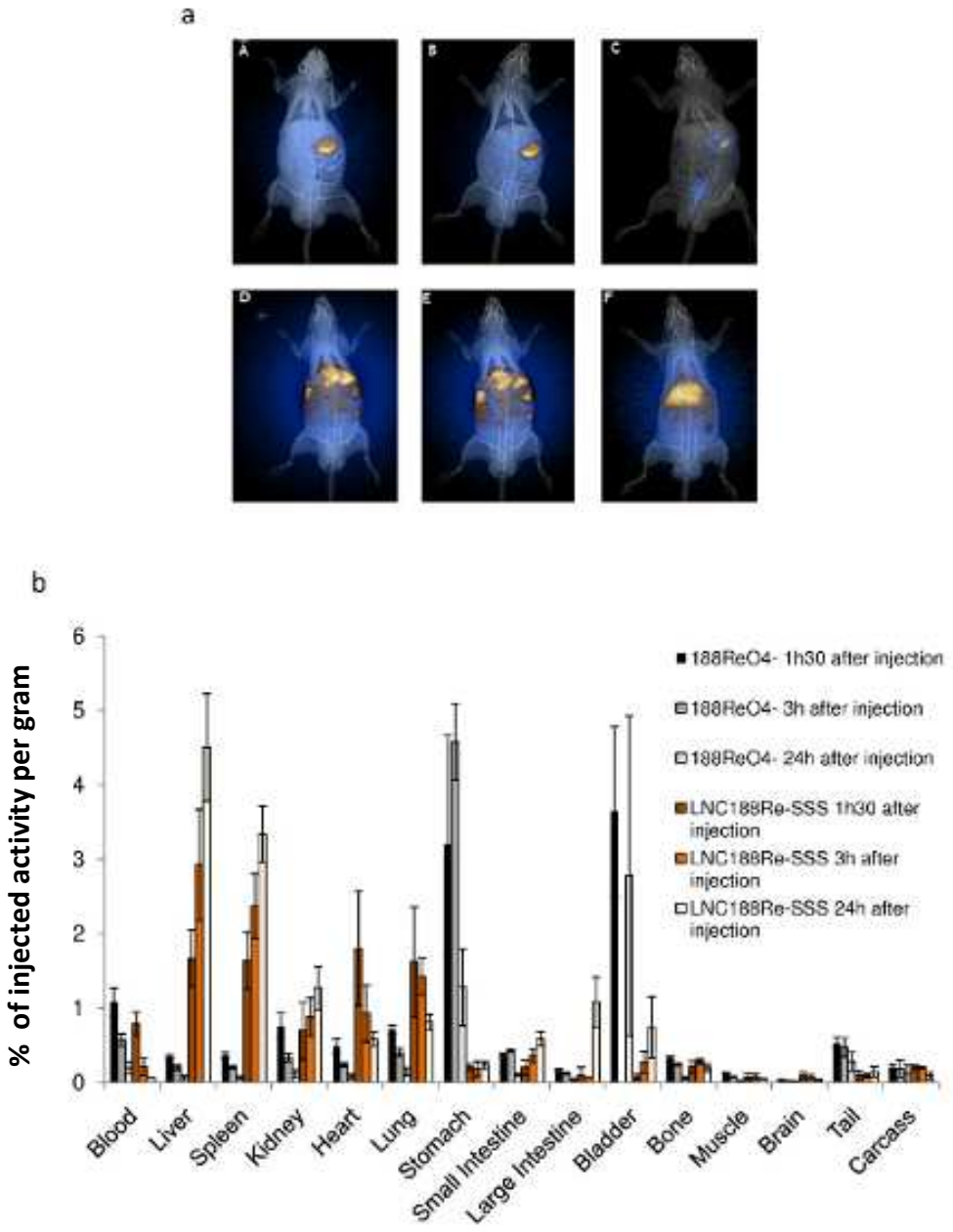

Figure 1: SPECT *images after the catheterization of the hepatic artery and tissue distributions.* **a:** A, B, and C: SPECT images after 1.5 h, 3 h, and 24 h of the ^{188}Re-perrhenate solution; D, E, and F: SPECT images after 1.5 h, 3 h, and 24 h of the LNC^{188}Re-SSS solution **b:** Organ biodistribution of $^{188}ReO_4^-$ (n=12) and LNC^{188}Re-SSS (n=12) solutions 1.5 h, 3 h, and 24 h following the intra-hepatic injection. Results are expressed as a percent of injected activity per gram of organ, mean ± SD

Survival study

The descriptive and statistical data from the survival study are summarized in Table 2.

As shown in Figure 2, all animals of the control groups died due to tumor progression at D105, with a median survival time of 51 ± 19 days, 77 ± 19 days, and 57 ± 24 days for blank LNC, sham, and $^{188}ReO_4^-$ groups, respectively. There was no significant difference between the three control groups (p>0.05).

Following treatment with LNC^{188}Re-SSS (80 MBq) therapeutic efficiency was demonstrated by an increase in the median survival from 54 to 107% as compared to control groups with up to 7/12 long-term survivors in the LNC^{188}Re-SSS group (80 MBq). Even if a slight difference in median survival time was observed between LNC^{188}Re-SSS – 80MBq (118 ± 27 days) and LNC^{188}Re-SSS – 120 MBq (97 ± 18 days), comparison with these two groups was not significant (p=0.4431).

Tumor volume assessment was performed using two different evaluation methods: MRI and macroscopic study. Figure 3 shows MRI and macroscopic views of control groups (sham, $^{188}ReO_4^-$ and blank LNC) and LNC^{188}Re-SSS – 80 MBq rats at D100 (MRI) and D101 (macroscopy) after the end of tumor induction. Liver tumors represented approximately 100% of the liver parenchyma for control rats, while they occupied only 50% of the liver tissue for LNC^{188}Re-SSS – 80 MBq rats. Therefore, 50% of healthy liver tissue appeared to be preserved following LNC^{188}Re-SSS – 80 MBq treatment. This observation was confirmed by histopathological analysis (data not shown).

Table 2: *Descriptive and statistical data from the survival study.* The increase in the median survival time (IMST%) is calculated in comparison to the sham and the ^{188}Re-perrhenate groups. Comparisons of survival data using the log-rank test (Mantel-Cox test) versus sham group (*p<0.05), blank LNC ($^{£}p$<0.05), $^{188}Re0_4^-$ group ($^{\$}p$<0.05), LNC^{188}Re-SSS – 80 MBq ($^{§}p$<0.05), LNC^{188}Re-SSS – 120 MBq ($^{\#}p$<0.05).

	Median survival time (days)	IMST (%)		Max survival time (days)	Min survival time (days)	Long-term survivors		*p* values versus sham	*p* values versus blank LNC	*p* values versus $^{188}ReO_4^-$	*p* values versus LNC^{188}Re-SSS 80 MBq	*p* values versus LNC^{188}Re-SSS 120 MBq
		Sham	**$^{188}ReO_4^-$**			**Sham**	**$^{188}ReO_4^-$**					
LNC^{188}Re-SSS - 80 MBq (n=12)	118 ± 27	54	107	154	72	1	7	0.0139*	0.0118$^{£}$	0.0102 $^{\$}$	-	0.4431
LNC^{188}Re-SSS -120 MBq (n=11)	97 ± 18	26	70	140	74	0	2	0.0367	0.0236$^{£}$	0.0219$^{\$}$	0.4431	-
Sham (n=12)	77 ± 19	6	34	105	49	0	0	-	0.2440	0.4247	0.0139§	0.0367
Blank LNC (n=7)	51 ± 19	-34	-11	92	38	0	0	0.0749	-	0.7237	0.0118§	0.0236$^{\#}$
$^{188}ReO_4^-$ (n=4)	57 ± 24	-26	-	90	41	0	0	0.4247	0.7237	-	0.0102§	0.0219$^{\#}$

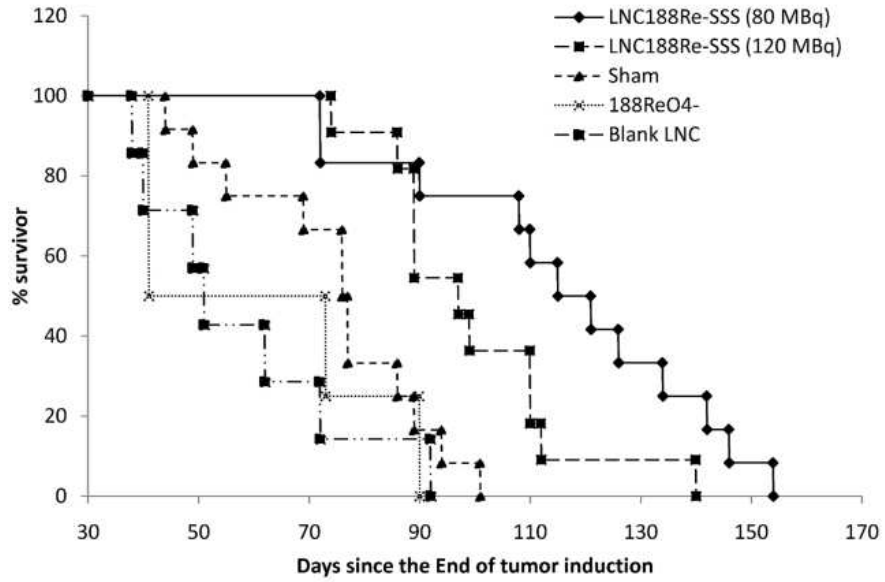

Figure 2: *Kaplan-Meier survival curves of rats with induced HCC*
On D10, rats were treated with 80MBq (n=12) and 120 MBq (n=11) of LNC^{188}Re-SSS, sham rats (n=12), blank LNC (n=8) and 80MBq of ^{188}Re-perrhenate solution (n=4).

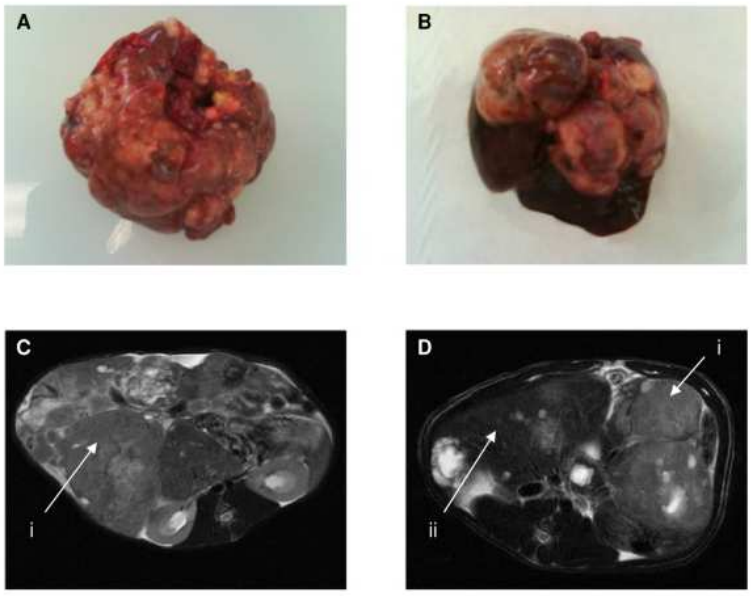

Figure 3: *Tumor volume assessment by MRI*
A and B represent macroscopic views at <D101 of control rats and LNC^{188}Re-SSS rats, respectively; T2-weighted images of control rats (C) and LNC^{188}Re-SSS (D) at D100 after the end of tumor induction. Tumors appear as hypersignals (i arrows); healthy liver (ii arrow)

Transaminase assessment

Transaminases were assessed in each group and compared to healthy rat data. As shown in Tables 3 and 4, the AST and ALT kinetics were very similar, with a slight liver toxicity starting at D12 for the LNC^{188}Re-SSS– 80 MBq group (AST, LNC^{188}Re-SSS – 80MBq group: 104 UI/mL, sham group: 74 UI/mL, $^{188}ReO_4^-$ group: 87 UI/mL, blank LNC group: 84 UI/mL, healthy rats: 76 UI/mL), which faded with normalization of AST levels at D55 (LNC^{188}Re-SSS– 80 MBq: 80 UI/mL, sham group: 95 UI/mL, $^{188}ReO_4^-$ group: 106 UI/mL, blank LNC: 93 UI/mL, healthy rats: 98 UI/mL) and at D90 for ALT levels (LNC^{188}Re-SSS – 80 MBq: 78 UI/mL, sham group: 66 UI/mL, $^{188}ReO_4^-$ group: 78 UI/mL, blank LNC: 76 UI/mL, healthy rats: 87 UI/mL). On the other side, hepatotoxicity was highlighted after a single injection of 120 MBq of LNC^{188}Re-SSS with ALT and AST levels higher in comparison with control groups at D12 (AST, LNC^{188}Re-SSS – 120MBq group: 151 UI/mL; ALT, LNC^{188}Re-SSS – 120 MBq group: 146 UI/mL) up to D105 (AST, LNC^{188}Re-SSS – 120MBq group: 129 UI/mL; ALT, LNC^{188}Re-SSS – 120 MBq group: 122 UI/mL).

Table 3: *AST Kinetics*

	AST UI/mL					
	$LNC^{188}Re$-SSSS	**$LNC^{188}Re$-SSSS**	**Sham**	**$^{188}ReO_4^-$**	**Blank LNC**	**Healthy rats**
	Group 1	**Group 2**	**Group 3**	**Group 4**	**Group 5**	**Group 6**
	(80MBq ; n=12)	**(120MBq ; n=11)**	**n=12**	**n=4**	**n=10**	**n=10**
	***p* values vs Group 6**	***p* values vs Group 6**	***p* values vs Group 6**	***p* values vs Group 6**	***p* values vs Group 6**	**-**
d12	104 ± 7.26	151 ± 9.48	74 ± 19.8	87 ± 11.31	84 ± 11.67	76 ± 11.78
	0.421*	0.0283*	0.2547	0.1292	0.1361	-
d18	97 ± 8.12	147 ± 14.62	77 ± 16.32	97 ± 9.73	78 ± 9.56	82 ± 9.45
	0.0489*	0.0193*	0.3415	0.0418*	0.3190	-
d25	102 ± 10.76	143 ± 10.78	88 ± 12.78	92 ± 10.72	95 ± 15.74	79 ± 10.32
	0.0374*	0.0342	0.2172	0.0426*	0.0435*	-
d30	114 ± 11.85	140 ± 15.04	85 ± 18.59	96 ± 8.43	106 ± 22.16	89 ± 13.57
	0.0372*	0.0187*	0.7341	0.3517	0.1214	-
d45	109 ± 12.64	129 ± 3.11	105 ± 20.1	110 ± 11.87	108 ± 25.9	97 ± 9.74
	0.464*	0.0231*	0.1322	0.1212	0.1189	-
d55	80 ± 20.36	127 ± 6.8	95 ± 16.62	106 ± 19.95	93 ± 11.43	98 ± 12.78
	0.4522	0.0251*	0.3781	0.1429	0.5123	-
d65	84 ± 7.14	126 ± 4.89	82 ± 14.85	95 ± 12.38	85 ± 14.75	109 ± 21.32
	0.5631	0.0467	0.5515	0.4287	0.5744	-
d80	87 ± 10.89	128 ± 19.99	92 ± 13.67	88 ± 10.24	97 ± 17.59	89 ± 10.38
	0.1865	0.0359*	0.1432	0.3428	0.4682	-
d90	77 ± 5.92	131 ± 8.83	137 ± 40.12	84 ± 8.56	79 ± 7.64	94 ± 4.66
	0.5349	0.0321*	0.0287*	0.4864	0.5276	-
d105	84 ± 30.81	129 ± 10.65	188 ± 85.87	-	-	103 ± 23.61
	0.4326	0.0211*	0.0083**	-	-	-
d130	91 ± 9.79	136 ± 14.32	-	-	-	85 ± 8.4
	0.1218	0.0107	-	-	-	-
d152	159 ± 57.98	-	-	-	-	76 ± 27.40
	0.0066**	-	-	-	-	-

The determination of the AST content in plasma samples for $LNC^{188}Re$-SSS (80 MBq and 120 MBq groups), sham, $^{188}ReO_4^-$, and blank LNC groups at D12, D18, D24, D25, D30, D45, D55, D65, D80, D90, D105, D130, and D152 after the end of tumor induction. Results are expressed in IU/mL of AST, mean ± SD. Comparisons of AST content versus healthy rats (*p<0.05; **p<0.01).

Table 4: *ALT Kinetics*

ALT UI/mL

	$LNC^{188}Re$-SSSS Group 1 (80MBq ; n=12) *p* values vs Group 6	$LNC^{188}Re$-SSSS Group 2 (120MBq ; n=11) *p* values vs Group 6	Sham Group 3 n=12 *p* values vs Group 6	$^{188}ReO_4^-$ Group 4 n=4 *p* values vs Group 6	Blank LNC Group 5 n=10 *p* values vs Group 6	Healthy rats Group 6 n=10 -
d12	95 ± 8.72	146 ± 9.78	64 ± 10.01	83 ± 8.48	74 ± 9.12	67 ± 12.14
	0.0392*	0.0083**	0.1281	0.1042	0.2148	-
d18	101 ± 13.62	148 ± 12.64	73 ± 9.41	74 ± 7.62	68 ± 12.56	72 ± 7.65
	0.0261*	0.0021**	0.0021**	0.1118	0.3512	-
d25	98 ± 10.37	141 ± 10.56	83 ± 13.67	69 ± 11.74	82 ± 10.86	87 ± 10.29
	0.0437*	0.0092**	0.3163	0.0912	0.1006	-
d30	87 ± 14.67	134 ± 12.76	79 ± 10.98	84 ± 8.94	79 ± 9.67	76 ± 8.34
	0.1872	0.0017**	0.4113	0.2275	0.3127	-
d45	99 ± 14.14	128 ± 6.78	83 ± 22.05	93 ± 11.57	95 ± 20.11	86 ± 11.33
	0.0439*	0.0376*	0.1024	0.3510	0.3121	-
d55	88 ± 12.63	133 ± 13.95	76 ± 6.51	67 ± 7.84	77 ± 7.12	80 ± 9.52
	0.1132	0.0051**	0.2941	0.2230	0.1949	-
d65	90 ± 15.65	126 ± 12.56	79 ± 8.94	72 ± 5.78	81 ± 9.53	84 ± 14.48
	0.0734	0.0421*	0.4376	0.3311	0.2414	-
d80	73 ± 12.84	125 ± 24.29	72 ±7.36	84 ± 9.23	92 ± 15.67	79 ± 7.48
	0.5635	0.0034**	0.2037	0.1882	0 .0613	-
d90	78 ± 0.74	129 ± 10.85	66 ± 9.95	78 ± 10.45	76 ± 6.89	87 ± 15.03
	0.4523	0.0288*	0.4579	0.1776	0.2430	-
d105	86 ± 24.74	122 ± 11.43	120 ± 14.81	-	-	77 ± 5.02
	0.2649	0.0107*	0.0119*	-	-	-
d130	74 ± 11.65	139 ± 9.52	-	-	-	69 ± 10.61
	0.3498	0.0034**	-	-	-	-
d152	123 ± 27.98	-	-	-	-	73 ± 12.59
	0.0056**	-	-	-	-	-

The determination of the ALT content in plasma samples for $LNC^{188}Re$-SSS (80 MBq and 120 MBq groups), sham, $^{188}ReO_4^-$, and blank LNC groups at D12, D18, D24, D25, D30, D45, D55, D65, D80, D90, D105, D130, and D152 after the end of tumor induction. Results are expressed in IU/mL of AST, mean ± SD. Comparisons of ALT content versus healthy rats (*p<0.05; **p<0.01).

VEGF quantification

Results showed major differences between LNC^{188}Re-SSS – 80MBq and the control groups (Figure 4). At D65, the VEGF concentration was approximately half as high in LNC^{188}Re-SSS rats versus each control group (LNC^{188}Re-SSS – 80MBq group: 21.27 pg/mL; sham rats: 49.31 pg/mL; $^{188}ReO_4^-$ group: 51.57 pg/mL; blank LNC group: 42.28 pg/mL) ($p_{LNC188Re\text{-}SSS/sham}$ = 0.0083; $p_{LNC188Re\text{-}SSS/blank\ LNC}$ = 0.016; $p_{LNC188Re\text{-}SSS/188ReO4-}$ = 0.0008). This remains lower up to D80 (LNC^{188}Re-SSS – 80MBq group: 69 pg/mL; sham rats: 131.50 pg/mL; $^{188}ReO_4^-$ group: 108.7 pg/mL; blank LNC group: 91.21 pg/mL) ($p_{LNC188Re\text{-}SSS/sham}$ = 0.043; $p_{LNC188Re\text{-}SSS/blank\ LNC}$ = 0.0188; $p_{LNC188Re\text{-}SSS/188ReO4-}$ = 0.0023).

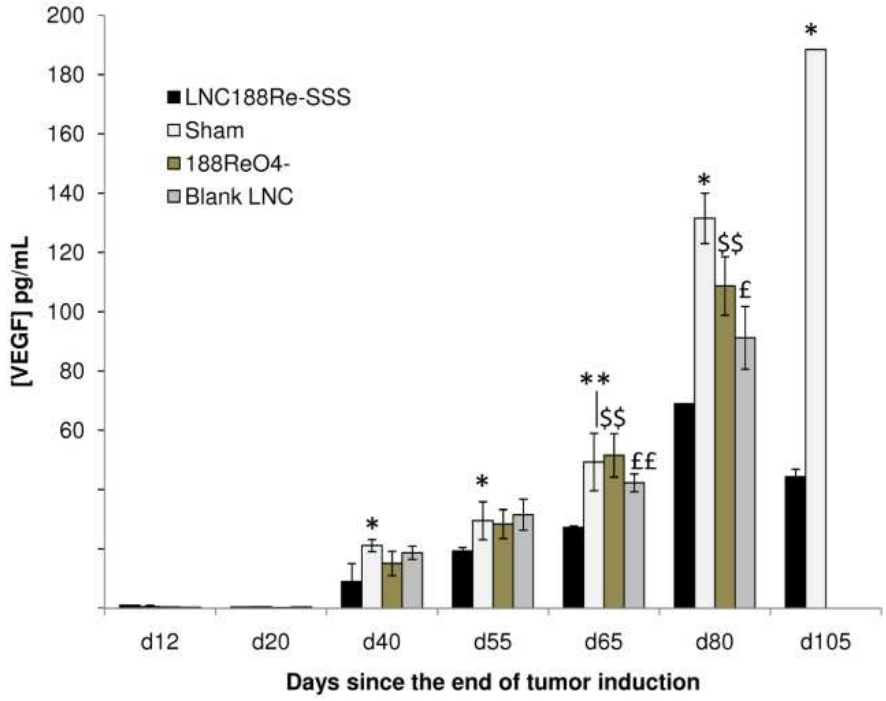

Figure 4: *Determination of the VEGF content in plasma samples*
The concentration of VEGF for each group. Results are expressed in pg/mL of VEGF, mean ± SD; comparison of the VEGF content in the LNC^{188}Re-SSS versus the sham group (*p<0.05; **p<0.01), $^{188}ReO_4^-$ group ($^{\$\$}$p<0.01), and blank LNC ($^{£}$p<0.05; $^{££}$p<0.01)

DISCUSSION

The use of LNCs, with a structure similar to lipoproteins, could represent a promising therapeutic modality for HCC management, as they modify the biodistribution of entrapped therapeutic agents [12-14]. These nano-objects include only FDA-approved excipients and are composed of a lipidic core leading to the entrapment of lipophilic molecules such as ^{188}Re-SSS [12], surrounded by a tension-active shell which induce physico-chemical properties different from those of the drug. Additionally, their nanometric scale (LNC^{188}Re-SSS mean diameter: 50 nm), and their low polydispersity index but also, the reduced viscosity of the drug, represent real advantages. It could likely avoid the excessive embolization process observed with chemoembolization (DC-beads™ – mean diameter: 300 – 500 µm [15]) and may penetrate more deeply inside the tumor blood vessels in comparison with ^{90}Y-microspheres devices (mean diameter around: 20 - 40 µm).

The first step in this study was to demonstrate the relevance of the encapsulation of Rhenium-188 for selective internal radiotherapy on a HCC rat model. The observed liver uptake following LNC^{188}Re-SSS injection and ^{188}Re-perrhenate accumulation in the stomach, which have been already reported in the literature [13, 14], validate the interest of the encapsulation of Rhenium-188. Organ biodistribution results indicated that LNC^{188}Re-SSS clearance from the blood was mainly ascribed to the liver. The enhancement permeability retention effect (EPR) may account for these findings [6]. This phenomenon could be explained by the size of LNC^{188}Re-SSS but Küpffer cells could be another explanation for these observations. In fact, it has been demonstrated that Küpffer cells and some

macrophages are involved in nanoparticle capture [16]. Thus, the physico-chemical properties of particulate systems improve the liver uptake of Rhenium-188.

The internal radiotherapy study by intra-arterial injection of LNC^{188}Re-SSS was carried out on a chemically induced (DENA) HCC rat model. 100% tumor take was observed, with a median survival time ranging from 51 to 77 days after the end of tumor. Three control groups were performed: ^{188}Re-perrhenate, blank LNC and sham groups. Neither the injection of the ^{188}Re-perrhenate solution nor the injection of blank LNC significantly modified rat survival, as the median survival time was 58 and 51 days respectively. The median survival time of the sham group (77 days) was higher than that of the ^{188}Re-perrhenate and blank LNC groups. This could be explained by a less invasive surgery, as neither hepatic artery catheterization nor injection, which could modify the hemodynamic parameters, were performed. As a consequence, treated groups (LNC^{188}Re-SSS – 80MBq; LNC^{188}Re-SSS – 120MBq) were compared with both ^{188}Re-perrhenate or blank LNC groups and sham group.

The LNC^{188}Re-SSS – 80MBq treatment was the most effective with 7/12 or 2/12 rats being long-term survivors and an IMST ranging from 107% to 54% according to the control group (^{188}Re-perrhenate groups or sham, respectively). These results correlated with MR images and macroscopic views, demonstrating a slowdown in tumor progression in the LNC^{188}Re-SSS – 80MBq group.

Increasing the absorded dose to the liver has shown no interest in terms of survival efficacy as LNC^{188}Re-SSS – 120 MBq group gave rise to the worse increase in median survival (IMST% ranging from 26% to 70% according to the control group). Hepatotoxicity demonstrated by higher levels of transaminases, could explain its less efficiency in term of survival.

Angiogenesis plays a key role in the pathogenesis of many cancers [17]. HCC, a hypervascular tumor, is mainly supplied by hepatic artery, whereas normal liver parenchyma and dysplastic nodules are largely supplied by the portal vein [18]. HCCs have been shown to express many angiogenic factors including VEGF [19]. Moreover, VEGF expression by the tumor and VEGF levels in patients' blood have been shown to correlate with the size, invasiveness, metastases, and prognosis of HCC [20]. As a consequence, the assessment of VEGF concentrations in plasma samples was carried out in each group except for LNC^{188}Re-SSS – 120 MBq group, which demonstrated worse results in terms of survival and hepatotoxicity. The lower VEGF levels, in LNC^{188}Re-SSS – 80 MBq group in comparison with control groups, could reflected an altered angiogenesis in the rat HCC model, which could reduced tumor progression confirmed by MRI.

Our results pointed out the advantage in using lipid nanocapsules, a drug delivery system for SIRT. In that field, an important breakthrough for HCC treatment has been done, with drug eluting beads (DEB, DC-beads™), ^{90}Y-microspheres (TheraSphere®, SIR-Sphere®), ^{188}Re-microspheres and nanocarriers. Dhanasekaran *et al.* demonstrated that doxorubicin DEB therapy with unresectable HCC provides a survival advantage over treatment with conventional chemoembolization [21]. However, micrometric size of DC-beads (300 to 500 µm) could generate excessive embolisation leading to Post-Embolization Syndrome (PES) [22]. Meanwhile DC-beads, SIRT with ^{90}Y-microspheres is another palliative HCC treatment option, with up to 50% in tumor HCC size reduction [23-26]. ^{188}Re-microspheres were also developed for HCC treatment with decrease in tumor growth after ^{188}Re-microsphere injection [27, 28].

Nanocarriers [29, 30] enable to load chemotherapeutic agents such as docetaxel [31] or oligonucleotides [32] were developed in order to reduce PES observed with DC-beads.

Results demonstrated a slowdown in tumor progression but most of these preclinical studies assessed their efficacy on a subcutaneous HCC model.

We have developed 50nm-lipid nanocapsules loaded with Rhenium-188 for selective internal radiotherapy and have assessed their efficiency on a chemically induced HCC rat model, known for its physiological properties similar to human hepatocarcinoma. Due to their nanometric scale, no embolisation process was possible. This could represent a real advantage as tumoral hypoxia areas could be reduced allowing a better efficiency of ionizing radiations.

Recently, sorafenib, an inhibitor of the VEGF receptor, has been shown to prolong the median survival time by 3 months in patients with advanced HCC [33]. As LNC^{188}Re-SSS seems to alter angiogenic process, their combination with sorafenib as an adjuvant therapy could be a valuable approach in the treatment of advanced HCC.

In conclusion, ^{188}Re-loaded LNCs appear to be an encouraging new radiopharmaceutical carrier for HCC internal radiotherapy which could penetrate more deeply inside the tumor blood vessels. A comparative study of LNC^{188}Re-SSS and ^{90}Y-microspheres SIRT, already used in clinical application, will probably provide informations of the effect of the size of particle systems and also in term of dosimetry.

ACKNOWLEDGEMENTS

We would like to thank Dr. Virginie Cadeillan for the kits kindly provided by the organic synthesis platform of the *Cancéropôle Grand Ouest, axe vectorisation tumorale et radiothérapie* (Grand Ouest Cancer Centre, tumor vectorization and radiotherapy section). . We are also grateful to Camille Belloche for her technical assistance in the animal experiments and to Dr. Sophie Michalak for the histopathological characterization. This work received grants from the Grand Ouest Cancer Centre and the *Ligue Contre le Cancer* (League Against Cancer, the Maine et Loire departmental committee). Claire Vanpouille-Box was a fellow from Angers Loire Métropôle.

REFERENCES

1. Cha, C.H., M.W. Saif, B.H. Yamane, and S.M. Weber, *Hepatocellular carcinoma: current management.* Curr Probl Surg, 2010. **47**(1): p. 10-67.
2. Cheng, J.C., J.K. Wu, C.M. Huang, D.Y. Huang, S.H. Cheng, Y.M. Lin, et al., *Radiation-induced liver disease after radiotherapy for hepatocellular carcinoma: clinical manifestation and dosimetric description.* Radiother Oncol, 2002. **63**(1): p. 41-45.
3. Brown, D.B., J.E. Gould, D.A. Gervais, S.N. Goldberg, R. Murthy, S.F. Millward, et al., *Transcatheter therapy for hepatic malignancy: standardization of terminology and reporting criteria.* J Vasc Interv Radiol, 2009. **20**(7 Suppl): p. S425-434.
4. Heurtault, B., P. Saulnier, B. Pech, J.E. Proust, and J.P. Benoit, *A novel phase inversion-based process for the preparation of lipid nanocarriers.* Pharm Res, 2002. **19**(6): p. 875-880.
5. Decuzzi, P., R. Pasqualini, W. Arap, and M. Ferrari, *Intravascular delivery of particulate systems: does geometry really matter?* Pharm Res, 2009. **26**(1): p. 235-243.
6. Maeda, H., J. Wu, T. Sawa, Y. Matsumura, and K. Hori, *Tumor vascular permeability and the EPR effect in macromolecular therapeutics: a review.* J Control Release, 2000. **65**(1-2): p. 271-284.
7. Lepareur N, G.E., Noiret N and J.Y. Herry, *A kit formulation for the labelling of lipiodol with generator-produced 188Re.* Journal of Labelled Compounds and Radiopharmaceuticals, 2004. **47**(12): p. 857-867.
8. Zeng, Z.C., Z.Y. Tang, B.H. Yang, K.D. Liu, Z.Q. Wu, J. Fan, et al., *Comparison between radioimmunotherapy and external beam radiation therapy for patients with hepatocellular carcinoma.* Eur J Nucl Med Mol Imaging, 2002. **29**(12): p. 1657-1668.

9. Garin, E., B. Denizot, J. Roux, N. Noiret, N. Lepareur, M. Moreau, et al., *Description and technical pitfalls of a hepatoma model and of intra-arterial injection of radiolabelled lipiodol in the rat.* Lab Anim, 2005. **39**(3): p. 314-320.

10. Kumar, A., D.N. Srivastava, T.T. Chau, H.D. Long, C. Bal, P. Chandra, et al., *Inoperable hepatocellular carcinoma: transarterial 188Re HDD-labeled iodized oil for treatment--prospective multicenter clinical trial.* Radiology, 2007. **243**(2): p. 509-519.

11. Lacoeuille, F., F. Hindre, F. Moal, J. Roux, C. Passirani, O. Couturier, et al., *In vivo evaluation of lipid nanocapsules as a promising colloidal carrier for paclitaxel.* Int J Pharm, 2007. **344**(1-2): p. 143-149.

12. Ballot, S., N. Noiret, F. Hindre, B. Denizot, E. Garin, H. Rajerison, et al., *99mTc/188Re-labelled lipid nanocapsules as promising radiotracers for imaging and therapy: formulation and biodistribution.* Eur J Nucl Med Mol Imaging, 2006. **33**(5): p. 602-607.

13. Deutsch, E., K. Libson, J.L. Vanderheyden, A.R. Ketring, and H.R. Maxon, *The chemistry of rhenium and technetium as related to the use of isotopes of these elements in therapeutic and diagnostic nuclear medicine.* Int J Rad Appl Instrum B, 1986. **13**(4): p. 465-477.

14. Hsieh, B.T., J.F. Hsieh, S.C. Tsai, W.Y. Lin, H.T. Huang, G. Ting, et al., *Rhenium-188-Labeled DTPA: a new radiopharmaceutical for intravascular radiation therapy.* Nucl Med Biol, 1999. **26**(8): p. 967-972.

15. Malagari, K., K. Chatzimichael, E. Alexopoulou, A. Kelekis, B. Hall, S. Dourakis, et al., *Transarterial chemoembolization of unresectable hepatocellular carcinoma with drug eluting beads: results of an open-label study of 62 patients.* Cardiovasc Intervent Radiol, 2008. **31**(2): p. 269-280.

16. Gibaud, S., M. Demoy, J.P. Andreux, C. Weingarten, B. Gouritin, and P. Couvreur, *Cells involved in the capture of nanoparticles in hematopoietic organs.* J Pharm Sci, 1996. **85**(9): p. 944-950.

17. Folkman, J., *Fundamental concepts of the angiogenic process.* Curr Mol Med, 2003. **3**(7): p. 643-651.

18. Semela, D. and J.F. Dufour, *Angiogenesis and hepatocellular carcinoma.* J Hepatol, 2004. **41**(5): p. 864-880.

19. Yamaguchi, R., H. Yano, A. Iemura, S. Ogasawara, M. Haramaki, and M. Kojiro, *Expression of vascular endothelial growth factor in human hepatocellular carcinoma.* Hepatology, 1998. **28**(1): p. 68-77.

20. Jinno, K., M. Tanimizu, I. Hyodo, Y. Nishikawa, Y. Hosokawa, T. Doi, et al., *Circulating vascular endothelial growth factor (VEGF) is a possible tumor marker for metastasis in human hepatocellular carcinoma.* J Gastroenterol, 1998. **33**(3): p. 376-382.

21. Dhanasekaran, R., D.A. Kooby, C.A. Staley, J.S. Kauh, V. Khanna, and H.S. Kim, *Comparison of conventional transarterial chemoembolization (TACE) and chemoembolization with doxorubicin drug eluting beads (DEB) for unresectable hepatocelluar carcinoma (HCC).* J Surg Oncol, 2010. **101**(6): p. 476-480.

22. Malagari, K., E. Alexopoulou, K. Chatzimichail, B. Hall, J. Koskinas, S. Ryan, et al., *Transcatheter chemoembolization in the treatment of HCC in patients not eligible for curative treatments: midterm results of doxorubicin-loaded DC bead.* Abdom Imaging, 2008. **33**(5): p. 512-519.

23. Dancey, J.E., F.A. Shepherd, K. Paul, K.W. Sniderman, S. Houle, J. Gabrys, et al., *Treatment of nonresectable hepatocellular carcinoma with intrahepatic 90Y-microspheres.* J Nucl Med, 2000. **41**(10): p. 1673-1681.

24. Lau, W.Y., S. Ho, T.W. Leung, M. Chan, R. Ho, P.J. Johnson, et al., *Selective internal radiation therapy for nonresectable hepatocellular carcinoma with intraarterial infusion of 90yttrium microspheres.* Int J Radiat Oncol Biol Phys, 1998. **40**(3): p. 583-592.

25. Salem, R., R.J. Lewandowski, B. Atassi, S.C. Gordon, V.L. Gates, O. Barakat, et al., *Treatment of unresectable hepatocellular carcinoma with use of 90Y microspheres (TheraSphere): safety, tumor response, and survival.* J Vasc Interv Radiol, 2005. **16**(12): p. 1627-1639.

26. Kulik, L.M., B. Atassi, L. van Holsbeeck, T. Souman, R.J. Lewandowski, M.F. Mulcahy, et al., *Yttrium-90 microspheres (TheraSphere) treatment of unresectable hepatocellular carcinoma: downstaging to resection, RFA and bridge to transplantation.* J Surg Oncol, 2006. **94**(7): p. 572-586.

27. Wunderlich, G., J. Pinkert, M. Stintz, and J. Kotzerke, *Labeling and biodistribution of different particle materials for radioembolization therapy with 188Re.* Appl Radiat Isot, 2005. **62**(5): p. 745-750.

28. Hafeli, U.O., S. Casillas, D.W. Dietz, G.J. Pauer, L.A. Rybicki, S.D. Conzone, et al., *Hepatic tumor radioembolization in a rat model using radioactive rhenium (186Re/188Re) glass microspheres.* Int J Radiat Oncol Biol Phys, 1999. **44**(1): p. 189-199.

29. Wang, Q., L. Zhang, W. Hu, Z.H. Hu, Y.Y. Bei, J.Y. Xu, et al., *Norcantharidin-associated galactosylated chitosan nanoparticles for hepatocyte-targeted delivery.* Nanomedicine, 2010. **6**(2): p. 371-381.

30. Xu, Y., Z. Wen, and Z. Xu, *Chitosan nanoparticles inhibit the growth of human hepatocellular carcinoma xenografts through an antiangiogenic mechanism.* Anticancer Res, 2009. **29**(12): p. 5103-5109.

31. Xu, Z., L. Chen, W. Gu, Y. Gao, L. Lin, Z. Zhang, et al., *The performance of docetaxel-loaded solid lipid nanoparticles targeted to hepatocellular carcinoma.* Biomaterials, 2009. **30**(2): p. 226-232.

32. Dai, L.C., X. Yao, X. Wang, S.Q. Niu, L.F. Zhou, F.F. Fu, et al., *In vitro and in vivo suppression of hepatocellular carcinoma growth by midkine-antisense oligonucleotide-loaded nanoparticles.* World J Gastroenterol, 2009. **15**(16): p. 1966-1972.

33. Llovet, J.M., S. Ricci, V. Mazzaferro, P. Hilgard, E. Gane, J.F. Blanc, et al., *Sorafenib in advanced hepatocellular carcinoma.* N Engl J Med, 2008. **359**(4): p. 378-390.

CONCLUSIONS

L'encapsulation du Rhénium-188 permet d'éviter une captation stomacale du ^{188}Re-perrhénate. Ainsi, nous avons observé qu'une seule injection de 80 MBq de NCL^{188}Re-SSS conduit à augmenter la médiane de survie des animaux jusqu'à 107% par rapport aux contrôles. Une légère hépatotoxicité a été démontrée avec des taux de transaminases (aspartate aminotransférase et alanine aminotransférase) plus élevés par rapport aux contrôles, cependant, cette toxicité hépatique est réversible puisque cette tendance s'estompe en fin d'expérimentation.

Une altération du processus angiogénique a également été démontrée par des taux plasmatiques de VEGF deux fois plus faibles en comparaison avec les animaux contrôles, ce qui pourrait expliquer le ralentissement tumoral observé aussi bien sur les courbes de survie que sur les images IRM.

Pour conclure ce chapitre, cette étude démontre le potentiel des NCL^{188}Re-SSS pour la radiothérapie interne du carcinome hépatocellulaire. Notons que les NCL^{188}Re-SSS réduisent la progression tumorale par altération du processus angiogénique tumoral après injection unique de NCL^{188}Re-SSS. Effectuer un fractionnement de la dose radioactive pourrait s'avérer intéressant afin de diminuer la toxicité hépatique d'une dose plus forte et de bénéficier d'un meilleur effet thérapeutique. Une appréciation des effets des NCL^{188}Re-SSS sur le processus angiogénique pourrait également être réalisée au sein d'un modèle de tumeur unique.

Chapitre II

Radiothérapie interne et gliomes

INTRODUCTION

Tout comme le carcinome hépatocellulaire, le gliome malin est une pathologie difficile à appréhender car aucun traitement curatif n'est efficace. En effet, la nature infiltrante de ces tumeurs ainsi que la présence de la barrière hémato-encéphalique limitent l'efficacité thérapeutique de l'exérèse et l'accès des agents-anticancéreux au site tumoral. La radiothérapie externe a toujours démontré une efficacité importante dans la prise en charge des patients atteints d'un gliome, cependant, l'irradiation des tissus sains adjacents représente un inconvénient majeur. Dans ce contexte, de nouvelles stratégies locorégionales avec notamment l'injection stéréotaxique par « Convection Enhanced-Delivery » (CED), une méthode d'injection permettant une distribution plus importante des agents anti-cancéreux (chimio- ou radio-thérapeutiques), ont été mises en place. Ainsi, la radiothérapie interne capable de créer une irradiation localisée a été développée. Cette stratégie peut utiliser un vecteur radiomarqué (anticorps radiomarqués, peptides radiomarqués, systèmes particulaires), on parle alors de radiothérapie interne vectorisée.

Ce chapitre a pour objectif de décrire les cibles cellulaires des gliomes ainsi que les vecteurs de radioéléments qui leur sont associés. Nous allons discuter de leur potentiel thérapeutique dans le traitement du gliome avec un intérêt particulier aux essais cliniques relevants.

Publication n°2 – Revue Bibliographique

Radiothérapie interne et gliomes.

“Focus on internal radiotherapy for malignant gliomas.”

Publication soumise dans «Journal of Nuclear Medicine»

FOCUS ON TARGETED INTERNAL RADIOTHERAPY FOR MALIGNANT GLIOMAS

Authors and Institutions: Claire Vanpouille-Box[1, 2], Emmanuel Garcion [1, 2], Olivier Couturier[1, 2], François Hindré[1, 2,*].

[1]PRES UNAM - INSERM U646, 10 rue A. Boquel, F-49100 Angers, France

[2]University of Angers, 10 rue A. Boquel, F-49100 Angers, France

*** For correspondence or reprints contact**: François HINDRE, INSERM U646, University of Angers, 10 rue A. Boquel, 49100 Angers (France); Telephone Number: (33) 2.41.73.58.50; Fax Number: (33) 2.41 .73.58.53; E-mail address: francois.hindre@univ-angers.fr

Keywords: Targeted radiotherapy, malignant brain tumors, peptide receptor therapy, radioimmunotherapy, radionuclide delivery systems

First Author: Claire Vanpouille-Box, PhD Student, INSERM U646, University of Angers, 10 rue A. Boquel, 49100 Angers (France). Telephone: +33 241 73 58 85; Fax: +33 241 73 58 53; Email: claire.vanpouille@gmail.com

short running foot line: Internal radiotherapy for gliomas

Abstract

Internal radiotherapy using radiolabeled vector, a strategy capable to deliver a localized irradiation, is the most promising modalities in terms of locoregional internal targeted radiotherapy for malignant gliomas. This review focuses in the various targeted radiotherapy which have been developed for the treatment of gliomas. Our purpose is to describe cellular target for glioma and radiolabeled vectors such as radiolabeled antibodies, peptides and radionuclide delivery systems. We will discuss their therapeutic potential in oncology with a particular interest to studies performed in clinical trials.

I- INTRODUCTION

Malignant gliomas are rare tumors with an incidence of 3.7 per 100,000 for men and 2.6 per 100,000 for women[1] which is more important in developed countries[2, 3] (Figure 1).

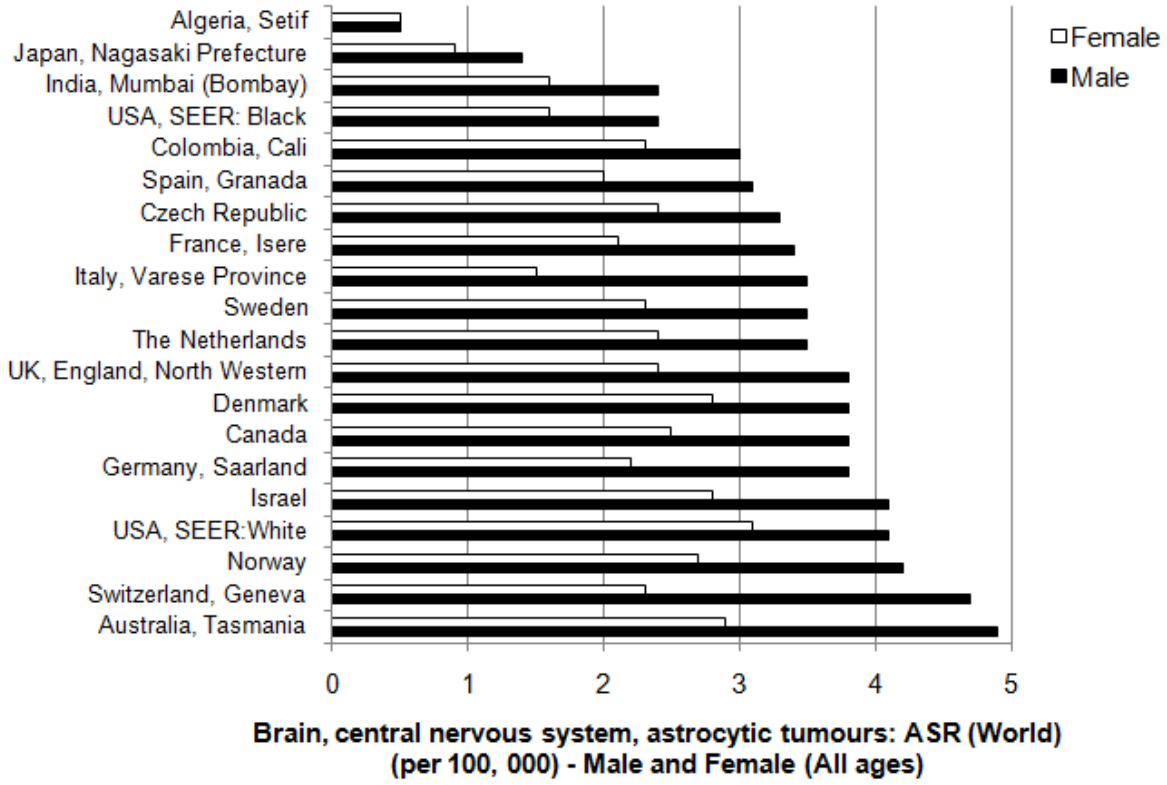

Figure 1: Incidence rates of astocytic tumours in the world. Source: In: Curado MP, Edwards B, Shin HR, Storm H, Ferlay J, Heanues M, Boyle P, editors. Cancer Incidence in Five Continents, vol. IX, No. 160 IARC Scientific Publications: Lyon, IARC; 2007.

It has been described that incidence of primary brain tumours is increasing since 1969[3, 4]. This can be explained by improved diagnostic methods such as modern radiologic imaging and better access to neurosurgical services[5, 6]. Indeed, incidental findings of gliomas increased with computed tomography (CT) and magnetic resonance imaging (MRI) technologies in 1980[4, 7]. However, the overall increased plateaued except for the older age groups which continues to increase[3]. Possible explanations are the duration exposure required for malignant transformation, the number of genetic alterations required to produce

clinical disease, the emergence of an environment that become permissive and/or a poorer immune surveillance advancing in age[6, 8, 9].

The prognosis is extremely poor and is based on several prognostic factors such as age, performance status, histological grade and extent of resection[10, 11]. Age is considered a strong negative factor on survival[12]. However, age should not be a reason for exclusion from aggressive treatment, because the few investigations of the treatment of malignant gliomas in the elderly have not identified specific prognostic factors in this subgroup[13].

Usually, surgery is the first therapeutic modality to proceed with macroscopically complete resection. However, genuine complete resection is impossible due to the infiltrative nature of malignant gliomas and relapse is yet inevitable.

Systemic chemotherapy is not either a good treatment option. Indeed, the failure of chemotherapy is due to the blood-brain barrier (BBB) which separates blood from the cerebral parenchyma. Its main function is to prevent penetration of drugs into the central nervous system. Hence, injecting chemotherapeutic agents intravenously is ineffective[14].

Stereotactic neurosurgery has been developed in order to bypasses BBB and to improve gliomas treatment. Indeed, locoregional therapies are promising approaches due to their ability to circumvent the BBB, to minimize systemic toxicity, and to concentrate therapy at the primary tumour site, which is well-recognized to be the site of tumour recurrence in most malignant gliomas.

The first approved locoregional therapy for malignant gliomas was Gliadel®, a controlled-release, biodegradable polymer releasing carmustine (BCNU). Results were encouraging but only demonstrate an increase in median survival up to 2-3 months[15, 16].

This can be explained by the low chemosensibility of glioma tumor cells and their high propensity in multidrug resistance phenomenon.

In a recent phase III study, results demonstrate that temozolomide (TMZ), an anticancer drug, improves survival in glioblastoma (GBM) patients when administered with concomitant external beam radiation (EBR)[17]. TMZ is an oral alkylator that leads to cells death by alkylation of the O^6 position of guanine and subsequent disturbance of DNA replication[18]. The

DNA repair protein O^6-methylguanine-DNA-methyltransferase (MGMT) has been implicated in the resistance of tumours cells to alkylating agents[19]. MGMT is expressed in gliomas and its contribution to resistance to TMZ has been reported[19-22]. Hence, nitrosoureas is not sufficient for gliomas treatment that is why more effective therapies are necessary.

EBR has been the standard treatment for the management of malignant gliomas[17], while systemic chemotherapy has had a limited role.

However, the non-specific nature of this conventional therapy for brain tumors often results in damage to adjacent areas of brain. Hence, administration of curative doses to tumor is limited because of the toxicity to normal brain which reduces the quality of life for the few patients with significant survival prolongation[23]. Thus, stereotactic radiosurgery (SR) and/or fractionated stereotactic radiotherapy (fSR) have emerged as logical adjuncts to current treatments for gliomas because of their ability to deliver high dose of radiation to a focal target[24].

With knowledge of the biology of malignant gliomas, identification of cellular targets led to the development of new kind internal radiation strategies. Indeed, five criteria are needed to meet with successful establishment of targeted radiotherapy:

(1) High and frequent expression of tumor-associated markers = specific target. (2) Availability of a high affinity targeting agents for reaching all distant sites of tumor cell infiltration. (3) Efficient radionuclide labeling of the targeting agent, i.e. preservation of binding properties. (4) *In vivo* stability of radioconjugate yielding long residence time on targeted tumor cells. (5) Radionuclide has to destroy tumor cells without irradiating adjacent normal brain areas.

Thus internal radiotherapy using radiolabeled vector has been developed. The main goal is to do a localized irradiation to glioma tumor cells. As such, radiolabeled peptide receptor therapies, radioimmunotherapy and radionuclide delivery systems represent the three most promising modalities in terms of locoregional internal targeted radiotherapy. Indeed, as it is still difficult to cross the BBB, administration technique for these three managements is often by stereotactic neurosurgery.

This review focuses on the various targeted radiotherapy modalities which have been developed for the treatment of malignant gliomas. Our purpose is to describe cellular target for gliomas and radiolabeled vectors such as radiolabeled peptides, antibodies and radionuclide delivery systems. We will discuss their therapeutic potential in oncology with a particular interest to studies performed in clinical trials.

II- RADIONUCLIDES FOR MALIGNANT GLIOMAS INTERNAL RADIOTHERAPY

Among all radionuclide, only a few are developed for radiotherapy. This can be explained by three inconvenients: (1) Availability of radionuclides with appropriate physical properties. (2) Interactions between the radionuclide and its biologic environment, i.e., the radiation biology of decaying moiety. (3) Identification of carrier with which to target such radionuclides to tumors.

In case of radionuclide, we have to consider its mode of decay, including the nature of the particulate radiation and their energies, its physical half-life and its chemistry in relation to the carrier.

For the carrier, one must define its stability and specificity, the biologic mechanisms that will bind it to the targeted cells (affinity…), the stability of the receptor-carrier complex, the distribution of the sites among cells and the microenvironment of the target.

Taken together, these criteria led to the development of 3 radiopharmaceuticals for internal radiation of malignant gliomas. Indeed, to date, the most common radionuclides used in clinic for radioimmunotherapy of malignant gliomas are, yttrium-90, iodine-131 and rhenium-188, while yttrium-90 is used in peptide receptor radionuclide therapy. The main physical characteristics of these radioisotopes are shown in Table 1.

A radionuclide with a long physical half-life will deliver more decay energy than one with a short half-life even if both have the same initial activity and biokinetics in the target tissue. For biological reasons, higher dose rates delivered over shorter treatment times are more effective than lower doses rates delivered over longer periods. Hence, a radionuclide with a short half-life will tend to be more biologically effective than one with similar emission energy but with a longer half-life[25]. So, rhenium-188 has the advantage over iodine-131 and yttrium-90 during the first day of treatment and 5 days after, the total dose delivered to the

target by rhenium-188, iodine-131 or yttrium-90 is quite similar. Indeed, if both yttrium-90 and rhenium-188 were separately conjugated to the same carrier with high specific activity and high *in vivo* stability, it would be suffice to administrate approximatively 3-4 times more initial activity of rhenium-188 than with yttrium-90 to deliver the same total absorbed dose to the target tissues. However a significant greater absorbed-dose rate for rhenium-188 during the first day of treatment will be achieve.

Even if rhenium-188 has favorable characteristic, yttrium-90 and iodine-131 present more simple chemistry that is why rhenium-188 is less used in clinical practice. Indeed, iodination process is well known since the 70's[26] and allow radiolabeling of monoclonal antibodies in the 80's.

Table 1 General characteristic of therapeutic radionuclides used for malignant gliomas treatment

Radionuclide	Half-life (h)	Energy of the main gamma emission (MeV) [abundance (%)]	Mean energy of beta particles emitted per disintegration (MeV)	Maximum energy of beta particles emitted per disintegration (MeV)	Mean beta-particle range in soft tissue (mm)	Maximum beta-particle range in soft tissue (mm)	Reference
^{188}Re	16.9	0.155 [15]	0.764	2.12	3.1	10.4	Casaco et al. (2008), Torres et al. (2008)
^{90}Y	64.1	-	0.935	2.28	4.0	11.3	Riva et al. (1999), Riva et al. (2000), Hofer et al. (2001), Schumacher et al. (2002), Bodei et al. (2004), Beutler et al. (2005), Heute et al. (2010)
^{131}I	192	0.208 [6.1]	0.133	0.497	0.23	1.8	Epenetos et al. (1985), Riva et al. (1994), Riva et al. (1995), Brown et al. (1996), Riva et al. (1997), Bigner et al. (1998), Akabani et al. (2000), Cokgor et al. (2000), Reardon et al. (2002), Reardon et al. (2006), McLendon et al. (2007), Reardon et al. (2008)
^{125}I	1425.6	0.0355 [6.7]	-	-			Kalofonos et al. (1989), Brady et al. (1990), Brady et al. (1992), Faillot et al. (1996)

III- RADIOIMMUNOTHERAPY (RIT)

This modality takes advantage of the antigenic specificity of tumors cells. The possibility to produce monoclonal antibodies (MAbs), firstly described by Kölher et al. in 1975[27], was the starting point of radioimmunotherapy (RIT). Indeed, development of monoclonal antibodies conjugated to a suitable isotope quickly followed with Levine et al. [28] which firstly described uptake kinetics of ^{131}I-MH-15 in a mouse model. However, the first application of radiolabelled-MAbs was for radioimmunodiagnosis[29-34]. Indeed, RIT was not described until the case report of Epenetos et al. [35] in 1985.

At the beginning, radiolabeled-MAbs were administered by intra-venous or intra-arterial routes but very low accumulation in the target tissue was noticed limiting therapeutic efficiency[36, 37]. Locoregional strategy with direct stereotactic injection of radiolabeled-MAb was then developed and has demonstrated its interest with the first locoregional study investigated by Hopkins et al. in 1997[38]. Indeed, radiolabeled-MAbs implanted by radiosurgery with stereotactic injection led to spares normal brain and distant critical organs. Moreover, radiolabeled-MAbs can easily react with its specific antigenic receptors expressed by malignant glioma tissues. Hence, three stereotactic modalities have emerged: locoreginal treatment may be intracavitary[39, 40], interstitial[15, 41] or intratumoral[34, 42, 43].

To be optimal, RIT needs to have a specific target of gliomas tumor cells. Hence, several MAbs have been investigated but only two specific targets have led to relevant clinical trials: epidermal growth factor receptor (EGFR), and tenascin (TN).

Epidermal Growth Factor Receptor (EGFR)

Epidermal Growth Factor Receptor (EGFR) was the first well-define target which led to clinical trial for malignant gliomas[36]. Indeed, EGFR is a tyrosine kinase transmenbrane glycoprotein that binds EGF and transforming growth factor α[44]. EGFR has an important role in normal cell proliferation and in the genesis of several cancers. Indeed, it has been

described that EGFR is overexpressed in malignant gliomas[45-48]. Hence, having specific MAbs to this epitope is interesting.

The murine-425 (M-425) MAb labeled with iodine-131 was firstly investigated for RIT by *Epenetos et al*.[35]. M-425 monoclonal antibody was radiolabeled with the Iodogen method[26] and immunoreactivity of ^{131}I-labeled-425 monoclonal antibody was checked before patient injection. Its intravenous injection result in tumor regression and improved the quality of life in patient with recurrent grade IV glioma. Moreover, authors described that a dosage of 1665 MBq of radiolabeled-425 monoclonal antibody could deliver to tumor 55 Gy and 130, 600 and 600 mGy to the whole body, liver and kidneys respectively.

This case report study was completed with *Brady et al*. studies which demonstrated interest of ^{125}I-425 monoclonal antibody for malignant glioma treatment. Indeed, in a first study, 15 patients with malignant astrocytoma were treated with one to three intra-arterial injections of ^{125}I-425 MAb. The total dose was 925 to 4810 GBq. Median survival time from antibody treatment alone was 8 ± 6.6 months[36]. At this stage, authors concluded on the ineffective treatment with radiolabeled-425 antibody by intra-arterial route. In a second study, *Brady et al.* decided to assess ^{125}I-425 MAb as adjuvant treatment of malignant astrocytomas. Hence, 25 patients received post-operative radiation therapy (mean dose 61 Gy in 6.5 weeks) before receiving ^{125}I-425 MAb. The average total doses of ^{125}I-425 MAb was 5587 MBq and resulted in a median survival up to 15.6 months[49].

However, intravenous or intra-arterial injections of radiolabeled-425 monoclonal antibody had demonstrated several adverse effects, with notably radiation of healthy[35, 36]. Indeed, mainly hepatocytes and epithelial cells also expressing EGFR which makes it inappropriate for treating malignant gliomas by systemic routes.

To avoid this main inconvenient, *Casaco et al*. opted for stereotactic radiosurgery modality and reported therapeutic effects of intracavitary injection of nimotuzumab (h-R3) in adult recurrent high-grade glioma[39]. Authors decided to use h-R3, a humanized antibody, in

order to circumvent the Human Anti-Mouse Antibodies (HAMA) response, already described in RIT[50, 51].

Indeed, most monoclonal antibodies are produced from cells of rodents (rats, mice, hamsters, rabbits). Thus, after injection, patients react against the monoclonal antibody as if they were a foreign substance and created a new set of antibodies with production of Human Anti-Mouse Antibodies (HAMA). This immune response by antibodies production progressively inactivates monoclonal antibody. Hence, modification of Fc fragments of the original species by human Fc fragments led to humanized antibodies development.

Nimotuzumab (h-R3) is a humanized antibody directed against EGFR and was the first radiolabeled-humanized antibody investigated for RIT of malignant gliomas treatment. Promising results were reported after a unique injection of 3 mg of h-R3 labeled with 370-555 MBq of rhenium-188 with a median survival up to 18.7 months for patients with recurrent high grade gliomas[39].

Biodistribution study of a single injection of 3 mg of ^{188}Re-h-R3 was then realized by *Torres et al*[52]. Dose-escalation was performed in order to determine Maximum Tolerated Dose (MTD) of 370 MBq and 555 MBq in recurrent high grade gliomas. Results demonstrated high retention in surgically created resection cavity (SCRC) with 85.5 ± 10.3 % injected activity 1h post-injection. Mean absorbed dose in the tumor area was about 24.1 ± 2.9 and 31.1 ± 6.4 Gy for patients with 370 MBq and 555 MBq respectively. Two patients of 555 MBq showed severe adverse effects, so Maximum Tolerated Dose (MTD) was determined at 370 MBq.

Locoregional of single injection of ^{188}Re-nimotuzumab seems to be an effective and safe treatment for recurrent high grade gliomas and need to be investigated in a phase II study.

Tenascin (TN)

Tenascin (TN) is a glycoprotein antigen which is present in the extracellular matrix in many cancers. In malignant brain tumors, tenascin is detected in 90% of all gliomas. Its overexpression in malignant gliomas is correlated with a high proliferation index and a high

vascularisation[53-55]. Hence, tenascin has emerged as logical specific target for malignant gliomas.

Several antitenascin-MAbs that binds to different epitope on the tenascin molecule have been investigated: BC-2, BC-4 and 81C6[41, 42, 56-64]. BC-2, 81C6 MAbs bind with spliced regions of the tenascin molecule whereas BC-4 reacts with an epitope in the epidermal growth factor-like repeat found on all tenascin isoforms[65]. As such, BC-2 and 81C6 MAbs should increase reactivity with tumor compared to liver, spleen and normal organs that express tenascin.

Mainly clinical trials involving BC-4 and BC-2 were conducted by *Riva et al.* [66-70]. Indeed, a pilot study of 24 patients with malignant gliomas reported biodistribution and dosimetry results of an intralesional RIT with BC-2 or BC-4 monoclonal antibodies labeled with iodine-131[68]. A dose more than 3019.2 MBq of ^{131}I was administered and had not demonstrated adverse effects due to ionizing radiations. The median survival was about 16 months with 5 patients with tumors stabilization (9 months), 3 with partial remissions (11 months) and 4 with complete responses (15 months).

The number of patients (n=24) was small, that is why these data were completed with another trial in 1995. Authors divided patients into two groups: group A with recurrent glioma lesion (n=12) and group B with newly diagnosed glioma tumors (n=4)[66]. No adverse effects concerning ionizing radiations were noticed but, 69% of patient produced human antimouse antibodies (HAMA). This was due to the migration of the murine proteins or their catabolic products from the place of injection into the blood stream, which elicited an immune response from the immunocompetent cells. Survival was increased compares to the precedent study with a median survival up to 18 months (group A) and 23 months (group B). These data were confirmed by *Riva et al* study in 1997 which demonstrated the interest of intralesional RIT as an adjuvant to current available therapies (surgery and conventional radiotherapy)[69]. However, in these two studies, patients with recurrent lesion do not respond as well as patients with newly diagnosed gliomas to the RIT. This can be explained by the use of iodine-131 (^{131}I) which has a restricted energy and cannot penetrate into tissues > 1

mm. Hence, further developments were conducted with BC-2 and BC-4 monoclonal antibodies labeled with yttrium-90 (^{90}Y), a pure β emitter with 2.284 MeV[71]. Contrary to ^{131}I, ^{90}Y wan penetrate tissues up to 0.5-0.7 cm, so radiolabeled-monoclonal antibodies can reach more distant neoplastic elements.

No survival results have been highlighted because of the advanced stage of the disease during RIT. However, maximum tolerated dose (MTD) to the brain was determined at 925 MBq.

It is also important to notice that the average dose to the tumor was 3200 cGy/mCi whereas, doses to the liver, bone marrow and kidneys were below 10 cGy/mCi. So, this biodistribution study clearly demonstrated that antibodies labeled with yttrium-90 reach only the neoplastic areas[71]. In a phase II clinical trial, authors reported an increased in median survival up to 31 months when RIT is associated with conventional therapies (neurosurgery, external beam radiation)[72].

Meanwhile the evaluation of BC-2 and BC-4 labeled antibodies, assessment of 81C6 labeled with iodine-131 was realized and has demonstrated promising results with several clinical trials[41, 56, 57, 59, 60, 73-75]. Patients were treated with ^{131}I-81C6MAb directly administered by means of Ommaya reservoir placed in the surgical created resection cavity (SCRC). Results showed an increased in median survival up to 12.69 and 15.9 months for recurrent[59] and newly diagnosed GBM[60] respectively.

Dose escalation was also realized in order to determine MTD of 3700 MBq[59] to 4440 MBq[60] for recurrent and newly diagnosed GBM respectively.

Recently, it has been described that ^{131}I-ch81C6, a humanIgG2/mouse chimeric antitenascin 81C6 (ch81C6) monoclonal antibody, exhibited higher tumor accumulation and enhanced stability compared with its murine parent[73]. Maximum tolerated dose (MTD) was determined at 2960 MBq with an increase in median survival time about 20.4 and 15 months for newly diagnosed and recurrent glioblastomas respectively.

IV- PEPTIDE RECEPTOR THERAPIES

Radiolabeled monoclonal antibody therapies was an important breakthrough 30 years ago for the treatment of glioma[76]. However, excessive molecular mass of antibodies led to the development of new targeting strategies such as the peptide receptor radiotherapy [43, 77].

Peptides are composed with amino acids. So, their size (1.5 kDa) depends on the number of amino acids (from 2 to 50). They do not have a well-defined three dimensional (tertiary) structure such as proteins and are not “natural”. In fact, most peptides are synthesized that is why there is a large number of peptide. These molecules are hydrophilic with a good permeability property which allows an easy and rapid access to tumor site after systemic injection. Moreover, their diffuse properties led to reach invading tumor cell clusters that migrate along vascular clefts.

However, peptides will not cross a normal blood-brain barrier (BBB) after systemic injection, but they are able to reach the tumor site when the BBB is disturbed [78-80] notably in case of malignant gliomas.

Few radiolabeled-peptides have been developed for peptide receptor therapy. Indeed, some authors studied EGF[81], oxytocin[82] and chlorotoxin[83] radiolabeled peptides but most relevant studies concerned somatostatin as specific target to malignant gliomas.

Somatostatin (SST)

Somatostatin (SST) is a natural small cyclic peptide hormone. Its activity is mediated through 5 specific receptors (SSTR-1 to SSTR-5) located on the membrane of the target cells. SSTR-3 mediates apoptosis in endocrine cells whereas inhibition of cell proliferation is mediated by activation of SSTR-1, SSTR-2 and SSTR-5 [84]. In addition to these biological actions, SST is known to be a neurotransmitter and neuromodulator in the brain [85]. Moreover, it also been described that brain tumors contain SSTR [79, 86] with an overexpression of SSTR-2 in malignant gliomas [87-89]. Hence, SST appears to be a good target for the treatment of gliomas with peptide receptor radiotherapy.

However, the conformation of SST makes it extremely sensitive to peptidase [90]. So stables analogs which incorporate a Phe-(D)Trp-Lys-Thr (or similar sequence) and which metabolically stabilized at both the N- and C- terminals were developed for clinical application. Thus, three commercially available SST analogs were developed: octreotide ([(D)-Phe-Cys-Phe-(D)Trp-Lys-Thr-Cys-Thr(ol)], lanreotide [(D)βNal-Cys-Tyr-(D)Trp-Lys-Val-Cys-Thr-NH_2] and vapreotide [(D)Phe-Cys-Tyr-(D)Trp-Lys-Val-Cys-Trp-NH_2] (cf. Figure 2). The main advantage of these compounds consists in a longer action and a much prolonged half-life in plasma and tissues compares to SST [91].

Their radiolabeling was often performed through the macrocyclic chelator DOTA (1, 4, 7, 10-tetraazacyclododecane-1, 4, 7, 10-tetraacetic acid), the gold standard chelator enable to encapsulate hard metals such as yttrium-90 for radiotherapy. Hence, octreotide, lanreotide and vapreotide peptides can be labeled with yttrium-90 (^{90}Y) resulting in stable radioconjugate such as ^{90}Y-DOTATOC ([^{90}Y]-DOTA^{0}-D-Phe^{1}-Tyr^{3}-octreotide)[92-94].

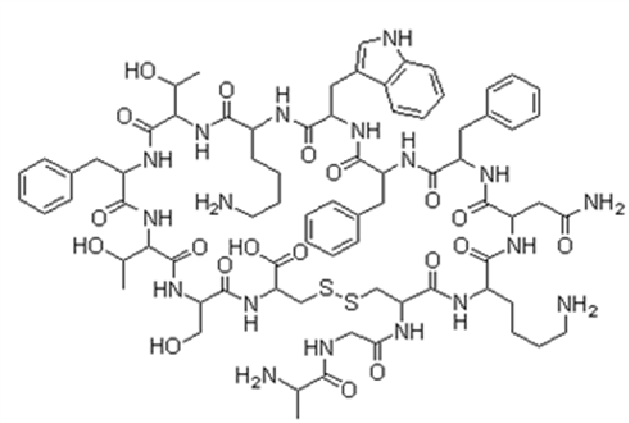

Somatostatin

Ala-Gly-Cys-Lys-Asn-Phe-Phe-Trp-Lys-Thr-Phe-Thr-Ser-Cys

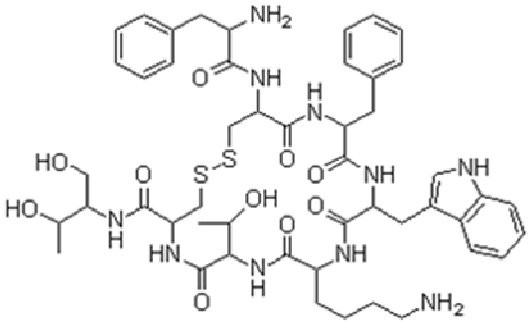

Octreotide

(D)Phe-Cys-Phe-(D)Trp-Lys-Thr-Cys-Threoninol

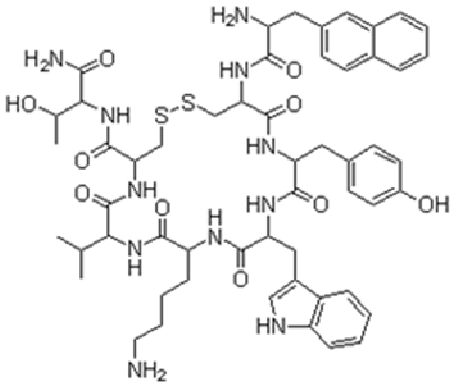

Lanreotide

(D)βNal-Cys-Tyr-(D)Trp-Lys-Val-Cys-Thr-NH_2

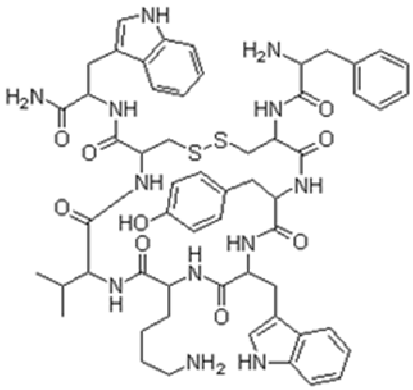

Vapreotide

(D)Phe-Cys-Tyr-(D)Trp-Lys-Val-Cys-Trp-NH_2

Figure 2: Structure of somatostatin analogs

To date, only ^{90}Y-DOTATOC (cf. Figure 3) radiolabeled peptide is assessed through clinical trials for malignant glioma peptide receptor therapy[95-98]. Indeed, *in vitro* and *in vivo* studies have demonstrated that radiolabeled-DOTATOC is a high-affinity ligand for SSTR-2, the somatostatin receptor-2 overexpressed in malignant gliomas[93, 99].

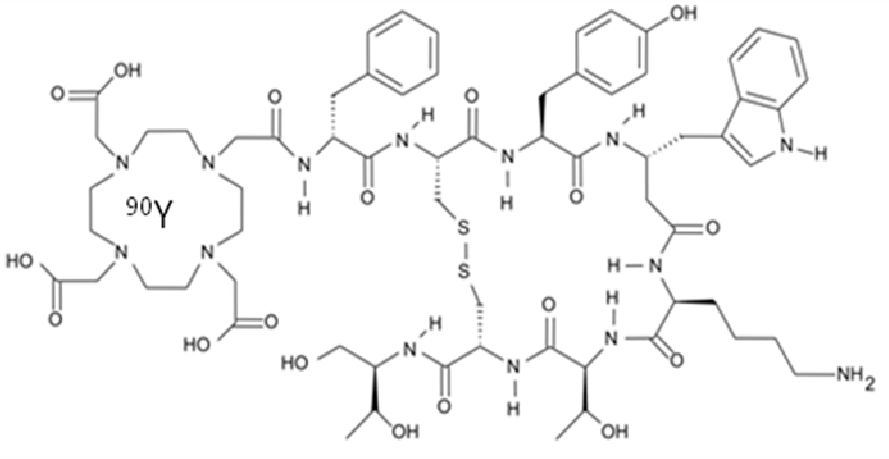

Figure 3: Structure of ^{90}Y-DOTATOC

Many studies were conducted by *Mäcke et al.* team and have firstly demonstrated in 1999 that ^{90}Y-DOTATOC competes specially with somatostatin binding to somatostatin receptor 2 in the low nanomolar range[92]. In this pilot study, eleven patients received one to four fractions of direct injection of ^{90}Y-DOTATOC into a Port-a-cath. Activity of ^{90}Y-DOTATOC per injection ranged between 185 and 1100 MBq and total cumulative activity per patient was between 370 MBq to 3330 MBq. Authors reported 1 patient with complete remission, 6 with disease stabilizations, and 4 with slow deterioration due to disease progression. Additionnal data were then reported by *Schumacher et al.* study[98] which demonstrated arrest of tumor progression for 13-45 months in all five patients with low-grade and anaplastic tumor types.

More recently, *Heute et al.*[100] described another pilot study of 3 patients with recurrent glioblastoma. After locoregional injection of ^{90}Y-DOTATOC (cumulated dose of 1.7 to 2.2 GBq in 3/4 fractions), 1 patient observed a complete remission and 2 a partial remission.

However, the limited number of patient makes it difficult to obtain relevant survival results.

Nevertheless, this study clearly highlighted receptor –mediated radionuclide therapy with ^{90}Y-DOTATOC as an attractive strategy for malignant gliomas.

V- RADIONUCLIDE DELIVERY SYSTEMS

Progress in pharmaceutical research field has been exploited in the design of tumor-targeting nanoscale[101] and microscale[102] carriers able to deliver radionuclides. Indeed, encapsulation of drug improves biodistribution and bioavaibility and so allows controlling tissular and cellular distribution profiles of drugs[103].

Nanovectors have a particulate interest since they can be classified into three categories. The first generation of nanocarrier is known for its rapid clearance from the blood stream and high uptake in macrophages due to opsonisation following intravenous injection.

To prolong blood circulation time of nanoparticle, their surface properties have been modified by binding hydrophilic poly(ethylene glycol) (PEG) chains[104, 105] ledding the second generation of nanocarriers.

Further developments on nanovectors have been performed in order to bind ligands (i.e. antibodies…) to their surface. Hence active targeting property of nanocarriers is the main characteristic of the third nanoparticle category[106].

During the last decades, many drug delivery systems have been developed, but no clinical studies were performed for malignant gliomas treatment. This can be explained by the novelty of this new internal radiation strategy.

However, among these different drug delivery systems, only lipid nanocapsules developed by *Benoit et al.* were assessed as new radionuclide delivery system for malignant gliomas[107-109] in preclinical studies.

Lipid Nanocapsules

Lipid nanocapsules (LNC) are biomimetic nanocarriers that mimic lipoproteins (cf. figure 4)[110]. Their size ranges from 20 to 100 nm depending on excipient quantities and they are characterized by a hybrid structure between polymer nanocapsules and liposomes. LNC are prepared by solvent free, soft energy procedure and present a great stability. Their lipidic

core is achieving through medium-chain triglycerides surrounded by a membrane made from a mixture of lecithin and pegylated surfactant.

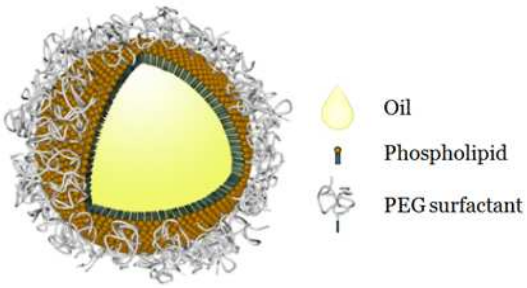

Figure 4 Schematic representation of LNC prepared by the phase-inversion temperature method

LNC formulation is very simple and is based on a phase inversion temperature (PIT) method[111]. Briefly, during three cycles of progressive heating and cooling, the Oil/Water emulsion is inverted into Water/Oil emulsion by passing through a phase-inversion zone. During the last cycle, rapid cooling with cold water is performed at the PIT, leading to the formation of lipid nanocapsules. All components are approved by the FDA for oral, topical and parenteral administration. Various drugs such as etoposide, docetaxel, paclitaxel, technetium-99m, rhenium-188… are encapsulated into these lipid nanovectors[103, 107, 108, 112-115].

Lipid Nanocapsules and rhenium-188

Lipid nanocapsules have a lipidic core. Hence, loading radiopharmaceutical compounds within lipid nanocapsules is possible only if the radioisotope has undergone chemical modifications to assign it lipophilic properties.

Recent progress in rhenium-188 chemistry led to the development of a patented lipophilic complex of rhenium-188 (^{188}Re-SSS) [116, 117]. The complex [^{188}Re ($PhCS_3$)$_2$ ($PhCS_2$)] (^{188}Re-SSS)] (cf. figure 5) is synthesized in two steps, with an intermediate compound of degree V ([$^{188}ReO(gluc)_2^-$]) chelated by sodium dithiobenzoate ($PhCS_2H$):

STEP 1: ^{188}Re-perrhenate ($^{188}ReO_4^-$) + Sodium Gluconate ⟶ $[^{188}ReO(gluc)_2^-]$

STEP 2: $[^{188}ReO(gluc)_2^-]$ + $PhCS_2H$ ⟶ $[^{188}Re(PhCS_3)_2(PhCS_2)]$

Encapsulation of this lipophilic complex of rhenium-188 (^{188}Re-SSS) can create high activity nano-objects for internal radiation application. Its incorporation within lipid nanocapsules is achieving though the PIT method, described above, after adding ^{188}Re-SSS in the other lipid nanocapsules components.

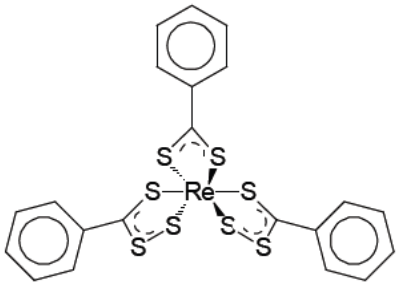

Figure 5 The complex $[^{188}Re(PhCS_3)_2(PhCS_2)]$

Lipid Nanocapsules loaded with rhenium-188 and malignant gliomas

Lipid nanocapsules proved to perfuse brain tumor after convection enhancement delivery (CED) injection[118] and have demonstrated their feasibility as a new strategy for internal radiation of malignant gliomas[107]. Indeed, a single injection of LNC^{188}Re-SSS (2.8 MBq) by CED injection have demonstrated promising results in a rat glioblastoma model with an increase in median survival time up to 83%[107]. To date, further developments concerning internal radiation using LNC^{188}Re-SSS after fractionated dose is conducted and results seems very interesting. However, this study has to be completed in order to definitively conclude on LNC^{188}Re-SSS efficacy.

Meanwhile evaluation of 1st generation of lipid nanocapsules by passive targeting, *Béduneau et al.*[108] studied active targeting of lipid nanocapsules. OX26 is a monoclonal antibody directed against the transferring receptor (TfR) highly expressed on the cerebral endothelium. Hence, TfR represent a good target and coupling OX26-MAb to lipid nanocapsules could improve their distribution within the brain.

Biodistribution study on healthy rats showed a concentration of 0.04%IA/g of OX26-immunonanocapsules in the brain 1h after intravenous injection. Thus these results clearly demonstrate the ability of these nano-objects to target the brain via TfR.

VI- CONCLUSIONS

In malignant gliomas management, there is a real need in developing new modalities since there is no curative treatment for this pathology. External beam radiation has always shown its effectiveness alone or in combination with neurosurgery and chemotherapy (temozolomide). However, intolerance of normal brain tissues to ionizing radiations limits its use. Research field in nuclear medicine with targeted internal radiation led to deliver high dose of radiation to a focal target and is therefore a promising modality in malignant gliomas treatment. Three different strategies (radiolabeled-antibodies, radiolabeled-peptides, radionuclide delivery systems) have emerged and have demonstrated its interest for the management of glioma tumors. However, their assessment in clinical practice (radioimmunotherapy and peptide receptor therapy) is in the early stage of nuclear medicine research since no phase III studies have been performed or has not yet started (radionuclide delivery systems).

VII- REFERENCES

1. Bondy, M.L. et al. Brain tumor epidemiology: consensus from the Brain Tumor Epidemiology Consortium. *Cancer* **113**, 1953-1968 (2008).
2. Curado MP, E.B., Shin HR, Storm H, Ferlay J, Heanues M and Boyle P Cancer Incidence in Five Continents. *Lyon: IARC* **IX** (2007).
3. Hess, K.R., Broglio, K.R. & Bondy, M.L. Adult glioma incidence trends in the United States, 1977-2000. *Cancer* **101**, 2293-2299 (2004).
4. Lonn, S. et al. Incidence trends of adult primary intracerebral tumors in four Nordic countries. *Int J Cancer* **108**, 450-455 (2004).
5. Gurney, J.G. & Kadan-Lottick, N. Brain and other central nervous system tumors: rates, trends, and epidemiology. *Curr Opin Oncol* **13**, 160-166 (2001).
6. Wrensch, M., Minn, Y., Chew, T., Bondy, M. & Berger, M.S. Epidemiology of primary brain tumors: current concepts and review of the literature. *Neuro Oncol* **4**, 278-299 (2002).
7. Preston, D.L. et al. Tumors of the nervous system and pituitary gland associated with atomic bomb radiation exposure. *J Natl Cancer Inst* **94**, 1555-1563 (2002).
8. Kleihues, P. & Ohgaki, H. Primary and secondary glioblastomas: from concept to clinical diagnosis. *Neuro Oncol* **1**, 44-51 (1999).
9. Kleihues, P. & Ohgaki, H. Phenotype vs genotype in the evolution of astrocytic brain tumors. *Toxicol Pathol* **28**, 164-170 (2000).
10. Lacroix, M. et al. A multivariate analysis of 416 patients with glioblastoma multiforme: prognosis, extent of resection, and survival. *J Neurosurg* **95**, 190-198 (2001).
11. Laws, E.R. et al. Survival following surgery and prognostic factors for recently diagnosed malignant glioma: data from the Glioma Outcomes Project. *J Neurosurg* **99**, 467-473 (2003).

12. Nazzaro, J.M. & Neuwelt, E.A. The role of surgery in the management of supratentorial intermediate and high-grade astrocytomas in adults. *J Neurosurg* **73**, 331-344 (1990).

13. Brandes, A.A., Compostella, A., Blatt, V. & Tosoni, A. Glioblastoma in the elderly: current and future trends. *Crit Rev Oncol Hematol* **60**, 256-266 (2006).

14. Bredel, M. Anticancer drug resistance in primary human brain tumors. *Brain Res Brain Res Rev* **35**, 161-204 (2001).

15. Brem, H. et al. Placebo-controlled trial of safety and efficacy of intraoperative controlled delivery by biodegradable polymers of chemotherapy for recurrent gliomas. The Polymer-brain Tumor Treatment Group. *Lancet* **345**, 1008-1012 (1995).

16. Westphal, M. et al. A phase 3 trial of local chemotherapy with biodegradable carmustine (BCNU) wafers (Gliadel wafers) in patients with primary malignant glioma. *Neuro Oncol* **5**, 79-88 (2003).

17. Stupp, R. et al. Radiotherapy plus concomitant and adjuvant temozolomide for glioblastoma. *N Engl J Med* **352**, 987-996 (2005).

18. Friedman, H.S., Kerby, T. & Calvert, H. Temozolomide and treatment of malignant glioma. *Clin Cancer Res* **6**, 2585-2597 (2000).

19. Sharma, S. et al. Role of MGMT in tumor development, progression, diagnosis, treatment and prognosis. *Anticancer Res* **29**, 3759-3768 (2009).

20. Esteller, M. et al. Inactivation of the DNA-repair gene MGMT and the clinical response of gliomas to alkylating agents. *N Engl J Med* **343**, 1350-1354 (2000).

21. Hegi, M.E. et al. MGMT gene silencing and benefit from temozolomide in glioblastoma. *N Engl J Med* **352**, 997-1003 (2005).

22. Sasai, K. et al. Careful exclusion of non-neoplastic brain components is required for an appropriate evaluation of O6-methylguanine-DNA methyltransferase status in glioma: relationship between immunohistochemistry and methylation analysis. *Am J Surg Pathol* **32**, 1220-1227 (2008).

23. Belka, C., Budach, W., Kortmann, R.D. & Bamberg, M. Radiation induced CNS toxicity--molecular and cellular mechanisms. *Br J Cancer* **85**, 1233-1239 (2001).

24. Romanelli, P. et al. Role of stereotactic radiosurgery and fractionated stereotactic radiotherapy for the treatment of recurrent glioblastoma multiforme. *Neurosurg Focus* **27**, E8 (2009).

25. Kassis, A.I. Therapeutic radionuclides: biophysical and radiobiologic principles. *Semin Nucl Med* **38**, 358-366 (2008).

26. Fraker, P.J. & Speck, J.C., Jr. Protein and cell membrane iodinations with a sparingly soluble chloroamide, 1,3,4,6-tetrachloro-3a,6a-diphrenylglycoluril. *Biochem Biophys Res Commun* **80**, 849-857 (1978).

27. Kohler, G. & Milstein, C. Continuous cultures of fused cells secreting antibody of predefined specificity. *Nature* **256**, 495-497 (1975).

28. Levine, G. et al. Localization of I-131-labeled tumor-specific monoclonal antibody in the tumor-bearing BALB/c mouse. *J Nucl Med* **21**, 570-573 (1980).

29. Epenetos, A.A. et al. Targeting of iodine-123-labelled tumour-associated monoclonal antibodies to ovarian, breast, and gastrointestinal tumours. *Lancet* **2**, 999-1005 (1982).

30. Epenetos, A.A. et al. Detection of human cancer in an animal model using radio-labelled tumour-associated monoclonal antibodies. *Br J Cancer* **46**, 1-8 (1982).

31. Farrands, P.A. et al. Radioimmunodetection of human colorectal cancers by an anti-tumour monoclonal antibody. *Lancet* **2**, 397-400 (1982).

32. Kemshead, J.T., Jones, D.H., Goldman, A., Richardson, R.B. & Coakham, H.B. Is there a role for radioimmunolocalization in diagnosis of intracranial malignancies?: discussion paper. *J R Soc Med* **77**, 847-854 (1984).

33. Sfakianakis, G.N. & DeLand, F.H. Radioimmunodiagnosis and radioimmunotherapy, 1982. *J Nucl Med* **23**, 840-850 (1982).

34. Yoshida, J. et al. Tumor-specific binding of radiolabeled G-22 monoclonal antibody in glioma patients. *Neurol Med Chir (Tokyo)* **32**, 125-129 (1992).

35. Epenetos, A.A. et al. Antibody guided irradiation of brain glioma by arterial infusion of radioactive monoclonal antibody against epidermal growth factor receptor and blood group A antigen. *Br Med J (Clin Res Ed)* **290**, 1463-1466 (1985).

36. Brady, L.W. et al. Iodine125 labeled anti-epidermal growth factor receptor-425 in the treatment of malignant astrocytomas. A pilot study. *J Neurosurg Sci* **34**, 243-249 (1990).

37. Zalutsky, M.R. et al. Monoclonal antibody and F(ab')2 fragment delivery to tumor in patients with glioma: comparison of intracarotid and intravenous administration. *Cancer Res* **50**, 4105-4110 (1990).

38. Hopkins, K., Papanastassiou, V., Zananiri, F.A. & Kemshead, J.T. A model to estimate the dose to tumour following intracavity administration of radioimmunoconjugates to patients with malignant gliomas. *Br J Radiol* **70**, 1152-1161 (1997).

39. Casaco, A. et al. Phase I single-dose study of intracavitary-administered Nimotuzumab labeled with 188 Re in adult recurrent high-grade glioma. *Cancer Biol Ther* **7**, 333-339 (2008).

40. Popperl, G. et al. Serial O-(2-[(18)F]fluoroethyl)-L: -tyrosine PET for monitoring the effects of intracavitary radioimmunotherapy in patients with malignant glioma. *Eur J Nucl Med Mol Imaging* **33**, 792-800 (2006).

41. Reardon, D.A. et al. Phase II trial of murine (131)I-labeled antitenascin monoclonal antibody 81C6 administered into surgically created resection cavities of patients with newly diagnosed malignant gliomas. *J Clin Oncol* **20**, 1389-1397 (2002).

42. Boiardi, A. et al. Intratumoral delivery of mitoxantrone in association with 90-Y radioimmunotherapy (RIT) in recurrent glioblastoma. *J Neurooncol* **72**, 125-131 (2005).

43. Behr, T.M. et al. Experimental studies on the role of antibody fragments in cancer radio-immunotherapy: Influence of radiation dose and dose rate on toxicity and anti-tumor efficacy. *Int J Cancer* **77**, 787-795 (1998).

44. Schlessinger, J. Cell signaling by receptor tyrosine kinases. *Cell* **103**, 211-225 (2000).

45. Voelzke, W.R., Petty, W.J. & Lesser, G.J. Targeting the epidermal growth factor receptor in high-grade astrocytomas. *Curr Treat Options Oncol* **9**, 23-31 (2008).

46. Carlsson, J. et al. Planning for intracavitary anti-EGFR radionuclide therapy of gliomas. Literature review and data on EGFR expression. *J Neurooncol* **77**, 33-45 (2006).

47. Ekstrand, A.J. et al. Genes for epidermal growth factor receptor, transforming growth factor alpha, and epidermal growth factor and their expression in human gliomas in vivo. *Cancer Res* **51**, 2164-2172 (1991).

48. Wong, A.J. et al. Increased expression of the epidermal growth factor receptor gene in malignant gliomas is invariably associated with gene amplification. *Proc Natl Acad Sci U S A* **84**, 6899-6903 (1987).

49. Brady, L.W. et al. Malignant astrocytomas treated with iodine-125 labeled monoclonal antibody 425 against epidermal growth factor receptor: a phase II trial. *Int J Radiat Oncol Biol Phys* **22**, 225-230 (1992).

50. Goldenberg, D.M. The role of radiolabeled antibodies in the treatment of non-Hodgkin's lymphoma: the coming of age of radioimmunotherapy. *Crit Rev Oncol Hematol* **39**, 195-201 (2001).

51. Wersall, P. et al. Intratumoral infusion of the monoclonal antibody, mAb 425, against the epidermal-growth-factor receptor in patients with advanced malignant glioma. *Cancer Immunol Immunother* **44**, 157-164 (1997).

52. Torres, L.A. et al. Biodistribution and internal dosimetry of the 188Re-labelled humanized monoclonal antibody anti-epidemal growth factor receptor, nimotuzumab, in the locoregional treatment of malignant gliomas. *Nucl Med Commun* **29**, 66-75 (2008).

53. Behrem, S., Zarkovic, K., Eskinja, N. & Jonjic, N. Distribution pattern of tenascin-C in glioblastoma: correlation with angiogenesis and tumor cell proliferation. *Pathol Oncol Res* **11**, 229-235 (2005).

54. Orend, G. Potential oncogenic action of tenascin-C in tumorigenesis. *Int J Biochem Cell Biol* **37**, 1066-1083 (2005).

55. Orend, G. & Chiquet-Ehrismann, R. Tenascin-C induced signaling in cancer. *Cancer Lett* **244**, 143-163 (2006).

56. Reardon, D.A. et al. A pilot study: 131I-antitenascin monoclonal antibody 81c6 to deliver a 44-Gy resection cavity boost. *Neuro Oncol* **10**, 182-189 (2008).

57. Reardon, D.A. et al. Salvage radioimmunotherapy with murine iodine-131-labeled antitenascin monoclonal antibody 81C6 for patients with recurrent primary and metastatic malignant brain tumors: phase II study results. *J Clin Oncol* **24**, 115-122 (2006).

58. Brown, M.T. et al. Intrathecal 131I-labeled antitenascin monoclonal antibody 81C6 treatment of patients with leptomeningeal neoplasms or primary brain tumor resection cavities with subarachnoid communication: phase I trial results. *Clin Cancer Res* **2**, 963-972 (1996).

59. Bigner, D.D. et al. Iodine-131-labeled antitenascin monoclonal antibody 81C6 treatment of patients with recurrent malignant gliomas: phase I trial results. *J Clin Oncol* **16**, 2202-2212 (1998).

60. Cokgor, I. et al. Phase I trial results of iodine-131-labeled antitenascin monoclonal antibody 81C6 treatment of patients with newly diagnosed malignant gliomas. *J Clin Oncol* **18**, 3862-3872 (2000).

61. Merlo, A. et al. Biodistribution of 111In-labelled SCN-bz-DTPA-BC-2 MAb following loco-regional injection into glioblastomas. *Int J Cancer* **71**, 810-816 (1997).

62. Paganelli, G. et al. Antibody-guided three-step therapy for high grade glioma with yttrium-90 biotin. *Eur J Nucl Med* **26**, 348-357 (1999).

63. Spaeth, N. et al. Radioimmunotherapy targeting the extra domain B of fibronectin in C6 rat gliomas: a preliminary study about the therapeutic efficacy of iodine-131-labeled SIP(L19). *Nucl Med Biol* **33**, 661-666 (2006).

64. Goetz, C.M. et al. Distribution of labelled anti-tenascin antibodies and fragments after injection into intact or partly resected C6-gliomas in rats. *Cancer Immunol Immunother* **54**, 337-344 (2005).

65. Zalutsky, M.R. Current status of therapy of solid tumors: brain tumor therapy. *J Nucl Med* **46 Suppl 1**, 151S-156S (2005).

66. Riva, P. et al. Local treatment of malignant gliomas by direct infusion of specific monoclonal antibodies labeled with 131I: comparison of the results obtained in recurrent and newly diagnosed tumors. *Cancer Res* **55**, 5952s-5956s (1995).

67. Riva, P. et al. Glioblastoma therapy by direct intralesional administration of I-131 radioiodine labeled antitenascin antibodies. *Cell Biophys* **24-25**, 37-43 (1994).

68. Riva, P. et al. Intralesional radioimmunotherapy of malignant gliomas. An effective treatment in recurrent tumors. *Cancer* **73**, 1076-1082 (1994).

69. Riva, P. et al. Local application of radiolabeled monoclonal antibodies in the treatment of high grade malignant gliomas: a six-year clinical experience. *Cancer* **80**, 2733-2742 (1997).

70. Riva, P. et al. 131I radioconjugated antibodies for the locoregional radioimmunotherapy of high-grade malignant glioma--phase I and II study. *Acta Oncol* **38**, 351-359 (1999).

71. Riva, P. et al. Loco-regional radioimmunotherapy of high-grade malignant gliomas using specific monoclonal antibodies labeled with 90Y: a phase I study. *Clin Cancer Res* **5**, 3275s-3280s (1999).

72. Riva, P. et al. Role of nuclear medicine in the treatment of malignant gliomas: the locoregional radioimmunotherapy approach. *Eur J Nucl Med* **27**, 601-609 (2000).

73. Reardon, D.A. et al. Novel human IgG2b/murine chimeric antitenascin monoclonal antibody construct radiolabeled with 131I and administered into the surgically created resection cavity of patients with malignant glioma: phase I trial results. *J Nucl Med* **47**, 912-918 (2006).

74. McLendon, R.E. et al. Tumor resection cavity administered iodine-131-labeled antitenascin 81C6 radioimmunotherapy in patients with malignant glioma: neuropathology aspects. *Nucl Med Biol* **34**, 405-413 (2007).

75. Akabani, G. et al. Dosimetry and dose-response relationships in newly diagnosed patients with malignant gliomas treated with iodine-131-labeled anti-tenascin monoclonal antibody 81C6 therapy. *Int J Radiat Oncol Biol Phys* **46**, 947-958 (2000).

76. Lee, Y.S. et al. Therapeutic efficacy of antiglioma mesenchymal extracellular matrix 131I-radiolabeled murine monoclonal antibody in a human glioma xenograft model. *Cancer Res* **48**, 559-566 (1988).

77. Reubi, J.C. Peptide receptors as molecular targets for cancer diagnosis and therapy. *Endocr Rev* **24**, 389-427 (2003).

78. Black, K.L. & Ningaraj, N.S. Modulation of brain tumor capillaries for enhanced drug delivery selectively to brain tumor. *Cancer Control* **11**, 165-173 (2004).

79. Haldemann, A.R. et al. Somatostatin receptor scintigraphy in central nervous system tumors: role of blood-brain barrier permeability. *J Nucl Med* **36**, 403-410 (1995).

80. Mehdipour, A.R. & Hamidi, M. Brain drug targeting: a computational approach for overcoming blood-brain barrier. *Drug Discov Today* **14**, 1030-1036 (2009).

81. Sundberg, A.L. et al. Combined effect of gefitinib ('Iressa', ZD1839) and targeted radiotherapy with 211At-EGF. *Eur J Nucl Med Mol Imaging* **30**, 1348-1356 (2003).

82. Chini, B. et al. Improved radiotracing of oxytocin receptor-expressing tumours using the new [111In]-DOTA-Lys8-deamino-vasotocin analogue. *Br J Cancer* **89**, 930-936 (2003).

83. Shen, S., Khazaeli, M.B., Gillespie, G.Y. & Alvarez, V.L. Radiation dosimetry of 131I-chlorotoxin for targeted radiotherapy in glioma-bearing mice. *J Neurooncol* **71**, 113-119 (2005).

84. Patel, Y.C. & Srikant, C.B. Somatostatin receptors. *Trends Endocrinol Metab* **8**, 398-405 (1997).

85. Cammalleri, M. et al. Functional effects of somatostatin receptor 1 activation on synaptic transmission in the mouse hippocampus. *J Neurochem* **111**, 1466-1477 (2009).

86. Reubi, J.C., Lang, W., Maurer, R., Koper, J.W. & Lamberts, S.W. Distribution and biochemical characterization of somatostatin receptors in tumors of the human central nervous system. *Cancer Res* **47**, 5758-5764 (1987).

87. Barbieri, F. et al. Somatostatin receptors 1, 2, and 5 cooperate in the somatostatin inhibition of C6 glioma cell proliferation in vitro via a phosphotyrosine phosphatase-eta-dependent inhibition of extracellularly regulated kinase-1/2. *Endocrinology* **149**, 4736-4746 (2008).

88. Lamszus, K., Meyerhof, W. & Westphal, M. Somatostatin and somatostatin receptors in the diagnosis and treatment of gliomas. *J Neurooncol* **35**, 353-364 (1997).

89. Reubi, J.C. et al. Coincidence of EGF receptors and somatostatin receptors in meningiomas but inverse, differentiation-dependent relationship in glial tumors. *Am J Pathol* **134**, 337-344 (1989).

90. Patel, Y.C. Somatostatin and its receptor family. *Front Neuroendocrinol* **20**, 157-198 (1999).

91. Pawlikowski, M. & Melen-Mucha, G. Somatostatin analogs - from new molecules to new applications. *Curr Opin Pharmacol* **4**, 608-613 (2004).

92. Merlo, A. et al. Locoregional regulatory peptide receptor targeting with the diffusible somatostatin analogue 90Y-labeled DOTA0-D-Phe1-Tyr3-octreotide (DOTATOC): a pilot study in human gliomas. *Clin Cancer Res* **5**, 1025-1033 (1999).

93. Otte, A. et al. DOTATOC: a powerful new tool for receptor-mediated radionuclide therapy. *Eur J Nucl Med* **24**, 792-795 (1997).

94. Otte, A. et al. Yttrium-90-labelled somatostatin-analogue for cancer treatment. *Lancet* **351**, 417-418 (1998).

95. Beutler, D. et al. Three-year recurrence-free survival in a patient with recurrent medulloblastoma after resection, high-dose chemotherapy, and intrathecal Yttrium-

90-labeled DOTA0-D-Phe1-Tyr3-octreotide radiopeptide brachytherapy. *Cancer* **103**, 869-873 (2005).

96. Bodei, L. et al. Receptor radionuclide therapy with 90Y-[DOTA]0-Tyr3-octreotide (90Y-DOTATOC) in neuroendocrine tumours. *Eur J Nucl Med Mol Imaging* **31**, 1038-1046 (2004).

97. Hofer, S. et al. Successful diffusible brachytherapy (dBT) of a progressive low-grade astrocytoma using the locally injected peptidic vector and somatostatin analogue [90Y]-DOTA0-D-Phe1-Tyr3-octreotide (DOTATOC). *Swiss Med Wkly* **131**, 640-644 (2001).

98. Schumacher, T. et al. Local injection of the 90Y-labelled peptidic vector DOTATOC to control gliomas of WHO grades II and III: an extended pilot study. *Eur J Nucl Med Mol Imaging* **29**, 486-493 (2002).

99. de Jong, M. et al. Yttrium-90 and indium-111 labelling, receptor binding and biodistribution of [DOTA0,d-Phe1,Tyr3]octreotide, a promising somatostatin analogue for radionuclide therapy. *Eur J Nucl Med* **24**, 368-371 (1997).

100. Heute, D. et al. Response of recurrent high-grade glioma to treatment with (90)Y-DOTATOC. *J Nucl Med* **51**, 397-400 (2010).

101. Ting, G., Chang, C.H. & Wang, H.E. Cancer nanotargeted radiopharmaceuticals for tumor imaging and therapy. *Anticancer Res* **29**, 4107-4118 (2009).

102. Salem, R. et al. Radioembolization for hepatocellular carcinoma using Yttrium-90 microspheres: a comprehensive report of long-term outcomes. *Gastroenterology* **138**, 52-64 (2010).

103. Garcion, E. et al. A new generation of anticancer, drug-loaded, colloidal vectors reverses multidrug resistance in glioma and reduces tumor progression in rats. *Mol Cancer Ther* **5**, 1710-1722 (2006).

104. Beduneau, A. et al. Pegylated nanocapsules produced by an organic solvent-free method: Evaluation of their stealth properties. *Pharm Res* **23**, 2190-2199 (2006).

105. Hoarau, D., Delmas, P., David, S., Roux, E. & Leroux, J.C. Novel long-circulating lipid nanocapsules. *Pharm Res* **21**, 1783-1789 (2004).

106. Beduneau, A., Saulnier, P. & Benoit, J.P. Active targeting of brain tumors using nanocarriers. *Biomaterials* **28**, 4947-4967 (2007).

107. Allard, E. et al. 188Re-loaded lipid nanocapsules as a promising radiopharmaceutical carrier for internal radiotherapy of malignant gliomas. *Eur J Nucl Med Mol Imaging* **35**, 1838-1846 (2008).

108. Beduneau, A. et al. Brain targeting using novel lipid nanovectors. *J Control Release* **126**, 44-49 (2008).

109. Ballot, S. et al. 99mTc/188Re-labelled lipid nanocapsules as promising radiotracers for imaging and therapy: formulation and biodistribution. *Eur J Nucl Med Mol Imaging* **33**, 602-607 (2006).

110. Heurtault, B., Saulnier, P., Pech, B., Proust, J.E. & Benoit, J.P. A novel phase inversion-based process for the preparation of lipid nanocarriers. *Pharm Res* **19**, 875-880 (2002).

111. Shinoda K, S.H. The Stability of O/W type emulsions as functions of temperature and the HLB of emulsifiers: The emulsification by PIT-method. *Journal of Colloid And Interface Science* **30**, 258-263 (1969).

112. Allard, E. et al. Lipid nanocapsules loaded with an organometallic tamoxifen derivative as a novel drug-carrier system for experimental malignant gliomas. *J Control Release* **130**, 146-153 (2008).

113. Huynh, N.T., Passirani, C., Saulnier, P. & Benoit, J.P. Lipid nanocapsules: a new platform for nanomedicine. *Int J Pharm* **379**, 201-209 (2009).

114. Lacoeuille, F. et al. In vivo evaluation of lipid nanocapsules as a promising colloidal carrier for paclitaxel. *Int J Pharm* **344**, 143-149 (2007).

115. Morille, M. et al. Long-circulating DNA lipid nanocapsules as new vector for passive tumor targeting. *Biomaterials* **31**, 321-329 (2010).

116. Lepareur, N. et al. Syntheses and reactivity of 'sulfur rich' Re(iii) and Tc(iii) complexes containing trithioperoxybenzoate, dithiobenzoate and dithiocarbamate ligands. *Dalton Trans*, 2866-2875 (2005).

117. Lepareur N, N.N.a.H.J. A kit formulation for the labelling of lipiodol with generator-produced 188Re. *Journal of Labelled Compounds and Radiopharmaceuticals* **47**, 857-867 (2004).

118. Vinchon-Petit, S. et al. In vivo evaluation of intracellular drug-nanocarriers infused into intracranial tumours by convection-enhanced delivery: distribution and radiosensitisation efficacy. *J Neurooncol* (2009).

Chapitre III

Radiothérapie Nanovectorisée appliquée au modèle de gliome 9L

INTRODUCTION

Comme déjà vu dans le chapitre précédent, beaucoup d'études ont montré l'intérêt d'une radiothérapie interne vectorisée via les anticorps et les peptides radiomarqués. Le potentiel des systèmes particulaires n'a été que très peu étudié puisque seule la faisabilité d'une radiothérapie interne par nanocapsules lipidiques chargées en Rhénium-188 pour le traitement du gliome malin a été reporté. L'objectif de la 1ère partie de ce chapitre est d'optimiser notre stratégie de radiothérapie interne nanovectorisée par injection intra-craniales répétées de NCL^{188}Re-SSS.

Depuis ces dix dernières années, plusieurs études ont démontré que la radiothérapie externe pouvait contribuer à la mise en place d'une nouvelle voie de mort cellulaire avec activation du système immunitaire. Ainsi, les interactions entre cellules irradiées, microenvironnement et système immunitaire peuvent résulter en l'acquisition d'une immunité spécifique anti-tumorale aussi bien aux sites primaires qu'aux sites métastatiques. La 2nde partie de ce chapitre a été d'évaluer les interactions entre les radiations ionisantes et le système immunitaire après radiothérapie interne nanovectorisée.

Publication n°3

Radiothérapie interne fractionnée à l'aide de NCL^{188}Re-SSS pour le traitement du glioblastome.

"Fractionated internal radiation with ^{188}Re-loaded lipid nanocapsules bypasses immunosuppressive barriers in malignant glioma tumors."

Publication soumise dans «Journal of Experimental Medicine»

FRACTIONATED INTERNAL RADIATION WITH ^{188}RE-LOADED LIPID NANOCAPSULES LEADS TO MAJOR TUMOR ERADICATION AND BYPASSES IMMUNOSUPPRESSIVE BARRIERS IN RAT GLIOMA.

Short title: LNC^{188}Re-SSS study using a glioma model

Authors and institutions: Claire Vanpouille-Box[1], Franck Lacoeuille[1,2], Camille Belloche[1], Nicolas Lepareur[3], Laurent Lemaire[1], Jean-Jacques LeJeune[1,2], Jean-Pierre Benoît[1], Philippe Menei[1, 4], Olivier Couturier[1,2], Emmanuel Garcion[1*#] and François Hindré[1*#].

[1]PRES UNAM - INSERM U646, 10 rue A. Boquel, F-49100 Angers, France - University of Angers, 10 rue A. Boquel, F-49100 Angers, France

[2]Nuclear Medicine department, Angers CHU, F-49100, France

[3]Medical imaging departments, CRLCC Eugene Marquis, F-35042 Rennes, France – European University of Brittany, F-35000 Rennes, France

[4]Neurosurgery department, Angers CHU, F-49100 Angers, France

***For correspondence or reprints contact:** Emmanuel Garcion, INSERM U646, University of Angers, 10 rue A. Boquel, 49100 Angers (France); Telephone: +33 241 73 58 85; Fax: +33 241 58 53; Email: emmanuel.garcion@univ-angers.fr; François Hindré, INSERM U646, University of Angers, 10 rue A. Boquel, 49100 Angers (France); Telephone: +33 241 73 58 99; Fax:+33 241 73 58 53; Email: francois.hindre@univ-angers.fr

#These authors contributed equally to this work.

First Author: Claire Vanpouille-Box, PhD Student, INSERM U646, University of Angers, 10 rue A. Boquel, 49100 Angers (France). Telephone: +33 241 73 58 85; Fax: +33 241 73 58 53; Email: claire_vanpouille@yahoo.fr

Grant support: This work received grants from the Maine-et-Loire *La Ligue Contre le Cancer* (League Against Cancer) and the *Cancéropôle Grand Ouest, axe vectorisation tumorale et radiothérapie* (Grand Ouest Cancer Centre, tumor vectorization and radiotherapy section).

ABSTRACT

To date, glioblastoma treatments have only been palliative. Regarding new medical devices, locoregional drug delivery strategies, which allow for blood-brain barrier bypass and the reduction of systemic toxicity, are of major significance. Recent progress in nanotechnology led to the development of colloidal carriers of radiopharmaceutics including lipid nanocapsules loaded with rhenium-188 (LNC^{188}Re-SSS), which can be implanted in the brain. In our study, we demonstrated that fractionated internal radiation using LNC^{188}Re-SSS triggers remarkable survival responses in a rat orthotopic glioma model (cure rates of 83%). We highlighted the importance of the radioactivity dose gradient obtained by the combination of a simple injection with convection-enhanced delivery. Basing ourselves on the overproduction of peripheral cytokines, tumor recruitment of immune cells, and memory response in long-term survivor animals, we established the role of the immune system in the treatment's efficacy. Due to the brain's immune privileges, these results appear crucial to overcome glioblastoma.

INTRODUCTION

Glioblastomas (GBM) are the most common and lethal primary brain tumors (1). Although surgery and external beam radiation therapy, with or without chemotherapy, slightly improve the prognosis, treatments are never curative (2). Systemic toxicity, normal brain tissue sensitivity and the presence of the blood-brain barrier (BBB) are the main responsible of the treatment failure (3).

Ionizing radiation is the gold-standard adjuvant treatment for malignant gliomas, that is why efforts in developing internal radiation have been done in order to prevent harm to healthy tissues. In that context, locoregional drug delivery modalities, such as stereotactic radiosurgery, which allow for blood-brain barrier (BBB) bypass and the reduction of systemic toxicity, are of major of significance. Clinical trials on GBM patients supported the usefulness of local radiolabeled peptide receptor therapy (^{90}Y-DOTATOC (4)) and radioimmunotherapy (^{131}I-tenascin antibodies (5), ^{188}Re-nimotuzumab (6)). Nanomedicine holds great promises for the development of effective targeted therapies for gliomas. When incorporated, the distribution of the radionuclide will not only be dependant from its intrinsic properties but from those of the nanocarrier (7). Hence, the benefit expected on the encapsulation of the radionuclide is to avoid its elimination following its injection.

In this field, colloidal drug delivery systems with a size below 100 nm have been designed to incorporate radionuclide. Among these, lipid nanocapsules (LNC), which are synthesized through a phase inversion process without any organic solvent, can be described as a lipid core surrounded by a tensioactive shell (8). These LNCs, which mimics the structure of lipoprotein, provide extensive drug encapsulation capacity (9-12) and also exhibit biological effects such as the inhibition of the P-gp (13-15), the endo-lysosomal escape (16) and biological barrier crossing (16). LNCs can be implanted in the brain tumors using stereotactic

injections for locoregional therapy. We recently established the faisability of using 50nm-LNC loaded with a lipophilic complex of Rhenium-188 (LNC^{188}Re-SSS - half-life: 16.9 hours; β^- emitter: 2.12 MeV; γ emitter: 155 keV) for internal radiation therapy in malignant glioma and have demonstrated a median survival up to 45 days after a single injection of LNC^{188}Re-SSS in an orthotopic 9L-glioma model (17).

In order to optimize internal radiation strategy, we assessed the efficacy of repeated brain administrations of LNC^{188}Re-SSS following 9L cells implantation. As simple stereotactic injections (SI) and convection-enhanced delivery (CED) lead to distinct LNC distribution volumes (18), these two LNC^{188}Re-SSS infusion techniques were chosen to study the impact of the dose gradient.

The current rationale of ionizing radiation is based on its ability to kill tumoral cells by the induction of an apoptotic program through excessive reactive oxygen species generation (19, 20). Nevertheless, several lines of evidence established that radiotherapy creates dose-dependent bystander effects such as adaptative responses, genomic instability and abscopal effects (21-27). One such dose-dependent bystander effect is the recruitment of biological effectors outside the treatment field with activation of innate immune cells such as macrophages (26, 28-32) and/or dendritic cells (33) depending on the release of danger signals by irradiated tumoral cells.

According to the fractionated internal radiotherapy protocol used in our study, different dose gradients could be apply and may enhance different bystander effect such as the establishment of an anti-tumoral immune response.

Meanwhile, biomaterials of the nanoparticle can also function as “danger signal” that activate dendritic cells and could induce subsequent T-cell immunity (34-38). As gliomas are infiltrative tumors, radiation-induced apoptosis might be insufficient for its eradication. The

modification of the tumor microenvironment by ionizing radiation associated with synthetic adjuvant, such as nanoparticles, could be very advantageous in the tumor eradication as immune cells effectors could be co-stimulated.

In that context, this study aims to investigate fractionated internal radiation using LNC^{188}Re-SSS and to clarify the impact of nanovectorized internal radiotherapy on the immune system on a rat glioma model.

MATERIALS AND METHODS

Materials

Lipoïd® S75-3 (soybean lecithin at 69% of phosphatidylcholine) and Solutol® HS15 (a mixture of polyethylene glycol 660 and polyethylene glycol 660 hydroxystearate) were kindly donated by Lipoïd Gmbh (Ludwigshafen, Germany) and BASF (Ludwigshafen, Germany), respectively. NaCl and dichloromethane were provided by Sigma (St-Quentin, Fallavier, France). Deionized water was obtained from a Milli-Q plus system (Millipore, Paris, France). Lipophilic Labrafac® CC (caprylic-capric acid triglycerides) was provided by Gattefosse S.A. (Saint-Priest, France).

Preparation of the ^{188}Re-SSS complex

^{188}Re as carrier-free Na [$^{188}ReO_4^-$] in physiological solution was obtained by saline elution and concentration of ^{188}W/^{188}Re generator (*Institut des Radioéléments*, Fleurus, Belgium). The ^{188}Re-SSS complex was prepared according to the method developed by Lepareur *et al*. (39). In brief, the ^{188}Re-SSS complex was obtained by the reaction of the ligand sodium dithiobenzoate (Plateform of organic synthesis, Rennes, France) with a freeze-dried formulation containing 30mg sodium gluconate, 30mg ascorbic acid, 40mg potassium oxalate, and 4mg $SnCl_2.2H_2O$ reconstituted in 0.5mL of physiological serum. 1 110MBq of ^{188}Re-perrhenate ($^{188}ReO_4^-$; in 0.5mL) was added, and the solution was mixed for 15 minutes at room temperature. Next, 20mg of sodium dithiobenzoate (in 0.5mL; pH=7) was added before being heated at 100°C for 30 minutes, which allowed for the formation of the ^{188}Re-

SSS complex. Due to its precipitation in aqueous media, the ^{188}Re-SSS complex was extracted with dichloromethane (1mL) and washed three times with 1mL of deionized water. The radiochemical purity (RCP) of the complex was checked by thin-layer chromatography as the ratio of migrated radioactivity to total radioactivity. Thin-layer chromatography was carried out using silica gel 60-F_{254} alumina plates (Merck) and a solution of petroleum ether/dichloromethane (6/4; v/v) as an eluant. Radioactivity was assessed with a phosphor-imaging machine (Packard, Cyclone storage phosphor system).

Nanocapsule formulation and characterization

The overall study was performed on 50nm diameter LNCs, which were prepared according to a phase-inversion process described by Heurtault *et al.* (8). In brief, 25mg Lipoïd® S75-3, 282mg Solutol® HS15, 342.7mg Labrafac®, 29.7mg NaCl, and 987.5mg deionized water were mixed by magnetic stirring. The ^{188}Re-SSS complex extracted with dichloromethane (1mL) was then added to the other components of the emulsion. The organic solvent was removed by being heated at 60°C for 15 minutes. Three cycles of progressive heating and cooling between 85°C and 60°C were then carried out and followed by an irreversible shock, induced by dilution with 4.16mL of 0°C deionized water, which was added to the mixture at 70°C. Afterwards, slow magnetic stirring was applied to the suspension for 5 minutes. LNC^{188}Re-SSS were dialyzed during 2 hours with deionized water at room temperature by magnetic stirring. The mean diameter and polydispersity index were then determined using a Malvern Zetasizer® Nano Serie DTS 1060 (Malvern Instruments S.A., Worcestershire, UK). The encapsulation yield was assessed with a gamma counter (Packard Auto-Gamma 5,000 series) according to the equation below.

Encapsulation yield (%):

$$= \frac{\text{LNC}^{188}\text{Re-SSS solution activity after dialysis}}{\text{LNC}^{188}\text{Re-SSS solution activity before dialysis}} \text{ X } 100$$

Tumor cells

9L (European Collection of Cell Culture, n° 94110705, Salisbury, UK), a rat gliosarcoma cell line, was maintained in Dulbecco's modified Eagle's medium (DMEM, BioWhittaker, Verviers, Belgium) containing 10% fetal calf serum (FCS) (BioWhittaker, Verviers, Belgium) and 1% antibiotic and antimycotic solution (Sigma, St Quentin Fallavier, France) in a humidified incubator gassed with 5% CO_2 (37°C) until reaching 80–90% confluence. The number of 9L passages at the time of use for the experiments was between P10-P11.

Animals

Female syngeneic Fisher 344 rats aged 9 to 10 weeks were obtained from Charles River (L'arbresle, France). The experiments were conducted in line with the French Minister of Agriculture and the European Communities Council Directive of 24 November 1986 (86/609/EEC). The animals were kept in polycarbonate cages in a room with controlled temperature (20-22°C), humidity (50-70 %), and light (12 hours' light/dark cycles). Room air was renewed at the rate of 10 vol/hour. Tap water and diet were provided *ad libitum.*

Intracerebral tumor implantation

Tumor cells for intracerebral implantation were trypsinized, counted, and checked for viability by trypan blue exclusion. Cells were washed twice with Eagle's minimal essential

medium (EMEM, BioWhittaker, Verviers, Belgium) without FCS or antibiotics, and a final suspension of $1x10^5$cells/mL in EMEM was obtained. Animals were anesthetized with an intraperitoneal injection of 0.75–1.5mL/kg of a solution containing 2/3 of ketamine (100 mg/mL; Clorketam®, Vétoquinol, Lure, France) and 1/3 xylazine (20mg/mL; Rompun®, Bayer, Puteaux, France). Using a stereotactic head frame and a 10µL Hamilton syringe (Hamilton® glass syringe 700 series RN), 10µL of $1x10^3$9L cells were injected into the rat's right striatum. The coordinates used for the intracerebral injection were 1mm posterior to the bregma, 3mm lateral to the saggital suture (right hemisphere), and 5mm below the dura.

Fractionated internal radiation, protocols, and groups

A fractionated internal radiation study was performed at an early and a late stage of tumor progression. In a first study, animals underwent internal radiotherapy with 2.8MBq of LNCs loaded with rhenium-188 (LNC^{188}Re-SSS) on D6 and D12 following 9L cell implantation. In a second study, the efficacy of LNC^{188}Re-SSS was assessed at a late stage of tumor progression, and the animals therefore received internal radiotherapy on D12 and D18. Two different administration types of LNCs (LNC^{188}Re-SSS) were chosen: a SI with a final volume of 10µL and a flow of 1µL/min, and a CED injection with a final volume of 60µL and a flow of 0.5µL/min. Depending on the administration technique chosen, four injection protocols were carried out, notably protocol 1: SI at D6 and D12; protocol 2: CED injections at D6 and D12; protocol 3: CED injection at D6 (or D12) and SI at D12 (or D18); protocol 4: SI at D6 (or D12) and CED injection at D12 (or D18). Each protocol was composed of four groups: a

LNC^{188}Re-SSS group (n=6), a blank LNC group (n=4), a $^{188}ReO_4^-$ group (n=4), and a saline solution group (n=4).

Simple injection and convection enhancement delivery procedures

The animals were anesthetized with an intraperitoneal injection of 0.75 – 1.5mL/Kg of a solution containing 2/3 of ketamine (100mg/mL; Clorketam®, Vétoquinol, Lure, France) and 1/3 xylazine (20mg/mL; Rompun®, Bayer, Puteaux, France). For the "standard" injection, 10µL were injected into the rat striatum at a flow of 1µL/min using a 10µL syringe (Hamilton® glass syringe 700 series RN) with a 32-G needle (Hamilton ®). For this purpose, rats were immobilized in a stereotactic head frame (Lab Standard Stereotactic; Stoelting, Chicago, IL). Coordinates were 1mm posterior to the bregma, 3mm lateral to the saggital suture, and 5mm below the dura. Following the injection, the needle was left in place for an additional 5 minutes to avoid expulsion of the suspension from the brain during the removal of the syringe.

Convection enhancement delivery (CED) injection was similar, except that the 10µL Hamilton® syringe with a 32-G needle was connected to a 100µL Hamilton ® 22-G syringe containing the product (Harvard Apparatus, Les Ulis, France) through a cannula (CoExTMPE/PVC tubing, Harvard Apparatus, Les Ulis, France). CED was performed using an osmotic pump PHD 2,000 infusion (Harvard Apparatus, Les Ulis, France) by controlling a 0.5µL/min rate for 2 hours.

Tissue distribution study

A tissue distribution study was carried out using 16 female Fisher rats 6 days following 9L implantation. They were divided into two groups: one injected with LNC^{188}Re-SSS after a SI (n=8) and one with LNC^{188}Re-SSS following a CED injection (n=8). In both groups, the animals were sacrificed at post-injection interval times of 24 hours (n=4) and 96 hours (n=4). The organs were removed, washed, and weighed (blood, liver, spleen, kidneys, heart, lung, stomach, small intestine, large intestine, bladder, bone, muscle, brain, and carcass). The content activity of each organ was determined using a gamma counter (Packard Auto-Gamma 5,000 series).

Autoradiography

Female Fisher rats 6 days following 9L cell implantation received 2.8MBq after SI and CED injections of LNC^{188}Re-SSS (n=3 per group).Twenty-four hours following the LNC^{188}Re-SSS injection, the brain was extracted and fixed with 4% of paraformaldehyde in phosphate-buffered saline 1X (pH=7.3). Coronal sections (1mm thick) were prepared from brains on an acrylic brain matrix. Brain slices were then placed on phosphor screens for 1 minute, and read by the Cyclone Phosphor Imaging System (Packard Instruments).

MRI

MRI was performed with a Bruker Avance DRX 300 (Germany) machine equipped with a magnet of 7T. Rapid T2-weighted images were obtained using rapid acquisition with relaxation enhancement (RARE) sequence (TR=2,000ms; mean echo time [Tem]=31.7ms;

RARE factor=8; FOV=3x3cm; matrix 128x128; nine contiguous slices of 1mm; eight acquisitions).

IL-2 and IFN$_\gamma$ quantifications

Blood samples were collected from the tail vein using heparinized tubes in each protocol from a fractionated internal radiation study (D6/D12) at D8, D16, and D24 following 9L cell implantation. After centrifugation at 1 000g for 20 minutes, the rat IL-2 and rat IFN$_\gamma$ ELISA tests (Duoset, R&D Systems Europe, Lille, France) were immediately performed according to manufacturer's instructions.

Immunohistochemistry

Brains from tumor-bearing animals were frozen at D15, D24, and D32 in isopentane cooled by liquid nitrogen and stored at -80°C. Fourteen-micron cryosections were fixed with 4% of paraformaldehyde in phosphate-buffered saline 1X (pH=7.3) and washed three times with phosphate-buffered saline (PBS). In order to block nonspecific binding, sections were incubated 1 hour in PBS containing 4% BSA and 10% normal goat serum, and washed twice with PBS. All incubations with primary antibodies (OX18 antibody: mouse, 1/100, BD Sciences; OX6 antibody: mouse, 1/100, BD Sciences; OX62 antibody: mouse, 1/100, BD Sciences; CD161a antibody: mouse, 1/100, BD Sciences; OX42 antibody: mouse, 1/100, BD Sciences; CD4 antibody: mouse, 1/100, BD Sciences; CD8b antibody: mouse, 1/100, BD Sciences; and IgG isotypes) were performed overnight at 4°C at a 1/100 final dilution. Primary antibodies were detected using a rat-absorbed biotinylated anti-mouse IgG secondary antibody (BD Biosciences). After 1 hour of incubation at 4°C, the sections were

washed twice with PBS containing 4% of BSA. Sections were developed with Alexa 488-conjugated secondary antibody (Streptavidin Alexa Fluor 488 conjugate S11223, Invitrogen) at a final concentration of 2.5µg/mL after an incubation of 1 hour at 4°C and washed four times with PBS 1X. After immunostaining, DAPI (4', 6-Diamidino-2-phenylindole dihydrochloride D9542, 0.1µg/mL, Sigma, St Quentin Fallavier, France) was added for 20 minutes at room temperature to stain the nuclei.

Re-challenging

Long-term survivors obtained from fractionated internal radiation studies (D6/D12 and D12/D18) were re-challenged with 1 000 9L cells in the left striatum. The animals were anesthetized with an intraperitoneal injection of 0.75 – 1.5mL/kg of a solution containing 2/3 of ketamine (100mg/mL; Clorketam®, Vétoquinol, Lure, France) and 1/3 xylazine (20mg/mL; Rompun®, Bayer, Puteaux, France). The intracerebral tumor implantation procedure was described above, but the coordinates used were modified: 1mm posterior to the bregma, 3mm lateral to the saggital suture (left hemisphere), and 5mm below the dura.

Statistical analysis

Results are expressed as mean ± standard deviation (SD). For the survival study, comparisons between all the control groups were made using the log-rank test (Mantel-Cox test). For other studies, statistical analysis was performed using the *t* test. Data was considered to be significant when $p<0.05$.

RESULTS

Biodistribution of nanovectorized radionuclide: importance of the administration route.

In order to highlight the importance of the administration route, biodistribution of LNC^{188}Re-SSS were performed. At Day 6 following 9L cell implantation, we assessed the usefulness of the encapsulation of rhenium-188 within LNCs so as to maintain high levels of radiopharmaceutics for a long time period in the brain. Rhenium-188 entrapping is essential, as only 4% and 65% of the injected activity were eliminated in urine and feces 96 hours following the injection of LNC^{188}Re-SSS and the solution of ^{188}Re-perrhenate ($^{188}ReO_4^-$), respectively (Figure 1a). Depending on the rhenium-188 formulation, different distributions were obtained, while the two administration techniques (SI; CED) had no impact on the elimination process (Figures 1b-c). The role of rhenium-188 entrapping is corroborated by biodistribution studies, with 86% and 78% of the injected activity found in the brain 24 hours and 96 hours following the injection, respectively, regardless of the administration technique used (Figure 1d).

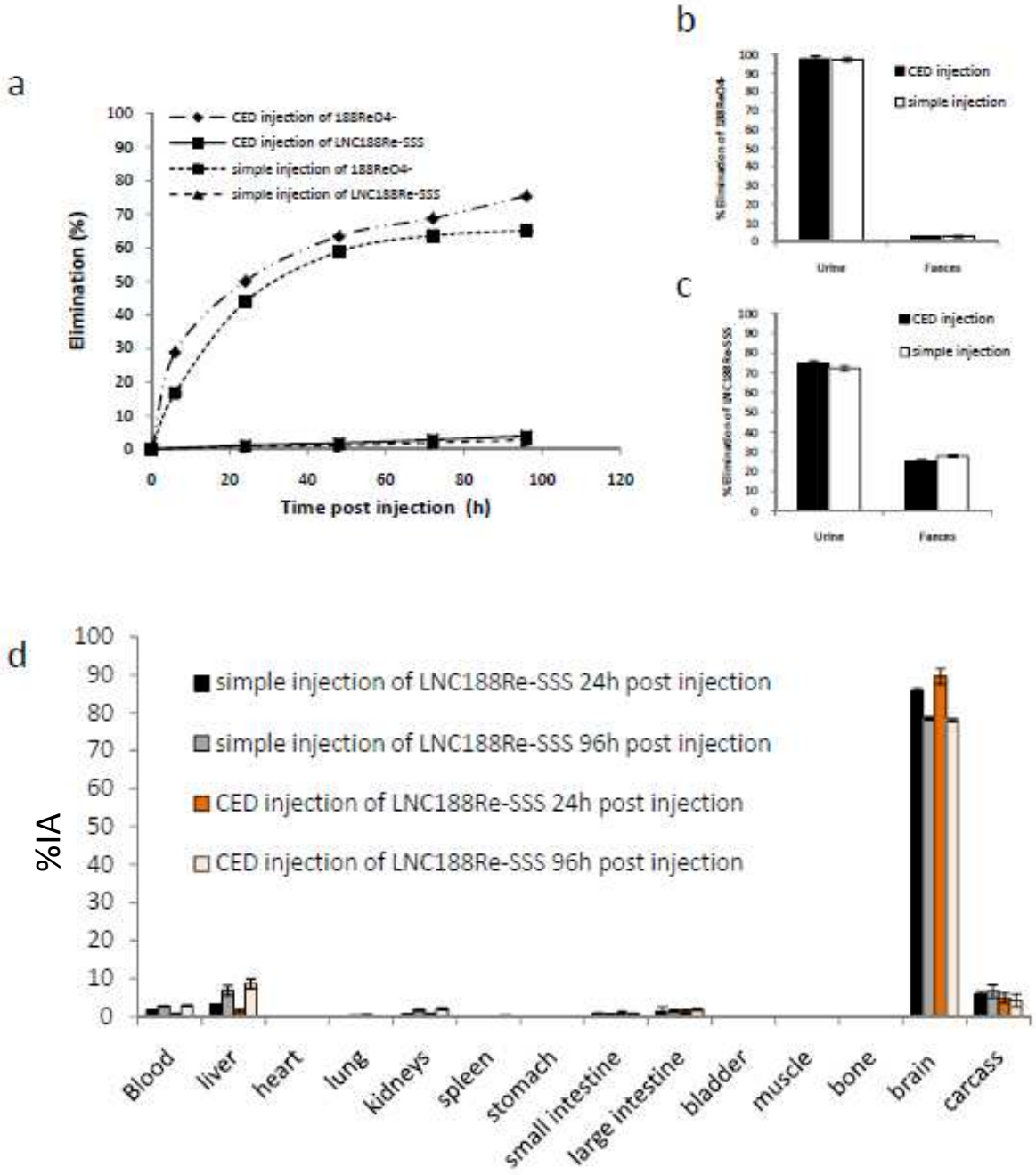

<u>Figure 1:</u> Distribution of LNCs loaded with rhenium-188

a: ^{188}Re elimination measured in urine and feces by a gamma counter during 96 hours following SI and CED injections of $^{188}ReO_4^-$ and LNC^{188}Re-SSS in 9L glioma-bearing rats 6 days following 9L implantation. Repartition between urine and feces for $^{188}ReO_4^-$ (**b**) and LNC^{188}Re-SSS (**c**). **d**: Organ biodistribution of $^{188}ReO_4^-$ (n=8) and LNC^{188}Re-SSS (n=8) solutions 24 hours and 96 hours following the injection; results are expressed as a percentage of the injected activity per gram of organ, mean ± SD

Importance of the administration route on the dose gradient.

To address the distribution of LNC^{188}Re-SSS within the brain, autoradiography views were performed 24 hours following simple and CED injections (Figure 2). Even if biodistributions were similar using SI or CED injections, the distribution within the brain tissue itself revealed a greater rhenium-188 spread with CED injections than with SI administration with a LNC^{188}Re-SSS area of 34.74 ± 0.72 mm² and 21.57 ± 0.78 mm² respectively (p=0.00004) (Figure 2a,c). Relative radioactivity was quantified using OptiQuant software and was expressed as the mean radioactivity density (DLU/mm²). Results revealed a radioactivity content more concentrated for the simple injection with 64.54 ± 1.99 DLU/mm² and 23.24 ± 2.68 DLU/mm² for simple and CED injections respectively (p=0.0006) (Figure 2a,b).

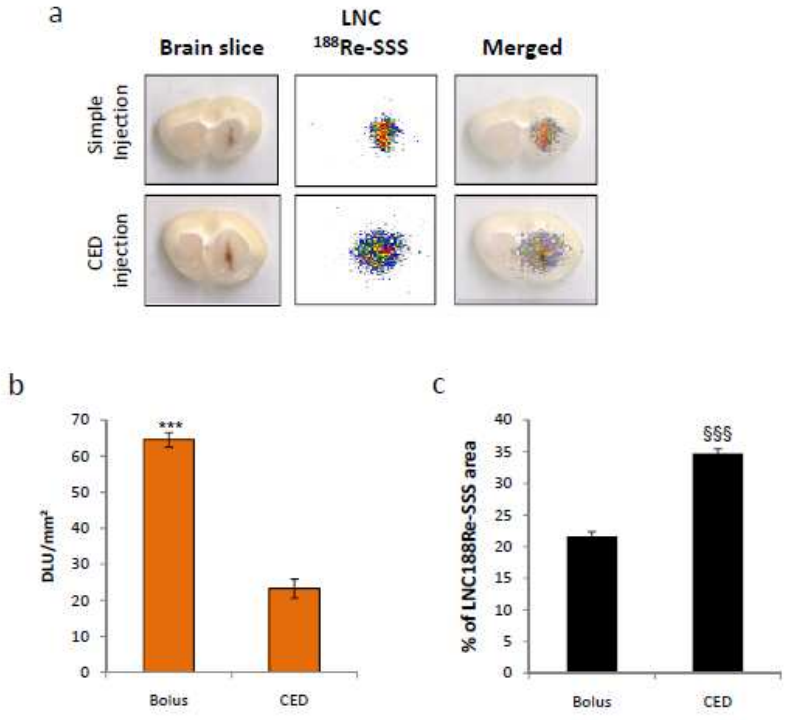

Figure 2: Autoradiography

a: Autoradiography views of LNC^{188}Re-SSS injected by SI and CED injections 24 hours following the injection. **b**: Relative amount of radioactivity in brain slices after bolus and CED injections of LNC^{188}Re-SSS. **c**: Percentage of LNC^{188}Re-SSS area after bolus and CED injections.

Treatment efficacy at day 6 and day 12 following tumor implantation.

Together with the characterization of the LNC^{188}Re-SSS distribution, the efficacy of fractionated internal radiation therapy was studied. Rats were treated with stereotactic injections of 2.8MBq of LNC^{188}Re-SSS 6 days (D6) and 12 days (D12) after 9L cell implantation. Depending on the administration technique (SI or CED), four injection protocols were assessed, notably protocol 1: SI at D6 and D12; protocol 2: CED at D6 and D12; protocol 3: CED at D6 and SI at D12; protocol 4: SI at D6 and CED at D12. In control group animals, the median survival time was close to 30 days for $^{188}ReO_4^-$ and 28 days for both blank LNC and saline solutions (Figures 3a-d). There were no significant differences between the control groups ($p>0.05$), regardless of the injection protocol used. Treatments with LNC^{188}Re-SSS were associated with an increased median survival time (IMST) of 37.5% and 35.7% for protocols 1 and 2, with 13% and 0% of long-term survivors, respectively (Figures 3a-b). Long-term survivors were defined as animals that survived for more than 120 days following 9L cell implantation (40). MRI monitoring corroborated this observation, with no tumor progression at that stage. Combination of CED and SI strongly improved animal survival, with an IMST of 176% with protocol 3 and 257% with protocol 4 (Figure 3c-d). Combining the two administration types that displayed distinct dose gradients had a strong impact on survival (7 in 12 animals were long-term survivors for protocols 3 and 4 against only one in 12 for protocols 1 and 2). MRI follow-up, which can detect 9L glioma tumors from Day 9, confirmed these findings with similar tumor progression between control groups, as demonstrated by representative images obtained with physiological serum (Figure 3e). Protocols 1 and 2 resulted in a comparable evolution with a slightly delayed tumor progression. In contrast, protocols 3 and 4 resulted in tumor eradication (Figure 3e).

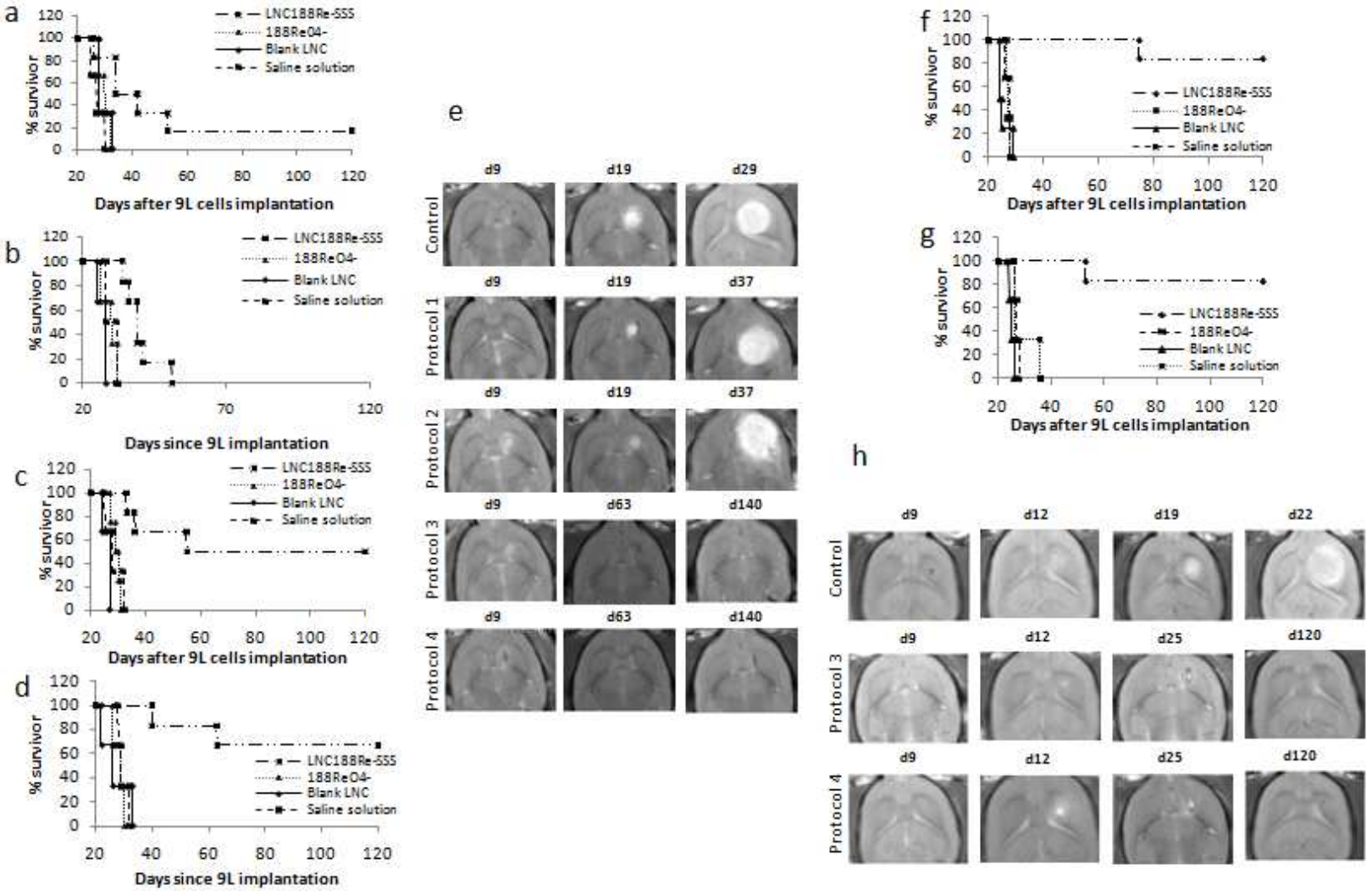

<u>Figure 3:</u> Efficacy of fractionated internal radiation with LNCs loaded with rhenium-188

a-d: Kaplan-Meier survival curves of rats treated at D6 and D12, 5.6MBq of LNC^{188}Re-SSS (n=6), 5.6MBq of $^{188}ReO_4^-$ (n=4), blank LNC (n=4), and saline solution (n=4) **a**: Protocol 1, SI at D6 and D12. One in six rats was a long-term survivor (>120 days) **b**: Protocol 2, CED injections at D6 and D12 **c**: Protocol 3, CED and SI at D6 and D12. Three in six rats were long-term survivors (>120 days) **d**: Protocol 4, SI and CED injections at D6 and D12. Four in six rats were long-term survivors **e**: T2-weighted images of control rats and LNC^{188}Re-SSS in each protocol of the D6/D12 fractionated internal study **f-g**: Kaplan-Meier survival curves of rats treated at D12 and D18, 5.6MBq of LNC^{188}Re-SSS (n=6), 5.6MBq of $^{188}ReO_4^-$ (n=4), blank LNC (n=4), and saline solution (n=4) **f**- Protocol 3, CED and SIs at D12 and D18. Five in six rats were long-term survivors (>120 days) **g**: Protocol 4, SI at D12 and CED injection at D18. Five in six rats were long-term survivors (>120 days) **h**: T2-weighted images of control rats and LNC^{188}Re-SSS in each protocol of the D12/D18 fractionated internal study

Treatment efficacy after tumor detection.

In order to mimic late-stage tumor progression, fractionated internal radiation was performed at D12 and D18 following 9L cell implantation. Protocols 3 and 4, which provided the best survival results during the previous treatment, were used. As expected, no significant differences between the control groups were detected, with a median survival close to 28 days. In contrast, with protocols 3 and 4, five in six rats (83%) were long-term survivors (Figures 3-g). MRI confirmed these results, with a tumor lesion at D9 following 9L cell implantation, which grew up until D25 and then regressed, with long-term survivor animals free of brain tumors (Figure 3h).

Effect of LNC^{188}Re-SSS on the production of peripheral cytokines.

As over-expression of interleukin-2 (IL-2) and interferon-γ (IFNγ) cytokines produced by T cells are importance for enabling anti-tumoral brain immune reponses (41), IL-2 and IFNγ were quantified at D8, D16, and D24 in blood of control and LNC^{188}Re-SSS-treated animals for protocols 3 and 4 (Figures 4a-b). No significant differences between the control groups were observed (saline solution, blank LNC and ^{188}Re-perrhenate solution); hence results of control groups were illustrated as a mean ± standard deviation of all control groups data. LNC^{188}Re-SSS treatment resulted in an overproduction of peripheral cytokines IL-2 and IFNγ as major increases in IL-2 and IFNγ were observed in LNC^{188}Re-SSS groups.

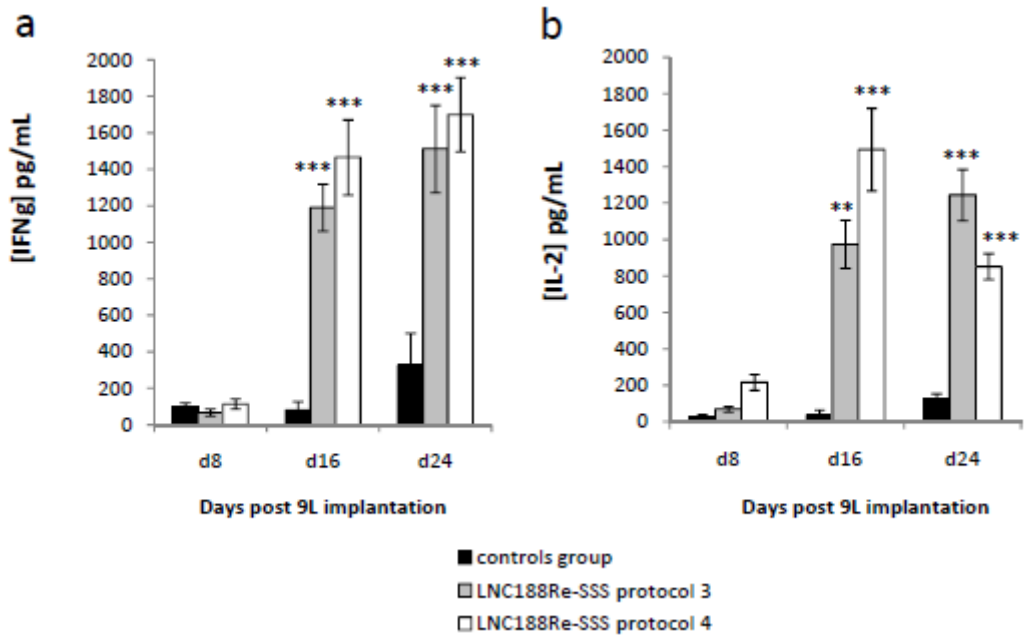

<u>Figure 4</u>: Peripheral cytokines (interleukin-2 and interferon-ɣ) quantification
Concentrations of interferon-γ (IFNγ) (**a**) and interleukine-2 (IL-2) (**b**) for control group and LNC^{188}Re-SSS of each protocol. Results are expressed in pg/mL of IL-2 and IFNγ, mean ± SD. Comparison of IL-2 content in LNC^{188}Re-SSS groups versus control groups; **p<0.01; ***p<0.001

<u>Recruitment and activation of immune and inflammatory cells within the central nervous system after LNC^{188}Re-SSS treatment.</u>

In order to evaluate locoregional immunostimulating effects of LNC^{188}Re-SSS versus blank LNC, the immunostaining of central nervous system (CNS) infiltrating or resident immune cells was assessed and illustrated for protocol 4, with results similar to those observed in protocol 3 (Figures 5a-b). Immunostaining of brain cryosections at D15 demonstrated a stronger activation of monocyte-macrophage-microglia in LNC^{188}Re-SSS-treated animals, as proven by the ameboid shape of OX42-positive cells (42, 43) .In addition, an improved recruitment of natural killer (CD161a) and dendritic cells (OX62) was observed from D15 to D25, with a slight decrease at D32.

MHC class II (OX6) over-expression in LNC^{188}Re-SSS-treated rats confirmed the recruitment and activation of inflammatory and immune cells in the CNS. Strong induction of MCH class I (OX18), whether it was present on the glioma cells themselves or on antigen-presenting cells, provided evidence in favor of an improved capability to develop an antitumor immune response. As effectors of the antitumor immune response, such as CD4 and CD8 positive cells, were absent at D15, they were progressively recruited in the CNS tumors at D25 and D32 (Figures 5a-b).

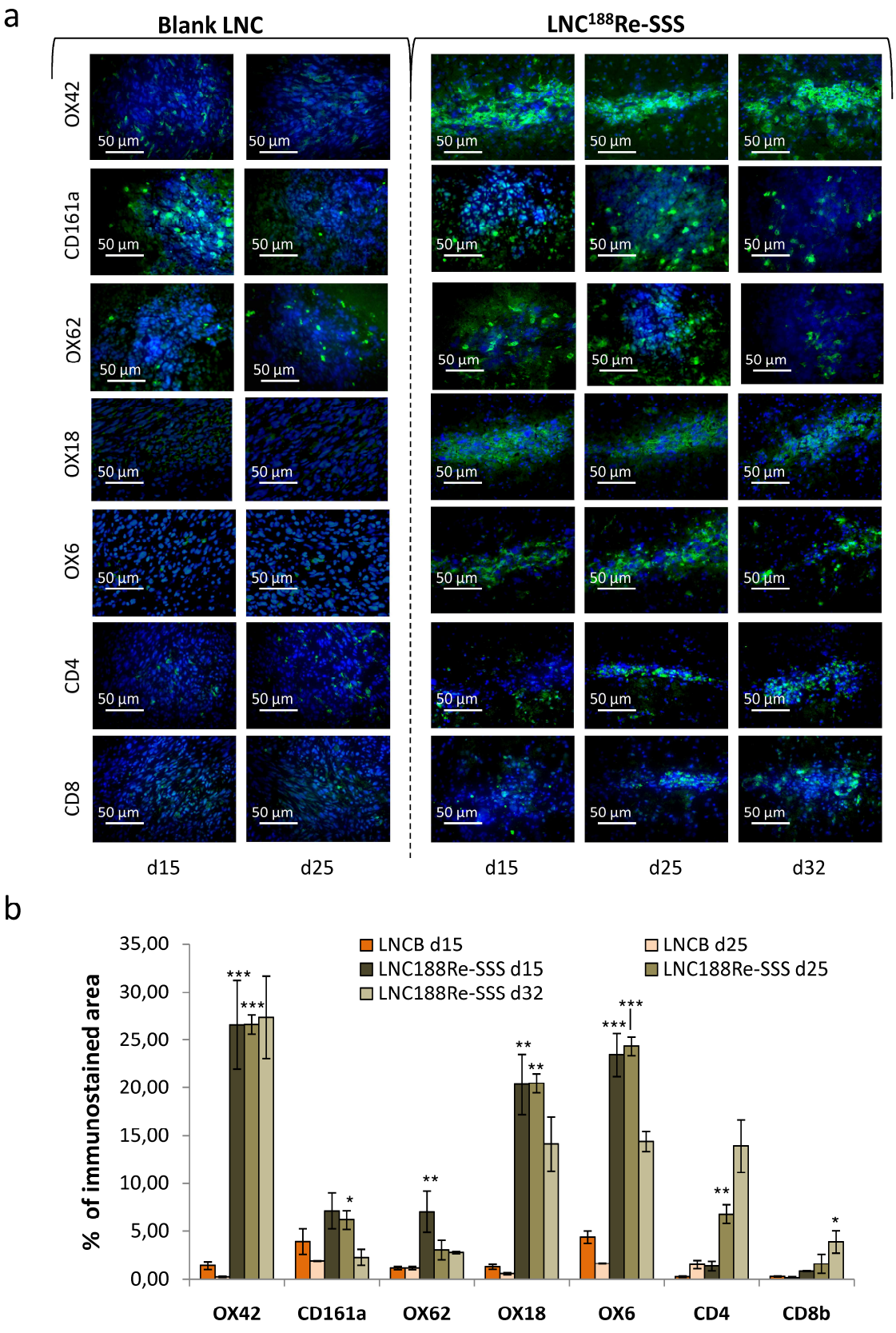

Figure 5: Recruitment and activation of immune and inflammatory cells within the central nervous system after LNC^{188}Re-SSS treatment.

a: Immunohistochemistry staining of macrophage cells (OX42), natural killer cells (OX61), major histocompatibility (class I - OX18; class II – OX6), dendritic cells (CD161a), and T lymphocytes cells (CD4 and CD8) of protocol 3 and 4 of the D6/D12 fractionated study. **b**: Semi-Quantitative results of immunohistochemistry. Results are expressed in % of immunostaining area after their determination with MetaMorph software.

Rechallenge in long-term survivors reveals immune protection.

In order to validate this immune response, long-term animal survivors obtained with protocols 3 and 4 were re-challenged with implantation of 1 000 9L cells in the left striatum. Regardless of the fractionated internal radiation timing used (D6/D12, Figure 6a; D12/D18, Figure 6b), median survival was significantly improved (from 35 to 37 days) when compared to control animals (25 days). Moreover, one long-term survivor was obtained for treatment at D6/D12 with protocol 4 and for treatment at D12/18 with protocols 3 and 4, thus representing 3 in 17 animals included in the study.

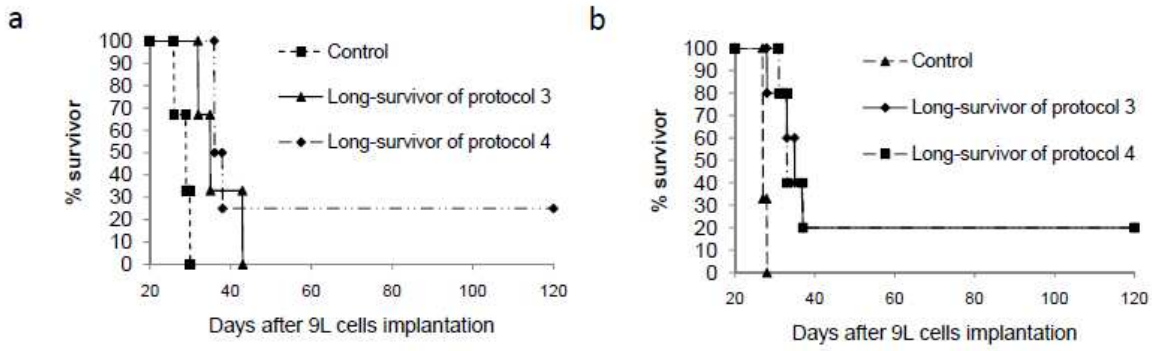

Figure 6: Rechallenge in long-term survivors.

a: Kaplan-Meier survival curves of re-challenged long-term survivors from the D6/D12 fractionated internal radiation study. **b**: Kaplan-Meier survival curves of re-challenged long-term survivors from the D12/D18 fractionated internal radiation study

DISCUSSION

In this study, we evaluated internal radiation using lipid nanocapsules loaded with Rhenium-188 and resulting dose-dependent bystander effects on an orthotopic glioma model.

The first part of this manuscript highlights the advantages of using lipid nanocapsules for entrapping Rhenium-188 as physico-chemical properties of LNC prevail over those of Rhenium-188. As a consequence, elimination of Rhenium-188 is very low and the main radioactivity is maintained within the brain.

The originality of this strategy is to apply a dose gradient as the best survival benefits were observed after the combination of the simple and CED injections. This therapeutic effect can be explained by the cellular heterogeneity of the tumor mass. Indeed, solid tumor are heterogenous from the point of view of histology with inflammatory infiltrates and vascular structures (44). Moreover, it has been established that the tumor mass is hierarchically organized with different subpopulation of cancer cells (45). Recently, a highly tumorogenic glioma tumor subpopulation, termed cancer stem cell or tumor-initiating cell (46-49), has been shown to promote therapeutic resistance and could be an explanation of the treatment failure of glioblastoma (50, 51). Thus, we can assume that the injection of LNC^{188}Re-SSS by the combination of the simple and CED injections, target different types of radiosensitive and radioresistant sub-cellular populations within the tumor mass. This hypothesis needs to be supported by further developments, however, these conclusions are important to consider as it is not possible to modify the distribution of the radiations with external beam radiation, the gold-standard adjuvant treatment for gliomas.

Although radiation-induced apoptosis has extensively been studied over the past decade, it is not a major form of cell death (approximately for 20%) (52). Other forms of non-apoptotic cell death have been described which include mitotic catastrophe, necrosis, autophagy and senescence (53). Taken together, our data suggest that distribution of ionizing radiation were different according the simple and CED injections. Hence, we can suppose that these two techniques might lead to different kind of cell death which could be effective in the eradication of glioma tumors when they are associated.

In this study we decided to treat animals at days 6/12 and 12/18 following 9L cells implantation. No significant differences were noticed between early and late care of the tumor. Nevertheless, D12/D18 fractionated internal radiation study highlights bystander effects as tumor regression, observed on MRI images, only began 7 days after the last LNC^{188}Re-SSS injection (25 following 9L cells implantation). Thus, excessive reactive oxygen species production cannot be the only reason of this treatment efficacy.

Considerable evidences indicate that radiation therapy effects extend beyong the induction of apoptosis with the ability of radiation therapy to create dose-dependent bystander effects. In our study, we have investigated whether an adaptative immune response was involved in the tumor regression observed after internal radiation with combined protocols (Protocol 3: CED+simple; Protocol 4: simple+CED). A peripheral stimulation of the immune system was highlighted with major increase of interleukin-2 (IL-2) and interferon-γ (IFNγ) cytokines at days 16 and 24 following 9L cells implantations. Moreover, we established that cells involved in the induction of inflammatory responses, innate immunity, and adaptative immunity were present form early to late stages of glioblastoma development after nanovectorized internal radiation. Our internal radiation strategy also gave rise to the

induction of a memory antitumor response as long-term survivors were partially or totally immunized after re-injection of 9L cells.

To conclude, the fractionated locoregional implantation of LNC^{188}Re-SSS supported the reversal of immune suppressive barriers in the brain. Although the immunization process remained incomplete, as the animals were not all protected, these data are primary of significance for developing new anti-glioblastoma strategies.

ACKNOWLEDGEMENTS

We are grateful to Pr. Nicolas Noiret and Dr. Virginie Cadeillan for kits kindly provided by the organic synthesis plateform of the *Cancéropôle Grand Ouest, axe vectorisation tumorale et radiothérapie*. We are also grateful to Pierre Legras and Jérome Roux (*Service Commun d'Animalerie Hospitalo – Universitaire, Angers, France*) for their technical assistance in animal experiments. This work received grants from the *Cancéropôle Grand Ouest* and the *Ligue Contre le Cancer (*«équipe labellisée 2007» and «comité départemental du Maine-et-Loire»). Claire Vanpouille-Box was a fellow from Angers Loire Métropôle.

REFERENCES

1. Bondy, M.L., M.E. Scheurer, B. Malmer, J.S. Barnholtz-Sloan, F.G. Davis, D. Il'yasova, C. Kruchko, B.J. McCarthy, P. Rajaraman, J.A. Schwartzbaum, S. Sadetzki, B. Schlehofer, T. Tihan, J.L. Wiemels, M. Wrensch, and P.A. Buffler. 2008. Brain tumor epidemiology: consensus from the Brain Tumor Epidemiology Consortium. *Cancer* 113:1953-1968.
2. Stupp, R., W.P. Mason, M.J. van den Bent, M. Weller, B. Fisher, M.J. Taphoorn, K. Belanger, A.A. Brandes, C. Marosi, U. Bogdahn, J. Curschmann, R.C. Janzer, S.K. Ludwin, T. Gorlia, A. Allgeier, D. Lacombe, J.G. Cairncross, E. Eisenhauer, and R.O. Mirimanoff. 2005. Radiotherapy plus concomitant and adjuvant temozolomide for glioblastoma. *N Engl J Med* 352:987-996.
3. Muldoon, L.L., C. Soussain, K. Jahnke, C. Johanson, T. Siegal, Q.R. Smith, W.A. Hall, K. Hynynen, P.D. Senter, D.M. Peereboom, and E.A. Neuwelt. 2007. Chemotherapy delivery issues in central nervous system malignancy: a reality check. *J Clin Oncol* 25:2295-2305.
4. Schumacher, T., S. Hofer, K. Eichhorn, M. Wasner, S. Zimmerer, P. Freitag, A. Probst, O. Gratzl, J.C. Reubi, R. Maecke, J. Mueller-Brand, and A. Merlo. 2002. Local injection of the 90Y-labelled peptidic vector DOTATOC to control gliomas of WHO grades II and III: an extended pilot study. *Eur J Nucl Med Mol Imaging* 29:486-493.
5. Reardon, D.A., J.A. Quinn, G. Akabani, R.E. Coleman, A.H. Friedman, H.S. Friedman, J.E. Herndon, 2nd, R.E. McLendon, C.N. Pegram, J.M. Provenzale, J.M. Dowell, J.N. Rich, J.J. Vredenburgh, A. Desjardins, J.H. Sampson, S. Gururangan, T.Z. Wong, M.A. Badruddoja, X.G. Zhao, D.D. Bigner, and M.R. Zalutsky. 2006. Novel human IgG2b/murine chimeric antitenascin monoclonal antibody construct radiolabeled with 131I and administered into the surgically created resection cavity of patients with malignant glioma: phase I trial results. *J Nucl Med* 47:912-918.

6. Casaco, A., G. Lopez, I. Garcia, J.A. Rodriguez, R. Fernandez, J. Figueredo, L. Torres, A. Perera, J. Batista, R. Leyva, Y. Pena, Z. Amador, A. Gonzalez, B. Estupinan, M. Coca, A. Hernandez, M. Puig, M. Iglesias, A. Hernandez, M. Ramos, L. Rodriquez, and N. Suarez. 2008. Phase I single-dose study of intracavitary-administered Nimotuzumab labeled with 188 Re in adult recurrent high-grade glioma. *Cancer Biol Ther* 7:333-339.

7. Caruthers, S.D., S.A. Wickline, and G.M. Lanza. 2007. Nanotechnological applications in medicine. *Curr Opin Biotechnol* 18:26-30.

8. Heurtault, B., P. Saulnier, B. Pech, J.E. Proust, and J.P. Benoit. 2002. A novel phase inversion-based process for the preparation of lipid nanocarriers. *Pharm Res* 19:875-880.

9. Allard, E., N.T. Huynh, A. Vessieres, P. Pigeon, G. Jaouen, J.P. Benoit, and C. Passirani. 2009. Dose effect activity of ferrocifen-loaded lipid nanocapsules on a 9L-glioma model. *Int J Pharm* 379:317-323.

10. Hureaux, J., F. Lagarce, F. Gagnadoux, L. Vecellio, A. Clavreul, E. Roger, M. Kempf, J.L. Racineux, P. Diot, J.P. Benoit, and T. Urban. 2009. Lipid nanocapsules: ready-to-use nanovectors for the aerosol delivery of paclitaxel. *Eur J Pharm Biopharm* 73:239-246.

11. Lacoeuille, F., F. Hindre, F. Moal, J. Roux, C. Passirani, O. Couturier, P. Cales, J.J. Le Jeune, A. Lamprecht, and J.P. Benoit. 2007. In vivo evaluation of lipid nanocapsules as a promising colloidal carrier for paclitaxel. *Int J Pharm* 344:143-149.

12. Vonarbourg, A., C. Passirani, L. Desigaux, E. Allard, P. Saulnier, O. Lambert, J.P. Benoit, and B. Pitard. 2009. The encapsulation of DNA molecules within biomimetic lipid nanocapsules. *Biomaterials* 30:3197-3204.

13. Garcion, E., A. Lamprecht, B. Heurtault, A. Paillard, A. Aubert-Pouessel, B. Denizot, P. Menei, and J.P. Benoit. 2006. A new generation of anticancer, drug-loaded, colloidal vectors reverses multidrug resistance in glioma and reduces tumor progression in rats. *Mol Cancer Ther* 5:1710-1722.

14. Lamprecht, A., and J.P. Benoit. 2006. Etoposide nanocarriers suppress glioma cell growth by intracellular drug delivery and simultaneous P-glycoprotein inhibition. *J Control Release* 112:208-213.

15. Roger, E., F. Lagarce, E. Garcion, and J.P. Benoit. 2010. Reciprocal competition between lipid nanocapsules and P-gp for paclitaxel transport across Caco-2 cells. *Eur J Pharm Sci* 40:422-429.

16. Paillard, A., F. Hindre, C. Vignes-Colombeix, J.P. Benoit, and E. Garcion. 2010. The importance of endo-lysosomal escape with lipid nanocapsules for drug subcellular bioavailability. *Biomaterials* 31:7542-7554.

17. Allard, E., F. Hindre, C. Passirani, L. Lemaire, N. Lepareur, N. Noiret, P. Menei, and J.P. Benoit. 2008. 188Re-loaded lipid nanocapsules as a promising radiopharmaceutical carrier for internal radiotherapy of malignant gliomas. *Eur J Nucl Med Mol Imaging* 35:1838-1846.

18. Vinchon-Petit, S., D. Jarnet, A. Paillard, J.P. Benoit, E. Garcion, and P. Menei. In vivo evaluation of intracellular drug-nanocarriers infused into intracranial tumours by convection-enhanced delivery: distribution and radiosensitisation efficacy. *J Neurooncol* 97:195-205.

19. Bucci, B., S. Misiti, A. Cannizzaro, R. Marchese, G.H. Raza, R. Miceli, A. Stigliano, D. Amendola, O. Monti, M. Biancolella, F. Amati, G. Novelli, A. Vecchione, E. Brunetti, and U. De Paula. 2006. Fractionated ionizing radiation exposure induces apoptosis through caspase-3 activation and reactive oxygen species generation. *Anticancer Res* 26:4549-4557.

20. Guo, G., Y. Yan-Sanders, B.D. Lyn-Cook, T. Wang, D. Tamae, J. Ogi, A. Khaletskiy, Z. Li, C. Weydert, J.A. Longmate, T.T. Huang, D.R. Spitz, L.W. Oberley, and J.J. Li. 2003. Manganese superoxide dismutase-mediated gene expression in radiation-induced adaptive responses. *Mol Cell Biol* 23:2362-2378.

21. Morgan, W.F., and M.B. Sowa. 2007. Non-targeted bystander effects induced by ionizing radiation. *Mutat Res* 616:159-164.

22. Pasi, F., A. Facoetti, and R. Nano. 2010. IL-8 and IL-6 bystander signalling in human glioblastoma cells exposed to gamma radiation. *Anticancer Res* 30:2769-2772.

23. Galluzzi, L., M.C. Maiuri, I. Vitale, H. Zischka, M. Castedo, L. Zitvogel, and G. Kroemer. 2007. Cell death modalities: classification and pathophysiological implications. *Cell Death Differ* 14:1237-1243.

24. Formenti, S.C., and S. Demaria. 2009. Systemic effects of local radiotherapy. *Lancet Oncol* 10:718-726.

25. Apetoh, L., F. Ghiringhelli, A. Tesniere, M. Obeid, C. Ortiz, A. Criollo, G. Mignot, M.C. Maiuri, E. Ullrich, P. Saulnier, H. Yang, S. Amigorena, B. Ryffel, F.J. Barrat, P. Saftig, F. Levi, R. Lidereau, C. Nogues, J.P. Mira, A. Chompret, V. Joulin, F. Clavel-Chapelon, J. Bourhis, F. Andre, S. Delaloge, T. Tursz, G. Kroemer, and L. Zitvogel. 2007. Toll-like receptor 4-dependent contribution of the immune system to anticancer chemotherapy and radiotherapy. *Nat Med* 13:1050-1059.

26. Coates, P.J., J.K. Rundle, S.A. Lorimore, and E.G. Wright. 2008. Indirect macrophage responses to ionizing radiation: implications for genotype-dependent bystander signaling. *Cancer Res* 68:450-456.

27. Larsson, M., J.F. Fonteneau, and N. Bhardwaj. 2001. Dendritic cells resurrect antigens from dead cells. *Trends Immunol* 22:141-148.

28. Hallahan, D.E., D.R. Spriggs, M.A. Beckett, D.W. Kufe, and R.R. Weichselbaum. 1989. Increased tumor necrosis factor alpha mRNA after cellular exposure to ionizing radiation. *Proc Natl Acad Sci U S A* 86:10104-10107.

29. Hong, J.H., C.S. Chiang, I.L. Campbell, J.R. Sun, H.R. Withers, and W.H. McBride. 1995. Induction of acute phase gene expression by brain irradiation. *Int J Radiat Oncol Biol Phys* 33:619-626.

30. Hong, J.H., C.S. Chiang, C.Y. Tsao, P.Y. Lin, W.H. McBride, and C.J. Wu. 1999. Rapid induction of cytokine gene expression in the lung after single and fractionated doses of radiation. *Int J Radiat Biol* 75:1421-1427.

31. Ishihara, H., K. Tsuneoka, A.B. Dimchev, and M. Shikita. 1993. Induction of the expression of the interleukin-1 beta gene in mouse spleen by ionizing radiation. *Radiat Res* 133:321-326.

32. McBride, W.H., C.S. Chiang, J.L. Olson, C.C. Wang, J.H. Hong, F. Pajonk, G.J. Dougherty, K.S. Iwamoto, M. Pervan, and Y.P. Liao. 2004. A sense of danger from radiation. *Radiat Res* 162:1-19.

33. Roses, R.E., M. Xu, G.K. Koski, and B.J. Czerniecki. 2008. Radiation therapy and Toll-like receptor signaling: implications for the treatment of cancer. *Oncogene* 27:200-207.

34. Bennewitz, N.L., and J.E. Babensee. 2005. The effect of the physical form of poly(lactic-co-glycolic acid) carriers on the humoral immune response to co-delivered antigen. *Biomaterials* 26:2991-2999.

35. Hunter, R., F. Strickland, and F. Kezdy. 1981. The adjuvant activity of nonionic block polymer surfactants. I. The role of hydrophile-lipophile balance. *J Immunol* 127:1244-1250.

36. Little, S.R., D.M. Lynn, Q. Ge, D.G. Anderson, S.V. Puram, J. Chen, H.N. Eisen, and R. Langer. 2004. Poly-beta amino ester-containing microparticles enhance the activity of nonviral genetic vaccines. *Proc Natl Acad Sci U S A* 101:9534-9539.

37. Reddy, S.T., M.A. Swartz, and J.A. Hubbell. 2006. Targeting dendritic cells with biomaterials: developing the next generation of vaccines. *Trends Immunol* 27:573-579.

38. Yoshida, M., and J.E. Babensee. 2004. Poly(lactic-co-glycolic acid) enhances maturation of human monocyte-derived dendritic cells. *J Biomed Mater Res A* 71:45-54.

39. Lepareur N, N.N.a.H.J. 2004. A kit formulation for the labelling of lipiodol with generator-produced 188Re. *Journal of Labelled Compounds and Radiopharmaceuticals* 47:857-867.

40. Recinos, V.R., B.M. Tyler, K. Bekelis, S.B. Sunshine, A. Vellimana, K.W. Li, and H. Brem. 2010. Combination of intracranial temozolomide with intracranial carmustine improves survival when compared with either treatment alone in a rodent glioma model. *Neurosurgery* 66:530-537; discussion 537.

41. Roth, W., and M. Weller. 1999. Chemotherapy and immunotherapy of malignant glioma: molecular mechanisms and clinical perspectives. *Cell Mol Life Sci* 56:481-506.

42. Bhat, R., and L. Steinman. 2009. Innate and adaptive autoimmunity directed to the central nervous system. *Neuron* 64:123-132.

43. Carpentier, P.A., and T.D. Palmer. 2009. Immune influence on adult neural stem cell regulation and function. *Neuron* 64:79-92.

44. Adams, J.M., and A. Strasser. 2008. Is tumor growth sustained by rare cancer stem cells or dominant clones? *Cancer Res* 68:4018-4021.

45. Diehn, M., and M.F. Clarke. 2006. Cancer stem cells and radiotherapy: new insights into tumor radioresistance. *J Natl Cancer Inst* 98:1755-1757.

46. Galli, R., E. Binda, U. Orfanelli, B. Cipelletti, A. Gritti, S. De Vitis, R. Fiocco, C. Foroni, F. Dimeco, and A. Vescovi. 2004. Isolation and characterization of tumorigenic, stem-like neural precursors from human glioblastoma. *Cancer Res* 64:7011-7021.

47. Hemmati, H.D., I. Nakano, J.A. Lazareff, M. Masterman-Smith, D.H. Geschwind, M. Bronner-Fraser, and H.I. Kornblum. 2003. Cancerous stem cells can arise from pediatric brain tumors. *Proc Natl Acad Sci U S A* 100:15178-15183.

48. Lee, J., S. Kotliarova, Y. Kotliarov, A. Li, Q. Su, N.M. Donin, S. Pastorino, B.W. Purow, N. Christopher, W. Zhang, J.K. Park, and H.A. Fine. 2006. Tumor stem cells derived from glioblastomas cultured in bFGF and EGF more closely mirror the phenotype and genotype of primary tumors than do serum-cultured cell lines. *Cancer Cell* 9:391-403.

49. Singh, S.K., C. Hawkins, I.D. Clarke, J.A. Squire, J. Bayani, T. Hide, R.M. Henkelman, M.D. Cusimano, and P.B. Dirks. 2004. Identification of human brain tumour initiating cells. *Nature* 432:396-401.

50. Bao, S., Q. Wu, R.E. McLendon, Y. Hao, Q. Shi, A.B. Hjelmeland, M.W. Dewhirst, D.D. Bigner, and J.N. Rich. 2006. Glioma stem cells promote radioresistance by preferential activation of the DNA damage response. *Nature* 444:756-760.

51. Dean, M., T. Fojo, and S. Bates. 2005. Tumour stem cells and drug resistance. *Nat Rev Cancer* 5:275-284.

52. Verheij, M., and H. Bartelink. 2000. Radiation-induced apoptosis. *Cell Tissue Res* 301:133-142.

53. Lefranc, F., J. Brotchi, and R. Kiss. 2005. Possible future issues in the treatment of glioblastomas: special emphasis on cell migration and the resistance of migrating glioblastoma cells to apoptosis. *J Clin Oncol* 23:2411-2422.

54. Vinchon-Petit, S., D. Jarnet, A. Paillard, J.P. Benoit, E. Garcion, and P. Menei. 2010. In vivo evaluation of intracellular drug-nanocarriers infused into intracranial tumours by convection-enhanced delivery: distribution and radiosensitisation efficacy. *J Neurooncol* 97:195-205.

CONCLUSIONS

Pour cette étude, une radiothérapie interne fractionée par injections stéréotaxiques de NCL^{188}Re-SSS a été menée dans un modèle de gliome 9L. Deux types d'injection ont été retenus avec l'injection par SI (ijection simple ; volume final: 10 µL ; débit 1µL/min ; activité injectée: 2,8 MBq) et l'injection par « Convection Enhanced Delivery » (CED ; volume final: 60 µL : débit 0,5 µL/min ; activité injectée: 2,8 MBq). Nous avons pu observer que ces deux types d'injection n'influent pas sur la biodistribution puisqu'une rétention cérébrale de 78% jusqu'à 96h post-injection de NCL^{188}Re-SSS a été démontrée. Seule la distribution au sein du cerveau lui-même diffère, ce qui, par combinaison des deux types d'injection, conduit à l'application d'un gradient d'activité radioactif, à l'origine d'un bénéfice de survie remarquable (taux de guérison des animaux: 83%).

Comme supposé, l'activation du système immunitaire a été soulignée par stimulation périphérique des cytokines interleukine-2 et interféron-γ. Ceci s'accompagne également d'un recrutement local de cellules immunitaires effectrices (CD4+, CD8+) et d'un processus d'immunisation puisque 14/17 animaux sont partiellement ou totalement (3/17) immunisés après ré-injection de cellules 9L.

Cette étude est l'une des premières à décrire des effets indirects à l'intérieur et en dehors du champ de traitement après radiothérapie interne nanovectorisée. En raison du statut immunitaire privilégié du cerveau, cette étude suggère de nouvelles perspectives incluant les combinaisons de traitement à visée immunothérapeutique.

Chapitre IV

Nanocapsules lipidiques chargées en rhénium-188 et stimulation de la réponse immunitaire.

Dans le chapitre précédent, nous avons vu que des injections répétées de NCL^{188}Re-SSS permettent la mise en place d'une réponse immunitaire adaptative pouvant être à l'origine de la régression tumorale. Ces résultats offrent de nouvelles perspectives pour le traitement du glioblastome, cependant, il faut être prudent dans l'analyse de ces données puisque le modèle de tumeur 9L est caractérisé comme étant peu invasif et fortement immunogène (Barth and Kaur 2009) (Figure 1). C'est dans ce contexte que nous avons changé de modèle tumoral par un modèle de tumeur F98, connu pour simuler les glioblastomes humains avec notamment les caractères hautement invasifs, immunosuppresseurs et radiorésistants (Tzeng, Barth et al. 1991; Paul, Barth et al. 2000; Clavreul, Delhaye et al. 2006).

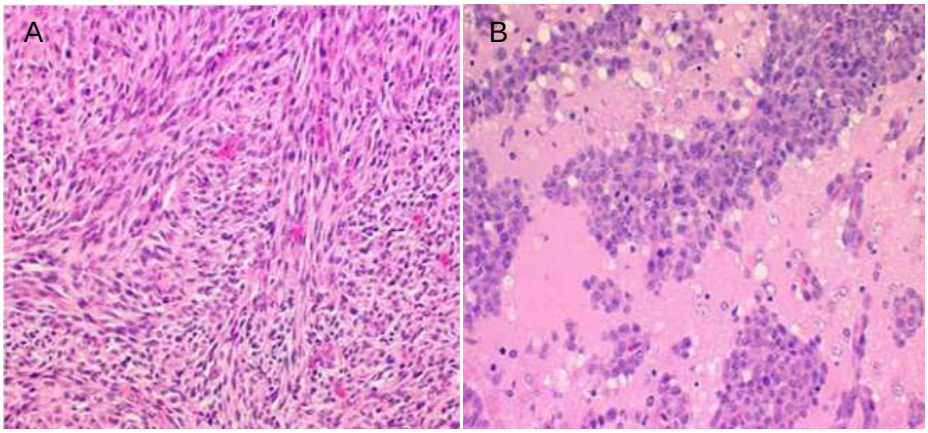

Figure 1: **A**- Le gliosarcome 9L composé de cellules fusiformes avec un aspect sarcomateux. Le modèle de croissance verticillée est observé avec une délimitation nette des zones tumorales et peu d'envahissement au niveau du cerveau normal contigu. **B**- Le gliome F98 est composé d'une population mixte de cellules et une sous-population de cellules polygonales avec des noyaux ronds à ovales. L'invasion tumorale dans le tissu sain adjacent est importante avec des îlots de cellules tumorales à distances variables de la masse tumorale principale (d'après Barth *et al*.)

I-NANOCAPSULES LIPIDIQUES CHARGEES EN RHENIUM-188 ET MODELE DE TUMORAL GLIAL F98.

I-1- Administration de 2,8 MBq par injection

L'évaluation d'une radiothérapie interne fractionnée a été réalisée pour le traitement des tumeurs gliales F98. Pour cela, des rats Fischer femelle de 10 semaines ont reçu deux injections de 2,8 MBq de $NCL^{188}Re$-SSS (dose équivalente approximative: 8Gy) aux jours 6 et 12 post-implantation de 500 cellules F98 (J0) (Figure 2).

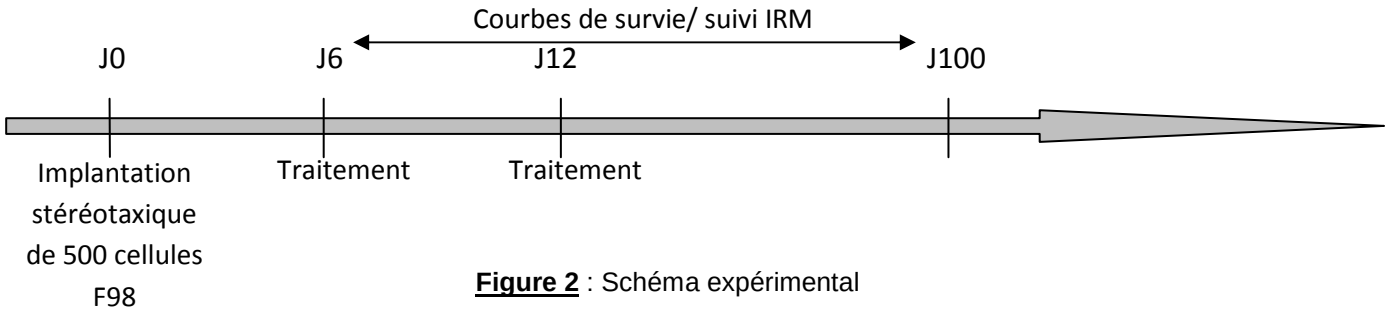

Figure 2 : Schéma expérimental

La combinaison des deux types d'injections (injection simple – SI – et CED) a démontré une efficacité remarquable en terme de survie au sein d'un modèle tumoral glial 9L (cf. chapitre III), ainsi, nous nous sommes focalisés sur les deux protocoles correspondant : le protocole 3 (CED+SI) et le protocole 4 (SI+CED). Chaque protocole comporte 3 groupes d'animaux randomisés selon les solutions administrées ($NCL^{188}Re$-SS, n=8; NCL Blanches, n=4 ; sérum physiologique, n=4). Les critères d'évaluations restent identiques au chapitre précédent, avec un suivi de la survie globale des animaux et de la progression tumorale par IRM.

Les résultats obtenus témoignent montrent un ralentissement de la progression tumorale, observée aussi bien sur les courbes de survie (Figure 3) que sur les images IRM (Figure 4). En effet, la médiane de survie des rats contrôles est de 26,5 jours tandis qu'elle

est de 36 et 40 jours pour les animaux ayant reçu une radiothérapie interne fractionnée selon les protocoles 3 et 4 respectivement. Cependant, la radiorésistance de ce modèle est responsable d'une augmentation de la médiane de survie nettement inférieure à celles obtenues avec le modèle 9L (Protocole 3 : médiane de survie de 77 jours ; Protocole 4 : médiane de survie >100 jours). Il semble donc nécessaire d'adapter notre stratégie de radiothérapie interne via les NCL^{188}Re-SSS selon le type tumoral à traiter.

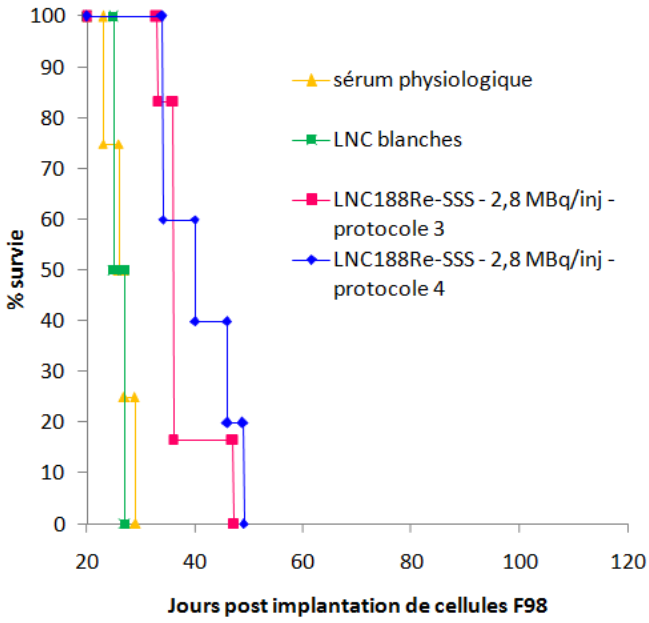

Figure 3 : Courbes de survie Kaplan-Meier des animaux traités aux jours 6 et 12 post implantation de cellules F98, 2,8 MBq aux jours 6 et 12 de NCL^{188}Re-SSS (n=6), nanocapsules blanches (n=4), sérum physiologique (n=4). (Protocole 3: CED + SI – Protocole 4: SI + CED)

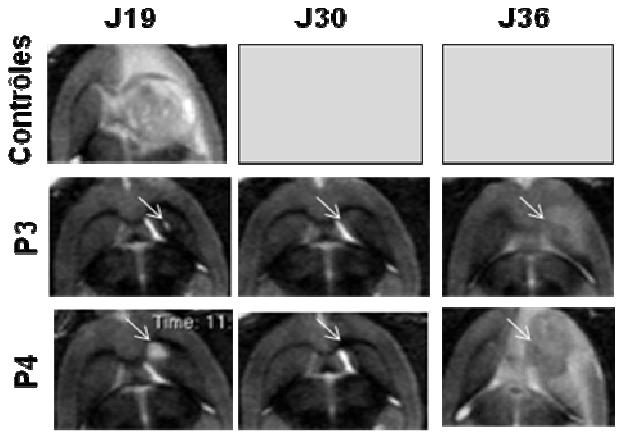

Figure 4 : Images IRM pondérées T2 des animaux contrôles et des rats traités via les NCL^{188}Re-SSS. (P3 : CED + SI – P4 : SI + CED)

I-2- Administration de 3,7 MBq par injection

Devant les résultats obtenus, nous avons décidé d'augmenter l'activité par injection de 3,7 MBq (dose équivalente approximative : 10Gy), le schéma expérimental reste identique avec deux injections de NCL^{188}Re-SSS aux jours 6 et 12 post-implantation de cellules F98 (protocoles 3 et 4 : CED+SI et SI+CED respectivement).

Comme l'illustrent les figures 5 et 6, les résultats sont encourageants avec une médiane de survie de 48,5 et 53 jours et l'obtention de 2/8 et 3/8 long-survivants pour les protocoles 3 et 4 respectivement (Figure 5 et 6).

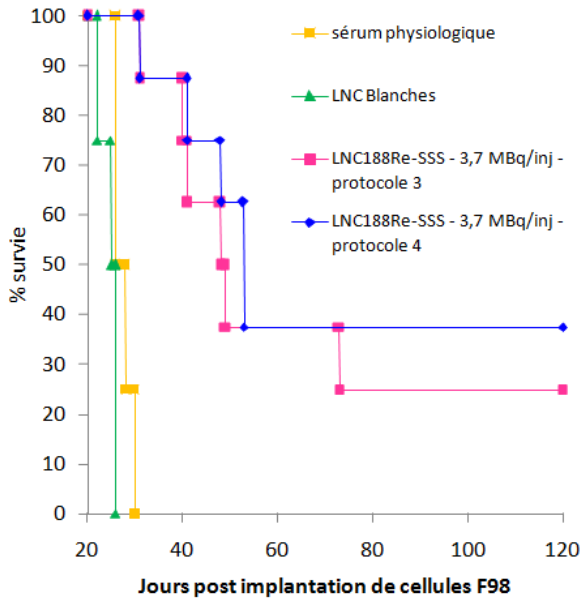

Figure 5 : Courbes de survie Kaplan-Meier des animaux traités aux jours 6 et 12 post implantation de cellules F98, 3,7 MBq aux jours 6 et 12 de NCL^{188}Re-SSS (n=8), nanocapsules blanches (n=4), sérum physiologique (n=4). (Protocole 3 : CED + SI; 2/8 long-survivant >120 jours – Protocole 4 : SI + CED; 3/8 long-survivant >120 jours)

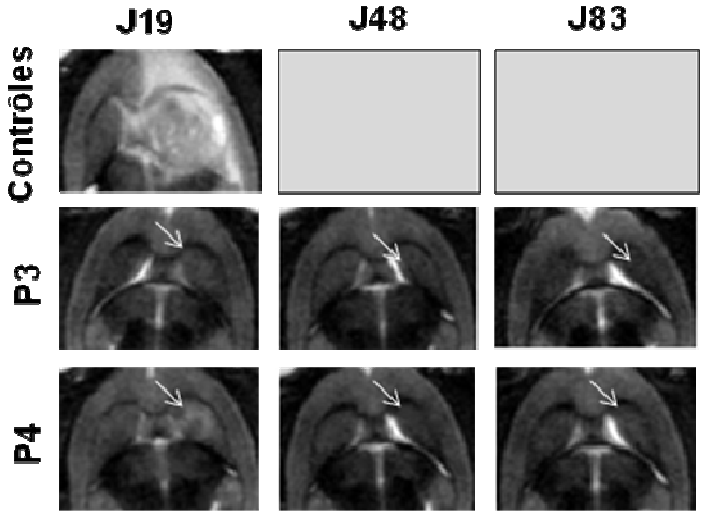

Figure 6: Images IRM pondérées T2 des animaux contrôles et des rats traités via les NCL^{188}Re-SSS. (P3: CED + SI – P4: SI + CED)

Même si l'augmentation de l'activité injectée a montré une meilleure efficacité, celle-ci reste inférieure à celle obtenue dans le chapitre précédent. Cette efficacité thérapeutique moins élevée peut s'expliquer par la faible immunogénicité du modèle tumoral F98. En effet, dans le chapitre précédent, nous avons démontré des effets indirects de l'irradiation, via les NCL^{188}Re-SSS, à l'extérieur du champ de traitement par l'acquisition d'une immunité spécifique anti-tumorale. L'efficacité thérapeutique de la radiothérapie interne nanovectorisée étant moins élevée dans un modèle connu comme étant peu immunogène, nous avons décidé de l'optimiser par la combinaison de stratégie à visée immunothérapeutique afin de renverser le caractère immunosuppresseur des F98 et donc permettre au système immunitaire d'interagir avec les radiations ionisantes comme observé dans le chapitre précédent.

II-NANOCAPSULES LIPIDIQUES CHARGEES EN RHENIUM-188 ET STIMULATION DU SYSTEME IMMUNITAIRE

II-1- Evaluation de la réponse immunitaire après injections répétées de 3,7 MBq

Afin de vérifier le caractère immunosuppresseur des tumeurs F98, nous avons, dans un premier temps, quantifié, par test ELISA, les cytokines interleukine-2 (IL-2) et interféron-γ (IFNγ) sur prélèvements plasmatiques aux jours 8, 16 et 24 après implantation de cellules F98. En effet, ces cytokines sont importantes dans la mise en place d'une réponse immunitaire anti-tumorale (Roth and Weller 1999).

Les résultats révèlent une activation du système périphérique avec une surproduction de ces cytokines à partir de J16 (Figure 7). Cependant, après comparaison aux résultats obtenus au sein du modèle 9L, les taux d'IL-2 et d'IFNγ sont deux fois inférieurs. L'activation du système pourrait donc être amoindrie, ce qui pourrait expliquer la faible efficacité de la radiothérapie interne nanovectorisée au sein du modèle de gliome F98.

Cette hypothèse a été vérifiée par immunomarquage des cellules immunitaires non spécifiques (macrophages – OX42, natural killer – CD161, cellules dendritiques – OX62) et des cellules immunitaires effectrices (complexe majeur d'histocompatibilité de classe I et de classe II – CMHI, OX18 et CMHII, 0X6; CD4+ et CD8+) (Figure 8).

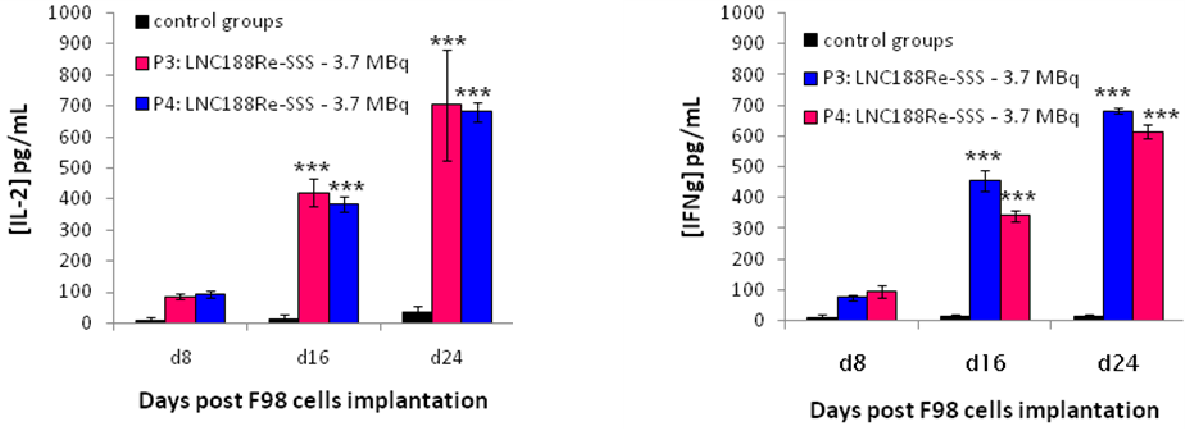

Figure 7 : Concentrations de l'interleukine-2 (IL-2) et de l'interféron-γ (IFNγ) pour les groupes contrôles et le groupe de NCL^{188}Re-SSS de chaque protocole. Les résultats sont exprimés en pg/mL d'IL-2 et d'IFNγ, moyenne ± écart-type. Comparaison des taux d'IL-2 et d'IFNγ par rapport aux groupes contrôles ; ***p<0,001.

Comme démontré dans le chapitre précédent, les NCL^{188}Re-SSS engendrent des effets indirects à l'intérieur du champ de traitement par recrutement de cellules immunitaires avec la présence d'un infiltrat inflammatoire (présence de macrophage dès J15 post implantation de cellules F98…). Notons le très faible recrutement de cellules dendritiques (OX62), cellules immunitaires clefs dans la mise en place d'une réponse immunitaire adaptative.

Néanmoins, contrairement au modèle tumoral 9L, le recrutement de cellules immunitaires est très faible et décroît à J25 post implantation de cellules. On peut donc supposer que la radiothérapie nanovectorisée est à l'origine d'une activation du système immunitaire, mais que le caractère immunosuppresseur des tumeurs F98 empêche le système immunitaire de maintenir les effets indirects en dehors du champ de traitement.

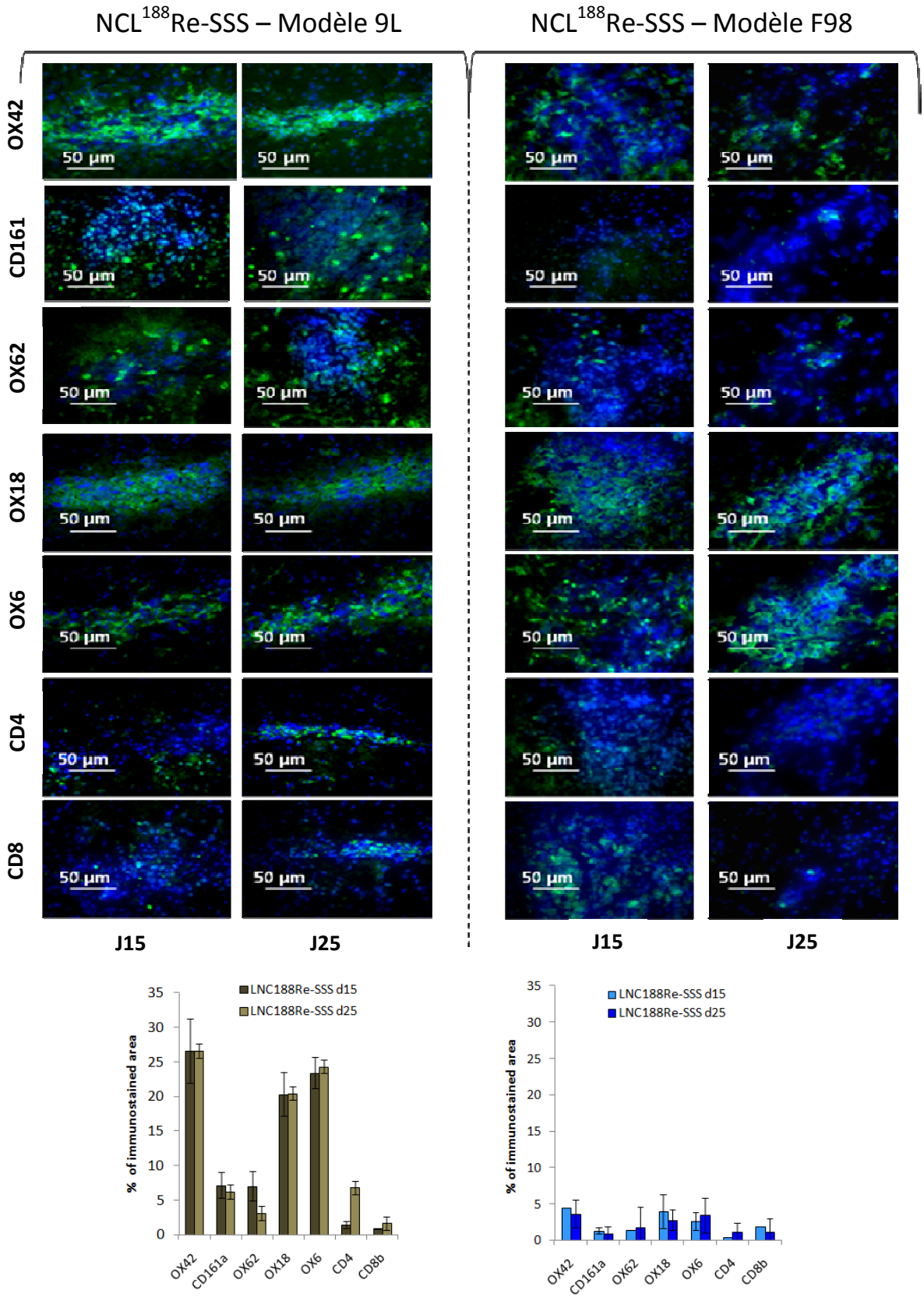

Figure 8 : Marquages immunohistochimiques des protocoles 3 (CED+SI) et 4 (SI+CED), des macrophages (OX42), des natural killer (CD161), des cellules dendritiques (OX62), CMHI (OX18), CMHII (OX6) et des cellules lymphocytaires (CD4+ et CD8+) dans les groupes NCL^{188}Re-SSS modèles 9L et F98 (J15, n=4 ; J25, n=4). Grossissement X400.

II-2- Stimulation du système immunitaire par vaccination de 2,5 millions de cellules F98 irradiées

Afin d'améliorer l'efficacité thérapeutique d'une radiothérapie interne nanovectorisée, nous avons débuté l'évaluation d'une stratégie de vaccination combinée aux NCL^{188}Re-SSS. En effet, exacerber le système immunitaire pourrait optimiser l'efficacité thérapeutique d'une radiothérapie nanovectorisée pour le traitement des tumeurs F98 puisque la stimulation périphérique des cytokines ainsi que le recrutement de cellules immunitaires sont moins élevés. Nous avons donc choisi de procéder à une vaccination de 2,5 millions de cellules F98 irradiées (40 Gy) que nous avons injectés en sous cutané (flanc droit) au jour 6 post-implantation de cellules F98 des animaux Fischer femelle de 10 semaines (Figure 10).

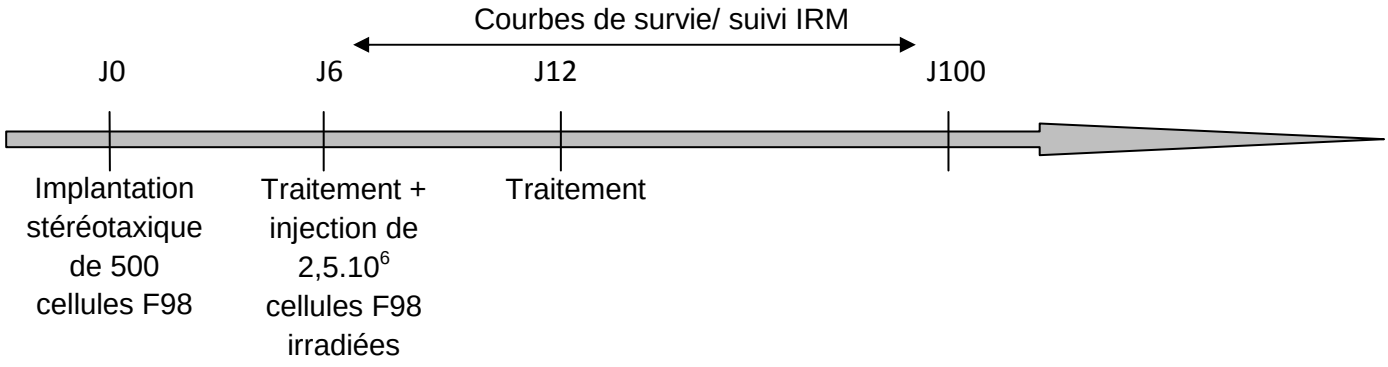

Figure 10 : Schéma expérimental

Nous nous sommes concentrés sur les protocoles 3 (CED+SI) et 4 (SI+CED). Chaque protocole compte 2 groupes d'animaux randomisés selon les solutions administrées (NCL^{188}Re-SSS + vaccination, n=8 ; sérum physiologique + vaccination, n=6). Les critères d'évaluations restent identiques au chapitre précédent, avec un suivi de la survie globale des animaux et de la progression tumorale par IRM, ainsi que l'évaluation du recrutement de cellules immunitaires.

La vaccination associée à la radiothérapie nanovectorisée conduit à une baisse de la médiane de survie pour le protocole 3 (médiane de survie de 42,5 jours au lieu de 48,5 jours

sans vaccination). Cependant, notons une légère augmentation de la médiane de survie au sein du protocole 4 avec une médiane de 65,5 jours au lieu de 53 jours sans vaccination (Figure 11).

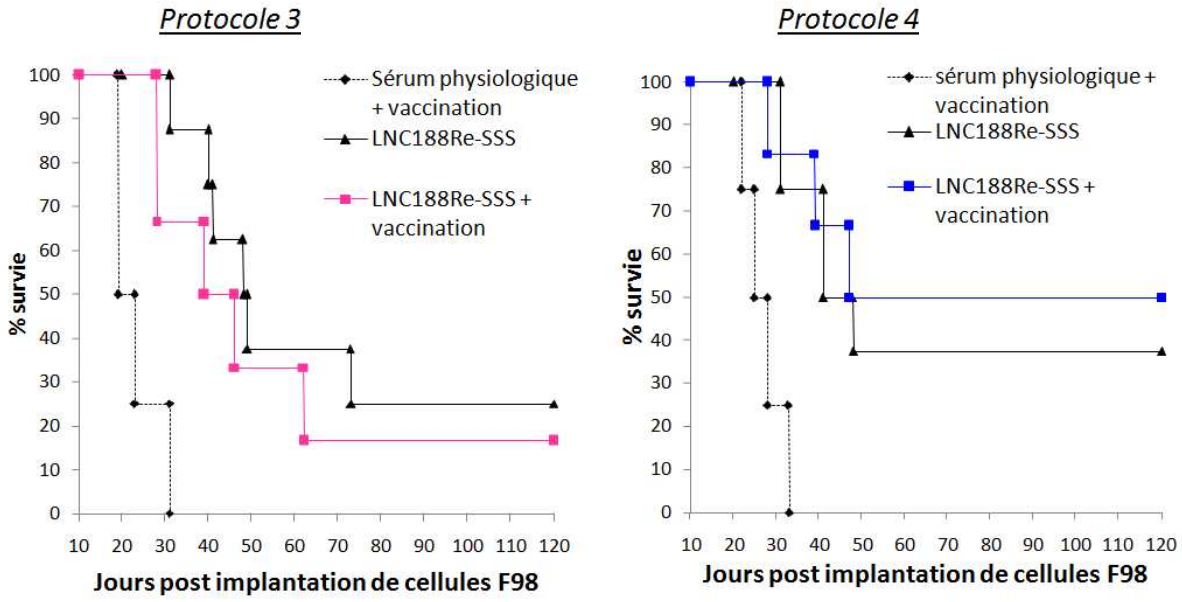

Figure 11 : Courbes de survie Kaplan-Meier des animaux traités via les NCL^{188}Re-SSS et ayant reçu 2,5.10^{6} cellules F98 irradiées aux jours 6 et 12 post implantation de cellules F98, 3,7 MBq aux jours 6 et 12 de NCL^{188}Re-SSS + vaccination (n=6), sérum physiologique + vaccination (n=4). (Protocole 3 : CED + SI; 1/6 long-survivant >120 jours – Protocole 4 : SI + CED; 3/6 long-survivant >120 jours)

Les résultats immunohistologiques démontrent un effet de la vaccination sur le recrutement cellulaire local lorsque celle-ci est associée aux NCL^{188}Re-SSS (Figure 12). Cependant, lorsque comparés avec les résultats obtenus dans le chapitre précédent, le recrutement des cellules immunitaires est toujours très faible, ce qui pourrait expliquer l'efficacité thérapeutique beaucoup moins élevée au sein de ce modèle F98 même après vaccination.

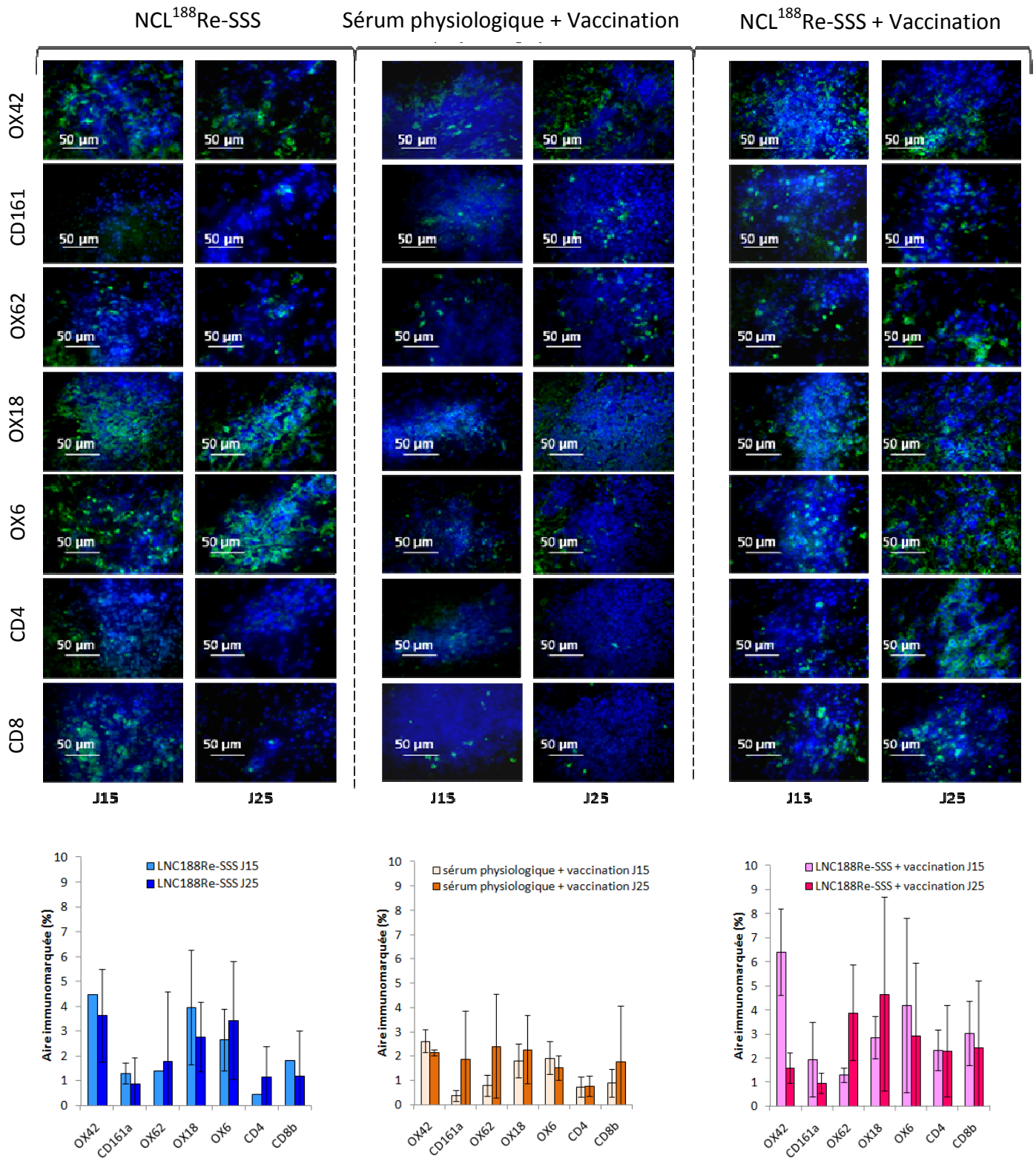

Figure 12 : Marquages immunohistochimiques des protocoles 3 (CED+SI) et 4 (SI+CED) des macrophages (OX42), des natural killer (CD161), des cellules dendritiques (OX62), du complexe majeur d'histocompatibilité de classe I (CMHI – OX18), du complexe majeur d'histocompatibilité de classe II (CMHII – OX6) et des cellules lymphocytaires (CD4+ et CD8+) dans les groupes NCL^{188}Re-SSS (n=8), sérum physiologique + vaccination (n=8) et NCL^{188}Re-SSS + vaccination (n=8) aux jours 15 et 25 post implantation de cellules F98. Grossissement X400.

III- CONCLUSIONS ET PERSPECTIVES

Pour conclure ce chapitre, notons que l'activation du système immunitaire semble être importante puisque la survie des animaux est moins élevée dans un modèle tumoral peu immunogène (modèle tumoral glial F98). La stimulation du système immunitaire par la vaccination de cellules F98 irradiées a pu montrer une amélioration du recrutement des cellules immunitaire, cependant, celle-ci reste trop faible pour induire une réponse immunitaire spécifique durable comme observé dans le modèle 9L (cf. chapitre III).

Le véritable challenge de la suite de ce travail réside dans la potentialisation du système immunitaire en association avec la radiothérapie nanovectorisée. En effet, le protocole vaccinal peut être modifié soit via une augmentation du nombre de cellules F98 irradiées injectées, soit via des injections répétées de cellules F98 irradiées. Le planning de vaccination peut également être amélioré, en effet, il est possible qu'une injection à J6 est trop précoce pour la stimulation du système immunitaire d'autant plus que les dosages de cytokines IL-2 et IFNγ indiquent une stimulation périphérique à partir de J16.
Une autre piste possible sera de modifié la stratégie vaccinale. En effet, l'immunothérapie des gliomes fait l'objet d'intenses recherches menant à d'autres thérapies prometteuses, toujours en cours d'évaluation. Parmi les stratégies les plus intéressantes, nous pouvons trouver le ciblage de l'EGFRvIII (Epidermal Growth Factor Receptor variant type III) et l'activation des cellules dendritiques par le Flt3L

III-1- Ciblage de l'EGFRvIII (Epidermal Receptor Growth Factor Receptor variant type III)

L'EGFRvIII est un exemple rare d'une mutation fréquente des tumeurs et joue un rôle central dans le processus néoplasique. Cette mutation consiste en une suppression de 801 paires

de bases du domaine extracellulaire de l'EGFR (Epidermal Growth Factor Receptor) qui va modifier un codon pour produire une nouvelle glycine au niveau de la jonction (Libermann, Nusbaum et al. 1985; Bigner, Humphrey et al. 1990). Cette mutation code pour une tyrosine active qui augmente la tumorogénécité (Batra, Castelino-Prabhu et al. 1995; Huang, Nagane et al. 1997), la migration (Boockvar, Kapitonov et al. 2003; Pedersen, Tkach et al. 2004) et la résistance aux traitements chimio- et radiothérapeutiques (Montgomery, Guzman et al. 2000; Lammering, Hewit et al. 2003; Lammering, Hewit et al. 2004; Lammering, Valerie et al. 2004). La mutation EGFRvIII est fréquemment rencontrée chez les patients atteints d'un glioblastome (Wong, Ruppert et al. 1992; Frederick, Wang et al. 2000; Heimberger, Hlatky et al. 2005). La nouvelle glycine insérée à la jonction des parties normales du domaine extracellulaire résulte en un épitope tumoral spécifique. Ainsi la spécificité tumorale de l'EGFRvIII, sa surexpression dans les glioblastomes, son absence dans les tissus normaux et son importance dans le phénotype oncogénique, font de l'EGFRvIII une cible idéale pour l'immunothérapie anti-tumorale des gliomes. Sampson *et al.* (Sampson, Archer et al. 2008) ont reporté les résultats d'une étude clinique de phase I/II démontrant qu'une vaccination ciblant le peptide EGFRvIII était à l'origine d'une augmentation de survie des patients après établissement d'une réponse immunitaire.

Ainsi, l'efficacité d'une vaccination anti-EGFRvIII associée à la radiothérapie interne via les NCL^{188}Re-SSS, pourrait conduire à une stimulation du système immunitaire intéressante.

III-2- Activation des cellules dendritiques et Flt3L (fems-like tyrosine 3 ligand)

Flt3L est un activateur de la différenciation des cellules dendritiques mais aussi de leur prolifération et de leur activation (Lyman, James et al. 1994; Maraskovsky, Brasel et al. 1996; Saunders, Lucas et al. 1996). Ces dix dernières années, des résultats encourageants ont été obtenus après administration de vecteurs d'expression utilisés pour délivrer le Flt3L soluble humain (adénovirus, vecteurs poloxamères). En se basant sur le fait que l'administration du Flt3L conduit à l'infiltration des cellules dendritiques au sein de la tumeur

(Lynch, Andreasen et al. 1997), l'équipe de Ali *et al*. (Ali, Curtin et al. 2004) a montré que l'expression élevée du transgène à l'intérieur des tumeurs gliales via les vecteurs adénoviraux optimise l'infiltration des cellules dendritiques et induit une réponse immunitaire anti-tumorale. En effet, une injection intra-craniale de ces vecteurs adénoviraux contenant le Flt3L résulte en une augmentation du temps de survie des animaux avec recrutement de cellules immunitaires effectrices telles que les cellules T CD8+.

Ainsi, combiner cette stratégie à la radiothérapie interne via les NCL^{188}Re-SSS pourrait également constituer un axe de recherche intéressant puisque la surexpression du Flt3L au sein de la tumeur stimule la réponse immunitaire anti-tumorale.

REFERENCES

Ali, S., J. F. Curtin, et al. (2004). "Inflammatory and anti-glioma effects of an adenovirus expressing human soluble Fms-like tyrosine kinase 3 ligand (hsFlt3L): treatment with hsFlt3L inhibits intracranial glioma progression." Mol Ther **10**(6): 1071-84.

Barth, R. F. and B. Kaur (2009). "Rat brain tumor models in experimental neuro-oncology: the C6, 9L, T9, RG2, F98, BT4C, RT-2 and CNS-1 gliomas." J Neurooncol **94**(3): 299-312.

Batra, S. K., S. Castelino-Prabhu, et al. (1995). "Epidermal growth factor ligand-independent, unregulated, cell-transforming potential of a naturally occurring human mutant EGFRvIII gene." Cell Growth Differ **6**(10): 1251-9.

Bigner, S. H., P. A. Humphrey, et al. (1990). "Characterization of the epidermal growth factor receptor in human glioma cell lines and xenografts." Cancer Res **50**(24): 8017-22.

Boockvar, J. A., D. Kapitonov, et al. (2003). "Constitutive EGFR signaling confers a motile phenotype to neural stem cells." Mol Cell Neurosci **24**(4): 1116-30.

Clavreul, A., M. Delhaye, et al. (2006). "Effects of syngeneic cellular vaccinations alone or in combination with GM-CSF on the weakly immunogenic F98 glioma model." J Neurooncol **79**(1): 9-17.

Frederick, L., X. Y. Wang, et al. (2000). "Diversity and frequency of epidermal growth factor receptor mutations in human glioblastomas." Cancer Res **60**(5): 1383-7.

Heimberger, A. B., R. Hlatky, et al. (2005). "Prognostic effect of epidermal growth factor receptor and EGFRvIII in glioblastoma multiforme patients." Clin Cancer Res **11**(4): 1462-6.

Huang, H. S., M. Nagane, et al. (1997). "The enhanced tumorigenic activity of a mutant epidermal growth factor receptor common in human cancers is mediated by threshold levels of constitutive tyrosine phosphorylation and unattenuated signaling." J Biol Chem **272**(5): 2927-35.

Lammering, G., T. H. Hewit, et al. (2004). "Inhibition of the type III epidermal growth factor receptor variant mutant receptor by dominant-negative EGFR-CD533 enhances malignant glioma cell radiosensitivity." Clin Cancer Res **10**(19): 6732-43.

Lammering, G., T. H. Hewit, et al. (2003). "EGFRvIII-mediated radioresistance through a strong cytoprotective response." Oncogene **22**(36): 5545-53.

Lammering, G., K. Valerie, et al. (2004). "Radiation-induced activation of a common variant of EGFR confers enhanced radioresistance." Radiother Oncol **72**(3): 267-73.

Libermann, T. A., H. R. Nusbaum, et al. (1985). "Amplification, enhanced expression and possible rearrangement of EGF receptor gene in primary human brain tumours of glial origin." Nature **313**(5998): 144-7.

Lyman, S. D., L. James, et al. (1994). "Cloning of the human homologue of the murine flt3 ligand: a growth factor for early hematopoietic progenitor cells." Blood **83**(10): 2795-801.

Lynch, D. H., A. Andreasen, et al. (1997). "Flt3 ligand induces tumor regression and antitumor immune responses in vivo." Nat Med **3**(6): 625-31.

Maraskovsky, E., K. Brasel, et al. (1996). "Dramatic increase in the numbers of functionally mature dendritic cells in Flt3 ligand-treated mice: multiple dendritic cell subpopulations identified." J Exp Med **184**(5): 1953-62.

Montgomery, R. B., J. Guzman, et al. (2000). "Expression of oncogenic epidermal growth factor receptor family kinases induces paclitaxel resistance and alters beta-tubulin isotype expression." J Biol Chem **275**(23): 17358-63.

Paul, D. B., R. F. Barth, et al. (2000). "B7.1 expression by the weakly immunogenic F98 rat glioma does not enhance immunogenicity." Gene Ther **7**(12): 993-9.

Pedersen, M. W., V. Tkach, et al. (2004). "Expression of a naturally occurring constitutively active variant of the epidermal growth factor receptor in mouse fibroblasts increases motility." Int J Cancer **108**(5): 643-53.

Roth, W. and M. Weller (1999). "Chemotherapy and immunotherapy of malignant glioma: molecular mechanisms and clinical perspectives." Cell Mol Life Sci **56**(5-6): 481-506.

Sampson, J. H., G. E. Archer, et al. (2008). "Tumor-specific immunotherapy targeting the EGFRvIII mutation in patients with malignant glioma." Semin Immunol **20**(5): 267-75.

Saunders, D., K. Lucas, et al. (1996). "Dendritic cell development in culture from thymic precursor cells in the absence of granulocyte/macrophage colony-stimulating factor." J Exp Med **184**(6): 2185-96.

Tzeng, J. J., R. F. Barth, et al. (1991). "Phenotype and functional activity of tumor-infiltrating lymphocytes isolated from immunogenic and nonimmunogenic rat brain tumors." Cancer Res **51**(9): 2373-8.

Wong, A. J., J. M. Ruppert, et al. (1992). "Structural alterations of the epidermal growth factor receptor gene in human gliomas." Proc Natl Acad Sci U S A **89**(7): 2965-9.

Discussion Générale

La radiothérapie interne minimise les effets systémiques, observés en radiothérapie externe, en focalisant les radiations ionisantes dans un tissu cible. La distribution des radiations ionisantes se fait soit via la mise en place de sources radioactives à l'intérieur de l'organisme (curiethérapie), soit via des vecteurs de radioéléments tels que les anticorps monoclonaux, les peptides et les systèmes particulaires (Bigner, Brown et al. 1998; Merlo, Hausmann et al. 1999; Bodei, Cremonesi et al. 2004; Reardon, Akabani et al. 2006). Dans le cas du carcinome hépatocellulaire et du gliome, le manque de dispositifs radioactifs (curiethérapie) et d'identifications de cibles biologiques spécifiques des cellules tumorales font de la radiothérapie interne, une modalité de traitement encore peu développée. Devant la constante augmentation des carcinomes hépatocellulaires et des gliomes, associée à la sensibilité des tissus hépatiques et cérébraux, il est important de développer de nouvelles stratégies pour la prise en charge de ces pathologies.

Dans ce contexte, l'objectif de ce travail a été d'évaluer le potentiel thérapeutique d'une radiothérapie interne nanovectorisée via les nanocapsules lipidiques chargées en Rhénium-188 (NCL^{188}Re-SSS) et d'en optimiser son utilisation au sein de deux modèles que sont les modèles de carcinome hépatocellulaire et de gliome. Ce type de radiothérapie interne, utilisant des nano-objets, n'a été introduit que très récemment puisque les premières études décrivant l'intérêt des vecteurs pour la radiothérapie interne datent de 2006 (Ballot, Noiret et al. 2006). En effet, encapsuler un radioélément au sein de vecteurs particulaire va permettre de modifier son devenir *in vivo* car les propriétés intrinsèques du vecteur vont prédominer sur celles du radioélément (Caruthers, Wickline et al. 2007). Parmi ces nouveaux systèmes particulaires, les nanocapsules lipidiques (NCL) sont des systèmes biocompatibles qui n'utilisent que des excipients approuvés par la FDA. Ils possèdent également la capacité d'encapsuler des substances lipophiles, comme les complexes lipophiles de Rhénium-188.

Ce travail de thèse s'inscrit dans une optique thérapeutique utilisant des NCL en tant que vecteur de radioélément pour la thérapie locorégionale du carcinome hépatocellulaire et du gliome. Nous avons choisi d'encapsuler un complexe métallique lipophile de Rhénium-188 (complexe hautement soufré [$^{188}Re(S_3CPh)_2(S_2CPh)$ ou ^{188}Re-SSS]) dans un système

nanocapsulaire afin d'évaluer à un stade préclinique leur application en radiothérapie nanovectorisée.

I- LE COMPLEXE DE RHENIUM-188

Dans un premier temps, nous avons adapté la formulation des NCL encapsulant le complexe de rhénium-188 (NCL^{188}Re-SSS) décrite par Allard *et al*. (Allard, Hindre et al. 2008) pour l'administration intra-hépatique, intracérébrale et pour une automatisation du procédé de formulation. L'objectif étant de s'affranchir des problèmes de radioprotection pour permettre le transfert vers la clinique.

Le complexe lipophile de rhénium-188 (^{188}Re-SSS) est synthétisé en deux étapes où un intermédiaire de degré V va être chelaté par un ligand labile, le dithiobenzoate de sodium ($PhCS_2H$). Une fois formé, le ^{188}Re-SSS est solubilisé dans une phase de dichlorométhane (CH_2Cl_2), puis ajouté aux autres excipients de la formulation. Une étape d'évaporation est nécessaire pour éliminer le solvant avant de réaliser les 3 cycles de chauffage-refroidissement entre 85 et 60°C. Les mesures de ta ille réalisées sur les NCL^{188}Re-SSS montrent que la présence du complexe ne modifie pas leur taille puisqu'elles sont inchangées par rapport aux NCL blanches avec une taille moyenne de 49,7 ± 2,7 nm et 50,7 ± 5,7 nm respectivement. Les indices de polydispersité sont inférieurs à 0,05 démontrant une distribution monodisperse.

II- MEILLEURE RETENTION HEPATIQUE ET CEREBRALE

Le Rhénium-188 possède une affinité stomacale identique à celle du technétium-99 et est éliminé par les voies urinaires après injection IV (Deutsch, Libson et al. 1986; Hsieh, Hsieh et al. 1999). Ainsi, les bénéfices attendus de son encapsulation est de modifier sa

distribution afin de maintenir une irradiation localisée au sein du tissu cible. Les résultats confirment l'intérêt de l'encapsulation du Rhénium-188 au sein des nanocapsules lipidiques (NCL^{188}Re-SSS) puisqu'elle permet d'éviter une captation stomacale et une élimination urinaire après injection intra-hépatique et injection intra-crânienne.

L'efficacité thérapeutique d'une radiothérapie interne est également fonction du temps d'exposition du tissu cible aux irradiations. Nous avons démontré que l'encapsulation du Rhénium-188 résultait en une modification de son profil de distribution, cependant, il est important de noter que les NCL^{188}Re-SSS résident au niveau du site d'injection aussi bien dans le modèle du carcinome hépatocellulaire et que dans le modèle tumoral glial. Ainsi, l'encapsulation du Rhénium-188 au sein des NCL permet non seulement de modifier sa distribution mais aussi de maintenir sa rétention jusqu'à 96 heures post-injection dans le tissu cible.

III- EFFICACITE THERAPEUTIQUE

III-1- Carcinome Hépatocellulaire

En terme de radiothérapie interne locorégionale, deux produits commerciaux de microsphères d'Yttrium-90, diamètre moyen de 40µm, sont mis sur le marché et utilisés en clinique après injection intra-artérielle (TheraSpheres® et SIR-Spheres®). On parle de radiothérapie interne sélective. En effet, compte-tenu de l'hypervascularisation du carcinome hépatocellulaire (CHC), les microsphères d'Yttrium-90, injectées dans l'artère hépatique, vont se propager dans le foie pour créer un phénomène d'embolisation, où l'approvisionnement sanguin de la tumeur pourra être potentiellement stoppé. Ce phénomène d'embolisation, associé aux rayonnements β^- de l'Yttrium-90, vont participer au bénéfice thérapeutique. Les résultats obtenus montrent une réduction de la masse tumorale jusqu'à 50%, en tant que traitement palliatif du CHC (Lau, Ho et al. 1998; Dancey, Shepherd

et al. 2000; Salem, Lewandowski et al. 2005; Kulik, Atassi et al. 2006). L'intérêt des systèmes particulaires pour le traitement du CHC est avérée.

La taille nanométrique des NCL^{188}Re-SSS, modulable en fonction de la proportion des excipients de leur formulation (Heurtault, Saulnier et al. 2002), pourrait offrir l'avantage d'une pénétration vasculaire plus profonde comparativement aux microsphères d'Yttrium-90.

Les NCL^{188}Re-SSS, utilisées pour ce travail de thèse, présentent une taille de 50-55 nm, une charge négative de -10mV et du PEG 660 à leur surface. Après injection unique de 80MBq (dose équivalente approximative : 40 Gy), la médiane de survie des animaux est augmentée jusqu'à 107% par rapport au groupe ^{188}Re-perrhénate et 58,33% des animaux sont considérés comme long-survivants. Ainsi, les NCL^{188}Re-SSS s'avèrent être un nouvel outil intéressant pour la radiothérapie interne du CHC.

Néanmoins, aujourd'hui, il nous est difficile de comparer l'efficacité d'une radiothérapie interne nanovectorisée par rapport à celle des systèmes micrométriques que sont les microsphères d'Yttrium-90. En effet, les études précliniques portant sur l'efficacité des microsphères ne sont pas accessibles ou ont été réalisées chez le chien (Wollner, Knutsen et al. 1988). Ainsi, réaliser une étude comparative NCL^{188}Re-SSS/^{90}Y-microsphères pourrait être un prochain axe de ce travail.

Cette stratégie présente toutefois quelques limites. En effet, la captation hépatique des NCL^{188}Re-SSS ne semble pas cibler de façon spécifique les nodules tumoraux du CHC. Dans ce contexte, il pourrait également être intéressant d'évaluer le rapport captation foie tumoral/captation foie sain dans un modèle de tumeur unique N1S1.

Une évaluation du processus angiogénique réalisée en parallèle constitue également la suite de ce travail.

Néanmoins, même si la stratégie de radiothérapie interne nanovectorisée via les NCL^{188}Re-SSS reste perfectible, ces données sont les premières à démontrer l'efficacité thérapeutique de ce système particulaire pour la radiothérapie interne du carcinome hépatocellulaire.

III-2- Gliomes

III-2-1- Radiothérapie externe

Des expérimentations préalables au laboratoire (Vinchon-Petit, Jarnet et al. 2010) avaient permis d'apprécier l'efficacité d'une radiothérapie externe fractionnée dans un modèle tumoral glial chez le rat. La médiane de survie est de 59,9 ± 8,2 jours pour des animaux ayant reçu 3 fractions de 6 Gy aux jours 8, 11 et 14 post-implantation de cellules 9L. La dose par fraction ainsi que le timing réalisé étant différents, nous avons effectué un protocole de radiothérapie externe identique à celui utilisé lors de notre stratégie de radiothérapie interne. L'objectif est ici de confronter la radiothérapie externe à la radiothérapie interne. Pour cela, des rats Fischer femelles de 10 semaines ont reçu deux fractions de 8 Gy aux jours 6 et 12 post-implantation de cellules 9L. Deux groupes d'animaux randomisés selon le traitement administré ont été réalisés. Les critères d'évaluation consistent en une étude de survie ainsi qu'un suivi de la progression tumoral par IRM (Figure 1). La radiothérapie externe résulte en une légère augmentation de survie avec une médiane de survie de 26,5 ± 2,1 jours et de 33,5 ± 1,5 jours pour les groupes contrôles et traités respectivement. Ainsi, ces données témoignent de la difficulté du traitement des gliomes par radiothérapie externe et la nécessité de développer de nouvelles stratégies telles que la radiothérapie interne nanovectorisée. Pour cette dernière, les résultats sont discutés dans le paragraphe suivant : III-2-3-.

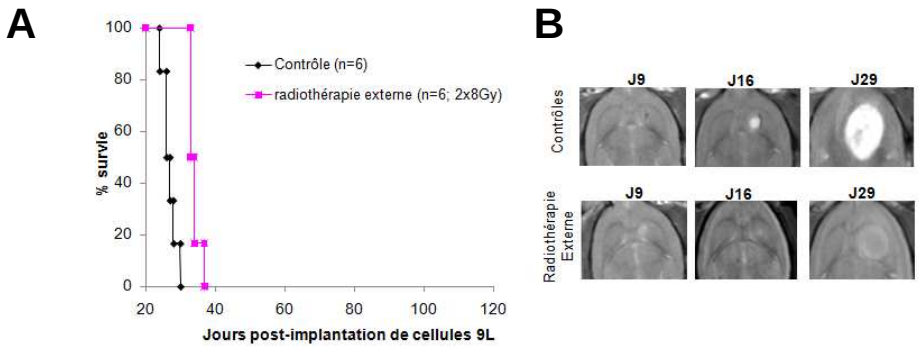

Figure 1 : **A**- Courbes Kaplan-Meier des animaux traités aux jours 6 et 12 post-implantation de cellules 9L. Groupe Radiothérapie externe (2x8Gy à J6 et J12 ; n=6) ; Groupe contrôle (anesthésie à l'isoflurane à J6 et J12 ; n=6). **B**- Images IRM des animaux aux jours 9, 16 et 29.

III-2-2- Injections par SI (injection simple) et par CED

D'après la bibliographie, peu de données concernant la radiothérapie interne via des systèmes particulaires ont été développés. Seule, une étude, effectuée au laboratoire, a établi la possibilité d'utiliser des NCL^{188}Re-SSS de 50 nm pour la radiothérapie interne du gliome (Allard, Hindre et al. 2008). Après une injection unique de NCL^{188}Re-SSS par la technique « Convection Enhanced Delivery » (CED), une augmentation de la médiane de survie de 80% a été observée pour une activité injectée efficace de 2,8 MBq, dans un modèle de rats porteur d'un gliome 9L.

Dans le but d'optimiser notre radiothérapie interne via les NCL^{188}Re-SSS et comme le fractionnement de dose est couramment utilisé en clinique (Stupp, Mason et al. 2005), nous avons évalué le bénéfice thérapeutique après injections intra-craniales répétées de 2,8 MBq de NCL^{188}Re-SSS dans un modèle de gliome 9L chez le rat. Pour cela, deux types d'injections stéréotaxiques ont été retenues : l'injection par SI (injection simple) et l'injection par CED.

La principale différence entre ces deux techniques réside dans le volume final injecté : 10 µL pour une injection par SI et 60 µL pour une injection par CED. Au laboratoire, la technique CED a été mise au point par Vinchon *et al.* (Vinchon-Petit, Jarnet et al. 2009). Elle utilise un pousse-seringue qui va permettre de délivrer le produit sous un effet de gradient de pression. L'infusion par CED des NCLs est réalisée grâce à une seringue de 32 gauges à une vitesse de 0,5µL/min pendant 2 heures tandis que l'infusion par SI est réalisée à une vitesse de 1µL/min pendant 10 min (Figure 2). Il a été démontré que la CED permettait un volume de distribution plus important des NCLs (Allard, Passirani et al. 2009; Vinchon-Petit, Jarnet et al. 2010). Ainsi, nous avons supposé que l'utilisation de ces deux types d'injection permettrait de modifier la distribution des NCL^{188}Re-SSS à l'intérieur du cerveau impliquant la création de gradients de dose différents.

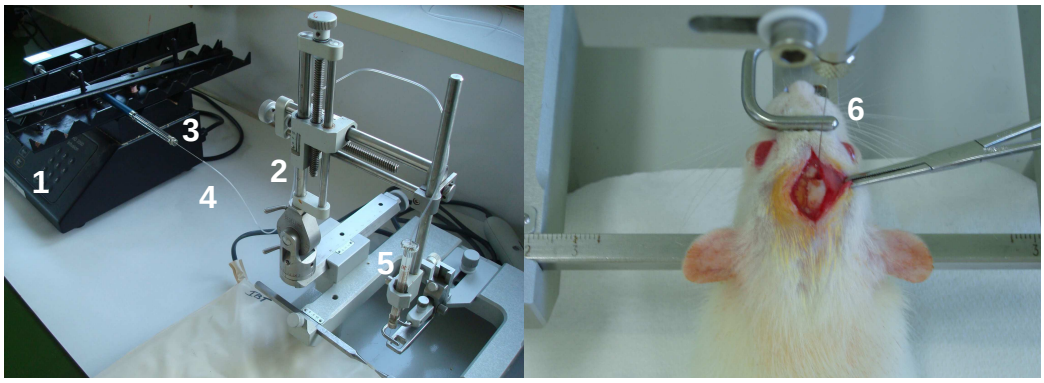

Figure 2 : Systèmes d'injection par SI et par CED. L'ensemble du dispositif comprend : une pompe Harvard PHD 2,000 (1), le cadre de stéréotaxie petit animal, la seringue Hamilton 100µL 22 gauges contenant les NCLs (3), la tubulure externe en PE/PVC (4), la seringue Hamilton 10 µL (5) et l'aiguille de 32G implantée dans le striatum droit du rat (6).

Comme attendu, l'infusion des NCL^{188}Re-SSS est plus importante et couvre un plus large volume après injection par CED comparativement à la SI pour une même activité injectée. Etant donné que l'hétérogénéité cellulaire est une des principales caractéristiques des masses tumorales gliales, la possibilité de moduler un gradient d'activité à l'intérieur du cerveau peut représenter un réel avantage en termes d'efficacité thérapeutique.

III-2-3- Radiothérapie interne fractionnée

L'évaluation d'une radiothérapie interne fractionnée a ensuite été évaluée pour le traitement des gliomes malins. La combinaison des injections par CED et par SI (protocoles 3 et 4) a montré les meilleurs bénéfices en terme de survie avec une augmentation du temps de survie de 176 et de 257% pour les protocoles 3 et 4 respectivement impliquant clairement l'impact du gradient d'activité dans le traitement. Ainsi, une radiothérapie interne fractionnée a permis d'augmenter le bénéfice thérapeutique des animaux comparativement à une injection seule de NCL^{188}Re-SSS avec l'obtention de 67% d'animaux considérés comme long-survivants. Même si notre stratégie de radiothérapie interne est très invasive, cette modalité augmente de façon remarquable l'index thérapeutique des animaux comparativement aux animaux traités par radiothérapie externe (augmentation du temps de

survie jusqu'à 198%) (cf. III-2-1). Ainsi, la radiothérapie interne nanovectorisée peut représenter une réelle alternative à la radiothérapie externe, « gold-standard » en matière de traitement adjuvant pour la thérapie des gliomes.

D'après la bibliographie, des séquelles neurologiques suite à l'injection unique de LNC^{188}Re-SSS dans un modèle tumoral 9L ont été démontré (Allard, Hindre et al. 2008). C'est pourquoi, nous nous sommes intéressés au comportement des animaux long-survivants, le but étant d'évaluer l'aspect cognitif en étudiant leur capacité d'apprentissage et de motricité. Pour cela, la spectroscopie par RMN a été réalisée au niveau du striatum droit (site d'injection de cellules 9L) versus striatum gauche (tissu sain) chez les animaux long-survivants. Les résultats n'ont pas montré de séquelles neurologiques particulières puisque les spectres du N-acétylaspartate, de la créatine et de la choline sont identiques entre les striata gauche et droit. Parallèlement, ces animaux ont effectué un test de motricité (ou « beam balance ») comme décrit par Shabitz *et al.* (Schabitz, Berger et al. 2004). Ce test a mis en évidence des difficultés de motricité et d'équilibre chez les rats long-survivants. Cependant, la répétition de ce test pendant 4 semaines a montré que ces difficultés étaient réversibles. En effet, les animaux long-survivants recouvrent les mêmes capacités motrices, d'équilibre et de mémoire au bout de 4 semaines que des animaux sains du même âge (Figure 3).

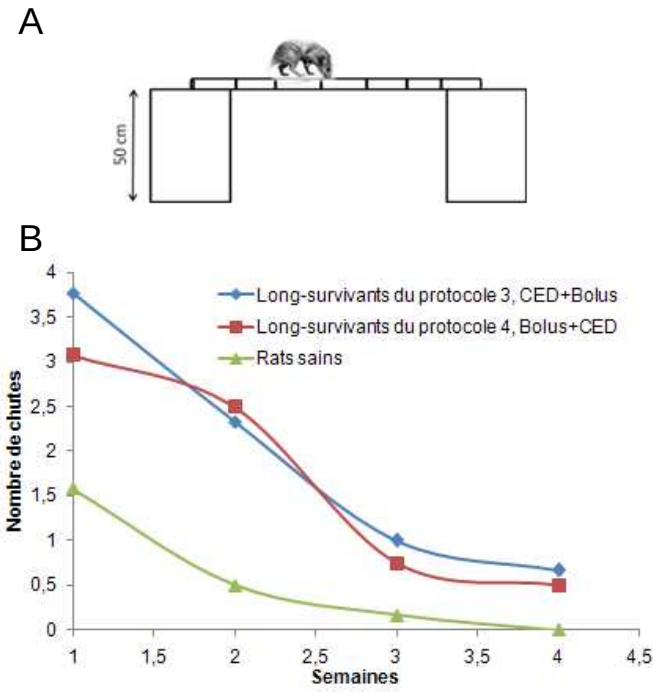

Figure 3: Test de Motricité. **A**- Dispositif, **B**- Courbe du nombre de chute lors d'un test de 1 minute réalisé chaque semaine pendant 4 semaines.

Ces résultats semblent surprenants car Allard *et al*. avaient décrit des séquelles neurologiques après une seule injection de NCL^{188}Re-SSS dans ce même modèle tumoral. Etant donné que deux injections de NCL^{188}Re-SSS n'induisent pas d'effets secondaires sévères, nous pouvons supposer que la concentration des NCL^{188}Re-SSS utilisées par Allard *et al*. pourraient en être la cause. En effet, d'après la littérature, les nanocapsules blanches peuvent être toxiques à des concentrations > 10 µmol/L (Garcion, Lamprecht et al. 2006; Paillard, Hindre et al. 2010). C'est dans ce contexte que nous avons préalablement adapté la formulation des NCL^{188}Re-SSS décrite par Allard *et al*. afin d'obtenir une concentration de 1,3 µmol/L de NCL^{188}Re-SSS. Cependant, cette hypothèse nécessite d'être approfondie par une étude de toxicité précise.

Il a été démontré que les tumeurs solides sont hétérogènes du point de vue histologique avec la présence de cellules tumorales, d'infiltrats inflammatoires et de structures vasculaires. De plus, il a été établi que des sous-populations hiérarchisées de cellules cancéreuses existent à l'intérieur de la masse tumorale (Diehn and Clarke 2006; Adams and Strasser 2008). Très récemment, il a été reporté que des cellules souches cancéreuses, connues pour être radiorésistantes, pouvaient être à l'origine de l'échec thérapeutique dans le traitement des glioblastomes (Bao, Wu et al. 2006; Rich 2007; Ropolo, Daga et al. 2009). Ainsi, l'application d'un gradient d'activité par l'association d'une injection simple et de la CED peut expliquer l'efficacité thérapeutique observée après radiothérapie interne nanovectorisée. En effet, nous pouvons supposer que les injections de NCL^{188}Re-SSS par combinaison des deux types d'injection, cible les différents types de sous-populations cellulaires radiosensibles et radiorésistantes. Cependant, cette hypothèse nécessite d'être étayée par une étude dosimétrique précise afin de déterminer le gradient d'activité créé après chaque type d'injection. De plus, il serait également important de vérifier quel type de cellules cancéreuses (radiorésistantes ou radiosensibles) sont touchées après administration des NCL^{188}Re-SSS par SI et par CED.

Outre l'application d'un gradient d'activité, l'efficacité thérapeutique de cette radiothérapie interne fractionnée via les NCL^{188}Re-SSS peut s'expliquer par une réponse directe des cellules tumorales aux radiations, avec l'ionisation des molécules d'eau (radiolyse) et d'oxygène à l'origine de la formation de radicaux libres (cf. introduction générale), mais également par le recrutement d'effecteurs biologiques à l'extérieur du champ de traitement (Apetoh, Ghiringhelli et al. 2007). En effet, il a été démontré que les radiations pouvaient modifier le microenvironnement tumoral avec, par exemple, l'activation de cellules immunitaire innées, telles que les macrophages, via les espèces réactives oxygénés produits par les cellules irradiées (Coates, Rundle et al. 2008). Cette hypothèse a été vérifiée par la quantification, par test ELISA, des cytokines interleukine-2 (IL-2) et interféron-ɣ (IFNɣ). En effet, ces cytokines sont importantes pour permettre la mise en place d'une réponse immunitaire adaptative (Roth and Weller 1999). Les résultats révèlent une stimulation

périphérique via une surproduction de ces cytokines à partir de J16 post-implantation de cellules 9L. Ainsi, nous pouvons en déduire que la deuxième injection de NCL^{188}Re-SSS est en partie responsable de ce phénomène puisque les taux d'IL-2 et d'IFNγ restent identiques à ceux obtenus pour les animaux contrôles (NCL blanches, sérum physiologique et ^{188}Re-perrhénate) à J8 post-implantation de cellules 9L.

La mise en place d'une réponse immunitaire adaptative a définitivement été observée avec l'augmentation des cellules immunitaires spécifiques, mais surtout par la mise en évidence du processus d'immunisation chez certains animaux. En effet, les animaux long-survivants obtenus précédemment, ont été ré-injectés par 1000 cellules 9L dans le deuxième striatum (gauche). Certains n'ont montré qu'une immunisation partielle avec un ralentissement de la progression tumorale tandis que d'autres n'ont pas développé de tumeur gliale.
Ainsi, la radiothérapie interne nanovectorisée engendre des effets thérapeutiques remarquables pouvant s'expliquer par l'effet d'un gradient d'activité et d'une réponse immunitaire adaptative.

IV- ADAPTATION DE LA DE RADIOTHERAPIE INTERNE NANOVECTORISEE SELON LE TYPE TUMORAL

Même si la radiothérapie interne nanovectorisée augmente considérablement l'index thérapeutique des animaux comparativement à la radiothérapie externe, il faut être prudent dans l'analyse de ces données puisque le modèle de tumeur 9L est caractérisé comme étant peu invasif et fortement immunogène (Barth and Kaur 2009). Dans ce contexte, nous avons changé de modèle tumoral glial par l'injection de 500 cellules F98 dans le striatum droit des rats Fischer afin d'évaluer notre stratégie de radiothérapie interne nanovectorisée en se focalisant sur les protocoles 3 et 4.

Les résultats obtenus ont souligné l'importance d'adapter l'activité injectée selon le type tumoral à traiter. En effet, la nature radiorésistant des tumeurs F98 nous a conduit à augmenter l'activité injectée à 3,7 MBq (dose équivalente approximative par injection : 10Gy) aux jours 6 et 12 dans le but d'obtenir une efficacité thérapeutique plus importante. Cependant, même après augmentation de l'activité injectée, le bénéfice en terme de survie est moins élevé comparativement au modèle 9L (Figure 3).

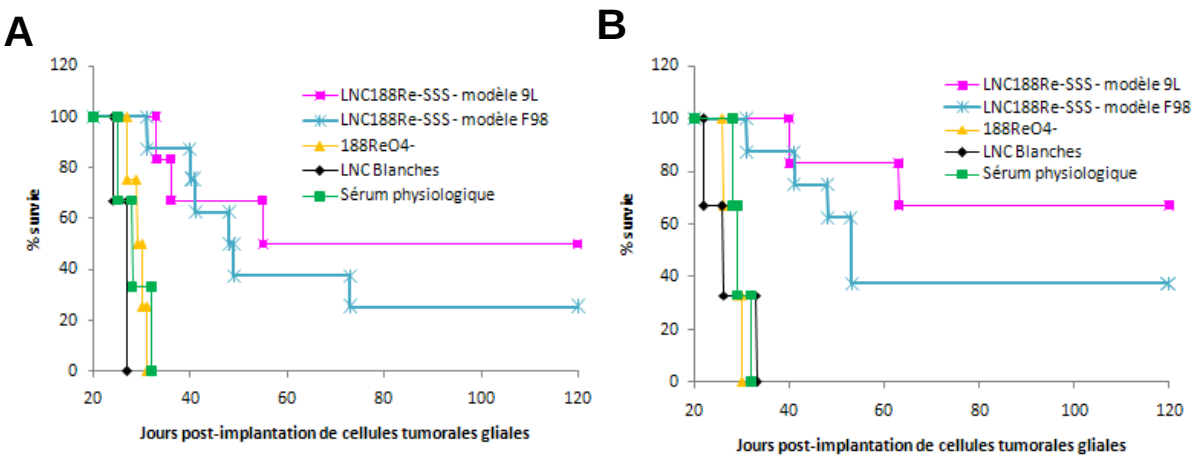

Figure 3 : Courbes de Kaplan-Meier des rats porteurs d'un gliome 9L et F98. Les animaux ont été traités avec 2,8 MBq (modèle 9L) et 3,7 MBq (modèle F98) de NCL^{188}Re-SSS. A- Protocole 3 : CED+SI ; B- Protocole 4 : SI+CED

Le modèle de tumeur F98 est très peu immunogène (Barth and Kaur 2009), nous avons alors supposé une différence dans l'activation du système immunitaire après radiothérapie interne fractionnée. Les résultats ont confirmé notre hypothèse puisque la stimulation immunitaire périphérique (taux IL-2 et d'IFNγ) est deux fois moins importante, ainsi que les recrutements de cellules immunitaires au niveau du site tumoral.

En conclusion de cette étude, la radiothérapie interne nanovectorisée via les NCL^{188}Re-SSS est un outil très prometteur car son efficacité thérapeutique a été démontrée non seulement sur le modèle tumoral 9L mais aussi sur un modèle radiorésistant et peu immunogène : le modèle tumoral F98. Toutefois l'action du système immunitaire joue un rôle important et semble limité dans le cadre du modèle F98.

V- STIMULATION DU SYSTEME IMMUNITAIRE ET RADIOTHERAPIE INTERNE NANOVECTORISEE

L'efficacité thérapeutique moins élevée chez le rat porteur d'un gliome F98, a motivé la dernière partie de ce travail. En effet, le modèle F98 étant peu immunogène, stimuler le système immunitaire chez ces animaux pourrait nous permettre d'optimiser notre stratégie de radiothérapie interne.

Nous avons choisi de stimuler le système immunitaire par vaccination en apportant des antigènes tumoraux au système immunitaire. Les cellules présentatrice d'antigène (CPA) vont pouvoir capter les antigènes pour les présenter de façon efficace aux cellules effectrices du système immunitaire que sont les lymphocytes T auxiliaires et les lymphocytes T cytotoxiques. Cependant, l'activation des CPA dépend des signaux environnants, ainsi la quantité et la nature des antigènes présentés sont des paramètres importants à prendre en compte lors de la mise en place d'un protocole vaccinal.

Irradier des cellules tumorales permet leur inactivation et arrête leur prolifération : les cellules deviennent apoptotiques (Ishikawa, Tsuboi et al. 2004). Une étude de vaccination préventive a démontré qu'une injection de 2.10^6 cellules 9L irradiées permet une protection contre le développement tumoral chez le rat Fischer femelle (Ishikawa, Tsuboi et al. 2004).

Pour cette partie, nous avons choisi de vacciner les animaux après établissement de la tumeur, il s'agit d'un protocole vaccinal curatif. Pour cela, des rats Fisher femelles ont été traités aux jours 6 et 12 par une injection de 3,7 MBq de NCL^{188}Re-SSS post-implantation de cellules F98. Parallèlement, les animaux ont reçu une injection sous-cutanée de 2.10^6 cellules F98 (flanc droit) 6 jours après injection de 500 cellules F98 dans le striatum droit. Les résultats obtenus ne sont pas satisfaisants car seule une faible d'augmentation de la médiane de survie des animaux a été observée. Cependant, les résultats immunohistochimiques montrent l'effet de la vaccination combinée à la radiothérapie interne puisque des cellules immunitaires spécifiques (CD4+, CD8+) semblent avoir été recrutées au

niveau du site tumoral. Néanmoins, en comparaison avec le modèle 9L, ce recrutement reste inférieur, ce qui pourrait expliquer les résultats moins élevés en terme de survie.

Pour conclure cette étude, notons que l'activation du système immunitaire semble être importante puisque la survie des animaux est moins élevée dans un modèle tumoral peu immunogène comme le modèle tumoral glial F98.
Le véritable challenge de la suite de ce travail réside dans la potentialisation du système immunitaire en association avec la radiothérapie nanovectorisée. En effet, le protocole vaccinal peut être modifié soit via une augmentation du nombre de cellules irradiées injectées, soit via des injections répétées de cellules irradiées. Le planning de vaccination peut également être amélioré. En effet, il est possible qu'une injection à J6 soit trop précoce pour la stimulation du système immunitaire d'autant plus que les dosages de cytokines IL-2 et IFNγ indiquent une stimulation périphérique à partir de J16 tandis qu'aucune modification par rapport aux contrôles n'a été observée à J8.

En conclusion, ce travail de thèse a permis d'explorer une nouvelle stratégie de radiothérapie interne : la radiothérapie nanovectorisée via les NCL^{188}Re-SSS. Son potentiel thérapeutique est majeur sur deux modèles animaux que sont les modèles de carcinome hépatocellulaire et de gliome. Les possibilités d'optimisation étant nombreuses (augmentation de l'activité injectée, injection répétées, stimulation de la réponse immunitaire…), cette stratégie offre de nouvelles perspectives dans le traitement du CHC et du gliome malin, qui aujourd'hui, restent des pathologies où aucun traitement curatif n'est satisfaisant.

RÉFÉRENCES

Adams, J. M. and A. Strasser (2008). "Is tumor growth sustained by rare cancer stem cells or dominant clones?" Cancer Res **68**(11): 4018-21.

Allard, E., F. Hindre, et al. (2008). "188Re-loaded lipid nanocapsules as a promising radiopharmaceutical carrier for internal radiotherapy of malignant gliomas." Eur J Nucl Med Mol Imaging **35**(10): 1838-46.

Allard, E., C. Passirani, et al. (2009). "Convection-enhanced delivery of nanocarriers for the treatment of brain tumors." Biomaterials **30**(12): 2302-18.

Apetoh, L., F. Ghiringhelli, et al. (2007). "Toll-like receptor 4-dependent contribution of the immune system to anticancer chemotherapy and radiotherapy." Nat Med **13**(9): 1050-9.

Ballot, S., N. Noiret, et al. (2006). "99mTc/188Re-labelled lipid nanocapsules as promising radiotracers for imaging and therapy: formulation and biodistribution." Eur J Nucl Med Mol Imaging **33**(5): 602-7.

Bao, S., Q. Wu, et al. (2006). "Glioma stem cells promote radioresistance by preferential activation of the DNA damage response." Nature **444**(7120): 756-60.

Barth, R. F. and B. Kaur (2009). "Rat brain tumor models in experimental neuro-oncology: the C6, 9L, T9, RG2, F98, BT4C, RT-2 and CNS-1 gliomas." J Neurooncol **94**(3): 299-312.

Bigner, D. D., M. T. Brown, et al. (1998). "Iodine-131-labeled antitenascin monoclonal antibody 81C6 treatment of patients with recurrent malignant gliomas: phase I trial results." J Clin Oncol **16**(6): 2202-12.

Bodei, L., M. Cremonesi, et al. (2004). "Receptor radionuclide therapy with 90Y-[DOTA]0-Tyr3-octreotide (90Y-DOTATOC) in neuroendocrine tumours." Eur J Nucl Med Mol Imaging **31**(7): 1038-46.

Caruthers, S. D., S. A. Wickline, et al. (2007). "Nanotechnological applications in medicine." Curr Opin Biotechnol **18**(1): 26-30.

Coates, P. J., J. K. Rundle, et al. (2008). "Indirect macrophage responses to ionizing radiation: implications for genotype-dependent bystander signaling." Cancer Res **68**(2): 450-6.

Dancey, J. E., F. A. Shepherd, et al. (2000). "Treatment of nonresectable hepatocellular carcinoma with intrahepatic 90Y-microspheres." J Nucl Med **41**(10): 1673-81.

Deutsch, E., K. Libson, et al. (1986). "The chemistry of rhenium and technetium as related to the use of isotopes of these elements in therapeutic and diagnostic nuclear medicine." Int J Rad Appl Instrum B **13**(4): 465-77.

Diehn, M. and M. F. Clarke (2006). "Cancer stem cells and radiotherapy: new insights into tumor radioresistance." J Natl Cancer Inst **98**(24): 1755-7.

Garcion, E., A. Lamprecht, et al. (2006). "A new generation of anticancer, drug-loaded, colloidal vectors reverses multidrug resistance in glioma and reduces tumor progression in rats." Mol Cancer Ther **5**(7): 1710-22.

Heurtault, B., P. Saulnier, et al. (2002). "A novel phase inversion-based process for the preparation of lipid nanocarriers." Pharm Res **19**(6): 875-80.

Hsieh, B. T., J. F. Hsieh, et al. (1999). "Rhenium-188-Labeled DTPA: a new radiopharmaceutical for intravascular radiation therapy." Nucl Med Biol **26**(8): 967-72.

Ishikawa, E., K. Tsuboi, et al. (2004). "X-irradiation to human malignant glioma cells enhances the cytotoxicity of autologous killer lymphocytes under specific conditions." Int J Radiat Oncol Biol Phys **59**(5): 1505-12.

Kulik, L. M., B. Atassi, et al. (2006). "Yttrium-90 microspheres (TheraSphere) treatment of unresectable hepatocellular carcinoma: downstaging to resection, RFA and bridge to transplantation." J Surg Oncol **94**(7): 572-86.

Lau, W. Y., S. Ho, et al. (1998). "Selective internal radiation therapy for nonresectable hepatocellular carcinoma with intraarterial infusion of 90yttrium microspheres." Int J Radiat Oncol Biol Phys **40**(3): 583-92.

Merlo, A., O. Hausmann, et al. (1999). "Locoregional regulatory peptide receptor targeting with the diffusible somatostatin analogue 90Y-labeled DOTA0-D-Phe1-Tyr3-octreotide (DOTATOC): a pilot study in human gliomas." Clin Cancer Res **5**(5): 1025-33.

Paillard, A., F. Hindre, et al. (2010). "The importance of endo-lysosomal escape with lipid nanocapsules for drug subcellular bioavailability." Biomaterials **31**(29): 7542-54.

Reardon, D. A., G. Akabani, et al. (2006). "Salvage radioimmunotherapy with murine iodine-131-labeled antitenascin monoclonal antibody 81C6 for patients with recurrent primary and metastatic malignant brain tumors: phase II study results." J Clin Oncol **24**(1): 115-22.

Rich, J. N. (2007). "Cancer stem cells in radiation resistance." Cancer Res **67**(19): 8980-4.

Ropolo, M., A. Daga, et al. (2009). "Comparative analysis of DNA repair in stem and nonstem glioma cell cultures." Mol Cancer Res **7**(3): 383-92.

Roth, W. and M. Weller (1999). "Chemotherapy and immunotherapy of malignant glioma: molecular mechanisms and clinical perspectives." Cell Mol Life Sci **56**(5-6): 481-506.

Salem, R., R. J. Lewandowski, et al. (2005). "Treatment of unresectable hepatocellular carcinoma with use of 90Y microspheres (TheraSphere): safety, tumor response, and survival." J Vasc Interv Radiol **16**(12): 1627-39.

Schabitz, W. R., C. Berger, et al. (2004). "Effect of brain-derived neurotrophic factor treatment and forced arm use on functional motor recovery after small cortical ischemia." Stroke **35**(4): 992-7.

Stupp, R., W. P. Mason, et al. (2005). "Radiotherapy plus concomitant and adjuvant temozolomide for glioblastoma." N Engl J Med **352**(10): 987-96.

Vinchon-Petit, S., D. Jarnet, et al. (2010). "External irradiation models for intracranial 9L glioma studies." J Exp Clin Cancer Res **29**: 142.

Vinchon-Petit, S., D. Jarnet, et al. (2009). "In vivo evaluation of intracellular drug-nanocarriers infused into intracranial tumours by convection-enhanced delivery: distribution and radiosensitisation efficacy." J Neurooncol.

Vinchon-Petit, S., D. Jarnet, et al. (2010). "In vivo evaluation of intracellular drug-nanocarriers infused into intracranial tumours by convection-enhanced delivery: distribution and radiosensitisation efficacy." J Neurooncol **97**(2): 195-205.

Wollner, I., C. Knutsen, et al. (1988). "Effects of hepatic arterial yttrium 90 glass microspheres in dogs." Cancer **61**(7): 1336-44.

Annexe

Publication Annexe

“The therapeutic potential of human multipotent mesenchymal stromal cells combined with pharmacologically active microcarriers transplanted in hemi-parkinsonian rats.”

Publication acceptée dans « Biomaterials ».

Biomaterials xxx (2010) 1–14

Contents lists available at ScienceDirect

Biomaterials

journal homepage: www.elsevier.com/locate/biomaterials

The therapeutic potential of human multipotent mesenchymal stromal cells combined with pharmacologically active microcarriers transplanted in hemi-parkinsonian rats

Gaëtan J.-R. Delcroix [a,b], Elisa Garbayo [a,b], Laurence Sindji [a,b], Olivier Thomas [a,b], Claire Vanpouille-Box [a,b], Paul C. Schiller [c,d], Claudia N. Montero-Menei [a,b,*]

[a] Inserm, U646, 10 rue André Boquel, Angers, F49100 France
[b] Univ Angers, UMR-S646, Angers, F49100 France
[c] GRECC and Research Service, Veterans Affairs Medical Center, Miami, FL, USA
[d] Geriatrics and Interdisciplinary Stem Cell Institutes and Departments of Medicine and Biochemistry & Molecular Biology, University of Miami Miller School of Medicine, FL, USA

ARTICLE INFO

Article history:
Received 30 September 2010
Accepted 19 October 2010
Available online xxx

Keywords:
Laminin
Mesenchymal stromal cells
Tissue engineering
Neurotrophin 3
Parkinson's disease
Pharmacologically active microcarriers

ABSTRACT

Multipotent mesenchymal stromal cells (MSCs) raise great interest for brain cell therapy due to their ease of isolation from bone marrow, their immunomodulatory and tissue repair capacities, their ability to differentiate into neuronal-like cells and to secrete a variety of growth factors and chemokines. In this study, we assessed the effects of a subpopulation of human MSCs, the marrow-isolated adult multilineage inducible (MIAMI) cells, combined with pharmacologically active microcarriers (PAMs) in a rat model of Parkinson's disease (PD). PAMs are biodegradable and non-cytotoxic poly(lactic-co-glycolic acid) microspheres, coated by a biomimetic surface and releasing a therapeutic protein, which acts on the cells conveyed on their surface and on their microenvironment. In this study, PAMs were coated with laminin and designed to release neurotrophin 3 (NT3), which stimulate the neuronal-like differentiation of MIAMI cells and promote neuronal survival. After adhesion of dopaminergic-induced (DI)-MIAMI cells to PAMs *in vitro*, the complexes were grafted in the partially dopaminergic-deafferented striatum of rats which led to a strong reduction of the amphetamine-induced rotational behavior together with the protection/repair of the nigrostriatal pathway. These effects were correlated with the increased survival of DI-MIAMI cells that secreted a wide range of growth factors and chemokines. Moreover, the observed increased expression of tyrosine hydroxylase by cells transplanted with PAMs may contribute to this functional recovery.

1. Introduction

Parkinson's disease (PD), mainly resulting from the degeneration of the nigrostriatal dopaminergic system, is a progressive neurodegenerative disorder that affects 2% of the population over 65 years of age. Currently the most efficient therapeutic treatment, L-DOPA, aims at replenishing the amount of dopamine missing in the striatum. However, this strategy slowly becomes less effective after long-term treatment and shows undesirable side effects [1,2]. Cell therapy is an alternative strategy to treat PD and many clinical studies using foetal dopaminergic cells or dopamine-producing cells, such as adrenal chromaffin cells and human retinal pigment epithelium have been performed [3–5]. These studies gave encouraging results that have provided the proof of principle for cell therapy in PD. However, the outcome was also highly variable between patients and the foetal grafts raised ethical and practical concerns [6], with a poor survival after transplantation [7–10].

Stem cells, that can self renew and further differentiate into dopaminergic precursors are currently the most studied candidates for cell therapy in PD. However, due to the difficulties in obtaining neural stem cells from adults and the inherent ethical problems to the use of foetal cells or of embryonic stem cells, multipotent mesenchymal stromal cells (MSCs), may represent an alternative cell source to repair the nervous system [5]. Indeed, as they are easily isolated from the bone marrow, autologous grafts can be performed avoiding ethical and availability concerns. MSCs may differentiate into progeny of the three embryonic layers *in vitro*, including neuronal-like cells, under the influence of matrix molecules and growth factors [11–14]. Using appropriate driving cues,

* Corresponding author. Inserm U646, 10 rue André Boquel, Angers, France. Tel.: +33 2 41 73 58 94; fax: +33 2 41 73 58 53.
E-mail address: claudia.montero-menei@univ-angers.fr (C.N. Montero-Menei).

0142-9612/$ – see front matter © 2010 Elsevier Ltd. All rights reserved.
doi:10.1016/j.biomaterials.2010.10.041

these cells that may partially originate from the neural crest [15], can be further directed toward a dopaminergic phenotype [16–18]. Recently, mesenchymal stem-like cells from endometrial origin have also been described as an interesting source of cells for PD therapy due to their ability to produce TH and restore dopamine level in parkinsonian mice [19]. In addition to their neuronal differentiation potential, MSCs possess immunomodulatory properties [20,21] and have the ability to migrate toward sources of lesions in the brain [22–26]. Furthermore, some studies showed a functional improvement in the rotational behavior of hemi-parkinsonian rats upon transplantation of rat or human MSCs [27–30]. As only a very small number of neuronal-like cells were observed in the brain [29], these effects were mostly attributed to the ability of MSCs to secrete various growth factors that protected the degenerating neuronal fibres. These reports encourage further studies with MSCs for cell therapy of PD, but also highlight the need to enhance MSC cell engraftment.

Tissue engineering, which combines cells with a supportive scaffold providing a 3D structure, may help to improve cell engraftment after transplantation [5,31]. In this way, microcarriers transporting foetal ventral mesencephalic (FVM) cells or adrenal chromaffin cells improved their long-term survival after intracerebral transplantation in hemi-parkinsonian rats [32–34]. A clinical trial has also reported the safety and efficacy of gelatine microcarriers conveying human retinal pigment epithelial cells for the treatment of PD [35,36]. Scaffolds providing a biomimetic surface of different extracellular matrix (ECM) molecules or their derived peptides, that stimulate cell survival and differentiation, may further enhance cell engraftment [5,37]. In this regard, various studies report that laminin (LM) enhances neurite outgrowth of neurons [38] as well as neural stem cell proliferation [39]. In addition, LM may also improve the integration of transplanted cells and their tissue regeneration potential in an *ex vivo* model of Parkinson's disease [40]. Finally, this ECM molecule is known to affect stem cell motility [41] and differentiation of MSCs toward a neuronal phenotype, in terms of morphology [42] but also of marker expression [43].

Another way to improve the efficiency of cell grafts is to engineer a scaffold that not only provides a biomimetic surface but also delivers a relevant bioactive growth factor that is released in a controlled manner, further affecting the fate of both transplanted and host cells (see for review [5,31,37]). Indeed, synergistic effects between adhesion and growth factor signals to guide and enhance cell differentiation have now been described [44]. In this sense, we have developed an adaptable and efficient device for tissue engineering, the pharmacologically active microcarriers (PAMs). They are biodegradable and non-cytotoxic polymeric microcarriers made of poly(lactic-co-glycolic acid) (PLGA), that with a functionalized surface provide an adequate 3D support for cell culture and/or for their administration. Their microcarrier role, the biomimetic surface and the programmed delivery of an appropriate therapeutic factor may act synergistically to induce and further maintain the survival and/or differentiation of the transplanted cells and their microenvironment, therefore enhancing their engraftment after complete degradation of the vector [45,46]. The efficacy of this tool was previously demonstrated in a rat PD paradigm using PAMs conveying PC12 cells and releasing nerve growth factor [47], but also with FVM cells attached to PAMs releasing glial cell line-derived neurotrophic factor [48]. In both cases, the PAMs stimulated cell survival and differentiation leading to an improved behavior of the animals.

The main goal of this study was to improve MSC survival, differentiation and tissue repair function after implantation in the striatum of hemi-parkinsonian rats, using PAMs tailored for this application. We chose to work with a homogeneous and well characterized subpopulation of human MSCs that express pluripotent stem cells markers. These cells termed "marrow-isolated adult multilineage inducible" (MIAMI) cells, may generate mature cells derived from all three embryonic germ layers [49,50]. EGF is now considered as an important factor able to enhance the therapeutic potential of MSCs (see for review Tamama et al. [51].). We recently demonstrated that exposing MIAMI cells to an EGF and bFGF pre-treatment enhances their neural specification and response to neuronal commitment [11]. MIAMI cells further differentiate toward the neuronal lineage on a fibronectin surface in an NT3-dependent manner [16] and this molecule increases β3-Tubulin expression by MIAMI cells [11] and MSCs [52] during *in vitro* neuronal differentiation. These results appoint NT3 as an ideal protein to encapsulate into PAMs and to use in combination with EGF-bFGF pre-treated MIAMI cells induced toward a dopaminergic phenotype. In order to choose the appropriate biomimetic surface for PAMs, we first screened the panel of integrins expressed by MIAMI cells by RT-qPCR and flow cytometry. We then studied the effect of LM, compared to fibronectin (FN), on the *in vitro* neuronal differentiation potential of MIAMI cells in terms of cell proliferation, cell length and expression of neuronal markers. Based on these results, PAMs with a biomimetic surface of LM and poly-D-lysine (PDL) were formulated and their total charge as well as the homogeneity of the LM biomimetic surface was characterized by zetametry and immunofluorescence imaging. PAMs delivering NT3 were formulated and the NT3 release kinetics characterized *in vitro*. These combined properties should act together to stimulate the survival and differentiation of the grafted MIAMI cells toward a neuronal phenotype. After adhesion of MIAMI cells to PAMs, these complexes were first characterized *in vitro*. Next, using a rat partial progressive 6-OHDA model of PD their effects on MIAMI cell survival and differentiation as well as on the motor behavior of the animals and tissue repair/protection were further evaluated.

2. Materials and methods

2.1. Bone marrow harvesting, selection & expansion of MIAMI cells

Whole bone marrow was obtained from vertebral bodies (T1–L5) of a 3 year old male cadaveric donor following guidelines for informed consent set by the University of Miami School of Medicine Committee on the Use of Human Subjects in Research. As previously described [49], isolated whole bone marrow cells were plated at a constant density of 10^5 cells/cm^2 in DMEM-low glucose, containing 5% foetal bovine serum (FBS) (Hyclone, South Logan, Utah) and antibiotics (AB) pansionredally plated in flaskrating steps this medium (100 U/mL penicillin, 0.1 mg/mL streptomycin, 0.25 μg/mL amphotericin B, Sigma, St-Quentin Fallavier, France) on an FN (Sigma), substrate under hypoxic conditions (3% O_2, 5% CO_2, 92% N_2). Fourteen days later, the non-adherent cells were removed and pooled colonies of adherent cells were selected and plated at low density for expansion (100 cells/cm^2) on 1.25 ng/cm^2 FN substrate in DMEM-low glucose (Gibco, Cergy Pontoise, France) containing 3% FBS and AB (40 mL/175 cm^2 flask) under hypoxic conditions. Cells were fed every 2–3 days by changing half the medium and split every 5 days, keeping 1/4 of old medium.

2.2. Neuronal differentiation in vitro

To assess the effects of the extracellular matrix molecules on the 3-step *in vitro* neuronal differentiation of MIAMI cells (passage 4–5) they were first expanded for 10 days in DMEM-low glucose with 20 ng/mL of both EGF and bFGF, 5 μg/mL heparin and a mixture of lipids (working concentration of 510 nM lipoic, 70 nM linolenic and 150 nM linoleic acid, all from Sigma) (pre-treatment step). As previously described [11], the protocol continued with the 3-step neuronal differentiation by plating the cells at 3000–4000 cells/cm^2 on either FN or LM (from human placenta, Sigma) coated dishes (all at 2 μg/cm^2) in DMEM-F12 (GIBCO) medium supplemented with 20% FBS, 20 ng/mL of both EGF-bFGF, 5 μg/mL heparin, antibiotics and cultured for 24 h in a normoxic atmosphere (Neural specification, step 1). Coating molecules were diluted in Dulbecco's phosphate buffered saline (DPBS) (without Ca and Mg) and coating was made in presence of 1 mM $CaCl_2$ for LM as it was previously reported to enhance its stabilization [53]. When plated on glass slides, LM coating was made at 0.5 μg/cm^2 as it allowed a sufficient attachment of cells during differentiation. At the end of step 1, cells were washed and neuronal commitment (step 2) was induced by exposing the cells to 1 mM β-mercaptoethanol (Sigma), 30 ng/ml NT3 (R&D Systems) for 2 days. Neuronal differentiation (step 3) was induced by washing and then exposing the cells to 100 μM butylated hydroxyanisole, 25 mM KCl, 2 mM

Please cite this article in press as: Delcroix GJ-R, et al., The therapeutic potential of human multipotent mesenchymal stromal cells combined with..., Biomaterials (2010), doi:10.1016/j.biomaterials.2010.10.041

valproic acid, 4 μM forskolin, 1 μM hydrocortisone, 5 μM insulin, 5 mM Hepes, 4 μM forskolin, 10 μM rolipram (all from Sigma), 30 ng/mL NT3, 10 ng/mL NGF (R&D Systems), and 30 ng/mL BDNF (R&D Systems) for 3 days.

For transplantation studies, EGF-bFGF pre-treated cells were used as such in some cases, or were further induced toward a dopaminergic phenotype (DI-MIAMI cells). DI-MIAMI cells were obtained prior to their attachment to PAM biomimetic surface (see Fig. 3A). Pre-treated cells were plated (3000–4000 cells/cm^2) on a 2 μg/cm^2 LM substrate in DMEM-F12 containing 20% FBS, 20 ng/mL of both EGF-bFGF and 5 μg/mL heparin for 24 h. Medium was then replaced by DMEM-F12 containing 200 ng/mL SHH and 100 ng/mL FGF8b for another 24 h (both from R&D Systems). Finally, cells were exposed to 0.5 μM retinoic acid (Sigma) during the last 24 h before attachment to PAMs.

2.3. Immunocytofluorescence & cell length analyses in vitro

Cells were plated on coated glass slides for NFM and β3-Tubulin immunocytofluorescence staining at the end of the neuronal differentiation protocol. After washing twice with DPBS, cells were fixed with 4% paraformaldehyde (PFA) (Sigma) at 4 °C for 15 min and then permeabilized for 5 min with DPBS containing 0.2% Triton X-100 (DPBS-T) (Sigma). Slides were blocked with DPBS-T, 10% normal goat serum (NGS) (Sigma), 4% bovine serum albumin (BSA) (Sigma) at room temperature (RT) for 45 min. After 3 washes in DPBS, slides were then incubated overnight at 4 °C with anti-NFM (1:50, clone NN18, Sigma) or anti-β3-Tubulin (1:1000, clone SDL.3D10, Sigma) antibodies in DPBS-T-4% BSA. Controls were made without primary antibody and with isotypic IgG1k (clone MOPC-31C, BD Biosciences) or IgG2bk (clone 27-35, BD Biosciences). After 3 further washes in DPBS, slides were incubated with 2.5 μg/mL secondary biotinylated anti-mouse antibody (Vector, Burlingame, CA, USA) in DPBS-T-4% BSA for 1 h at RT. Finally, after washing 3 times in DPBS, and following incubation with 20 μg/mL streptavidin FITC (Dako) in DPBS for 40 min at RT, slides were mounted and observed with a fluorescence microscope (Axioscop, Carl Zeiss, Le Pecq, France), a CoolSnap ES camera (Photometrics, Tucson, Arizona) and Metamorph™ software (Roper Scientific, Evry, France). Immunocytofluorescence results are presented as the mean ± average deviation of averaged object intensities calculated from 6 different images. Metamorph™ was also used for cell length analyses and results are presented as the average length of the 3 longer cells of 5 different images ± average deviation.

2.4. Reverse transcription and real-time quantitative PCR

Design of primers specific for human genes and PCR were performed as described elsewhere [11] (Table 1). Cells were lysed in a 1% β-mercaptoethanol containing buffer and RNA extracted following treatment by DNAse to remove any traces of genomic DNA (Total RNA isolation Nucleospin® RNA II, Macherey Nagel, Hoerdt, France). First strand cDNA synthesis was performed with a Ready-To-Go You-Prime First Strand Beads® kit in combination with random hexamers (Amersham Biosciences, Orsay, France) using 1 μg RNA according to the manufacturer's guidelines. Following first strand cDNA synthesis, cDNAs were purified (Qiaquick PCR purification kit, Qiagen, Courtaboeuf, France), eluted in 50 μL RNAse free water (Gibco). Five microliters of cDNA (1:20) were mixed with iQ SYBR Green Supermix (Biorad) and primer mix (0.2 μM) in a final volume of 15 μL. Amplification was carried on a Chromo4 thermocycler (Biorad) with a first denaturation step at 95 °C for 3 min and 40 cycles of 95 °C for 10 s, 55 °C for 15 s and 72 °C for 15 s. After amplification, a melting curve of the products determined the specificity of the primers for the targeted genes. A mean cycle threshold value (Ct) was obtained from 2 measurements for each cDNA. Several housekeeping genes, Glyceraldehyde-3-phosphate dehydrogenase (Gapdh, NM_002046), Hypoxanthine phosphoribosyltransferase 1 (Hprt1,NM_000194), Beta actin (Actb, NM_001101), 30S ribosomal protein S18 (Rps18, NM_001093779) and Heat shock 90 kD protein 1 beta (Hspcb, NM_007355) were tested for normalization. The GeNorm™ freeware (http://medgen.ugent.be/jvdesomp/genorm/) was used to determine that Gapdh, Hprt1 & Hspcb were the three most stable housekeeping genes. The relative transcript quantity (Q) was determined by the delta cT method $Q = E$ (Ct min in all the samples tested-Ct of the

Table 1
Human specific primer sequences.

Gene	Full name	NM accession number	Sequences	Amplicon
ITGB1	Integrin B1	002211-033666-033667-033669-033668-133376	F = 5′-CGGACAGTGTGTTTGTAGG-3′	161
			R = 5′-CAGTGTAGTTGGGGTTGC-3′	
ITGB3	Integrin B3	000212	F = 5′-TACAAACACGTGCTGACG-3′	196
			R = 5′-GAGTCTTGGCATCAGTGG-3′	
ITGB4	Integrin B4	000213-001005619-001005731	F = 5′-CTGCACCTACAGCTACACC-3′	173
			R = 5′-CACAGTACTTCCAGCATAGC-3′	
ITGA1	Integrin A1	181501	F = 5′-GGCCGTAGTTAAAGTGACC-3′	185
			R = 5′-GTGAATCTAGGGTGACACG-3′	
ITGA2	Integrin A2	002203	F = 5′-TCCAGACAGTACAGCTAACG-3′	187
			R = 5′-GCAACCAGAGCTAACAGC-3′	
ITGA3	Integrin A3	005501-002204	F = 5′-TGAGAACTTCTACCCAGACC-3′	187
			R = 5′-CTGTCTGGAAAGTGTGACC-3′	
ITGA4	Integrin A4	000885	F = 5′-CGCTTCAGTGATCAATCC-3′	166
			R = 5′-GGCACTCTGGTTGTAAGC-3′	
ITGA5	Integrin A5	002205	F = 5′-GAGCAGAACCATGTGTACC-3′	181
			R = 5′-CAAAGTAGTCACAGCTCAGG-3′	
ITGA6	Integrin A6	000210-001079818	F = 5′-CCCAGATATTGCAGTTGG-3′	200
			R = 5′-CTGAATCTGAGAGGGAACC-3′	
ITGA7	Integrin A7	002206	F = 5′-GACTCACTGCACTACTCAGG-3′	192
			R = 5′-CAGCTCTACCTCCAGTTCC-3′	
ITGA8	Integrin A8	003638	F = 5′-GAGATTCGGTAGTGCTATGG-3′	168
			R = 5′-ACTCCTTGCAGAACTTGG-3′	
ITGA9	Integrin A9	002207	F = 5′-ACTGGAGAGGAGGAGAGG-3′	195
			R = 5′-CCCCAAAGCTAGATACAGG-3′	
ITGA11	Integrin A11	001004439-012211	F = 5′-CATCCTGAAGACACCTAAGC-3′	183
			R = 5′-CTGGCATTGATCTGAACC-3′	
ITGAV	Integrin AV	002210	F = 5′-CAGTCCCATCTCAAATCC-3′	160
			R = 5′-CTGGCCCTGTATAAGATAGC-3′	
Nurr1 (NR4A2)[a]	nuclear receptor subfamily 4, group A, member 2	006186	F = 5′-TTGCCAGATGCGCTTCGACG-3′	414
			R = 5′-CCAACAGCCAGGCACTTCTG-3′	
DAT[a]	Dopamine transporter	001044	F = 5′-GAAGGTGGTATGGATCACAG-3′	121
			R = 5′-GTAGAAGTCAACGCTCAGGT-3′	
TH[a]	Tyrosine hydroxylase	199292-000360-199293	F = 5′-CACCATCTAGAGACCCGGCC−3′	290
			R = 5′-GCAATCAGCTTCCTGCGCTG−3′	
NT3	Neurotrophin 3	Commercial primers ordered from Qiagen, ref #QT00204218		
NGF	Nerve growth factor	Commercial primers ordered from Qiagen, ref #QT00001589		
BDNF	Brain-derived neurotrophic factor	Commercial primers ordered from Qiagen, ref #QT00235368		
GDNF	Glial cell line-derived neurotrophic factor	Commercial primers ordered from Qiagen, ref #QT00043330		
STC1[a]	Stanniocalcin 1	003155	F = 5′-AGGCAAGGCTGACTTCTCTG-3′	102
			R = 5′-AACTACTTGTCGCATTGGGG-3′	

[a] Primers ordered from Origen, USA.

Please cite this article in press as: Delcroix GJ-R, et al., The therapeutic potential of human multipotent mesenchymal stromal cells combined with..., Biomaterials (2010), doi:10.1016/j.biomaterials.2010.10.041

sample) where E is related to the primer efficiency ($E = 2$ if the primer efficiency = 100%). Relative quantities (Q) were normalized using the multiple normalization method described in Vandesompele et al. [54]. Q normalized = Q/(geometric mean of the 3 most stable housekeeping genes Q).

2.5. Integrin screening by flow cytometry

Cells were washed with DMEM-low glucose and detached with 10 mL Versene (Lonza) for 20 min at 37 °C. After pelleting at 295 g for 10 min, cells were washed twice before distribution in 296 well plates (10^5 cells/50 μL). 50 μL of 10 μg/mL mouse monoclonal anti-integrin antibodies (CD29, CD49e, CD49c and CD49b, all from BD Biosciences, Le Pont De Claix, France) or IgG1k isotypic antibody (BD Biosciences) solutions diluted in DPBS, 5% FBS, 0.02% azide were added and incubated for 1 h at 4 °C. After washing, 20 μg/mL FITC-conjugated anti-mouse antibody (Dako) was added for 30 min at 4 °C. Cells were rinsed 3 times before a final addition of DPBS, 0.02% azide and transfer to tubes containing DPBS, 0.02% azide, 0.7% formaldehyde. Every washing step was performed with DPBS, 5% FBS, 0.02% azide. Fluorescent signal was acquired using a FACScalibur flow cytometer (BD Biosciences) and data analysis was performed using the Cellquest™ software (BD Biosciences).

2.6. Formulation of NT3 solid particles and encapsulation within microspheres

PLGA microspheres of an average diameter of 60 μm were prepared using an s/o/w emulsion solvent extraction-evaporation process described in [55], with modifications. Polymer used was a poly(lactic-co-glycolic acid) (PLGA) copolymer with a lactic:glycolic ratio of 37.5:25 (MW: 25,000 Da) (Phusis, Saint Ismier, France). The protein loading was 1 μg of NT3 (Abcys, Paris, France) with 5 μg of human serum albumin (HSA) (Sigma)/mg of microspheres. First, NT3 and HSA were precipitated separately using a process previously described [55] and adapted to each protein. Briefly, 1.077 g of cold glycofurol was added to 10 μl of a NaCl solution (0.3 M) containing 50 μg NT3 and 1 mg poloxamer 188 (Lutrol F68, BASF). After 30 min on ice, the protein particles were harvested by 30 min centrifugation at 10,000 g. HSA solid particles were produced in a similar manner, adding 1.077 g of cold glycofurol on 25 μl of a NaCl solution (0.3 M) containing 250 μg HSA and 5 mg poloxamer. After supernatant removal, the NT3 and HSA solid particles were mixed with 670 μL of organic phase made of 50 mg PLGA dissolved in a 3:1 methylene chloride:acetone solution. This organic phase was emulsified in a poly(vinylalcohol) (Mowiol® 4-88, Kuraray Specialities Europe, Frankfurt, Germany) aqueous solution (90 ml, 4% w/v) maintained at 1 °C and mechanically stirred at 550 rpm for 1 min (Heidolph, RZR 2041, Merck Eurolab, Paris, France). After addition of 100 ml of deionized water and stirring for 10 min, the resulting o/w emulsion was added to 500 mL deionized water and stirred for a further 20 min to extract the organic solvent. Finally, the microparticles were filtered on a 0.45 μm filter (HVLP type, Millipore SA, Guyancourt, France), washed five times with 100 ml of deionized water and freeze-dried. The average volume diameter and the size distribution of the resulting microspheres were evaluated using a Multisizer™ Coulter Counter (Beckman Coulter, Roissy, France). Encapsulation yield was determined after dissolution of microspheres in acetone, centrifugation and evaporation, using a NanoOrange® protein quantification kit (Invitrogen, Cergy Pontoise, France) and following the manufacturer's guidelines. To assess the effects of NT3, microspheres without NT3 were also formulated and covered with a biomimetic surface. Thus, in the following, we will distinguish PAMs encapsulating NT3 (PAMs-NT3) and PAMs without NT3 (PAMs-Blank). When no precision is given, the term PAMs refers to both PAMs-NT3 and PAMs-Blank. For technical reasons, microspheres with a reduced diameter (mean of 25 μm) were also formulated to perform zeta potential measurements. We produced these microspheres using the above protocol with increased poly(vinylalcohol) concentration (6% w/v) and agitation speed (1000 rpm).

2.7. Formulation of PAMs

To obtain PAMs, PLGA microspheres were coated with LM. A combination of LM with the highly charged PDL (Sigma) molecules was used to favor cell attachment on PAM surface. 6 mg of microspheres were resuspended in DPBS and sonicated upon full dispersion of the microspheres. Coating solutions were prepared in DPBS, mixed to the microsphere suspension (final volume: 12 mL) and placed under rotation at 15 rpm at 37 °C during 4 h. After coating, PAMs were washed 3 times in distilled sterile water, lyophilized and finally kept at −20 °C for long-term storage. Every tube was covered with sigmacote ® (Sigma) to prevent product loss on the tube walls. The final concentration of the coating molecules was 40 μg/mL of LM or of a mixture of PDL/LM. For optimization of the PDL/LM coating, the ratio PDL-LM of 60/40 was changed to 40/60 after zeta potential evaluation, in order to maximize the quantity of LM adsorbed to the surface. The incubation time was finally decreased to 1.5 h as well as the total coating molecules concentration (15 μg/mL).

2.8. Zeta potential

A Zetasizer 2000 (Malvern Instruments, Orsay, France) operating at 150 V at RT was used to assess PAM electrical surface charge variations depending on the coating used. Briefly, PAMs were redispersed in 10 mL of 1 mM NaCl and sonicated prior to every measurement. The chamber was washed with ultrapure water (Millipore) between every sample. Results are presented as the average ± standard deviation of three experiments and 10 measurements were performed in each experiment.

2.9. PAM immunofluorescence

Tubes containing 1 mg coated or uncoated lyophilized PAMs were resuspended in DPBS, 4% BSA, 0.2% Tween 20 and placed for 30 min at RT under 15 rpm rotation. Samples were then washed three times with DPBS followed by a centrifugation step at 9000 g for 5 min and supernatant removal. Incubation with mouse monoclonal anti-laminin antibody (Sigma) diluted at 100 μg IgG/mL in DPBS, 4% BSA, 0.2% Tween 20 was performed at 37 °C for 1.5 h under rotation. For negative controls, incubation was performed in the same solution without anti-laminin antibody. After incubation, samples were washed again 4 times before incubation with anti-mouse biotinylated antibody (Vector) diluted at 2.5 μg/mL in DPBS, 4% BSA, 0.2% Tween 20 for 1 h at RT under rotation. After three washes, samples were incubated with streptavidine-fluoroprobe 547 (Interchim, Montluçon, France) diluted 1:500 in DPBS for 40 min at RT under rotation. Samples were finally washed three times with DPBS and observed under confocal microscopy (Olympus Fluoview™ TU 300, Rungis, France). Every condition was observed in triplicate and 3 independent experiments were performed.

2.10. In vitro NT3 release profile and bioactivity of the released protein

NT3 was labeled with ^{125}I by the iodogen method as previously described [56]. Briefly, 50 μL of $Na^{125}I$ (4.625 MBq) was added in a tube coated with 0.4 μg of iodogen (1,3,4,6-tetrachloro-3a,6a-diphrenylglycouril, Sigma) and mixed at RT during 3 min 50 μg of NT3 was dissolved in 100 μL of phosphate buffer (67 mM KH_2PO_4, 33 mM Na_2HPO_4 $12H_2O$; pH = 6.8) and then added to the tube containing $Na^{125}I$ and mixed during 45 min at RT. Free ^{125}I were separated from ^{125}I-labeled NT3 using a PD10 column (GE Healthcare) prior to precipitation and encapsulation within PAMs. An *in vitro* kinetic release was performed by placing 5 or 50 mg of PAMs in 500 μL of DPBS containing 0.1% BSA and 0.02% sodium azide. At different times, PAMs-NT3 were centrifugated for 5 min at 800 g and radioactivity measured in the supernatant using a gamma counter Minaxi AutoGammas 5000 (Packard, Australia). To assess the bioactivity of the released NT3, MIAMI cells were plated on fibronectin at 3000 cells/cm^2 in DMEM-F12 containing 20% FBS and 10 ng/mL bFGF. After 24 h, medium was changed with DMEM-F12 containing 1 mM β-me and diluted kinetics samples. After 48 h, the increased proliferation rate when exposed to NT3 was measured using the Cyquant cell proliferation assay® (Invitrogen), following the manufacturer's guidelines. NT3 concentration in the kinetics samples was estimated by comparing the obtained cell density with density of MIAMI cells exposed to known concentration of NT3. Presented radioactivity count results were obtained from a representative experiment and bioassay results expressed as average NT3 release ± standard deviation.

2.11. Formation of PAMs/DI-MIAMI cells complexes

DI-MIAMI cells were washed with DMEM-F12, detached with 0.16% trypsin (Sigma), 0.02% EDTA (Lonza) solution, and pelleted at 295 g for 10 min. Cell pellets were resuspended in culture medium supplemented with 3% FBS. 0.75 mg lyophilized microspheres were resuspended in coated Eppendorf tubes (Sigmacote, Sigma) containing DMEM-F12, 3% FBS for 15 min. PAM suspension was sonicated and briefly vortexed prior to addition of 0.5 mL cell suspension (2×10^5 cells/0.75 mg PAMs). The mixture was then gently flushed and plated in 1.9 cm^2 Costar ultra low cluster plate (#3473, Corning, Avon, France). Plates were incubated at 37 °C during 4 h to allow cell attachment on PAM surface. PAMs/cell aggregates were recovered, washed with DMEM-F12 and pelleted by centrifugation at 200 g for 2 min. Cell adhesion to PAM surface was assessed by microscopic observation and cells adhered to PAMs were quantified using the Cyquant cell proliferation assay®. A vehicle solution of CMC-Na-Tween 80-Mannitol (final concentration 0.125%, 0.125% and 0.5%, respectively) was added to the aggregates in a final volume of 10 μL just prior to transplantation. To allow cell tracking after transplantation, DI-MIAMI cells were labeled with the membrane dye PKH26 (Sigma) before attachment to PAMs. Briefly, cells were washed with medium after harvesting and resuspended in 0.5 mL diluent C. PKH26 dye diluted in 500 μL diluent C (1 μL PKH26/1 million cells) was then added to the cell suspension and carefully mixed before incubation at 37 °C for 5 min. Labeling reaction was stopped by washing three times with serum containing medium before proceeding to attachment onto PAMs.

2.12. Animals and surgical procedures

All animal experiments were conducted in accordance with the "Direction des Services Vétérinaires", the "Ministère de l'Agriculture" of France and with the European Communities Council Directive of 24 November 1986 (86/609/EEC). A total of 50 female Sprague–Dawley rats, 12 week old and about 250 g in weight, were used in this study. Rats were anaesthetized with xylazine (7.7 mg/kg) and ketamine (41.5 mg/kg) and positioned in a Kopf stereotaxic instrument. Two injections of 10 μg of 6-hydroxydopamine (Sigma, France, in 5 μl saline supplemented with 0.1% ascorbic acid) were performed to induce a unilateral partial progressive and retrograde lesion

Please cite this article in press as: Delcroix GJ-R, et al., The therapeutic potential of human multipotent mesenchymal stromal cells combined with..., Biomaterials (2010), doi:10.1016/j.biomaterials.2010.10.041

of the nigrostriatal system, a lesion model previously described [57]. The lesion coordinates were: (1) AP: 0.5, L: −2.5, and V: −5 mm, (2) AP: −0.5, L: −4.2, and V: −5 mm relative to Bregma and ventral from dura, with the tooth bar set at 0 mm. Only rats that showed more than 7, but less than 18 net ipsiversive turns per minute eleven days after the lesion were used. They were assigned to one of 6 treatment groups: animals receiving intrastriatal injection of vehicle solution only (carboxymethylcellulose (CMC)-Na-Tween 80-Mannitol), DI-MIAMI cells alone, PAMs conveying DI-MIAMI cells (PAMs-NT3 or PAMs-Blank), PAMs-NT3 alone and MIAMI cells only pre-treated with EGF-bFGF, without dopaminergic induction and without PAMs. On the day of transplantation, 2 weeks post-lesion, 1.5×10^5 cells alone or attached to 0.75 mg of PAMs were stereotactically implanted with a 20 gauges Hamilton microsyringe (with a modified 25° bevel, to allow a better sample aspiration) in the lesioned striatum at the following coordinates: AP+0.5; ML−2.8; DV−5; tooth bar−3.3.

2.13. Behavioral study

Amphetamine-induced rotational behavior was measured in an automated rotometer 11 days after the lesion and 2, 4, 6 & 8 weeks after grafting. The animals were weighed prior to each rotation test. All tests were conducted in a blind manner. 5 mg/kg of D-amphetamine (dissolved in NaCl 0.9%) (Sigma, France) was administered intraperitoneally. Animals were individually placed in circular plastic boxes and attached to the rotational leash 15 min before injection for accustoming. Immediately after amphetamine injection, the test began and the data were recorded for 90 min using a computerized system. A net rotational asymmetry score was expressed as full-body turns per minute in the direction ipsilateral to the lesion. Results are presented as the mean rotations of 5–6 rats per group ± average deviation.

2.14. Histological study

Eight weeks after cell transplantation, the animals were anaesthetized and perfused through the heart with 150 ml of ice-cold 0.9% saline, followed by 300 ml of ice-cold 4% PFA, 2.5% sucrose (Sigma) in DPBS pH 7.4. Brains were left 1.5 h in the PFA solution, then transferred to 10% sucrose solution gradually increased up to 30% during the next 48 h. Brains were finally frozen in cold isopentan (−40 °C) before storage at −80 °C. Striatal and substantia nigra sections, of 14 μm and 30 μm respectively, were made on a CM3050S cryotome (Leica Microsystems).

Immunohistochemistry was used to assess the extent of the striatal lesion using a mouse anti-tyrosine hydroxylase (TH) antibody (1:1000, clone 6D7, Covance, Emeryville, CA, USA). For the detection of DI-MIAMI cells, we used a human specific, mouse anti-mitochondria antibody (1:100, clone MTCO2, Abcam, Paris, France). A mouse anti-CD11b antibody (1:100, clone MRCOX42, Abd Serotec, Cergy Saint-Christophe, France) (specific for macrophage-microglia) and a mouse anti-β3-Tubulin (1:250, clone SDL.3D10, Sigma) were used to assess, respectively, the inflammatory reaction and the presence of neuronal cells. A polyclonal rabbit anti-human TH was also ordered from Eurogentec (AS-DOUB-LX immunization program, Liège, Belgium) after characterization of 2 sequences of peptides specific for human TH. Briefly, rabbits were immunized with both EDVRSPAGP & GTAAPAASYTPTPRS peptides. Serum was harvested 87 days later and used at a 1:250 dilution to detect human MIAMI cells expressing TH 8 weeks after grafting. Sections were first washed with DPBS, 0.1% Triton X-100 (DPBS-T). For TH staining, quenching of peroxidases was made with 0.3% H_2O_2 (Sigma) in DPBS-T, at RT for 15 min. After washing, blocking was performed with DPBS-T, 4% BSA, 10% NGS for 2 h at RT. Sections were incubated overnight at 4 °C with the primary antibodies diluted in DPBS-T, 4% BSA. After washing, sections were incubated at RT for 2 h with the secondary biotinylated anti-mouse antibodies (1:200, Vector) diluted in DPBS-T, 4% BSA. For TH staining, incubation with Vectastain® ABC reagent (Vector) in DPBS was made at RT for 1 h. Sections were washed and revealed with 0.03% H_2O_2, 0.4 mg/mL diaminobenzidine (DAB) (Sigma) in DPBS (2.5% nickel chloride was sometimes added to enhance the signal) and dehydrated before mounting. For human mitochondria and anti-CD11b staining, sections were incubated with Streptavidine-Fluoroprobes 488 ® (1:200, Interchim) diluted in DPBS for 40 min at RT before mounting with fluorescent mounting medium. Free floating TH staining of substantia nigra was performed with a similar treatment as for striatal TH staining, apart from the use of a polyclonal rabbit anti-TH (1:20000, Jacques Boy, Reims, France) and of a biotinylated anti-rabbit secondary antibody (1:500, Vector). At 8 weeks, human mitochondria fluorescent staining was used to quantify cell survival using the Metamorph™ software. For each group, an average fluorescent intensity was calculated from 2 pictures taken in the center of the injection site of3 different rats. The density of TH-positive fibres was also quantified using the Metamorph™ software in both ipsilateral and contralateral side of the striatum. The extent of the lesion was estimated by substracting the TH intensity of the contraleral side minus the intensity of the lesioned side. Results are presented as mean differences ± average deviation and were calculated from 3 slides taken from 5 different rats for each group, unless otherwise stated.

2.15. Statistical analysis

Data are presented as the mean value of three independent experiments ± standard deviation (SD), unless otherwise stated. Significant differences between samples were determined using a Student's *t*-test modified for small samples. $t'_0 = (m_1 - m_2)/(\sqrt{s_1^2/n_1 + s_2^2/n_2})$, differences were considered significant if $|t'_0| > t_{k';0.05}$, with k' being the closer integer of the calculated $k = (s_1^2/n_1 + s_2^2/n_2)^2/[(1/(n_1-1))(s_1^2/n_1)^2 v) + (1/(n_2-1))(s_2^2/n_2)^2)]$. Kruskal–Wallis test was used for multiple comparisons. Threshold *P*-value was set to 0.05, unless otherwise stated.

3. Results

3.1. MIAMI cells integrin subunit screening

In preliminary experiments we observed a higher number of MIAMI cells if expanded on FN compared to other substrates such as collagen (data not shown). This result, together with the reported neuronal inducing effects of LM, prompted us to screen in MIAMI cells the expression of integrins that may interact with FN or LM. During expansion of MIAMI cells, integrin subunits beta 1, alpha 2, 3, 5, 11 and V were highly expressed when evaluated by RT-qPCR. Subunits beta 3, 4 and alpha 1, 4, 6–9 were also detected but at much lower level (data not shown). The high expression of subunits beta 1, alpha 2, 3 and 5 was confirmed by flow cytometry (Fig. 1A), thus showing that FN and LM are adequate molecules for the biomimetic surface of PAMs.

3.2. In vitro neuronal differentiation on laminin vs. fibronectin

We previously demonstrated [11] that during a neuronal induction protocol performed on an FN substrate, EGF-bFGF pre-treated MIAMI-derived neuronal-like cells showed a diminished proliferation rate, presented long neurites (Fig. 1B) and acquired an expression pattern consistent with a neuronal differentiation program. Using Trypan blue counting, we observed that differentiating the EGF-bFGF pre-treated cells on a substrate of LM instead of FN led to a further decrease of cell proliferation that was abolished most of the time (0.61 ± 0.06 doublings on FN *vs.* 0.26 ± 0.05 doublings on LM) during *in vitro* neuronal differentiation. Importantly, dead cells were never observed during differentiation on either substrate. In addition to a decreased proliferation rate, total cell length was increased in most experiments at the end of differentiation; with longer neurites when plated on LM compared to glass or FN (Fig. 1C).

Finally, we also observed by immunocytofluorescence that at the end of the induction protocol MIAMI-derived neuronal-like cells expressed significantly higher levels of β3-Tubulin as well as, to a certain extent, NFM, when plated on LM compared to glass or FN (Fig. 1D, E). We can note that all these trends were also obtained with MIAMI cells not pre-treated with 20 ng/mL of EGF-bFGF, but to a much lower extent (data not shown).

3.3. Characterization of PAM biomimetic surface

Uncoated PLGA microspheres and LM-coated PAMs (40 μg/mL) presented a negative zeta potential (Fig. 2A), which was not satisfactory for cell adhesion. Conversely, PDL-coated PAMs exhibited a positive zeta potential (49.7 ± 2.1 mV). We therefore used a blend of PDL with LM to combine the benefits of a positively charged surface promoting cell adhesion and presenting the ECM molecule. The association of LM with PDL slightly decreased the zeta potential value compared to PDL alone. We next tested conditions allowing to optimize the ratio of PDL/LM, the concentration of coating molecules and the incubation time necessary for adsorption of the molecules on the surface. In this way, the ratio of LM was increased to 60% instead of 40%, the adsorption time decreased from 4 to 1.5 h and the total quantity of coating molecules decreased from 40 μg/mL to 15 μg/mL. We next confirmed these optimized parameters did not impair the positive surface charge, which was 34.5 ± 2.6 mV (Fig. 2A, top right bar), and the homogeneity of the LM surface. Immunofluorescence

Please cite this article in press as: Delcroix GJ-R, et al., The therapeutic potential of human multipotent mesenchymal stromal cells combined with..., Biomaterials (2010), doi:10.1016/j.biomaterials.2010.10.041

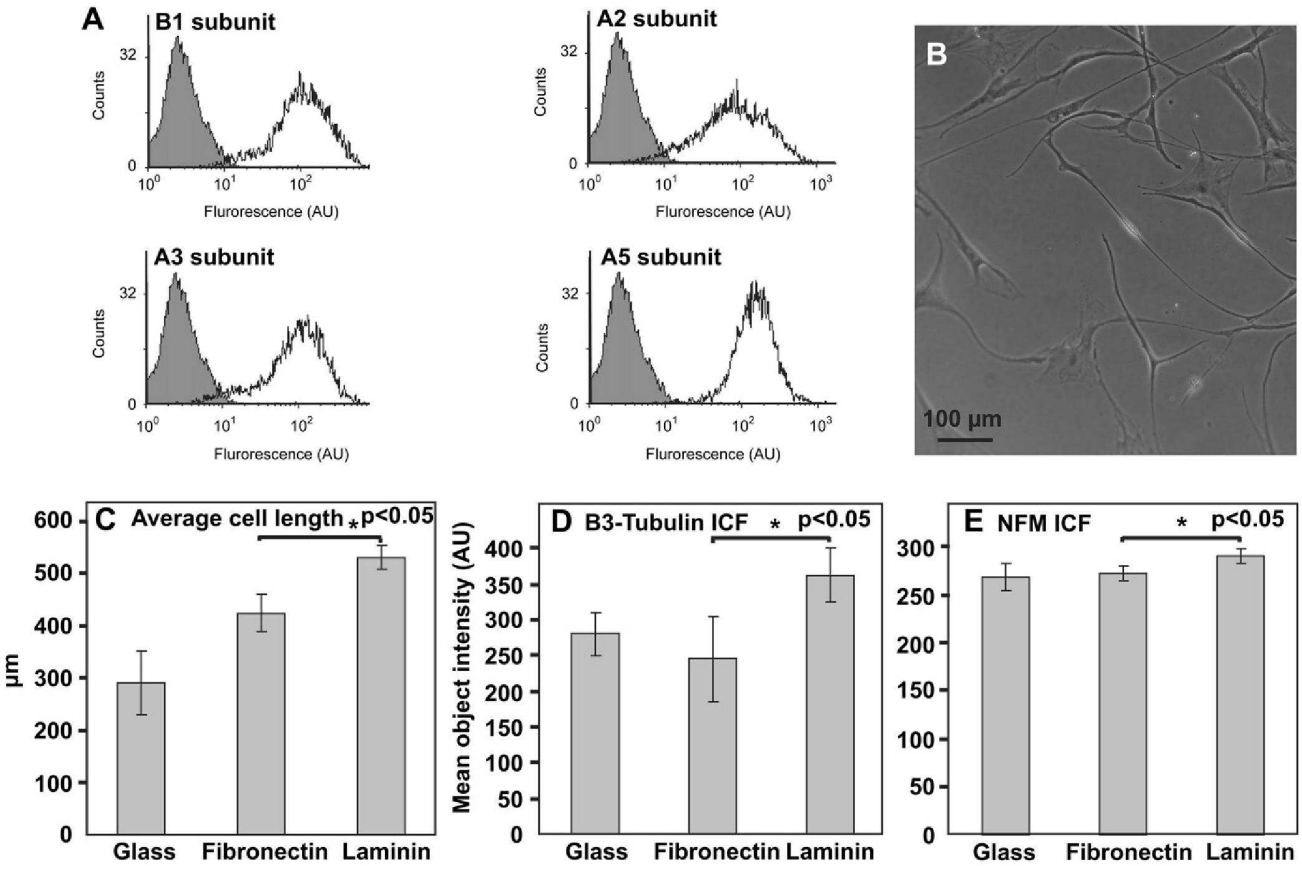

Fig. 1. Laminin (LM) enhanced the extent of MIAMI cell neuronal differentiation. Using flow cytometry, we observed that expanding MIAMI cells strongly expressed the integrin (ITG) subunits beta 1, alpha 2, 3 and 5, making both LM and FN suitable molecules for PAM biomimetic surface (isotypes in grey) (A). During neuronal differentiation, the cells acquired a neuronal morphology (B) and LM enhanced neurite formation and resulted in an increased cell length at the end of step 3 (C). The expression of neuronal markers, β3-Tubulin and NFM (D, E, respectively) were also enhanced at the end of step 3 using an LM substrate, compared to FN or glass as observed by immunocytofluorescence. Cell length results and immunocytofluorescence results are presented as mean length or intensities ± average deviation. Abbreviation: ICF: immunocytofluorescence.

imaging demonstrated that no background signal was observed on controls and uncoated microspheres (Fig. 2B, C) whereas the signal was intense and homogeneous all around the PAMs coated with a mixture of PDL/LM at a ratio of 40/60 (Fig. 2D, *E*). These optimized conditions were further used throughout this study.

3.4. NT3 encapsulation, in vitro release kinetics and bioactivity of the released protein

NT3 loaded microparticles presented a diameter of 57.4 ± 19.0 µm. The yield of the microencapsulation of NT3 was around 100%, as measured using the NanoOrange® protein quantification kit. The radiolabeling assay demonstrated that around 50% of the NT3 encapsulated was released in a sustained manner after 22 days, with only a small burst during the first hours. The bioassay performed with MIAMI cells confirmed that the NT3 was released under a bioactive conformation, meaning that the protein remains active through the precipitation/microencapsulation process and throughout the release (Fig. 2F). Thus, we could estimate that about 75 ng of bioactive NT3 could be released *in vivo* during the first 3 days upon transplantation of 0.75 mg of PAMs, the dose we used in our transplantation experiments.

3.5. In vitro characterization of PAMs/DI-MIAMI cell complexes

The LM biomimetic surface allowed the efficient attachment of 1.5×10^5 MIAMI cells on 0.75 mg of PAMs prior to transplantation, as calculated using the Cyquant cell proliferation assay ®. Importantly, almost all the cells attached to the PAM biomimetic surface after 4 h at 37 °C, and no free floating cells were observed (Fig. 2G). RT-qPCR demonstrated that gene expression of *Nurr1*, *DAT* and *TH* was not modified upon attachment to PAMs as observed by RT-qPCR. Only low levels of these markers were detected in MIAMI cells, without significant differences upon early dopaminergic induction (data not shown).

3.6. Behavioral study

Amphetamine-induced rotational behavior of sham-treated rats continuously increased from the implantation day until the end of the experiment, at 8 weeks. Implantation of DI-MIAMI cells alone did not significantly reduce the number of ipsilateral rotations compared to sham-treated rats (Fig. 3B). However, transplantation of DI-MIAMI cells adhered onto PAMs-NT3 affected the rotational behavior, which was strongly, and significantly, decreased compared to sham-treated rats or rats implanted with cells alone. In addition, PAMs-Blank resulted in a less important, but still significant, decrease in the animal rotational behavior compared to PAMs-NT3. These observations show a behavioral improvement in rats treated with PAMs/DI-MIAMI cells complexes, while neither improvement nor deterioration was observed in control experiments when grafting PAMs-NT3, but without cells (data not shown).

Please cite this article in press as: Delcroix GJ-R, et al., The therapeutic potential of human multipotent mesenchymal stromal cells combined with..., Biomaterials (2010), doi:10.1016/j.biomaterials.2010.10.041

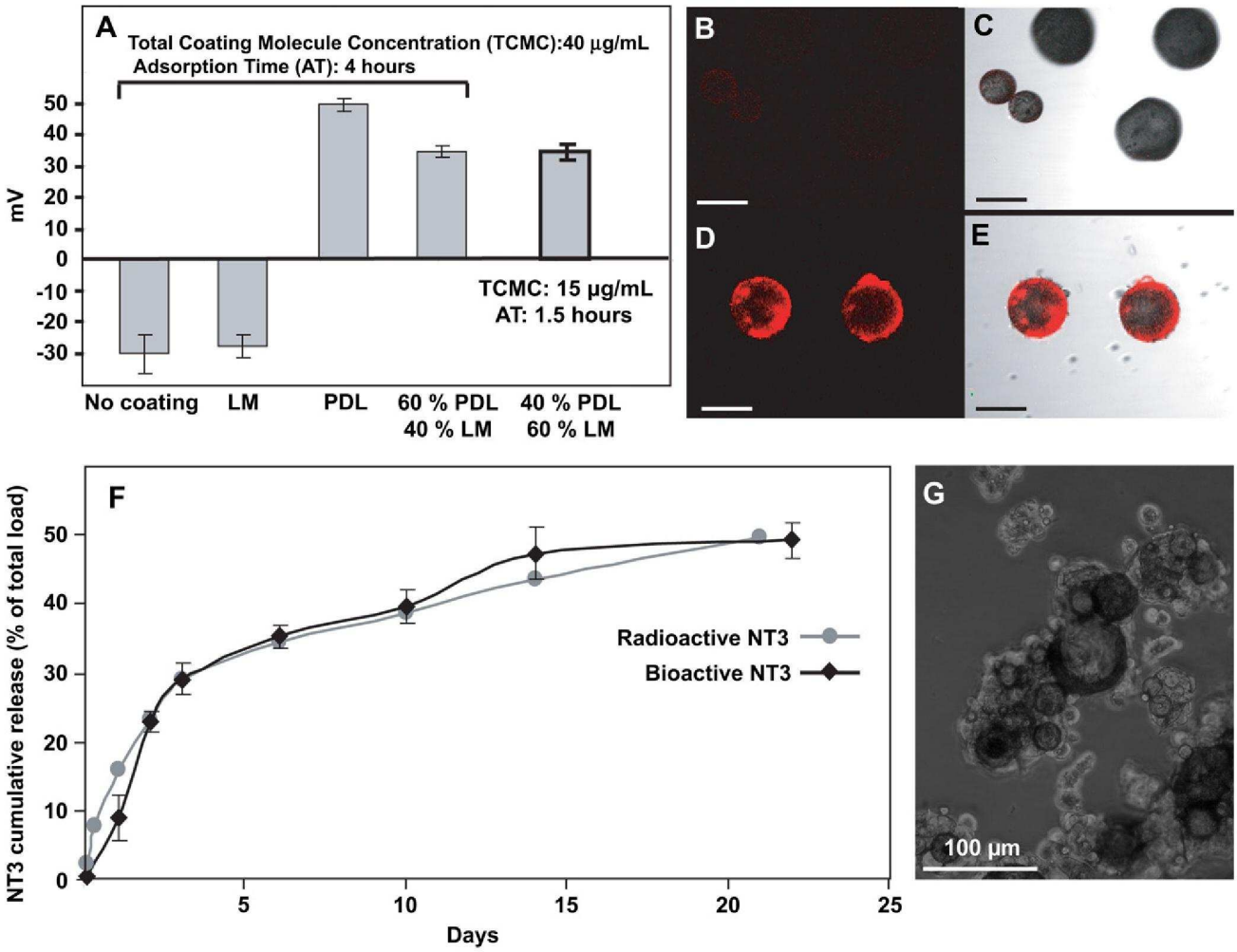

Fig. 2. PAM laminin (LM) biomimetic surface & NT3 release *in vitro*. LM induced a negative zeta potential whereas PDL shifted this potential toward positive values, favorable for cell attachment to the surface. PDL/LM-coated PAM formulation was optimized by using a ratio PDL/LM of 40/60 to increase the quantity of adsorbed LM (A). The adsorption time was decreased from 4 to 1.5 h, and the total molecule concentration used for coating was decreased from 40 µg/mL to 15 µg/mL. No changes in zeta potential were observed using these parameters (A, top right bar). Zeta potential results are presented as average Zeta potential ± standard deviation. Using anti-LM immunofluorescence, uncoated microspheres (B, C) show no staining whereas PDL/LM-coated microspheres (D, E) stained positive with the anti-LM antibody. NT3 encapsulated within PAMs was released in a bioactive conformation as observed using an *in vitro* bioassay (F). After 22 days *in vitro*, about 50% of the encapsulated NT3 was released, as observed by radioactivity counting and bioassay, which correspond to approximately 375 ng of NT3 for 0.75 mg PAMs transplanted per animals. Importantly, LM was homogeneously distributed over the PAM surface, which allowed adhesion of 1.5×10^5 cells to 0.75 mg of PAMs prior to transplantation (G). Presented results were obtained from a representative experiment and expressed as average NT3 release ± standard deviation. C, E: superposition of Nomarsky and fluorescent images. Scale bars: 50 µm. Abbreviations: NT3: neurotrophin 3, PAMs: pharmacologically active microcarriers.

3.7. *Protection of nigrostriatal pathway*

The rotational behavior was linked to the integrity of the lesioned nigrostriatal pathway, as observed using a rat specific anti-TH immunohistochemistry (Fig. 4). Only a few TH-positive fibres remained in the striatum of sham-treated rats 8 weeks after the lesion (Fig. 4A), suggesting that the retrograde neurodegeneration progressed in time concomitantly with the increased rotational behavior. The number of neurons in the ipsilateral substantia nigra (SN) was also importantly reduced compared to the contraletaral side. Transplantation of DI-MIAMI cells in combination with PAMs resulted in a significantly higher density of TH-positive fibres in the lesioned striatum (Fig. 4B, C), therefore demonstrating their neuro-repair properties. However, a higher number of dopaminergic neurons were also observed in the ipsilateral SN in 40% of the animals, suggesting that a neuroprotection of the nigrostriatal pathway occurred in addition to a repair mechanism due to fibre outgrowth. Transplantation of DI-MIAMI cells without PAMs induced only a small, non significant, protection of the striatal dopaminergic fibres compared to sham-treated rats (data not shown).

3.8. *Cell fate in vivo*

In vitro, the cytoplasmic membrane marker PKH26 did not diffuse to surrounding cells during co-culture experiments and was consequently used to track transplanted DI-MIAMI cells *in vivo*. PKH26-positive cells co-localized nicely with the anti-human mitochondria-positive cells in the grafted area, therefore confirming that a significant fraction of cells survived and integrated within the parenchyma 2 months after transplantation (Fig. 5A). No strong inflammatory reaction was observed with OX42 (CD11b) staining and only a small fraction of PKH26 dye co-localized with macrophage/microglia, suggesting phagocytosis occurred to a very limited extent (Fig. 5A). After 8 weeks, and as depicted by Fig. 5A,

Please cite this article in press as: Delcroix GJ-R, et al., The therapeutic potential of human multipotent mesenchymal stromal cells combined with..., Biomaterials (2010), doi:10.1016/j.biomaterials.2010.10.041

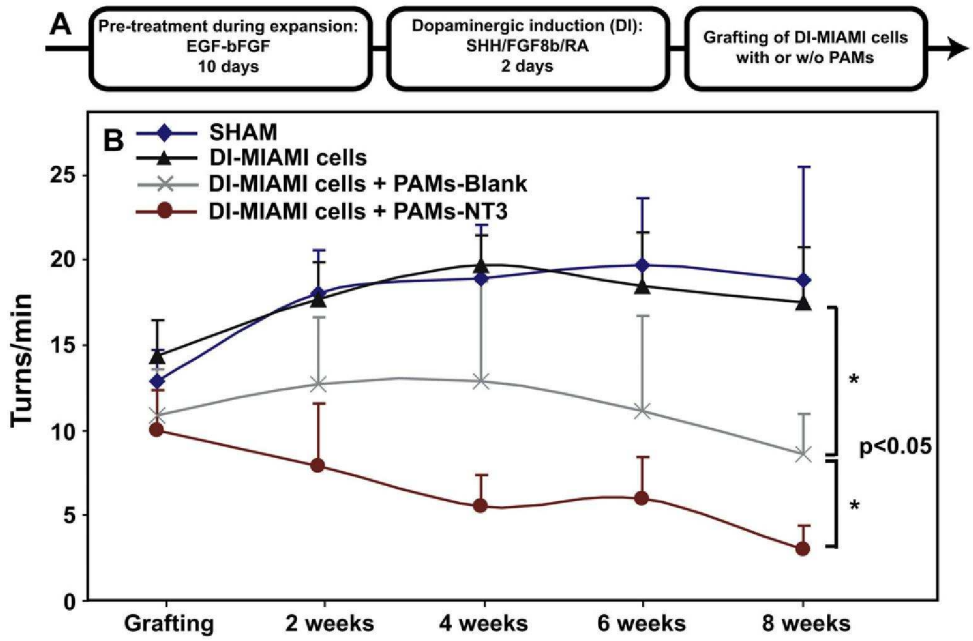

Fig. 3. Functional recovery during amphetamine-induced rotational behavior. Before transplantation, cells were pre-treated with EGF-bFGF and further induced toward a dopaminergic phenotype (DI-MIAMI cells) prior to their attachment to PAM biomimetic surface (A). Rats transplanted with medium alone (sham-operated) exhibited a constant increase of their rotational behavior during 6 weeks before stabilization at 8 weeks (B). Rats transplanted with DI-MIAMI cells alone did not exhibit a statistically significant reduced rotational behavior compared to sham-operated rats. However, DI-MIAMI cells adhering to PAMs-NT3 resulted in a constant, and statistically significant, decrease until the end of the experiment. PAMs-Blank also led to an improved rotational behavior, but to a lesser extent compared to PAMs-NT3. Results are presented as the mean rotations of 5–6 rats per group ± average deviation. Abbreviations: DI-MIAMI: dopaminergic-induced marrow-isolated adult multilineage inducible, NT3: neurotrophin 3, PAMs: pharmacologically active microcarriers.

a higher number of MIAMI cells was observed by immunostaining upon transplantation with PAMs-NT3. PAMs were also still detected at that time (Fig. 5B). This increased survival was confirmed by semi-quantification of human mitochondria-positive cells within the striatum after 8 weeks (Fig. 5C). These data demonstrated that PAMs increased by 2 fold the survival of DI-MIAMI cells, an effect that was even more significant (3 fold) if NT3 was released by the PAMs. This may explain the differential functional recovery observed between PAMs-NT3 and PAMs-Blank. In comparison, DI-MIAMI cells alone poorly survived within the striatum. After 8

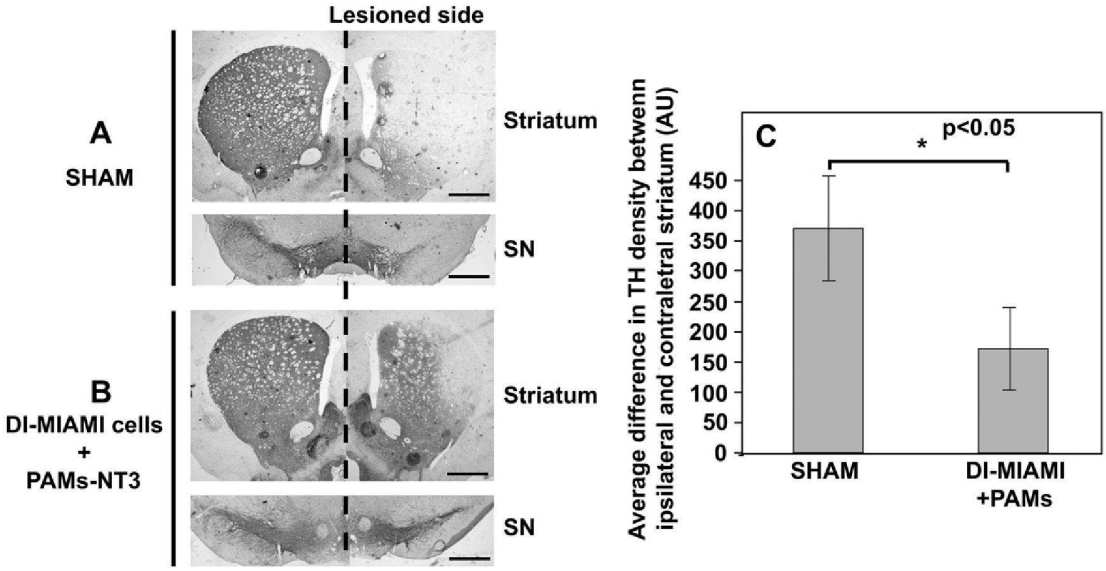

Fig. 4. Neuroprotection/reparation of nigrostriatal pathway induced by PAMs/DI-MIAMI cell complexes. Eight weeks after transplantation, only a few TH-positive fibres were observed in the striatum and a few TH-postive neurons were found in the SN of sham grafted rats (A). Transplantation of DI-MIAMI cells combined to PAMs resulted in an important neuroprotection of the nigrostriatal dopaminergic system, as observed in the striatum and SN (B) and confirmed by densitometric analysis (C). Scale bars: 1 mm. Abbreviations: SN: substantia nigra, DI-MIAMI: dopaminergic-induced marrow-isolated adult multilineage inducible, PAMs: pharmacologically active microcarriers, TH: tyrosine hydroxylase. Densitometric results are presented as mean difference intensities between contraleral and ipsilateral striatum ± average deviation.

Please cite this article in press as: Delcroix GJ-R, et al., The therapeutic potential of human multipotent mesenchymal stromal cells combined with..., Biomaterials (2010), doi:10.1016/j.biomaterials.2010.10.041

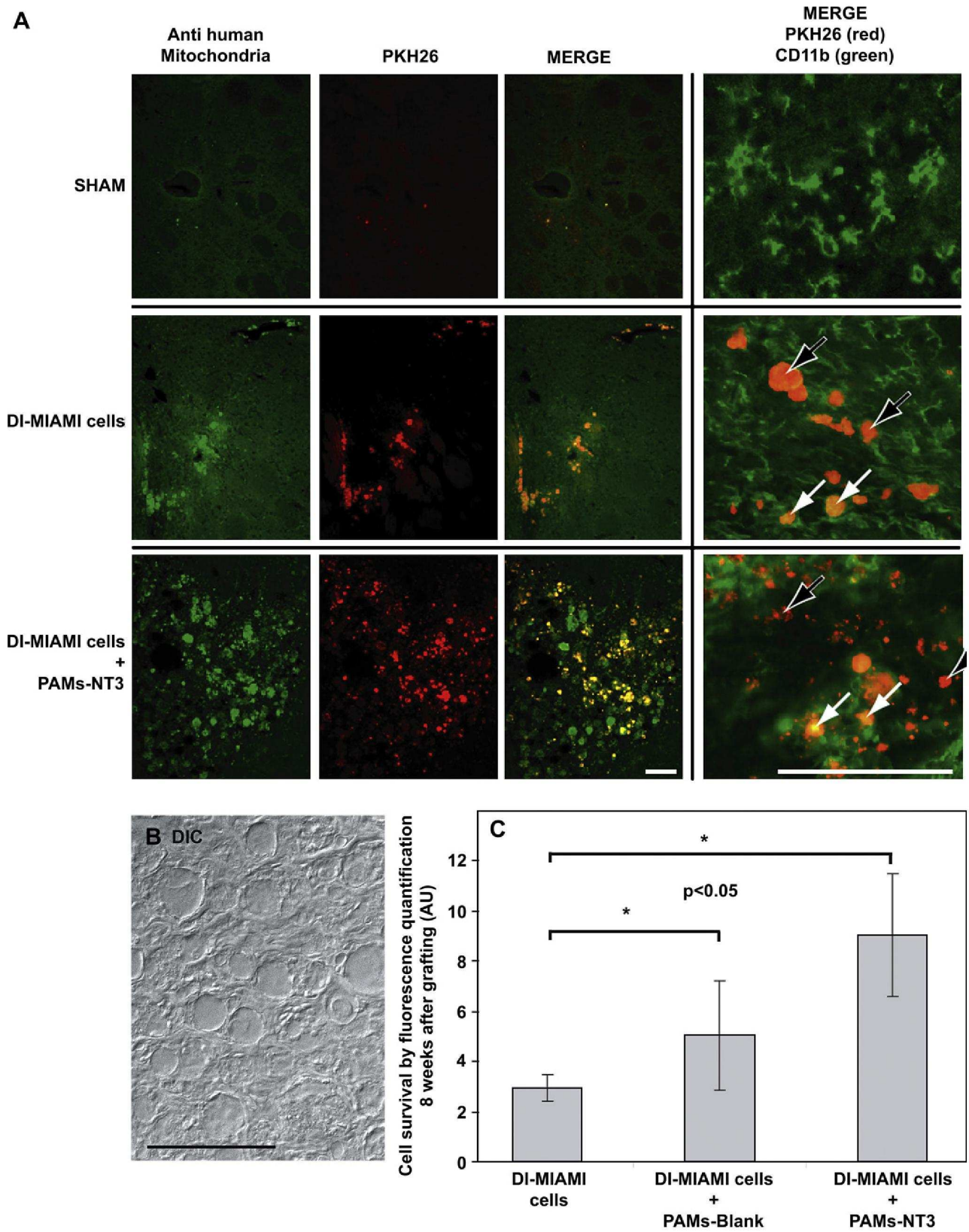

Fig. 5. PAMs increased MIAMI cell survival *in vivo*. Colocalization of PKH26 and anti-human mitochondria staining demonstrated that DI-MIAMI cells were still present in the striatum of rats 8 weeks after transplantation (A). There was no strong immune reaction, and most of the PKH26 staining observed did not co-localize with macrophage/microglia (black arrows). White arrows point to engulfed PKH26. DIC: differential interference contrast image showing PAMs at the implantation site 8 weeks after grafting (B). Eight weeks after transplantation, cell survival was almost 2 fold higher in presence of PAMs-Blank, and more than 3 fold higher in presence of PAMs-NT3 (C), as observed by quantification of human mitochondria fluorescent staining intensity. Results are presented as the mean cell survival ± average deviation. Scale bars: 100 μm. Abbreviations: DI-MIAMI: dopaminergic-induced marrow-isolated adult multilineage inducible, PAMs: pharmacologically active microcarriers, NT3: neurotrophin 3, TH: tyrosine hydroxylase.

Please cite this article in press as: Delcroix GJ-R, et al., The therapeutic potential of human multipotent mesenchymal stromal cells combined with..., Biomaterials (2010), doi:10.1016/j.biomaterials.2010.10.041

weeks, certain cells seemed to express a slight amount of β3-Tubulin in the striatum of rats. Most importantly, a fraction of DI-MIAMI cells expressed TH only if combined to PAMs (Fig. 6C, D), while this was almost not observed for DI-MIAMI cells alone (Fig. 6A, B).

3.9. EGF-bFGF pre-treated MIAMI cells, without dopaminergic induction

Interestingly, EGF-bFGF pre-treated MIAMI cells transplanted without PAMs survived as poorly as DI-MIAMI cells transplanted alone (Fig. 7A). However, and in opposition to DI-MIAMI cells alone, these cells did induce on their own a functional recovery and a high density of striatal TH-positive fibres, similarly to that observed upon PAMs/DI-MIAMI cell transplantation (Fig. 7B, C). This interesting effect of MIAMI cells only pre-treated with EGF-bFGF may be explained by their distinct profile of secretion of growth factors. Indeed, RT-qPCR demonstrated that MIAMI cells always expressed a low amount of the three neurotrophins (*NT3*, *NGF* and *BDNF*, data not shown), while EGF-bFGF pre-treated cells expressed a higher amount of molecules such as *GDNF* and *Stanniocalcin 1* (*STC1*) compared to DI-MIAMI cells, which may be one of the reasons for the benefits observed upon transplantation of EGF-bFGF pre-treated cells without dopaminergic induction. Noteworthy, adhesion onto PAMs tended to increase the expression profile of these molecules by DI-MIAMI cells, as observed by RT-qPCR (Fig. 7D, *E*). However, the potential role of these molecules in the observed functional recovery would need to be further examined as part of future studies.

4. Discussion

Adult cells may be easily isolated from the patient body, in particular from accessible tissues (i.e., blood, skin, bone marrow), therefore permitting autologous grafts to be performed in the clinic without ethical problems. For this reason, as well as for their immunomodulatory and tissue repair capacities, their ability to differentiate into neuronal-like cells and to secrete a variety of molecules, the potential of MSCs to treat neurodegenerative disorders, and especially PD, has been recently investigated [5]. However, the percentage of MSCs that survive and express neural/neuronal markers after transplantation in the brain remains very low [22,29]. Thus, functional improvements obtained in animal models of PD are thought to primarily derive from the action of growth factors and chemokines produced by transplanted MSCs [27,28], which also seems to be the case in several other defects [58–60]. Tissue engineering may be of great interest to help repair lesioned tissues/organs due to the possible increase in grafted cell survival, differentiation, or secretory profile induced by the supportive element or scaffold. In this study, we used carriers providing a biomimetic support and the delivery of a growth factor, the PAMs, combined with MIAMI cells to maximize the resulting protective/reparative effects on hemi-parkinsonian rats. We here demonstrated the efficacy of this tool in a rat model of PD, as an important motor function recovery was observed upon grafting with PAMs/DI-MIAMI cell complexes, while no major effects were observed with DI-MIAMI cells alone. This behavioral recovery upon attachment of MIAMI cells to PAMs was correlated with a neuroprotection/repair of the nigrostriatal pathway. These effects were mainly due to the increased survival and engraftment of transplanted cells which secrete a variety of neurotrophic factors and chemokines. Moreover, a fraction of the cells transplanted with the PAMs expressed human TH, strongly suggesting a neuronal dopaminergic phenotype. Therefore, these cells may have produced dopamine, which could have contributed to functional improvement. We thus demonstrate that the PAMs enhance the stem cell repair capacity by improving their survival and differentiation, as we previously observed with PC12 cells and embryonic dopaminergic cells [47,48].

To improve the known potential of MIAMI cells to differentiate toward a neuronal lineage [11,16], we studied their neuronal differentiation *in vitro* on 2 ECM molecules, FN and LM, for which the cells express a high level of integrin receptors [61]. Indeed, LM is known to induce Nestin expression, a marker of neuronal precursors, in MSCs [43] as well as morphological changes during neuronal differentiation, with a higher number of neurite-like branching [42]. In our hands, MIAMI cells differentiated on a substrate of LM *in vitro* exhibited longer neurite-like extensions together with an improved expression of neuronal proteins (β3-Tubulin and NFM, respectively) compared to FN. Noteworthy, no cell body retraction was observed upon culture on an LM substrate, therefore confirming that the increased expression of β3-Tubulin and NFM were not artifacts due to cellular shrinkage as it has sometimes been suggested [62,63]. Moreover, cell proliferation was almost abolished when cells were differentiated on LM. All these observations are commonly related to a normal stem cell differentiation process, thereby suggesting the bioactive signalling role of LM in the induction of MIAMI cells toward a neuronal lineage.

A biomimetic scaffold bearing LM should therefore be advantageous to implement MIAMI cell therapy in a context where an efficient neuronal differentiation is required. PAMs covered with LM alone presented a weak cell adhesion property so we designed PAMs with a surface made of LM blended with the highly charged PDL molecules. Addition of PDL to the LM surface efficiently switched the zeta potential of PAMs toward positive value, without detriment to LM distribution homogeneity around PAMs. From a practical point of view, formulation of PAM surface was optimized for easier implementation within future potential clinical studies, resulting in a shorter (from 4 h to 1.5 h) but also less expensive protocol as less protein was used without affecting surface characteristics in terms of zeta potential and homogeneity. Moreover, reducing LM adsorption time prevented an excessive loss of NT3 during formulation as a small burst release was observed during the first hours, as is usually the case from PLGA microspheres [55]. In addition to the use of an LM biomimetic surface, PAMs may further enhance MIAMI cells survival and neuronal differentiation by releasing neurotrophin 3, a factor known to play a role in this process [16]. This neurotrophin was encapsulated with a high efficiency within PAMs (100% encapsulation yield) and could be released in a prolonged manner under a bioactive conformation, with only a small burst during the first hours. Around 50% of the encapsulated protein was released after 22 days, suggesting that NT3 could have a long-term effect *in vivo*.

As reported earlier, PAMs may improve the integration of PC12 cells and embryonic dopaminergic cells within the brain parenchyma, after transplantation in hemi-parkinsonian rats, by improving their survival and differentiation [47,48]. An improved differentiation of MSCs toward a chondrogenic phenotype in combination with TGFβ3 PAMs, has also recently been described *in vitro* and *in vivo* [46]. In a similar manner, use of PAMs-NT3 in our study led to a 3 fold increased survival of DI-MIAMI cells 8 weeks after transplantation in hemi-parkinsonian rats, while PAMs-Blank only induced a 2 fold increase in cell survival compared to DI-MIAMI cells grafted alone. This result suggests that bioactive NT3 is being released from the PAMs *in vivo*, which contributes to the survival and differentiation of MIAMI cells and their induced functional recovery. Thus, PAMs could be an easy way to improve the low survival usually observed in long-term studies when grafting MSCs in PD rat brains [26–29]. In addition to an increased

Please cite this article in press as: Delcroix GJ-R, et al., The therapeutic potential of human multipotent mesenchymal stromal cells combined with..., Biomaterials (2010), doi:10.1016/j.biomaterials.2010.10.041

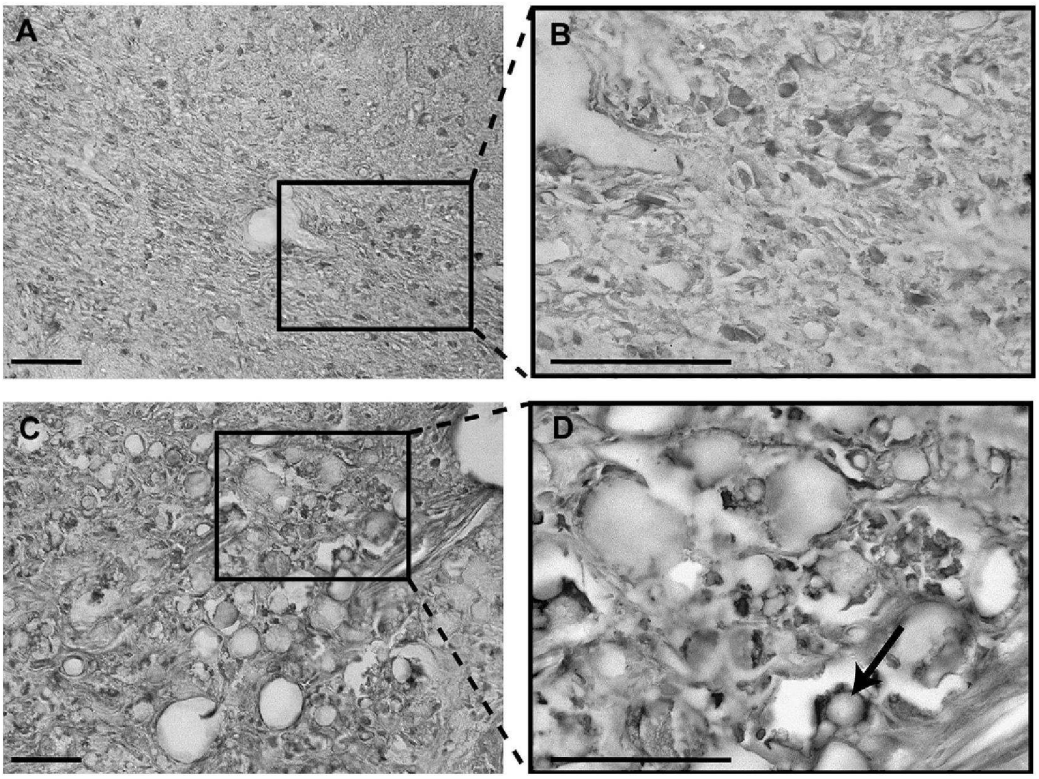

Fig. 6. PAMs enhanced the expression of TH by DI-MIAMI cells *in vivo*. Human specific anti-TH immunohistochemistry revealed that DI-MIAMI cells expressed almost no TH after 8 weeks if transplanted alone (A, B). Conversely, grafting of MIAMI cells in combination with PAMs resulted in a higher fraction of human TH-positive cells in the striatum after 8 weeks (C, D). Black arrow point to a PAM surrounded by TH-positive DI-MIAMI cells. Scale bar: 50 μm. Abbreviations: DI-MIAMI: dopaminergic-induced marrow-isolated adult multilineage inducible, PAMs: pharmacologically active microcarriers, TH: tyrosine hydroxylase.

survival, PAMs induced the differentiation of a fraction of DI-MIAMI cells, with TH expression observed 8 weeks after transplantation of the complexes, but not in the case of cells transplanted alone. Finally, these complexes successfully promoted a reduction of the amphetamine-induced rotational behavior, while cells alone did not induce a major recovery. A small fraction of TH-expressing human MSCs have already been described by another team in the context of PD [29], and the functional recovery they observed in the context of a total nigrostriatal lesion underlined the ability of human MSCs to produce dopamine *in situ*. Another study described functional improvements obtained by grafting dopaminergic-induced human MSCs in the same animal model of Parkinson's disease [27] as ours, despite an incomplete neuronal engagement *in vitro*, as is the case in our study. Thus, these authors concluded that the functional effects observed should mainly derive from secretion of growth factors, chemokines or cytokines from the transplanted cells, a property they previously observed *in vitro* [64]. This is also certainly the case in our study, although dopamine production by TH-expressing cells in presence of PAMs may also have contributed to the functional effect we observed.

In addition to the increased survival/differentiation of grafted cells, the functional effect observed in our study was correlated with a neuroprotection/reparation of the nigrostriatal pathway. This neuroprotection/repair process cannot be observed in studies using total nigrostriatal lesion models [16,29], in which the functional benefits are mainly derived from the secretion of dopamine by the transplanted cells. A repair of the nigrostriatal fibres has already been reported after GDNF striatal injection in not only pre-clinical but also clinical studies [65], and more recently with GDNF delivering microspheres (without cells) enabling the prolonged delivery of the factor [65–68]. Adhesion of DI-MIAMI cells to PAMs-NT3 induced an increased survival of cells but also resulted in an increased expression of *GDNF* and *Stanniocalcin 1* mRNAs. Therefore, in our study, a repair mechanism based on fibre sprouting and possibly driven by the secretion of growth factors such as GDNF may explain the high density of TH-positive fibres detected in the striatum with only a few TH-positive neurons in the substantia nigra. In comparison to the use of GDNF releasing scaffolds, our strategy advantageously results in the secretion of multiple growth factors and chemokines by surviving cells, with potential long-term effects. Importantly, combination of PAMs with DI-MIAMI cells not only led to repair but also to neuroprotection of the nigrostriatal pathway in 40% of the animals, with TH-positive fibres and neurons surviving in the striatum and in the substantia nigra after 8 weeks. This protection was also probably due to the secretion of growth factors and chemokines by the transplanted cells. Accordingly, Stanniocalcin 1 may have a role in protecting surrounding cells from apoptosis [69].

In opposition to DI-MIAMI cells, MIAMI cells only pre-treated with EGF-bFGF efficiently promoted a functional recovery, despite a poor survival due to the absence of PAMs. This observation confirms the potential of EGF-bFGF pre-treated cells for brain cell therapy [11] and supports the hypothesis that functional recovery mainly derives from secretion of growth factors, chemokines or cytokines from the transplanted cells. For example, it is now known that EGF-bFGF treatment increase the secretion of BDNF, GDNF and NGF by adipocyte-derived MSCs, an ability supposed to be responsible for the functional recovery the authors observed [30]. In a similar manner, we demonstrated that EGF-bFGF pre-treated MIAMI cells did produce a significantly higher amount of GDNF and

Please cite this article in press as: Delcroix GJ-R, et al., The therapeutic potential of human multipotent mesenchymal stromal cells combined with..., Biomaterials (2010), doi:10.1016/j.biomaterials.2010.10.041

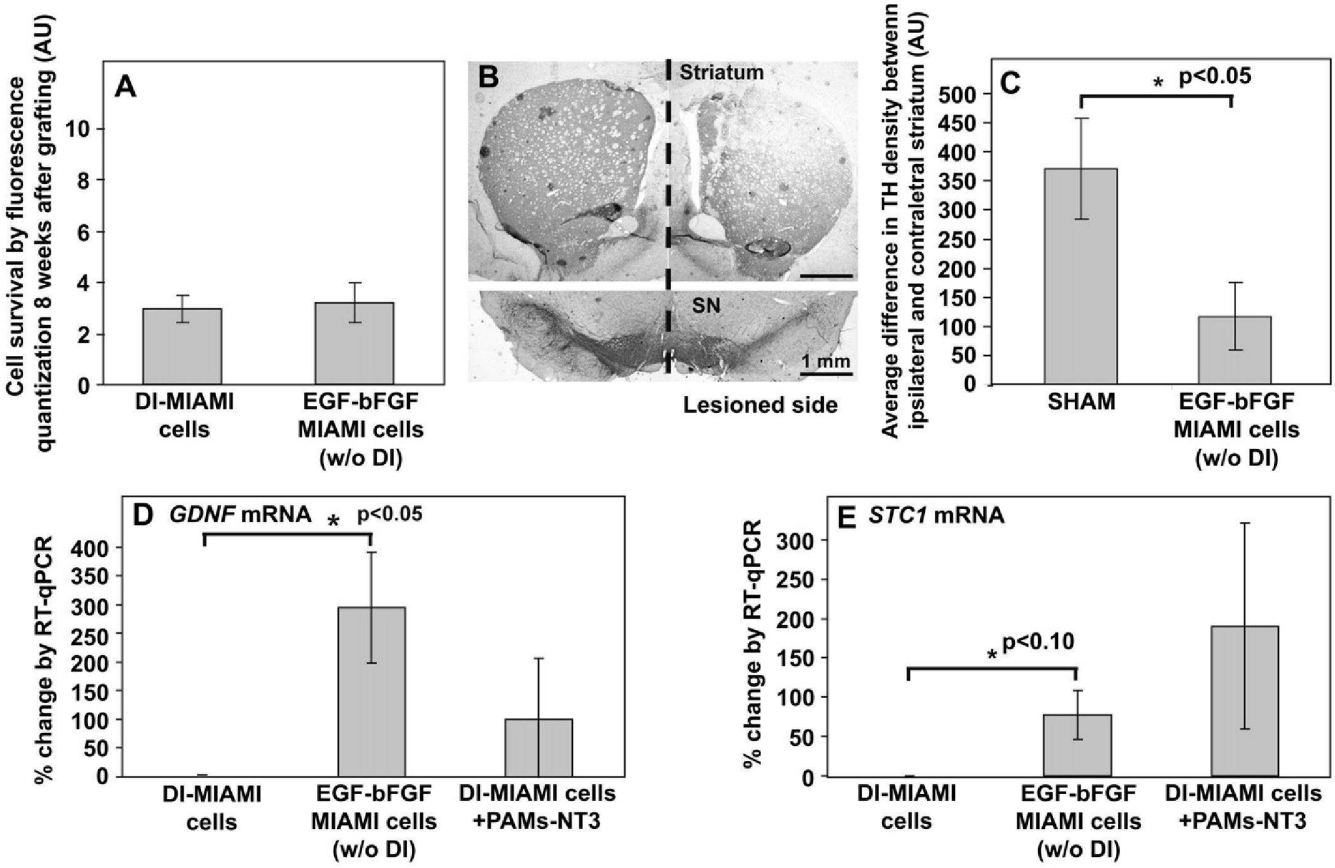

Fig. 7. Effects of EGF-bFGF pre-treated MIAMI cells, without dopaminergic induction. Similarly to DI-MIAMI cells, MIAMI cells only pre-treated with EGF-bFGF (without DI) and transplanted without PAMs poorly survived. Despite their poor survival, these cells induced a functional recovery, correlated with a high density of TH fibres in the striatum (B, C). This could be explained by their differential secretion of molecules such as *GDNF* and *Stanniocalcin 1*, as observed by RT-qPCR (D, E). Noteworthy, adhesion onto PAMs-NT3 tended to increased the secretion profile of DI-MIAMI cells (D, E, top right bar). TH density results are presented as mean differences ± average deviation calculated from 3 slides taken in 3 different rats for each group. RT-qPCR results were obtained from three different experiments and presented as the average % change of mRNA expression ± average deviation. Abbreviations: DI: dopaminergic induction, TH: tyrosine hydroxylase, *STC1*: *Stanniocalcin 1*.

Stanniocalcin 1 compared to MIAMI cells that were furthermore differentiated toward the dopaminergic lineage.

5. Conclusion

To conclude, PAMs-NT3 transporting MIAMI cells induced a strong functional recovery in rat models of PD, mainly via an improved survival and differentiation of grafted cells. Moreover, the secretion pattern of relevant neuroprotecting/repairing factors by MIAMI cells was positively modified upon combination with PAMs. These factors, secreted by surviving cells, may be responsible for the neuroprotection/repair of the nigrostriatal pathway observed, while a possible secretion of dopamine by differentiated cells could have also contributed to the functional effects. This adult cell therapy study demonstrates the benefits of biomaterials combining the biomimetic strategy with the controlled delivery of a growth factor to treat PD [5]. After deeper characterization of the underlying mechanisms, this tissue engineering strategy may ultimately set the ground for pre-clinical studies with non-human primates to increase the efficiency of MSC therapy of the brain.

Disclosure of interests

There is no disclosure of interest in this publication.

Acknowledgments

We thank the SCIAM (“Service Commun d’Imagerie et d’Analyse Microscopique”) of Angers for confocal microscopy images as well as the SCCAN (“Service Commun de Cytométrie et d’Analyse Nucléotidique”) of Angers for the use of PCR facilities. We are also thankful to Marie-Claire Venier and François Hindré (INSERM U646, Angers) for their precious scientific advices as well as to Kevin Curtis (Miami Miller School of Medicine, FL) for RT-qPCR analysis of dopaminergic markers.

Grant information: This work was supported by the “Région Pays de la Loire” & “Inserm”, France and the Department of Veterans Affairs, USA

Appendix

Figures with essential colour discrimination. Certain figures in this article, particularly, Figs. 2, 3 and 5 are difficult to interpret in black and white. The full colour images can be found in the on-line version, at doi:10.1016/j.biomaterials.2010.10.041.

References

[1] Papa SM, Engber TM, Kask AM, Chase TN. Motor fluctuations in levodopa treated Parkinsonian rats: relation to lesion extent and treatment duration. Brain Res 1994;662:69–74.

[2] Fahn S. Is levodopa toxic? Neurology 1996;47:S184–95.
[3] Drucker-Colin R, Verdugo-Diaz L. Cell transplantation for Parkinson's disease: present status. Cell Mol Neurobiol 2004;24:301–16.
[4] Lindvall O, Hagell P. Role of cell therapy in Parkinson's disease. Neurosurg Focus 2002;13:e2.
[5] Delcroix GJR, Schiller PC, Benoit J-P, Montero-Menei CN. Adult cell therapy for brain neuronal damages and the role of tissue engineering. Biomaterials 2010;31:2105–20.
[6] Lindvall O, Kokaia Z. Prospects of stem cell therapy for replacing dopamine neurons in Parkinson's disease. Trends Pharmacol Sci 2009;30:260–7.
[7] Schierle GS, Hansson O, Leist M, Nicotera P, Widner H, Brundin P. Caspase inhibition reduces apoptosis and increases survival of nigral transplants. Nat Med 1999;5:97–100.
[8] Kordower JH, Rosenstein JM, Collier TJ, Burke MA, Chen EY, Li JM, et al. Functional fetal nigral grafts in a patient with Parkinson's disease: chemoanatomic, ultrastructural, and metabolic studies. J Comp Neurol 1996;370:203–30.
[9] Kordower JH, Freeman TB, Chen EY, Mufson EJ, Sanberg PR, Hauser RA, et al. Fetal nigral grafts survive and mediate clinical benefit in a patient with Parkinson's disease. Mov Disord 1998;13:383–93.
[10] Brundin P, Barbin G, Isacson O, Mallat M, Chamak B, Prochiantz A, et al. Survival of intracerebrally grafted rat dopamine neurons previously cultured *in vitro*. Neurosci Lett 1985;61:79–84.
[11] Delcroix GJ, Curtis KM, Schiller PC, Montero-Menei CN. EGF and bFGF pretreatment enhances neural specification and the response to neuronal commitment of MIAMI cells. Differentiation 2010;80:213–27.
[12] Hermann A, Liebau S, Gastl R, Fickert S, Habisch HJ, Fiedler J, et al. Comparative analysis of neuroectodermal differentiation capacity of human bone marrow stromal cells using various conversion protocols. J Neurosci Res 2006;83:1502–14.
[13] Ross JJ, Verfaillie CM. Evaluation of neural plasticity in adult stem cells. Philos Trans R Soc Lond B Biol Sci 2008;363:199–205.
[14] Song S, Sanchez-Ramos J. Brain as the Sea of Marrow. Exp Neurol 2003; 184:54–60.
[15] Morikawa S, Mabuchi Y, Niibe K, Suzuki S, Nagoshi N, Sunabori T, et al. Development of mesenchymal stem cells partially originate from the neural crest. Biochem Biophys Res Commun 2009;379:1114–9.
[16] Tatard VM, D'Ippolito G, Diabira S, Valeyev A, Hackman J, McCarthy M, et al. Neurotrophin-directed differentiation of human adult marrow stromal cells to dopaminergic-like neurons. Bone 2007;40:360–73.
[17] Barzilay R, Kan I, Ben-Zur T, Bulvik S, Melamed E, Offen D. Induction of human mesenchymal stem cells into dopamine-producing cells with different differentiation protocols. Stem Cells Dev 2008;17:547–54.
[18] Trzaska KA, Kuzhikandathil EV, Rameshwar P. Specification of a dopaminergic phenotype from adult human mesenchymal stem cells. Stem Cells 2007; 25:2797–808.
[19] Wolff EF, Gao XB, Yao KV, Andrews ZB, Du H, Elsworth JD, et al. Endometrial stem cell transplantation restores dopamine production in a Parkinson's disease model. J Cell Mol Med. 2010, doi: 10.1111/j.1582-4934.2010.01068.x.
[20] Le Blanc K. Immunomodulatory effects of fetal and adult mesenchymal stem cells. Cytotherapy 2003;5:485–9.
[21] Nasef A, Mathieu N, Chapel A, Frick J, Francois S, Mazurier C, et al. Immunosuppressive effects of mesenchymal stem cells: involvement of HLA-G. Transplantation 2007;84:231–7.
[22] Delcroix GJ, Jacquart M, Lemaire L, Sindji L, Franconi F, Le Jeune JJ, et al. Mesenchymal and neural stem cells labeled with HEDP-coated SPIO nanoparticles: *in vitro* characterization and migration potential in rat brain. Brain Res 2009;1255:18–31.
[23] Mahmood A, Lu D, Wang L, Chopp M. Intracerebral transplantation of marrow stromal cells cultured with neurotrophic factors promotes functional recovery in adult rats subjected to traumatic brain injury. J Neurotrauma 2002;19:1609–17.
[24] Sykova E, Jendelova P. *In vivo* tracking of stem cells in brain and spinal cord injury. Prog Brain Res 2007;161:367–83.
[25] Jendelova P, Herynek V, Urdzikova L, Glogarova K, Kroupova J, Andersson B, et al. Magnetic resonance tracking of transplanted bone marrow and embryonic stem cells labeled by iron oxide nanoparticles in rat brain and spinal cord. J Neurosci Res 2004;76:232–43.
[26] Hellmann MA, Panet H, Barhum Y, Melamed E, Offen D. Increased survival and migration of engrafted mesenchymal bone marrow stem cells in 6-hydroxydopamine-lesioned rodents. Neurosci Lett 2006;395:124–8.
[27] Bouchez G, Sensebe L, Vourc'h P, Garreau L, Bodard S, Rico A, et al. Partial recovery of dopaminergic pathway after graft of adult mesenchymal stem cells in a rat model of Parkinson's disease. Neurochem Int 2008;52: 1332–42.
[28] Sadan O, Bahat-Stromza M, Barhum Y, Levy YS, Pisnevsky A, Peretz H, et al. Protective effects of neurotrophic factors secreting cells in a 6OHDA rat model of Parkinson disease. Stem Cells Dev 2009;18:1179–90.
[29] Levy YS, Bahat-Stroomza M, Barzilay R, Burshtein A, Bulvik S, Barhum Y, et al. Regenerative effect of neural-induced human mesenchymal stromal cells in rat models of Parkinson's disease. Cytotherapy 2008;10:340–52.
[30] McCoy MK, Martinez TN, Ruhn KA, Wrage PC, Keefer EW, Botterman BR, et al. Autologous transplants of Adipose-Derived Adult Stromal (ADAS) cells afford dopaminergic neuroprotection in a model of Parkinson's disease. Exp Neurol 2008;210:14–29.
[31] Orive G, Anitua E, Pedraz JL, Emerich DF. Biomaterials for promoting brain protection, repair and regeneration. Nat Rev Neurosci 2009;10:682–92.
[32] Saporta S, Borlongan C, Moore J, Mejia-Millan E, Jones SL, Bonness P, et al. Microcarrier enhanced survival of human and rat fetal ventral mesencephalon cells implanted in the rat striatum. Cell Transplant 1997;6:579–84.
[33] Borlongan CV, Saporta S, Sanberg PR. Intrastriatal transplantation of rat adrenal chromaffin cells seeded on microcarrier beads promote long-term functional recovery in hemiparkinsonian rats. Exp Neurol 1998;151: 203–14.
[34] Cherksey BD, Sapirstein VS, Geraci AL. Adrenal chromaffin cells on microcarriers exhibit enhanced long-term functional effects when implanted into the mammalian brain. Neuroscience 1996;75:657–64.
[35] Bakay RA, Raiser CD, Stover NP, Subramanian T, Cornfeldt ML, Schweikert AW, et al. Implantation of Spheramine in advanced Parkinson's disease (PD). Front Biosci 2004;9:592–602.
[36] Stover NP, Watts RL. Spheramine for treatment of Parkinson's disease. Neurotherapeutics 2008;5:252–9.
[37] Tatard VM, Menei P, Benoit JP, Montero-Menei CN. Combining polymeric devices and stem cells for the treatment of neurological disorders: a promising therapeutic approach. Curr Drug Targets 2005;6:81–96.
[38] Tucker BA, Rahimtula M, Mearow KM. Integrin activation and neurotrophin signaling cooperate to enhance neurite outgrowth in sensory neurons. J Comp Neurol 2005;486:267–80.
[39] Hall PE, Lathia JD, Caldwell MA, Ffrench-Constant C. Laminin enhances the growth of human neural stem cells in defined culture media. BMC Neurosci 2008;9:71.
[40] Kearns SM, Scheffler B, Goetz AK, Lin DD, Baker HD, Roper SN, et al. A method for a more complete in vitro Parkinson's model: slice culture bioassay for modeling maintenance and repair of the nigrostriatal circuit. J Neurosci Methods 2006;157:1–9.
[41] Kearns SM, Laywell ED, Kukekov VK, Steindler DA. Extracellular matrix effects on neurosphere cell motility. Exp Neurol 2003;182:240–4.
[42] Qian L, Saltzman WM. Improving the expansion and neuronal differentiation of mesenchymal stem cells through culture surface modification. Biomaterials 2004;25:1331–7.
[43] Ho M, Yu D, Davidsion MC, Silva GA. Comparison of standard surface chemistries for culturing mesenchymal stem cells prior to neural differentiation. Biomaterials 2006;27:4333–9.
[44] Nakajima M, Ishimuro T, Kato K, Ko IK, Hirata I, Arima Y, et al. Combinatorial protein display for the cell-based screening of biomaterials that direct neural stem cell differentiation. Biomaterials 2007;28:1048–60.
[45] Tatard VM, Venier-Julienne MC, Saulnier P, Prechter E, Benoit JP, Menei P, et al. Pharmacologically active microcarriers: a tool for cell therapy. Biomaterials 2005;26:3727–37.
[46] Bouffi C, Thomas O, Bony C, Giteau A, Venier-Julienne MC, Jorgensen C, et al. The role of pharmacologically active microcarriers releasing TGF-beta3 in cartilage formation in vivo by mesenchymal stem cells. Biomaterials 2010; 31:6485–93.
[47] Tatard VM, Venier-Julienne MC, Benoit JP, Menei P, Montero-Menei CN. In vivo evaluation of pharmacologically active microcarriers releasing nerve growth factor and conveying PC12 cells. Cell Transplant 2004;13:573–83.
[48] Tatard VM, Sindji L, Branton JG, Aubert-Pouessel A, Colleau J, Benoit JP, et al. Pharmacologically active microcarriers releasing glial cell line - derived neurotrophic factor: survival and differentiation of embryonic dopaminergic neurons after grafting in hemiparkinsonian rats. Biomaterials 2007;28: 1978–88.
[49] D'Ippolito G, Diabira S, Howard GA, Menei P, Roos BA, Schiller PC. Marrow-isolated adult multilineage inducible (MIAMI) cells, a unique population of postnatal young and old human cells with extensive expansion and differentiation potential. J Cell Sci 2004;117:2971–81.
[50] D'Ippolito G, Diabira S, Howard GA, Roos BA, Schiller PC. Low oxygen tension inhibits osteogenic differentiation and enhances stemness of human MIAMI cells. Bone 2006;39:513–22.
[51] Tamama K, Kawasaki H, Wells A. Epidermal growth factor (EGF) treatment on multipotential stromal cells (MSCs). Possible enhancement of therapeutic potential of MSC. J Biomed Biotechnol; 2010. 795385.
[52] Padovan CS, Jahn K, Birnbaum T, Reich P, Sostak P, Strupp M, et al. Expression of neuronal markers in differentiated marrow stromal cells and CD133+ stem-like cells. Cell Transplant 2003;12:839–48.
[53] Freire E, Gomes FC, Linden R, Neto VM, Coelho-Sampaio T. Structure of laminin substrate modulates cellular signaling for neuritogenesis. J Cell Sci 2002; 115:4867–76.
[54] Vandesompele J, De Preter K, Pattyn F, Poppe B, Van Roy N, De Paepe A, et al. Accurate normalization of real-time quantitative RT-PCR data by geometric averaging of multiple internal control genes. Genome Biol 2002;3. RESEARCH0034.
[55] Giteau A, Venier-Julienne MC, Marchal S, Courthaudon JL, Sergent M, Montero-Menei C, et al. Reversible protein precipitation to ensure stability during encapsulation within PLGA microspheres. Eur J Pharm Biopharm 2008;70:127–36.
[56] Fraker PJ, Speck Jr JC. Protein and cell membrane iodinations with a sparingly soluble chloroamide, 1,3,4,6-tetrachloro-3a,6a-diphrenylglycoluril. Biochem Biophys Res Commun 1978;80:849–57.
[57] Kirik D, Rosenblad C, Bjorklund A. Characterization of behavioral and neurodegenerative changes following partial lesions of the nigrostriatal dopamine system induced by intrastriatal 6-hydroxydopamine in the rat. Exp Neurol 1998;152:259–77.

Please cite this article in press as: Delcroix GJ-R, et al., The therapeutic potential of human multipotent mesenchymal stromal cells combined with..., Biomaterials (2010), doi:10.1016/j.biomaterials.2010.10.041

[58] Horwitz EM, Prather WR. Cytokines as the major mechanism of mesenchymal stem cell clinical activity: expanding the spectrum of cell therapy. Isr Med Assoc J 2009;11:209–11.
[59] Chen Q, Long Y, Yuan X, Zou L, Sun J, Chen S, et al. Protective effects of bone marrow stromal cell transplantation in injured rodent brain: synthesis of neurotrophic factors. J Neurosci Res 2005;80:611–9.
[60] Ohtaki H, Ylostalo JH, Foraker JE, Robinson AP, Reger RL, Shioda S, et al. Stem/progenitor cells from bone marrow decrease neuronal death in global ischemia by modulation of inflammatory/immune responses. Proc Natl Acad Sci U S A 2008;105:14638–43.
[61] Docheva D, Popov C, Mutschler W, Schieker M. Human mesenchymal stem cells in contact with their environment: surface characteristics and the integrin system. J Cell Mol Med 2007;11:21–38.
[62] Lu P, Blesch A, Tuszynski MH. Induction of bone marrow stromal cells to neurons: differentiation, transdifferentiation, or artifact? J Neurosci Res 2004;77:174–91.
[63] Khoo ML, Shen B, Tao H, Ma DD. Long-term serial passage and neuronal differentiation capability of human bone marrow mesenchymal stem cells. Stem Cells Dev 2008;17:883–96.
[64] Sensebe L, Deschaseaux M, Li J, Herve P, Charbord P. The broad spectrum of cytokine gene expression by myoid cells from the human marrow microenvironment. Stem Cells 1997;15:133–43.
[65] Hurelbrink CB, Barker RA. The potential of GDNF as a treatment for Parkinson's disease. Exp Neurol 2004;185:1–6.
[66] Garbayo E, Montero-Menei CN, Ansorena E, Lanciego JL, Aymerich MS, Blanco-Prieto MJ. Effective GDNF brain delivery using microspheres – a promising strategy for Parkinson's disease. J Control Release 2009;135:119–26.
[67] Jollivet C, Aubert-Pouessel A, Clavreul A, Venier-Julienne MC, Remy S, Montero-Menei CN, et al. Striatal implantation of GDNF releasing biodegradable microspheres promotes recovery of motor function in a partial model of Parkinson's disease. Biomaterials 2004;25:933–42.
[68] Bjorklund A, Rosenblad C, Winkler C, Kirik D. Studies on neuroprotective and regenerative effects of GDNF in a partial lesion model of Parkinson's disease. Neurobiol Dis 1997;4:186–200.
[69] Block GJ, Ohkouchi S, Fung F, Frenkel J, Gregory C, Pochampally R, et al. Multipotent stromal cells are activated to reduce apoptosis in part by upregulation and secretion of stanniocalcin-1. Stem Cells 2009;27:670–81.

Please cite this article in press as: Delcroix GJ-R, et al., The therapeutic potential of human multipotent mesenchymal stromal cells combined with..., Biomaterials (2010), doi:10.1016/j.biomaterials.2010.10.041

Curriculum Vitae

Claire VANPOUILLE-BOX
18, rue de la meignanne
49100 Angers
France
Française/28 ans/ mariée
06 15 36 02 89
claire.vanpouille.box@gmail.com

Doctorante en Pharmacologie Expérimentale et Clinique

FORMATION

Nov 2007 – aujourd'hui: **Doctorat** en pharmacologie expérimentale (1ère, 2ème, and 3ème années), Université d'Angers (France)

2006 – 2007: **Master** biophotonique des cellules et systèmes intégrés Université de Saint-Etienne (France)

2005 – 2002: **Licence** biologie, biochimie et chimie Université de Saint-Etienne (France)

EXPERIENCES PROFESSIONELLES

Nov 2007 – aujourd'hui — INSERM U646, Université d'Angers (France)

Radiothérapie vectorisée via les nanocapsules lipidiques chargées en rhénium-188 pour le traitement du carcinome hépatocellulaire et du gliome.

* formulation de systèmes particulaires vecteurs de radioéléments
* biologie cellulaire (immunohistochimie…)
* études pharmaco-cinétiques
* expérimentation animale: stéréotaxie, microchirurgie (niveau 1 en expérimentation animale)
* Techniques d'imagerie (IRM petit animal, scintigraphies…)
* 2 publications
* 2 publications soumises

Stage Master 2: 2007, 6 mois — Laboratoire de Biophysique et des radiopharmaceutiques, EA 3063, Université de Saint-Etienne (France)

Influence de la résistance multi-drogue sur la captation cellulaire de la (18)F-FCH dans un modèle de glioblastome.

* biologie cellulaire
* études de radiotraceurs
* 1 publication

Stage Master 1: 2006, 6 semaines — Laboratoire d'histologie, Université de Saint-Etienne (France)

Mise au point d'une technique d'hybridation in situ sur étalements broncho-pulmonaires

* marquages fluorescent

ACTIVITÉS D'ENSEIGNEMENT ET D'ENCADREMENT

Enseignement:

* Travaux pratique en 1ère année du DUT analyse biologique et biochimique. 96h. Contact: Lydie Bouvier
  - Multiplication cellulaire, Culture cellulaire
  - Osmose, perméabilité membranaire, échanges d'eau et de substances dissoutes
  - Reproduction sexuée chez les végétaux
  - Dissections appareils reproducteurs (souris femelle et souris mâle)
  - Dissection appareil digestif (rat)
  - Absorption intestinale (*ex vivo* chez le rat)
  - Histologie Animale et Végétale
  - Histo-cytochimie des constituants cellulaires végétaux
  - Photosynthèse

Encadrement:

* Encadrement d'étudiants en Master 1 Sciences, Technologies et Ingienerie de la Santé (5 semaines):
  - "Evaluation de la réponse immunitaire périphérique après radiothérapie interne nanovectorisée dans un modèle de gliome", Clara Marsac et Claire Goussault.
  - " Dosage des cytokines Interleukine-2 et Interferon-γ après radiothérapie interne dans un modèle de gliome chez le rat", Florent Maugin et Basile Gautier.
* Encadrement d'étudiants en Licence professionnelle Biologie Analytique et Expérimentale des Microorganismes du Végétal et de l'Animal (14 semaines):
  - "Caractérisation de la réponse immunitaire induite par la radiothérapie interne nanovectorisée dans un modèle de gliome", Camille Belloche.
  - "Etude de la stimulation du système immunitaire après radiothérapie interne nanovectorisée associée à une vaccination dans un modèle de gliome", Emeline Brocard.

COMPÉTENCES COMPLÉMENTAIRES

* Formation Expérimentation Animale Niveau 1, ONIRIS, Nantes
* Stage INSERM: Initiation gestion des risques
* Anglais: Lu, écrit, parlé
* Allemand: niveau scolaire
* Logiciels: Word, Excel, Power Point, GIMP, StatView, Endnote, MetaMorph

PUBLICATIONS

Vanpouille C, Le Jeune N, Kryza D, Clotagatide A, Janier M, Dubois F, Perek N. Eur J Nucl Med Mol Imaging, 2009 Aug; 36(8):1256-64. Epub Mar 20 - **Influence of multidrug resistance on (18)F-FCH cellular uptake in a glioblastoma model.**

Delcroix GJ, Garbayo E, Sindji L, Thomas O, Vanpouille-Box C, Schiller PC, Montero-Menei CN. Biomaterials,2011 Feb; 32(6):1560-732010s. Epub Nov 12 - **The therapeutic potential of human multipotent mesenchymal stromal cells combined with pharmacologically active microcarriers transplanted in hemi-parkinsonian rats.**

Vanpouille-Box C, Lacoeuille F, Roux J, Aubé C, Garcion E, Lepareur N, Oberti F, Bouchet F, Noiret N, Garin E, Benoit JP, Couturier O, Hindré F. PloS One, in press **– Lipid nanocapsules loaded with rhenium-188 reduce tumor progression in a rat hepatocellular carcinoma model.**

POSTER

Vanpouille C., Lacoeuille F., Garcion E., Lemaire L., Bouchet F., LeJeune JJ., Benoit JP., Couturier O., Hindré F. - **Radiothérapie interne fractionnée à l'aide des nanocapsules lipidiques chargées en rhénium-188 dans un modèle de glioblastome de rat** - 47ème Colloque de Médecine Nucléaire de Langue Française – 9th – 12th may, Brest 2009

Vanpouille C., Lacoeuille F., Roux J., Aubé C., Oberti F., Garin E., LeJeune JJ., Benoit JP, Couturier O., Hindré F. - **Internal radiation with 188Re-loaded lipid nanocapsules in a rat hepatocellular carcinoma** - 1srt TARCC international Workshop on targeted radionuclide therapy: "Advances in targeted radionuclide therapy", May 25th-26th, 2009 Nantes, France

COMMUNICATIONS ORALES

Vanpouille C., Lacoeuille F., Roux J., Aubé C., Oberti F., LeJeune JJ., Benoit JP, Couturier O., Hindré F. - **Injection intra-artérielle de nanocapsules lipidiques chargées en rhénium-188, pour le traitement du carcinome hépatocellulaire chez le rat** - 47ème Colloque de Médecine Nucléaire de Langue Française, 9th -12th may, Brest 2009, France

Vanpouille C., Lacoeuille F., Garcion E., Lemaire L., Bouchet F., Lepareur N., LeJeune JJ, Benoit JP, Couturier O, Hindré F. - **Stereotaxic injections of 188-Re loaded nanocapsules as fractionated internal radioation in a rat glioblastoma model** - 1srt TARCC international Workshop on targeted radionuclide therapy: "Advances in targeted radionuclide therapy", May 25th - 26th, 2009 Nantes, France

Vanpouille C, Lacoeuille F, Garcion E, Lemaire L, Bouchet F, Lepareur N, Noiret N, LeJeune JJ, Benoit JP, Couturier O, Hindré F. - **Fractionated internal radiation with stereotaxic injection of 188Re-loaded lipid nanocapsules in a rat glioblastoma model** - SNM 56th Annual Meeting, Toronto, Canada, June 13th - 17th 2009

Vanpouille C., Lacoeuille F., Roux J., Aubé C., Oberti F., Noiret N., LeJeune JJ., Benoit JP., Couturier O., Hindré F. - **Intra-arterial injection of lipid nanocapsules loaded with rhenium-188 for the radiotherapy of hepatocellular carcinomas in rats.** - SNM 56th Annual Meeting, Toronto, Canada, June 13th - 17th 2009

Vanpouille C., Lacoeuille F., Roux J., Aubé C., Oberti F., Noiret N., LeJeune JJ., Benoit JP., Couturier O., Hindré F. - **Intra-arterial injection of lipid nanocapsules loaded with rhenium-188 for the radiotherapy of hepatocellular carcinomas in rats. –** New trends in Molecular Imaging and Nuclear Medicine, Bologne, Italie, 14 septembre 2009. Award « Young Investigator award ».

Vanpouille C., Lacoeuille F., Roux J., Aubé C., Oberti F., Noiret N., Garin E., LeJeune JJ., Benoit JP., Couturier O., Hindré F. – **Administration of ^{188}Re-loaded nanocapsules into the hepatic artery involves neoangiogenesis alterations in a rat hepatocellular carcinoma model.** - Targeting and Imaging of the Tumor Microenvironment from the 23rd to 26th of September 2009 in Berder Island, France.

Vanpouille C., Garcion E., Lacoeuille F.,Lemaire L., Lepareu r N. , Le Jeune JJ ., Benoit JP. , Couturier O.,Hindré F. - **Evaluation des réponses immunitaires dans le cadre de la radiothérapie interne nanovectorisée du Glioblastome.** - 5ème journée de l'IFR132 « Stratégies de ciblage en thérapeutique », 7 mai 2010, Angers, France. 1st award « Best Oral Presentation ».

Vanpouille C., Garcion E., Lacoeuille F., Lemaire L., Lepareur N., Le Jeune JJ., Benoit JP , Couturier O., Hindré F. – **Evaluation of immune responses after nanovectorized internal radiotherapy for glioblastomas.** – 2010 World Molecular Congress, Kyoto, Japan, September 8th-11th 2010.

Vanpouille C., Garcion E., Lacoeuille F., Lemaire L., Lepareur N., Le Jeune JJ., Benoit JP , Couturier O., Hindré F. – **Evaluation of immune responses after nanovectorized internal radiotherapy for glioblastomas.** – Biology of ionizing radiation from the 22nd to 25th of September 2010 in Berder Island, France.

Vanpouille C., Garcion E., Lacoeuille F., Lepareur N., Le Jeune JJ., Benoît JP., Couturier O., Hindré F. – **Nanovectorized internal radiation therapy in a glioblastoma rat model**. – EANM'10, Annual Congress of the European Association of Nuclear Medicine, Vienna, Austria, 9-13 October 2010.

RESUME

La radiothérapie implique de limiter l'irradiation des tissus sains. Dans ce but, des nanocapsules lipidiques chargées en complexes lipophile de rhénium-188 (NCL^{188}Re-SSS) ont été utilisées afin de créer une irradiation localisée après injection intra-tumorale. Nous avons ainsi évalué la faisabilité d'une radiothérapie interne après injection intra-hépatique de NCL^{188}Re-SSS pour le traitement du carcinome hépatocellulaire (CHC) et, dans un deuxième temps, étudié l'efficacité d'un fractionnement de la dose radioactive après injections intra-crâniennes répétées pour le traitement des gliomes. La première partie de ce travail décrit l'intérêt d'une radiothérapie interne via les NCL^{188}Re-SSS pour le traitement du CHC avec une augmentation de la médiane de survie jusqu'à 107% dans un modèle CHC chimio-induit chez le rat. Dans une seconde partie, nous avons pu démontrer un bénéfice majeur, sur un modèle de gliome, avec 83% des animaux long-survivants. Cette efficacité thérapeutique pourrait s'expliquer par la mise en place d'une réponse immunitaire adaptative avec recrutement local de cellules immunitaires effectrices (CD4+, CD8+…). En revanche, les essais d'une radiothérapie interne nanovectorisée sur un modèle de rat peu immunogène et radiorésistant (modèle tumoral F98) ont montré des bénéfices moindres en terme de survie. Pour stimuler la réponse immunitaire anti-tumorale et optimiser l'efficacité thérapeutique, nous avons évalué la combinaison d'une radiothérapie interne nanovectorisée et d'une vaccination par cellules F98 irradiées. Un recrutement des cellules immunitaires effectrices a été observé, cependant, l'efficacité thérapeutique n'a pas été augmentée. Les perspectives qu'offre ce travail sont de deux ordres : évaluer l'impact du processus angiogénique dans le cas du modèle CHC et stimuler le système immunitaire en association avec la radiothérapie interne pour le modèle de gliome.

MOTS-CLEFS : NCL^{188}Re-SSS, gliomes, hépatocarcinome, gradient d'activité, réponse immunitaire adaptative, processus d'immunisation, vaccination.

ABSTRACT

Radiotherapy aims to preserve the irradiation of healthy tissues. For this purpose, lipid nanocapsules loaded with lipophilic complex of rhenium-188 (LNC^{188}Re-SSS) were used to create a localized irradiation after intratumoral injection. Hence, we assessed the feasibility of internal radiation therapy after intra-hepatic LNC^{188}Re-SSS for the treatment of hepatocellular carcinoma (HCC). Secondly, we examined the efficiency of repeated intra-cranial injections for the treatment of gliomas. The first part of this work describes the interest of internal radiotherapy with LNC^{188}Re-SSS for the treatment of HCC with increased median survival up to 107% in a chemically-induced HCC rat model. Meanwhile, we demonstrated a major benefit in terms of survival, with 83% of animals which were long-term survivors. This therapeutic effect could be explained by the establishment of an adaptive immune response with local recruitment of immune effector cells (CD4+, CD8+…). However, assessment on a weakly immunogenic and radioresistant model (tumor model F98) showed lower benefits in terms of survival. To stimulate an anti-tumor immune response and to optimize therapeutic efficiency, we evaluate the combination of fractionated internal radiotherapy with vaccination of F98 irradiated cells. Although an increase in the recruitment of immune cells was highlighted, the combination of these two strategies did not result in better survival benefit. The prospects offered by this work are twofold: to assess the impact of the angiogenic process in the case of the HCC model and stimulate the immune system in combination with internal radiation therapy for the glioma model.

KEYWORDS : LNC^{188}Re-SSS, gliomas, hepatocarcinoma, activity gradient, adptative immune response, immunization process, vaccination